IVW - Schriftenreihe Band 92
Institut für Verbundwerkstoffe GmbH - Kaiserslautern

Lada Antonova Gyurova

Sliding Friction and Wear of Polyphenylene Sulfide Matrix Composites: Experimental and Artificial Neural Network Approach

Bibliografische Information Der Deutschen Bibliothek

Die Deutsche Bibliothek verzeichnet diese Publikation in der Deutschen Nationalbibliografie; detaillierte bibliografische Daten sind im Internet über <http://dnb.ddb.de> abrufbar.

Bibliographic information published by Die Deutsche Bibliothek

Die Deutsche Bibliothek lists this publication in the Deutsche Nationalbibliografie; detailed bibliographic data is available in the Internet at <http://dnb.ddb.de>.

Herausgeber: Institut für Verbundwerkstoffe GmbH
Prof. Dr.-Ing. Peter Mitschang
Erwin-Schrödinger-Straße
TU Kaiserslautern, Gebäude 58
67663 Kaiserslautern
http://www.ivw.uni-kl.de

Verlag: Institut für Verbundwerkstoffe GmbH

Druck: Technische Universität Kaiserslautern
ZBT – Abteilung Foto-Repro-Druck

D 386

Als Manuskript gedruckt. Printed in Germany.
ISSN 1615-021X
ISBN 978-3-934930-88-9
ISBN 3-934930-88-3

Sliding Friction and Wear of Polyphenylene Sulfide Matrix Composites: Experimental and Artificial Neural Network Approach

Vom Fachbereich Maschinenbau und Verfahrenstechnik

der Technischen Universität Kaiserslautern

zur Verleihung des akademischen Grades

Doktor-Ingenieur (Dr.-Ing.)

genehmigte Dissertation

von

M.Sc. Lada Antonova Gyurova

aus Sofia, Bulgarien

Tag der mündlichen Prüfung: 08. März 2010

Prüfungsvorsitzender:	Prof. Dr.-Ing. Bernd Sauer
1. Berichterstatter:	Prof. Dr.-Ing. Dr. h.c. mult. Klaus Friedrich
2. Berichterstatter:	Prof. Dr.-Ing. Martin Maier
3. Berichterstatter:	Prof. Dr.-Ing. Karl-Heinz Zum Gahr

D 386

This work is dedicated to my family

Acknowledgements

First of all, I would like to express deep gratitude to my supervisor Prof. Dr.-Ing. Dr. h.c. mult. Klaus Friedrich whose support, both professional and personal, mentoring, constructive advice and criticism throughout my research work were invaluable. His great knowledge and professional commitment to excellence in research is at a level which I aspire to achieve.

I am indebted to the members of the examination commission, Prof. Dr.-Ing. Martin Maier and Prof. Dr.-Ing. Karl-Heinz Zum Gahr, for the time and effort they have spent on the co-reference of my thesis. I would also like to extend my gratitude to Prof. Dr.-Ing. Bernd Sauer for accepting the presidency of the examination committee.

Throughout the years (2005-2010) I have had the privilege of working in an outstanding environment from both a scientific and technical point of view at IVW. I hereby would like to thank Prof. Dr.-Ing. Alois K. Schlarb, Prof. Dr.-Ing. Peter Mitschang and Dr. rer. nat. Thomas Burkhart for providing me this opportunity and giving me the sovereignty to choose projects of interest to me.

During my stay at the institute, I benefited tremendously from the expertise of many of the technical staff, especially that of Materials Science Division. In this respect, I would like to thank Joachim Stephan who was always ready to lend a helping hand in the tribology lab, Hermann Giertzsch for his kind help in the preparation of the SEM micrographs, Stefan Schmitt for the work on the AFM images, Rolf Walter and Werner Schröck for their support in the extrusion lab, Ralf Schimmele for his assistance in performing the mechanical testing of the materials as well as Markus Hentzel. Well-deserved thanks go to Nora Opitz, who keeps things running smoothly in the division from administrative point and was very helpful, especially with urgent matters without complaining or failing to deliver.

I would like to thank Dr. Zhenyu Jiang and Prof. Zhong Zhang for introducing me to the world of artificial neural networks and Dr. Björn Lehmann for helping me to advance my expertise in thermoplastic processing. Help and advice from Dr. Frank Haupert and Andreas Noll are also gratefully acknowledged. All the colleagues at

IVW who have contributed over the years in one way or another: you have my personal and very sincere gratitude.

A big thank you to my students for their valuable contributions towards my research work: Xiang Yang, Nico Buhl, Jie Zou, Christian Hartmann, Patrick Schäfer, Tan Li, David Kuhn, Ramon Mazquiaran Oteiza, Carlos Bercianos Garcia, Paz Miniño-Justel, Jose Antonio Pérez Calvo, Ana Vinas Alonso and Asier Bereciartua Dudagoitia.

This whole project would not have been possible without the continuous financial support of the German Research Foundation (DFG) within DFG FR 675/45-1 as well as DFG SCHL 280/7-2, which I sincerely acknowledge. Equally, I would like to thank the companies Ensinger GmbH and Ticona GmbH for supplying some of the raw materials as well as the company FACT GmbH for lending the tool for injection molding.

I am grateful to my colleagues Thomas Bayerl, Markus Steeg, Michael Harrass, Bernd Wetzel, Nicole Knör, Martin Priebe, Lars Moser, Michael Bierer, Robert Lahr and Jens Schlimbach, whom I have over the years become good friends with for the nice and fruitful time both at work and in private.

My close friends Sandrine, Zdravka, Wenjing, Núria, Margit, Koji, Sergiy, Dietrich, Julia, Yota, Markus, Boriana, Irene, Konstantina, Ibrahim and Andreas Hölzer among many others I would like to thank for being there for me in making the hard moments bearable and made my stay in and outside Kaiserslautern unforgettable.

I would like to thank my partner Miro for his incredible support, patience and love during the last months of writing my thesis and preparing for the defense.

Finally, but most importantly, I would like to thank my parents and my sister who devotedly supported me, inspired me and helped me to come so far and become the person I am. To them, I give my heartfelt thanks and deepest appreciation.

Table of Contents

Abstract

In recent years the consumption of polymer based composites in many engineering fields where friction and wear are critical issues has increased enormously. Satisfying the growing industrial needs can be successful only if the costly, labor-intensive and time-consuming cycle of manufacturing, followed by testing, and additionally followed by further trial-and-error compounding is reduced or even avoided. Therefore, the objective is to get in advance as much fundamental understanding as possible of the interaction between various composite components and that of the composite against its counterface. Sliding wear of polymers and polymer composites involves very complex and highly nonlinear processes. Consequently, to develop analytical models for the simulation of the sliding wear behavior of these materials is extremely difficult or even impossible. It necessitates simplifying hypotheses and thus compromising accuracy. An alternative way, discussed in this work, is an artificial neural network based modeling. The principal benefit of artificial neural networks (ANNs) is their ability to learn patterns through a training experience from experimentally generated data using self-organizing capabilities.

Initially, the potential of using ANNs for the prediction of friction and wear properties of polymers and polymer composites was explored using already published friction and wear data of 101 independent fretting wear tests of polyamide 46 (PA 46) composites. For comparison, ANNs were also applied to model the mechanical properties of polymer composites using a commercial data bank of 93 pairs of independent Izod impact, tension and bending tests of polyamide 66 (PA 66) composites. Different stages in the development of ANN models such as selection of optimum network configuration, multi-dimensional modeling, training and testing of the network were addressed at length. The results of neural network predictions appeared viable and very promising for their application in the field of tribology.

A case example was subsequently presented to model the sliding friction and wear properties of polymer composites by using newly measured datasets of polyphenylene sulfide (PPS) matrix composites. The composites were prepared by twin-screw extrusion and injection molding. The dataset investigated was generated from pin-on-disc testing in dry sliding conditions under various contact pressures and slid-

ing speeds. Initially the focus was placed on exploring the possible synergistic effects between traditional reinforcements and particulate fillers, with special emphasis on sub-micro TiO_2 particles (300 nm average diameter) and short carbon fibers (SCFs). Subsequently, the lubricating contributions of graphite (Gr) and polytetrafluoroethylene (PTFE) in these multiphase materials were also studied. ANNs were trained using a conjugate gradient with Powell/Beale restarts (CGB) algorithm as well as a variable learning rate backpropagation (GDX) algorithm in order to learn composition-property relationships between the inputs and outputs of the system. Likewise, the influence of the operating parameters (contact pressure (p) and sliding speed (v)) was also examined. The incorporation of short carbon fibers and sub-micro TiO_2 particles resulted in both a lower friction and a great improvement in the wear resistance of the PPS composites within the low and medium pv-range. The mechanical characterization and surface analysis after wear testing revealed that this beneficial tribological performance could be explained by the following phenomena: (i) enhanced mechanical properties through the inclusion of short carbon fibers, (ii) favorable protection of the short carbon fibers by the sub-micro particles diminishing fiber breakage and removal, (iii) self-repairing effects with the sub-micro particles, (iv) formation of quasi-spherical transfer particles free to roll at the tribological contact. Still, in the high pv-range stick-slip sliding motion was observed with these hybrid materials. The adverse stick-slip behavior could be effectively eliminated through the additional inclusion of solid lubricant reservoirs (Gr and PTFE), analogous to the lubricants used in real ball bearings. Likewise, solid lubricants improved the wear resistance of the multiphase system PPS/SCF/TiO_2 in the high pv-range ($\geq$ 9 MPa·m/s). Yet, their positive effect, especially that of graphite, was limited up to certain volume fraction and loading conditions. The optimum results were obtained by blending comparatively low amounts of Gr and PTFE ($\approx$ 5 vol.% from each additive). An introduction of softer sub-micro particles did not bring the desired ball bearing effect and fiber protection. The ANN prediction profiles for PPS tribo-compounds exhibited very good or even perfect agreement with the measured results demonstrating that the target of achieving a well trained network was reached. The results of employing a validation test dataset indicated that the trained neural network acquired enough generalization capability to extend what it has learned about the training patterns to data that it has not seen before from the same knowledge domain.

Optimal brain surgeon (OBS) algorithm was employed to perform pruning of the network topology by eliminating non-useful weights and bias in order to determine if the performance of the pruned network was better than the fully-connected network. Pruning resulted in accuracy gains over the fully-connected network, but induced higher computational cost in coding the data in the required format. Within an importance analysis, the sensitivity of the network response variable (frictional coefficient or specific wear rate) to characteristic mechanical and thermo-mechanical input variables was examined. The goal was to study the relationships between the diverse input variables and the characteristic tribological parameters for a better understanding of the sliding wear process with these materials. Finally, it was demonstrated that the well-trained networks might be applied for visualization what will happen if a certain filler is introduced into a composite, or what the impacts of the testing conditions on the frictional coefficient and specific wear rate are. In this way, they might be a helpful tool for design engineers and materials experts to explore materials and to make reasoned selection and substitution decisions early in the design phase, when they incur least cost.

Kurzfassung

In den letzten Jahren haben sich die Einsatzgebiete für Polymer-Verbundwerkstoffe in vielen technischen Bereichen, in denen Reibung und Verschleiß kritische Faktoren sind, erheblich ausgeweitet. Um dem wachsenden Industriebedarf nachzukommen, sollte der teure, arbeitsintensive und zeitaufwendige Zyklus der Herstellung, gefolgt von Prüfung und einer weiteren Trial-and-Error Compoundierung verringert oder sogar komplett vermieden werden. Die Zielsetzung ist es daher ein grundlegendes Verständnis der Wechselwirkung sowohl zwischen den einzelnen Verbundkomponenten als auch zwischen dem Verbund und dem Gegenkörper zu erhalten. Gleitverschleiß bei Polymeren und Verbundwerkstoffen weist hochkomplexe und nichtlineare Vorgänge auf. Somit ist die Entwicklung analytischer Modelle für deren Simulation äußerst schwierig oder nahezu unmöglich. Sie erfordert die Vereinfachung von Hypothesen, wodurch die Genauigkeit deutlich vernachlässigt wird. Eine andere Alternative, welche in der vorliegenden Arbeit vorgestellt ist, bietet die künstliche neuronale Netzwerksmodellierung. Der größte Vorteil der künstlichen neuronalen Netze ist ihre Fähigkeit durch die wiederholte Eingabe von Trainingsmustern selbständig zu lernen.

Zunächst wurde das Potential des Ansatzes für die künstlichen neuronalen Netzwerke zur Vorhersage des Verschleißverhaltens von Polymeren und Verbundwerkstoffen unter Verwendung existierender, experimenteller Daten aus 101 unabhängigen Schwingverschleißuntersuchungen an Polyamid 46 (PA 46) analysiert. Zum Vergleich wurden künstliche neuronale Netzwerke eingesetzt, um die mechanischen Eigenschaften von Polymer-Verbundwerkstoffen unter Verwendung einer kommerziellen Datenbank (93 Paare von einzelnen Izod-Schlag, Zug- und Biege- Versuchen an Polyamid 66 (PA 66) Verbundwerkstoffen) zu modellieren. Unterschiedliche Phasen zur Entwicklung eines neuronalen Netzwerks sowie die Auswahl der optimalen Netzwerkskonfiguration, multidimensionale Modellierung, Netzwerk-Training und -Test wurden ausführlich erforscht. Die Ergebnisse der Vorhersage des neuronalen Netzes erschienen erfolgversprechend für deren Anwendung im Bereich der Tribologie.

Anschließend wurde anhand einer Fallstudie eine Analyse der Effizienz des Ansatzes zur Modellierung der Gleitreibung und des Verschleißverhaltens von Polymer-Verbundwerkstoffen durch die Verwendung von neu gemessenen Datensätzen an

Verbundwerkstoffen auf Polyphenylensulfidbasis (PPS) durchgeführt. Die Werkstoffe wurden mittels Doppelschneckenextrusionsverfahren hergestellt und durch Spritzgießverfahren weiterverarbeitet. Der experimentelle Datensatz wurde aus Stift-Scheibe Versuchen unter Trockenlaufbedingungen bei Anwendung unterschiedlicher Belastungskollektive generiert. Zu Beginn wurden die synergetischen Effekte zwischen konventionelle Verstärkung und Partikelfüllstoffen analysiert, wobei die einzelnen Schwerpunkte auf Titandioxid (TiO_2) Submikropartikeln (300 nm Durchschnittsdurchmesser) und kurzen Kohlenstofffasern lagen. Danach wurde die Mitwirkung von den Schmierstoffen Graphit und Polytetrafluorethylen (PTFE) bei diesen mehrphasigen Werkstoffen untersucht. Als Lernregel diente der konjugierten Gradientenabstieg (CGB) Algorithmus sowie das GDX Trainingsverfahren. Auch der Einfluss der Versuchsparameter (Flächenpressung (p) und Gleitgeschwindigkeit (v)) wurde betrachtet. Werkstofflich ergab die Einarbeitung kurzer Kohlenstofffasern und Titandioxid Submikropartikeln eine signifikante Verbesserung in der Verschleißfestigkeit der PPS-Tribowerkstoffe im unteren bis mittleren pv-Bereich. Die mechanischen Eigenschaften und Oberflächencharakterisierung nach dem Verschleißtest ließen erkennen, dass diese positive Wirkung auf die tribologischen Eigenschaften mit den folgenden Phänomenen erklärt werden konnte: (i) verbesserte mechanische Eigenschaften mit den Kohlenstofffasern, (ii) erfolgreicher Schutz der Kohlenstofffasern durch die Titandioxid-Submikropartikel mit einer Verminderung des Faserbruches und der Faserherauslösung, (iii) selbstreparierende Effekte mit den Submikropartikeln, (iv) Entstehung quasi-sphärischer Verschleißpartikel, die zum Teil frei in der Kontaktoberfläche (Grenzschicht) abrollen können. Dennoch wiesen diese hybriden Werkstoffsysteme ein Stick-Slip-Verhalten im höheren pv-Bereich auf. Das gefürchtete Stick-Slip-Verhalten konnte wirksam beseitigt werden durch zusätzliche Einarbeitung von Festschmierstoffen (Graphit und PTFE), welche als Reservoir dienen, analog zu den Schmierstoffen in realen Kugellagern. Ebenso haben die Festschmierstoffe die Verschleißfestigkeit des mehrphasigen Systems PPS/SCF/TiO_2 im höheren pv-Bereich ($\geq$ 9 MPa·m/s) verbessert. Allerdings war ihre positive Wirkung, insbesondere die von Graphit, beschränkt auf bestimmte Volumenanteile und Lastbedingungen. Die bestmöglichen Ergebnisse wurden durch die Kombination von relativ geringen Mengen an Graphit und PTFE ($\approx$ 5 vol.% von jedem Zusatzstoff) erzielt. Die Einführung von weicheren Submikropartikeln brachte nicht den gewünschten Kugellager-

Effekt und den Faserschutz. Die vorhergesagten Eigenschaftsprofile durch das neuronale Netzwerk zeigten eine sehr gute beziehungsweise perfekte Übereinstimmung mit den experimentell gemessenen Ergebnissen und bewiesen, dass die Zielsetzung, ein gut trainiertes Netzwerk zu generieren, gelungen ist. Die Ergebnisse mit dem Validierungsdatensatz wiesen darauf hin, dass das trainierte neuronale Netzwerk eine ausreichende Generalisierungsfähigkeit erworben hatte und in der Lage ist, die richtigen Ausgabewerte für die nicht im Trainingssatz enthaltenen Eingabedaten zu liefern. Ein Optimal Brain Surgeon (OBS) Verfahren wurde eingesetzt, um unnötige Verbindungsgewichte und Schwellenwert, die keine Relevanz auf das Ergebnis haben, zu eliminieren. Nachher wurde überprüft, ob der Pruning Algorithmus OBS für die untersuchte Aufgabenstellung bessere Ergebnisse bezüglich Generalisierung als das ebenfalls untersuchte, voll vernetzte neuronale Netzwerk aufwies. Trotz Zugewinn an Genauigkeit mit der signifikant reduzierten Netzwerkstopologie war dieses Verfahren äußerst rechenintensiv, da eine Datenkodierung im obligatorischen Format erforderlich war. Innerhalb einer Wichtigkeitsanalyse wurde die Abhängigkeit der Netzwerk-Ausgangsgröße (Reibungskoeffizient oder spezifische Verschleißrate) von charakteristischen, mechanischen und thermomechanischen Eingangsgrößen untersucht. Zielsetzung war es die Ableitung möglicher Schlüsse aus dem ANN-Ansatz, die zum Verständnis der Mechanismen des Verschleißvorganges bei diesen Werkstoffen beitragen können, zu ermitteln. Schließlich wurde gezeigt, dass erfolgreich trainierte neuronale Netzwerke für eine Visualisierung des Einflusses gewisser Füllstoffe oder Prüfbedingungen auf die Verschleißeigenschaften angesetzt werden könnten. Dadurch könnten solche Netzwerke ein hilfreiches und nützliches Instrument für die Entwicklungsingenieure und Werkstoff-Experten sein, um neue Materialien zu erforschen und begründete Entscheidungen zur Auswahl und Umtausch von Werkstoffen schon in einer sehr frühen Entwicklungsphase zu treffen, um dadurch die Kosten so gering wie möglich zu halten.

List of Abbreviations and Symbols

Abbreviations	
AF	Aramid fiber
AFM	Atomic force microscope
Ag_2S	Silver sulfide
Al_2O_3	Aluminium oxide (alumina)
ANN	Artificial neural network
APS	Average particle size
Au	Gold
BFG	BFGS quasi-Newton algorithm
BP	Backpropagation
C	Carbon
CaO	Calcium oxide
CaS	Calcium sulfide
$CaSiO_3$	Wollastonite (calcium inosilicate mineral)
CF	Carbon fiber
CGB	Conjugate gradient with Powell/Beale restarts algorithm
COD	Coefficient of determination
CPU	Central processing unit
Cr	Chromium
CuF_2	Copper fluoride
CuO	Copper oxide
CuS	Copper sulfide
DAP	Diallyl-phthalate
dia.	diameter
DMTA	Dynamic Mechanical Thermal Analysis
DS	Dataset
DWCNT	Double-walled carbon nanotubes
EDX	Energy dispersive X-ray spectroscopy

et al.	and others
etc.	and the rest
Fe	Iron
FeO	Iron (II) oxide, ferrous oxide
Fe_3O_4	Iron (II,III) oxide, ferrous-ferric oxide, magnetite
FeS	Iron (II) sulfide, ferrous sulfide
$FeSO_4$	Iron (II) sulfate, ferrous sulfate
$Fe_2(SO_4)_3$	Iron (III) sulfate, ferric sulfate
FPE	Final prediction error
GDM	Gradient descent algorithm with momentum
GDX	Variable learning rate backpropagation algorithm
Gr	Graphite
GUI	Graphical user interface
HDPE	High density polyethylene
LM	Levenberg-Marquardt algorithm
long.	longitudinal
MAE	Mean absolute error
MFD	Melt flow direction
MoS_2	Molybdenum disulfide
MRA	Multiple regression analysis
MRE	Mean relative error
MWCNT	Multi-walled carbon nanotubes
NiS	Nickel sulfide
No.	Number
O	Oxygen
OBS	Optimal brain surgeon
PA	Polyamide
PAI	Polyamide-imide
PAr	Polyarylate
Pb	Lead
PbO_3	Lead oxide
Pb_3O_4	Trilead tetroxide
PbS	Lead sulfide

PbSe	Lead selenide
PbTe	Lead telluride
PC	Personal computer
Pd	Paladium
PE	Polyethylene
PEI	Polyetherimide
PEEK	Polyetheretherketone
PI	Polyimide
PMIA	Poly(m-phenylene isophalamide)
PMMA	Polymethyl methacrylate
P-o-D	Pin-on-Disc
POM	Polyoxymethylene
PPS	Polyphenylene sulphide
PPESK	Poly(phthalazinone ether sulfone ketone)
PS	Polystyrene
PTFE	Polytetrafluoroethylene
PUR	Polyurethane
PVC	Polyvinylchloride
RMSE	Root mean squared error
S	Sulphur
SCF	Short carbon fiber
SCG	Scaled conjugate gradient algorithm
SEM	Scanning electron microscope
SFRP	Short fiber-reinforced polymer
SFR-PA	Short fiber-reinforced polyamide
SGF	Short glass fiber
SiC	Silicon carbide
Si_3N_4	Silicon nitride
SiO_2	Silicon dioxide
SNNS	Stuttgart neural network simulator
SnS	Tin sulfide
SSA	Specific surface area
St.Dev	Standard deviation

SWCNT	Single-walled carbon nanotube
Ti	Titanium
TiO_2	Titanium dioxide
UD	Unidirectional
UFD	Ultrafine diamond
UHMWPE	Ultra high molecular weight polyethylene
vs.	versus
WC	Tungsten carbide
WS_2	Tungsten disulfide
XPS	X-ray photoelectron spectroscopy
Zn	Zinc
ZnF_2	Zinc fluoride
ZnO	Zinc oxide
ZnS	Zinc sulfide
ZrO_2	Zirconia
3D	Three-dimensional

Symbols

a_{cN}	[kJ/m^2]	Notch Charpy impact strength
B		Coefficient of determination
d_i		Desired output value
E_c	[MPa]	Compression modulus of elasticity
E_t	[MPa]	Tensile modulus of elasticity
E’	[MPa]	Storage modulus
E'_{Tg}	[MPa]	Value of storage modulus at glass transition temperature
E’’	[MPa]	Loss modulus
f()		Function
f’()		Derivative of function f()
F_F	[N]	Friction force
F_N	[N]	Normal load

k*	[mm^3/Nm]	Wear factor
k_0*	[mm^3/Nm]	Basic wear factor
n		Number of data (total number of entries)
N_h		Number of neurons in the (last) hidden layer
N_{in}		Number of neurons in the input layer
N_{out}		Number of neurons in the output layer
o		Average predicted output value by ANN
o_i		Predicted output value i by ANN
p	[MPa]	Normal contact pressure
R_a	[μm]	Average surface roughness
t	[s]	Testing time
t_k		Output target pattern k
T	[°C]	Temperature
T_g	[°C]	Glass transition temperature
$T_g^{E''}$	[°C]	Glass transition temperature determined from the peak of loss modulus (peak temperature of the loss modulus peak)
T_g^{onset}	[°C]	Glass transition temperature determined according to 2% offset-method
v	[m/s]	Sliding speed
v_{0j}		Bias on hidden unit j
v_{ij}		Weight from input unit i to hidden unit j
w_{0k}		Bias on output unit k
w_{jk}		Weight from hidden unit j to output unit k
w_s	[mm^3/Nm]	Specific wear rate
w_t	[nm/s] or [μm/h]	Time-related depth wear rate
x_i		Input (output) signal i
X_i		Input unit i
y_in_k		Net input to output unit k
y_k		Output signal (activation) of output unit k
Y_k		Output unit k
z_in_j		Net input to hidden unit j

z_j		Output signal (activation) of hidden unit j
Z_j		Hidden unit j
α		Learning rate
δ_in_j		Sum of delta inputs
δ_j		Portion of error correction weight adjustment that is due to backpropagation of error information from the output layer to the hidden unit j
δ_k		Portion of error correction weight adjustment that is due to an error at output unit k; also, the information about the error at output unit k that is propagated back to the hidden units that feed into output unit k
tanδ		Mechanical loss factor
$\tan\delta_{max}$		Maximum value of mechanical loss factor
$\tan\delta_{Tg}$		Value of mechanical loss factor at glass transition temperature
ΔG	[kJ/mol]	Gibbs free energy change
Δh	[nm]	Reduction in specimen height
Δm	[mg]	Mass loss of specimen
Δv_{0j}		Bias correction term used to update v_{0j}
Δv_{ij}		Weight correction term used to update v_{ij}
Δw_{0k}		Bias correction term used to update w_{0k}
Δw_{jk}		Weight correction term used to update w_{jk}
ε_M^c		Compression strain at compressive strength
ε_M^t		Tensile strain at tensile strength
η		Momentum term
μ, μ		Coefficient of friction, frictional coefficient
ρ	[g/cm^3]	Density
σ_M^c	[MPa]	Compressive strength
σ_M^t	[MPa]	Tensile strength

1 Introduction

Friction and wear initiate from multiple sets of complex interactions on a microscopic scale between surfaces that are in mechanical contact and slide against each other. These interactions depend on a complicated balance between materials, geometrical and topological characteristics of the surfaces and overall conditions under which the surfaces are made to slide against each other, e.g. loading, temperature, atmosphere, type of contact etc. [1]. Consequently, friction and wear are not inherent material properties, but unique features of the tribological system in which they are measured. The science and technology that focuses on friction, wear and lubrication of interacting surfaces in relative motion is referred to as tribology [1-3].

Friction is defined as the resistance to the sliding of one solid body over or along another. The magnitude or level of friction is expressed in terms of the coefficient of friction, in the following referred to as the frictional coefficient, which is the force needed to create sliding (friction force) divided by the applied normal load [4]:

$$\mu = \frac{F_F}{F_N} \tag{1.1}$$

In accordance to DIN 50 320, wear is the progressive removal of material in sliding or rolling contact against a counterface. Several fundamental wear modes are distinguished: adhesive wear, abrasive wear, wear caused by fatigue, and corrosive wear [1, 5]. Adhesive wear is initiated by the interfacial adhesive junctions that form if solid materials are in contact on an atomic scale. Abrasive wear may be described as damage to a surface by a harder material, mainly in form of sharp asperities. It is also sometimes referred to as scratching, scoring, or gouging depending on the degree of severity. Both adhesive and abrasive wear modes are generated under plastic contact. Fatigue wear refers to wear generated after repeated cycles, as it occurs often under rolling contact conditions. Corrosive wear is a general term relating to any form of material removal caused by a chemical or corrosive process. Fatigue wear and corrosive wear can be generated in both plastic and elastic contacts. The material removal in adhesive, abrasive, or fatigue wear mode is related to deformation and fracture in the contact region produced by mechanically induced strains and stresses. For that reason, this type of wear is described as mechanical wear. The material

removal in corrosive wear is governed by the development of chemical reaction film, where chemical reactions are triggered and accelerated by frictional deformation, frictional heating, micro-fracture, and successive elimination of reaction products. This mode of wear is generally described as tribochemical wear. In practical situations, several wear modes act simultaneously and the predominating wear mode may change from one to another depending on resultant changes in surface material properties and dynamic surfaces responses due to frictional heating, formation of transfer film, etc. [1, 3, 5, 6].

Sliding wear does not specify any wear mechanisms, but refers to the types of contact between two surfaces in relative motion. Nevertheless, wear in sliding contact is generally of great interest because of its common occurrence in many machine elements such as automotive under the hood parts, bearings and gears [1, 3, 7]. In practice, numerous geometrical test configurations for sliding wear evaluation have been developed (Fig. 1.1).

(a) (b)

Figure 1.1: Schematic illustrations of common sliding wear test configurations (a) block-on-ring, (b) pin-on-disc

Model tests based on block-on-ring (ASTM G77) [8] or pin-on-disc (ASTM G99) [9] are examples of American standards used most frequently. These tests allow material ranking and evaluation of the volume loss. From the volume loss, system properties can subsequently be evaluated based on the following equations [10]:

- Specific wear rate, w_s

$$w_s = \frac{\Delta m}{\rho \cdot v \cdot t \cdot F_N} \qquad [mm^3/Nm] \qquad (1.2)$$

- Depth wear rate (time-dependent wear rate), w_t

$$w_t = \frac{\Delta h}{t} \qquad [\mu m/h] \qquad (1.3)$$

in which the individual quantities have the following meanings: Δm is the mass loss, ρ is the density of the material being tested, v is the sliding speed, t is the testing time, F_N is the normal force applied on the specimen during sliding and Δh is the reduction in specimen height.

The individual wear rates can be interrelated as follows:

$$w_t = w_s \cdot (p \cdot v) \qquad (1.4)$$

The specific wear rate is equal to the so-called wear factor k*, which is often given in specialized literature for choosing materials for friction and wear applications. As long as w_s is independent of the operating parameters, there exists a linear relationship between w_t and the pv-product. Under these conditions, w_s is considered as a material property (dependent on the dominating wear mechanisms). If the latter remain the same over a certain pv-range, w_s can be designated as k_0*, the so-called basic wear factor. Above a certain pv-range the wear factor of the material is no longer a material property only, but increases with the operating parameters until an upper limit is surpassed beyond which severe wear occurs [10-12].

The pv-factor or load-carrying capacity is frequently used as basic performance criterion for characterizing bearing materials. In practice it may be represented in two different ways: (i) the pv-factor for permanent function at a given specific wear rate; (ii) the “limiting pv” above which a rapid increase in wear appears [12, 13].

To understand the complicated, detrimental process known as wear, to predict the wear rate and to minimize it, still remains one of the most complicated problems facing the engineers today [14]. To assess accurately the performance of a given material or a new compound under a broad range of operating conditions using a relatively small experimental dataset constitutes a quite attractive, cost-effective solution, taking into account that there are only few practical mathematics- or physics-based solutions. For that reason, the artificial neural network (ANN) technique has found many successful applications in modeling the relationship between wear and diverse influential factors, as reviewed by Zhang and Friedrich [15]. The principle benefit of neural network modeling compared to other approaches is in its capability for accu-

rate predictions when significant non-linearity and hysteresis are present simultaneously. The latter is not easy to attain with conventional curve fits. Furthermore, neural networks will readily handle irregular or random inputs [16]. Accordingly, an ANN approach seems to have good potential to save time and cut expenses in solving various friction and wear problems.

Polymers and polymer composites are presently viewed as key tribological materials because of their self-lubricating properties, exceptional corrosion resistance, high chemical stability, high compliance, high capacity for damping vibrations or for shock resistance, low noise emission, light weight, and low cost. In the usual case, unfilled or neat polymers are not appropriate due to intrinsic limitations (e.g. poor thermal conductivity, low load carrying capacity). Wear additives with enhanced thermal transfer as well as mechanical performance can compensate for this and provide an optimum balance of mechanical, self-lubricating, wear resistant, and operating temperature properties [11, 17-19]. Short fibers (glass, aramid or carbon) are regarded as classical tribo-reinforcements used to enhance properties such as stiffness, strength, impact resistance, and thermal conductivity yielding improved load carrying capacity accordingly [20, 21]. Due to their layered structure, solid lubricants, (e.g. graphite, PTFE, and molybdenum disulfide), assist in the formation of a thin, coherent transfer film on the counterface; this is one of the essential prerequisites for reducing friction and facilitating sliding [19, 22]. More recently nano-scale inorganic particles proved to be effective in improving both wear resistance and mechanical behavior of the neat matrix material [23-29]. In terms of the aforementioned, the major goals in designing wear resistant materials are enhancement of the “limiting pv” factor and reduction of the basic wear factor. These goals can successfully be accomplished with the appropriate combination of diverse fiber reinforcements, fillers and lubricants in a polymer matrix.

2 State-of-the-Art

2.1 Designing Wear Resistant Polymer Composites

2.1.1 Effect of Short Fibers and Internal Lubricants

2.1.1.1 Short Fibers

The bulk properties of pristine polymer can be changed remarkably by the addition of a short fiber reinforcement. The classical benefits of such reinforcement in polymer composites may be an improvement in: (i) mechanical properties such as compressive strength, impact strength, creep resistance, load-carrying capacity, (ii) coefficient of thermal expansion along with thermal conductivity, (iii) frictional coefficient, wear rate as well as life endurance. Furthermore, these fillers are uncomplicated to handle with respect to standard manufacturing techniques. Table 2.1 summarizes information on the physical properties of fibers commonly used for polymer reinforcement.

Table 2.1: Selected properties of common fibers used in polymer composites [30]

Fiber type	**Tensile strength [GPa]**	**Tensile modulus [GPa]**	**Density [g/cm^3]**	**Diameter [μm]**
Aramid	3.6-3.8	60-180	1.44-1.47	12
Carbon	2.1-7.1	230-830	1.70-2.18	5-10
Glass	3.5*	72	2.54	10-20

**Virgin strength values. Actual strength values prior to incorporation into composite are about 2.1 GPa.*

Short glass fibers (SGFs) are preferred common reinforcing agents owing to their low cost. Still, these are abrasive in nature, which results in increase in the frictional coefficient of polymer composites. As a rule, the reinforcement with glass fibers yields approximately 10 to 100 times higher abrasiveness when compared to short carbon fibers. By the incorporation of mineral and lubricating graphite the wear properties of glass fiber reinforced material can be enhanced to an intermediate level between those of neat glass and neat carbon fiber reinforcement [19, 31]. In general, the improved wear resistance of short glass fiber reinforced polymer systems is coupled to the increased rigidity and high modulus of fibers embedded in the polymer matrix [32-34]. Under sliding wear conditions the glass fibers are depleted layer by layer and

small abrasive fiber particles are only detaching from the fiber ends. The wear process is a combination of adhesive and abrasive modes. Depending on the corresponding matrix material as well as testing conditions the proportions of these two wear modes might alter [35, 36].

Of all three types of fiber reinforcement, short carbon fibers (SCFs) are regarded as fundamental filler in improving wear resistance of polymers. Compared to glass fibers, carbon fibers perform better, owing to their excellent mechanical properties and less abrasive nature [3, 11, 12, 20, 33, 37]. Moreover, in the process of sliding SCFs form a smooth carbon film on the counterface and increase thermal conductivity, as well as resistance to heat distortion of the polymer matrix [38]. Carbon fibers are derived either from polyacrilonitrile (PAN) or a special petroleum pitch. The PAN-derived fibers are generally referred to as high strength fibers, while pitch-based fibers are identified as high modulus fibers, which make them appealing for stiffness-decisive applications [19, 39]. Because of their low price, the pitch-based carbon fibers could be an alternative to PAN-carbon fibers for certain tribological applications [40]. Typical wear scenario with carbon fibers embedded into polymer matrix includes fiber thinning, break-down and interfacial removal [12, 27, 38, 41].

Table 2.2: Selected properties of commercial carbon fibers [19, 39]

Physical property	**PAN**	**Pitch**
Shape and size	Round, 7μm dia.	Round, 10 μm dia.
Density [kg/m^3]	1770	1990
Tensile strength [GPa]	3.65-4.28	1.38-3.10
Modulus of elasticity [GPa]	230-241	159-931
Elongation at failure at 25°C [%]	1.4	0.5
Coefficient of thermal expansion [·10^{-6}/°C]	-0.54 (long.)	-1.30 (long.)

Aramid fibers (AFs) are industrial fibers made of organic material. In contrast to glass and carbon fibers, aramid fibers are rather soft and flexible. This kind of fiber possesses almost 100% paracrystalline structure and a very high degree of orientation of fibrils along the fiber axis [42, 43]. Besides high strength, AFs possess a very good damage tolerance, impact resistance and vibration-damping characteristics, as well as lack of notch sensitivity. In the last few years short forms of aramid fibers have found important applications in wear parts such as clutches, brakes, thermosetting

bulk molding compounds [44]. The advantage of aramid fibers over the other fiber types is that they cause minimal wear to counterpart materials [45]. Still, low stability at high temperatures combined with moisture absorption behavior can sometimes be a problem with AFs in the field of tribology [40, 46]. Moreover, due to their high crystallinity the surface of AFs is chemically inert and smooth which leads to poor fiber/ matrix adhesion. Therefore, surface modification is crucial to improve their reinforcing effect [47, 48]. Additionally, these fibers exhibit poor properties in compression and suffer from rapid decrease in mechanical properties at temperatures above 200°C [49].

A comparison of the reinforcing function of diverse short fibers was done by Song and Ehrenstein [31] in polyamide 66 (PA 66), Lhymn and Bozolla [50] in PPS, Chen et al. [51] in high performance polyimide (PI), Davim and Cardoso [52] as well as Friedrich and coworkers [53] in polyetheretherketone (PEEK). In all these studies the friction and wear reduction was the strongest with short carbon fibers. The latter was attributed to the good thermal conductivity of the carbon fibers [50]. Likewise, it was demonstrated that in the process of dry sliding against a metal counterpart, the short glass fibers are easily abraded and prone to breakage. The broken fibers transfer to the interface and increase the surface roughness of the counterpart, thus leading to higher wear. With the short carbon fibers only slight microcracking and spalling could be observed [51].

A key factor in designing composites for specific application is the fiber loading fraction as it governs the mechanical and thermo-mechanical responses of these materials. In the process of optimizing the wear performance of polymer composites, several authors [12, 27, 33, 54-56] recognized the role of fiber content. Based on these works it can be concluded that a favorable friction and wear behavior can be achieved with carbon fiber content of 10-20 vol.%. A content higher than 20 vol.%, especially in the upper pv-range, can lead to stick-slip sliding motion. Likewise, for short glass fibers it was shown that the wear resistance decreases with a higher fiber loading fraction. Nevertheless, the frictional coefficient was found to be independent of the glass fiber volume content. However, results to the contrary were reported by Suresha [57].

Another important factor concerning reinforcement with short fibers involves the quality of the fiber/matrix interface along with fiber orientation. Strong fiber/matrix interfacial bonding helps keep the broken fiber pieces within the composite surface, thus preventing early formation of third body abrasives and enhanced wear. In this respect, different techniques can be applied to improve the adhesion between fiber and matrix [58]. Voss and Friedrich [59] demonstrated for short fiber reinforced PEEK composites a marked variation of the wear rate with the fiber orientation. The analysis of the corresponding wear mechanisms disclosed reduced fiber breakage and pulverization for fibers in the normal direction leading to lower wear rates compared to the parallel or anti-parallel fiber orientation. Consequently, scientists and engineers working with fiber-reinforced composites should consider all these aspects when designing a material for a specific service.

2.1.1.2 Internal Lubricants

In general it has been recognized that in metal-polymer sliding systems the formation of a thin, uniform, coherent transfer film is a must for reducing the specific wear rate. This transfer film prevents direct contact between the soft polymer surface and the much harder metal counterface leading to reduced abrasive action and improved wear resistance [60-66]. One of the mechanisms for facilitating transfer film development is the incorporation of internal lubricants such as polytetrafluoroethylene (PTFE), molybdenum disulfide (MoS_2) and graphite (Gr).

Among polymers, PTFE forms transfer film most readily [19]. PTFE is a unique polymer in the development of composite materials since it may either be a matrix forming polymer or a solid phase lubricant. It is chemically inert and does not absorb water leading to excellent dimensional stability [67, 68]. In the process of sliding the molecules of PTFE are stretching out parallel to the sliding direction. The symmetrical, non-polar configuration of the PTFE chains is responsible for weak intermolecular bonding. Once an oriented layer is built-up, slippage in this layer becomes very easy. The end result is a low frictional coefficient [19, 63, 69]. This effect is used to improve the frictional properties of other materials by lubricating them internally with PTFE. The filler is adherent, cannot be worn out easily and prevents stick-slip motion instabilities [63, 70]. Nevertheless, it should be considered that the use of PTFE in high-temperature applications is limited to an operation temperature of 250°C [33].

The positive contribution of PTFE in diminishing wear has already been established in diverse polymers e.g. PEEK [33], poly(m-phenylene isophalamide) (PMIA) [71], PPS, polyvinylchloride (PVC), polyarylate (PAr), polyoxymethylene (POM), polyimide (PI) and diallyl-phthalate (DAP) [72]. Concerning the optimum loading fraction, under standard pv-conditions Friedrich and coworkers [33] established for PEEK systems that the best wear resistance (i.e. the lowest wear rate) could be achieved with a PTFE content in the range of 5-10 vol.%. Still, for the frictional coefficient the lowest value was obtained at 10 to 20 vol.%. Beyond 20 vol.% the frictional coefficient increases, which is attributed to changes in microstructure. From the viewpoint of achieving both low friction and wear, the best loading fraction was found to be 15 vol.% PTFE. Different results were reported at lower pv-products, where the lowest wear rate was measured at 20 vol.% PTFE (both load and speed were varied during testing) [71].

The key to graphite as a lubricant is its layered-lattice structure and its ability to form strong chemical bonds with gases from the environment. The latter weakens the interlayer bonding forces and accordingly yields easy shear and transfer of crystallite platelets to the mating surface. For that reason graphite is very often used as filler with polymers run under lubrication or wet environment [73]. Additionally, graphite is an excellent thermal conductor [19, 74]. This property is particularly important in tribo-contacts, where frictional heat generated at the interface must be effectively dissipated.

A comparison of the lubricating function of PTFE and graphite in epoxy nanocomposites and poly(phthalazinone ether sulfone ketone) (PPESK) composites was provided by Chang [27] and Zhang et al. [75], respectively. For the epoxy matrix composite with PTFE the lowest peak value of the frictional coefficient and the shortest duration of the running-in stage were observed. However, graphite contributed to both lower stable frictional coefficient and average wear rate, mostly under high pressures [27]. Similar results were also observed with the incorporation of PTFE and graphite into PPESK matrix. Moreover, the transfer film of PTFE-filled PPESK was more compact and smoother than that of graphite-filled PPESK. The latter was attributed to the fact that PTFE wear debris deform more easily in the process of sliding than those of graphite [75].

The layer-lattice structure of MoS_2 is similar to that of graphite. Still, in the case of MoS_2 the “important layers “constitute of the MoS_2 molecules and are three atom layers thick. Although these layers possess strong covalent bonding within them, the bonding between them is of the weak van der Waals nature (for comparison in graphite the bonding between the layers is attributed to comparatively large Coulombic attractions). This great difference in the strength of the bindings causes easy slip parallel to the basal plane of the crystal lamellae and consequently very low sliding friction [67, 76]. Apart from its low friction properties, the other beneficial feature of MoS_2, important in lubrication, is its high load carrying capacity. Studies on the effect of MoS_2 incorporation into different polymers are summarized in [67]. MoS_2 is reported to decrease the wear rate of PTFE, PA 66, PI, polyamide-imide (PAI). It is recommended that the volume fraction of MoS_2 in polymer matrices generally should not exceed 30 vol.%, unless the material is designated to supply transfer lubrication. A negative outcome with MoS_2 was established by Yu et al. [77] and Wang et al. [78] for PPS and PA 1010, respectively. It was demonstrated that while graphite and PTFE contributed to an increase in wear resistance of PPS, MoS_2 exerted adverse effects. These adverse effects were related to poor mechanical properties and a tendency of the filler to segregate and extrude out of the matrix in the process of sliding. Yet, it should be taken into account that for both studies the lubricant concentration was comparatively high (≥ 10 vol.%). It has already been stated in the literature that with some polymers at concentrations of 10 vol.% or more MoS_2 can significantly reduce the structural strength of a composite [67].

2.1.1.3 Combining Short Fibers and Internal Lubricants

The effects on the tribological performance of polymer composites when incorporating both short fibers and internal lubricants were studied in numerous publications [11, 36, 78-86]. The improved wear resistance and low frictional coefficient with these multiphase materials was attributed to the load-supporting effect of the fibers combined with the effective transfer film formation by the lubricants. An extensive summary on the present topic was given by Lu [87] for composite materials that were tested at both room and elevated temperatures. This study revealed that with such systems high load bearing capacities can be realized also at higher temperatures

(220°C), which opens new opportunities for their usage in industrial sectors like the chemical process industry and transportation sector.

Until recently the low temperature technology has been applied to space applications, superconductivity or medical diagnostics. However, new applications such as hydrogen technologies for environmentally friendly energy supply and transportation are on the way to win interest [88]. Therefore, it is important to search for adequate system design that can meet the requirements of these new applications. Klein [89] summarized the research done on different PTFE/PEEK/CF systems in a cryogenic environment (-196°C). It was established that whereas at room temperature, factors such as filler volume fraction dominate the wear behavior of the composites, in the low temperature range the properties of the matrix and not those of the filler play the key role.

2.1.2 Effect of Particulate Fillers

2.1.2.1 From Micro- to Sub-micro- and Nano- Level

Composites reinforced with various micron-sized particles belong to the most widely used composites in everyday materials. Such materials offer low cost and ease of fabrication. Usually, they are added to increase the matrix elastic modulus and yield strength [90, 91]. The tribological behavior of polymers filled with inorganic microfillers (e.g. CuO, CuS, PbO_3, CuF_2, PbS, Ag_2S) was extensively studied in the past. Bahadur and coworkers [92-97] showed that certain fillers like CuO, CuS, CuF_2, Pb_3O_4, CaS, CaO and Ag_2S were beneficial for the wear resistance of neat PEEK and/or PA. At the same time other fillers like sulfides and fluorides of Zn and Pb brought adverse effects [96]. The wear resistance of PPS was improved by microparticles such as Ag_2S, NiS, CuS and CuO and deteriorated with PbTe, PbSe, ZnF_2, CaF_2 and SnS [60, 61, 64, 98]. The mechanism of wear reduction with such microfillers was explained in terms of chemical reaction between the filler and metal counterface, leading to enhanced adhesion of the transfer film along with mechanical interlocking of the transfer film into the crevices of the counterface asperities [61, 63, 98, 99]. Further, the deformability of the particles might also contribute to better wear resistance [64].

When working with micro-scale particles it must be taken into account that the mechanical behavior of the filler tends to follow the one of the bulk filler material. Likewise, the particle angularity plays a decisive role for such compounds. In this respect, rigid fillers are not suitable due to unwanted abrasive effects [62]. Therefore, it is expected that the smaller the particle size, the more efficient their reinforcing role should be, which is also experimentally confirmed [100]. By scaling the particle size down to a nanometer range the influence from particle's angularity greatly shrinks. Nanoparticles possess a large surface-to-volume ratio and are referred to as being "interface-dominated" materials [101]. The latter increases the possibility of enhanced bonding between the filler and the surrounding, and would produce a stronger transfer film [65, 102]. It is well-recognized in the community that the formation of transfer film in polymer tribology is of essential character owing to its direct effect on the wear rate [102, 103]. Material removal would be restricted because of the smaller particle size, being of the same order as the segments of the surrounding polymer chains (severe abrasion would be replaced by mild abrasive wear) [102, 104]. Moreover, the high thermal conductivity of ceramic nanoparticles might increase the thermal conductivity of the composite leading to less heat development in the contact area during sliding [28, 105]. In diverse studies the potential of this method for designing wear resistant materials has already been investigated and proved [106-112]. In the following subchapter the relationship between the sub-micro/nano-filler volume content and wear resistance of their composites will be more comprehensively analyzed.

2.1.2.2 Sub-micro/Nanoparticle Volume Fraction

Several observations were made so far concerning the influence of nanoparticle volume fraction on the tribo-performance of nanocomposites. Bahadur et al. [62, 66] studied the tribological behavior of PPS filled with different inorganic nanoparticles such as Al_2O_3, TiO_2, ZnO, CuO and SiC. The maximum filler loading in these studies was 10 vol.%. A decrease in the wear rate was observed with 2 vol.% Al_2O_3, TiO_2 and CuO. Increasing the filler content to 3 vol.% or more worsened the wear resistance of the composites when compared to that of unfilled PPS. The adverse behavior with higher filler loading was related to: (i) abrasion of the transfer film by the hard ceramic particles, (ii) weakening of the transfer film bonding aroused from the polishing effect of the agglomerated nanoparticles on the counterface [62]. Wang et al.

[106, 110, 113-116] recognized a similar tendency for PEEK reinforced with SiC, ZrO_2, Si_3N_4, and SiO_2. The incorporation of 0.5-4 vol.% nano-SiO_2 (13 nm) in PEEK [29] led to a strong improvement in the wear resistance yielding optimum results at 1 vol.% nano-SiO_2. The reduced shear deformation of PEEK combined with reduced tangential plastic flow of the surface layer involved in friction process are considered to play important roles in this case. Wetzel and coworkers [23, 24, 109], Sreekala and Eger [117] investigated the effect of different size inorganic particle reinforcement in epoxy. A gradual increase in the wear resistance as well as stiffness and impact strength of epoxy was observed with rising filler content until an optimum value of 4 vol.% was reached. Higher filler loadings led to properties deterioration [23]. The addition of small amounts of Al_2O_3 (13 nm) seemed also effective only at low filler content (1-2 vol.%) [24]. Similarly, the incorporation of approximately 2 wt.% (~ 1.3 vol.%) silica (20 nm) in PA 6 matrix resulted in a three fold reduction of frictional coefficient and 140-fold lower specific wear rate. The use of higher silica loadings was less successful [118]. In Fig. 2.1, reported wear rates for selected composites reinforced with sub-micro or nanoparticles are displayed as a function of filler volume fraction. The variation in the optimum filler content can be attributed to the particles size and dispersion state [29].

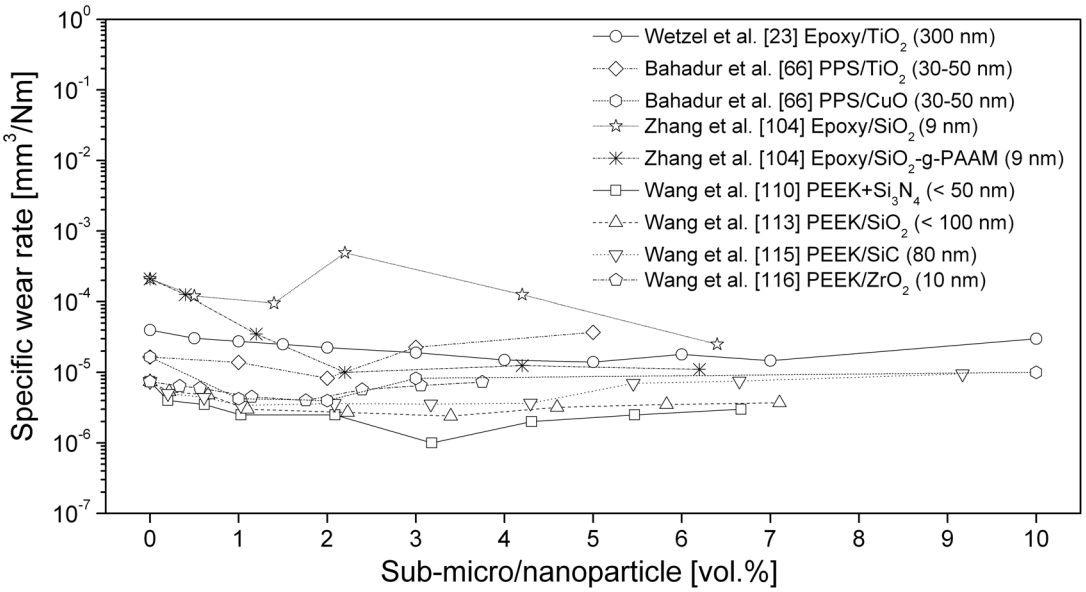

Figure 2.1: Dependence of the specific wear rate on sub-micro/nanoparticle content for selected polymer composites

In view of the aforementioned, it can be concluded that the optimum filler content for acquiring adequately good enhancement in friction and wear behavior with sub-micro/nanoparticles lies within the limits 1-5 vol.%, except for PTFE matrix, which case will be discussed in the next subchapter. A comparable tendency was formerly established by Friedrich, Zhang and coworkers [25, 26, 28].

2.1.2.3 Sub-micro/Nanoparticle Volume Fraction in PTFE

Contrary to other polymer matrices, the wear of PTFE reinforced by 20 vol.% TiO_2 (agglomeration of fine particles less than 300 nm in size) was much higher than that of PTFE incorporating ZrO_2 (ranging from several microns to about 50 μm) particles. This was explained in terms of the inability of small scale fillers to prevent large scale destruction of the PTFE banded structure [68]. Nevertheless, with the boom of nanotechnology in recent years few attempts were made to improve the wear behavior of PTFE by incorporating nano-ZnO (average particle size 50 nm) [119], nano-alumina (average particle size 40 nm) [120] or nano-attapulgite (fibrous clay mineral having length of 100-1000 nm and width 10-25 nm) as fillers [121]. The reported optimum nano-filler content was on the order of 15 vol.% or more for both sliding wear [119] and fretting wear [120] conditions. As already mentioned, this content was much higher when compared to other polymer matrices. Li et al. [119] suggested that in this case the uniformly distributed nanoparticles at the subsurface of PTFE prevent the destruction of the PTFE banded structure. Sawyer et al. [120] presumed that the higher volume fraction of nanoparticles provide a casing for the matrix material. This casing interrupts surface crack propagation and therefore keeps the virgin PTFE islands isolated so that damage in one region cannot easily spread into the other. However, it was the hypothesis of Gyurova and Schlarb [122] that with the higher nanoparticle volume fraction agglomerates build up. These agglomerates function similarly to microparticles and have a load-supporting function for the soft PTFE matrix. Recently, Burris et al. [123] incorporated irregularly shaped alumina (80 nm) and reported a 3000-fold improvement over unfilled PTFE at very low filler content of 1 wt% (~ 2.2 vol.%). The very much improved wear resistance was related to the irregular shape of the nano-filler. This allows sufficient mechanical entanglement with the matrix to take place and consequently facilitates filler accumulation at the sliding interface. Another interesting investigation was that of Lai et al. [124] who evaluated

the friction and wear properties of PTFE filled with ultrafine diamond (10 nm in diameter). Ultrafine diamond (UFD) possesses unique properties of nano-scale material combined with those of a diamond. The experimental results showed no significant change in the frictional coefficient, but orders of magnitude lower wear rate with increasing filler concentration when compared to neat PTFE. This effect was analyzed in terms of improved heat absorption capacity of the composite as well as the assistance in transfer film formation, and enhancement of the bonding between the transfer film and the counterpart. Finally, it was suggested that the UFD particles function as roller bearings in the frictional interface [124].

2.1.2.4 Surface Modification

It has already been recognized in the community that uniform dispersion of nanoparticles is essential prerequisite for improving their mechanical and tribological properties [125]. To realize this various both physical and chemical methods were employed in the praxis such as surface modification of nanoparticles using coupling agents, compatibilizers, grafting agents, etc. [102]. In a number of friction and wear studies [102, 104, 111, 126, 127] the effect of both surface treated and untreated nanoparticles dispersed in a polymer matrix was compared. An irradiation grafting method was applied, where nanoparticles surfaces are equally activated both outside and inside the agglomerates. Due to their low molecular weight nature, the monomers can enter into the agglomerated nanoparticles easily, fill the interstitial volume and react with the activated sites of the nanoparticles, accordingly helping in separating the agglomerated nanoparticles. Moreover, the surface of the nanoparticles will also become hydrocarbon due to an increased hydrophobicity resulting from the grafting polymer. This is beneficial for the filler/matrix miscibility and hence for the ultimate properties [102, 111]. The experimental results from dry sliding tests revealed that both the frictional coefficient and specific wear rate were lower than those of the neat matrix as well as nanocomposites filled with the unmodified fillers. These results were associated with the strong adhesion between the modified particles and the matrix leading to better resistance against the periodic friction stress and prevention of friction induced crack initiation, coalescence and propagation. Similarly, strengthening of the transfer film could be achieved through improved interaction of the grafted nanoparticles with the wear debris [111, 126, 127].

2.1.2.5 Counterface Surface Roughness

One additional aspect, relevant to the effect of sub-micro/nanoparticles incorporation in polymer matrices, involves the counterface surface roughness. In general, the surface roughness of the steel counterface correlates directly to the real average distance of two sliding surfaces [128] and plays an important role for the formation of a thin, uniform, transfer film as well as for wear reduction. An example of this effect was provided by Zhang et al. [41] and Bahadur et al. [62]. It has been shown that both, the wear rate and frictional coefficient of the composites increased strongly when sliding against the smoother counterface, having lower arithmetic average surface roughness (30 nm) than the particles average size (300 nm) [41]. For PPS filled with nano-scale alumina (33 nm) [62], the lowest wear rate was reached again when sliding against counterfaces having surface roughness higher than the nanoparticles average size (Fig. 2.2). In the opposite case (sliding against a counterface of smaller surface roughness than the particles size) patchy transfer film was formed, which could not cover the asperities completely. Therefore, nanoparticles could not position themselves in the counterface asperities and provide the required effective anchoring for the transfer film [35]. Another possible explanation for this behavior can be that in this case the very small nanoparticles do not act as individuals, but form agglomerates. These agglomerates must be of the same order as the counterpart surface roughness or even slightly higher, so that they act as spacers and reduce wear.

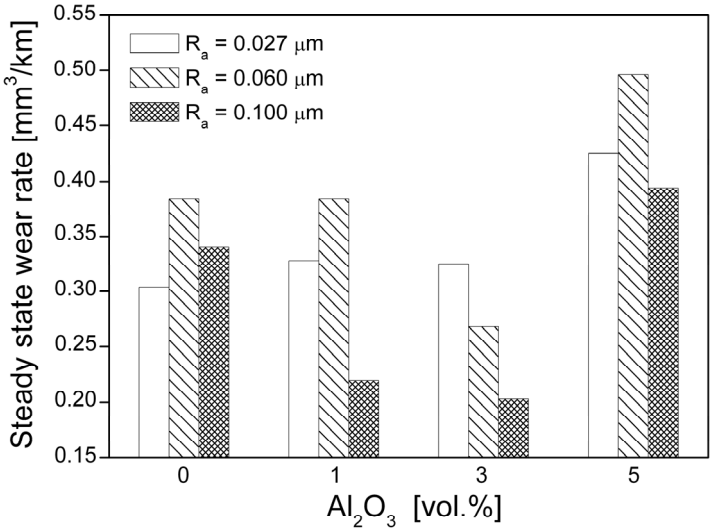

Figure 2.2: Dependence of the steady state wear rate of PPS filled with nano-scale alumina (33 nm average diameter) on the average counterface surface roughness R_a (adapted from [62])

2.1.3 Combinative Action of Traditional and Particulate Fillers

2.1.3.1 Traditional Fillers with Inorganic Microparticles

Wang et al. [78] considered the interaction between micron size MoS_2 and a short carbon fiber reinforcement in nylon 1010 (PA 1010) and reported a major reduction in both friction and wear. Palabiyik and Bahadur [129] studied the effect of mixing micro-CuO particles with PTFE and short glass fibers in blends of PA and high density polyethylene (HDPE). Bahadur and coworkers [130, 131] added particulate micro-sized CuS or CuO along with PTFE to carbon fiber and glass fabric reinforced PA. The incorporation of particulate filler alone did not lead to any improvement in the wear resistance of the composite. With the auxiliary integration of PTFE the desired synergistic effect was achieved. In this case the wear process was influenced by several factors such as preferential load support by the fibers, development of uniform transfer film on the counterface by the lubricant, back transfer of material from the counterface to the pin as well as decreased fiber breakage [131]. Friedrich and coworkers [132] added micro-$CaSiO_3$ to polyetherimide (PEI) filled additionally with both short carbon fibers and graphite. The gained enhancement in the tribological properties was attributed to the reinforcing effect of the microparticles. The incorporation of inorganic micro-sized CuS and PTFE [133] in a PEEK matrix proved also beneficial for the friction and wear properties of the composite. This was explained in terms of chemical reactions increasing the adhesion of the transfer film to the steel counterface.

2.1.3.2 Traditional Fillers with Inorganic Sub-micro/Nanoparticles

In the process of designing a composite the material properties are modified to achieve the desired performance profile over various length scales. The expansion of length scales from meters (finished woven composite parts), micrometers (fiber diameter), sub-micrometers (fiber/matrix interface) to nanometers opens great opportunities for novel approaches in processing, characterization and modeling of new generation of composite materials. There are two different reasons that distinguish the properties of nano-materials from other materials: from one side increased relative surface area and from the other quantum effects [134]. In the field of tribology more and more research activities are focused today on inorganic nanoparticles due to their special advantages: low price, high surface-to-volume ratio, reduced angular-

ity, strengthening of the transfer film, much milder material removal as compared to conventional composites (q.v. subchapter 2.1.2.1). Short carbon fibers are already recognized in the community as indispensable filler for improving the sliding wear resistance of polymers (q.v. subchapter 2.1.1.1). The concept of hybrid reinforcement with inorganic sub-micro/nanoparticles and short carbon fibers as well as internal lubricants was rigorously investigated in the last few years by Zhang and coworkers [25, 41, 80, 81, 132, 135-138]. For a series of epoxy-based composites [135] it was shown that an optimum (100-fold) reduction could be achieved with 5 vol.% TiO_2 (average size 300 nm), 15 vol.% SCF (average diameter 14.5 μm and average length 90 μm) and 15 vol.% graphite (average size 20 μm). The latter was the result of the superimposed wear-reducing mechanisms of the different phases in this multiphase system. Moreover, the incorporation of the particulate filler in epoxy already reinforced by traditional fillers could increase its wear resistance by a factor of two [27, 135]. Larsen et al. [139] established reduced friction and wear in epoxy through the addition of small amount of nano-CuO (up to 0.4 vol.%) and PTFE. Zhang and Schlarb [140] investigated the effect of low loading (1 vol.%) nano-SiO_2 particles (13 nm) on the tribological behavior of PEEK filled with SCF, PTFE and graphite. It was found that under low pressure (1 MPa) the nanoparticles played a negative role. Still, in the higher pressure range their incorporation led to better wear resistance. Two factors were assumed to interact simultaneously. On one side the increased stiffness of PEEK matrix by the nano-SiO_2 might reduce stress concentration on SCF and alleviate friction; on the other side the increased matrix stiffness might reduce the deformation of SCF in tension mode. Guo et al. [141] showed that the simultaneous addition of nano-SiO_2 (12 nm) and short pitch based carbon fibers in epoxy resin was beneficial for improving the tribological performance of the composite in terms of improved surface hardness, reduction of fiber pull-out and interfacial abrasion as well as rapid formation of uniform, stable transfer film. McCook et al. [142] blended nanoparticles of ZnO (53 nm) and PTFE in small loading fractions with epoxy and established lessening of both friction and wear. This effect was ascribed to the wear debris size, which is regulated by the control of particles dispersion. It has already been observed in experimental tribology that fine debris usually accompany lower wear rates, reduced friction and building of uniform transfer films. Su et al. [143] reported on the improvement of the tribo-performance of hybrid glass/PTFE fabric com-

posite by the inclusion of surface modified nano-ZnO (15-25 nm). The authors attributed this improvement to the achievement of good dispersion with the nano-ZnO, enhancement of the composite's structural integrity, formation of thin and uniform transfer film as well as three-body rolling effect of the nano-ZnO being incorporated in the wear debris. Xian et al. [144] also found that the combination of TiO_2 (300 nm) and graphite was beneficial for the wear performance of neat epoxy, due to the easy transfer film formation as well as reinforcing effect of the nanoparticles. In a more recent study Su et al. [145] showed that the addition of proper content of nano-TiO_2 (5-10 nm) might significantly augment the wear resistance and load-carrying capacity of hybrid glass/PTFE fabric composites as well as the friction reducing abilities of these composites, especially under high load.

Research activities were carried out to establish the optimum sub-micro/nano-filler volume fraction in these multiphase systems. The volume content of the other fillers was kept constant. The results showed that the most favorable volume fraction of the sub-micro/nano filler lies in the range 4-6 vol.% [27, 41, 135, 137]. The synergistic effect of such hybrid reinforcement with nano, sub-micro and micro-sized fillers was ascertained also in thermoplastic polymer matrices such as PA 66 and PEI [27,132, 137, 138].

Zhang and coworkers [25-28, 41, 135-138, 146-148] suggested a positive rolling effect of the sub-micro/nanoparticles at the sliding interface. This rolling mechanism causes lower frictional coefficient and shear stresses between the two mating surfaces, in particular at the edge of the fibers. Accordingly, fiber removal is greatly reduced and the fibers are protected against more severe wear, above all in the high pv-range. Still, one should bear in mind that the rolling mechanism is so far only hypothetical and further experimental investigations are required to verify it. A similar rolling hypothesis has already been reported in the community with ultrafine diamond in PTFE [124], with fullerene-like WS_2 [149-154], MoS_2 [155-157] as well as TiS_2 [158] nanoparticles.

Finally, it should be considered that adverse effects are also possible when combining nanoparticles with traditional reinforcing agents. These unfavorable effects might result from chemical reactions between the two reinforcing phases being detrimental to the transfer film formation [159].

2.1.4 Reinforcement with Carbon Nanotubes

Carbon nanotubes exist in the form of graphite sheets rolled into seamless tubes (i.e. tubes made of carbon with acicular single-crystal structure much like a tubular modification of fullerene). Two structural classes of carbon nanotubes can be synthesized (Fig. 2.3): single-walled carbon nanotubes (SWCNTs) and multi-walled carbon nanotubes (MWCNTs). There exist also double-walled carbon nanotubes (DWCNTs), which are a special case of MWCNTs with two concentric graphene layers.

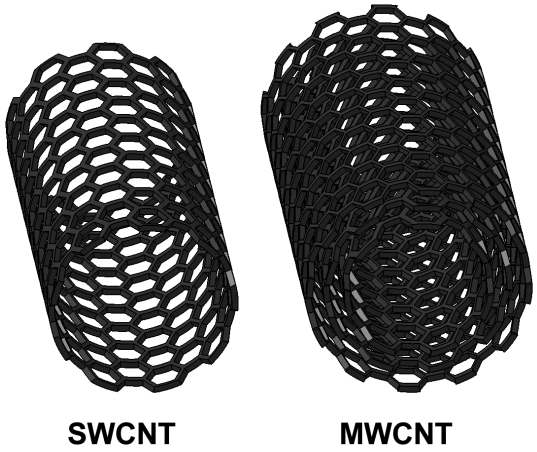

Figure 2.3: A schematic representation of carbon nanotube structural classes

Since their documented discovery in 1991 by Iijima, nanotubes have received much attention owing to their remarkable properties. Nanotubes are the stiffest known fibers with a measured Young's modulus in the TPa range and a tensile strength of 100-150 GPa [90, 134, 160-162]. The density of CNT is about one-half that of aluminum [90, 161].

Recently, both SWCNTs and MWCNTs were employed as a reinforcing phase for polymer matrices for improving their mechanical and electrical properties. Review articles on this subject can be found in Thostenson et al. [90], Hussain et al. [134], Khare and Base [160] as well as Ahir and Terentjev [161]. In order to take advantage of the superior reinforcement with carbon nanotubes two critical issues should be fulfilled: (i) homogeneous dispersion of the nanotubes, (ii) carefully engineered interface that will ensure effective load transfer in such systems [90, 134, 163, 164].

Nanotubes are also expected to yield attractive tribological properties: with their nanometric size, they can easily be active in the contact area; their structure without dangling bonds provides chemical inertness. Likewise, the use of carbon materials in

tribological applications is a field of research widely explored and many carbon compounds have already been considered for their tribological properties [165]. The tribological behavior of CNTs incorporated in metal, ceramic or polymer matrices [162, 166-183] has been studied scarcely up to now. With respect to polymer matrices, it was found that the inclusion of even a small amount of nanotubes (~ 0.5 vol.%) might lower the wear rate of the composite (Fig. 2.4).

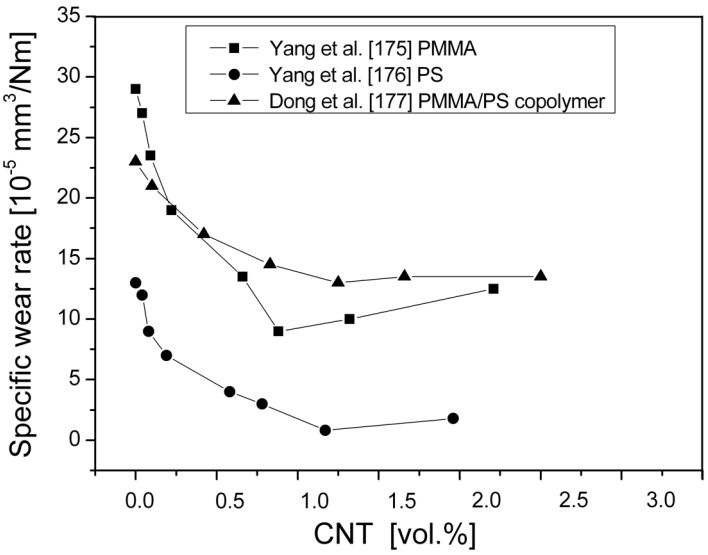

Figure 2.4: Dependence of the specific wear rate on CNT loading fraction in polymer matrices

This beneficial effect of the CNTs was explained by the following factors: (i) the incorporation of carbon nanotubes augments the mechanical properties and hence contributes to better wear resistance, (ii) the carbon nanotubes being uniformly dispersed can prevent the contact between the two sliding surfaces which leads to reduction in the frictional coefficient and slows down wear, (iii) in the process of sliding, the nanotubes are released from the matrix and transferred to the interface, where their self-lubricating properties come into play [175-177]. CNTs were also beneficial for the reduction of friction and wear of PTFE [183]. Nevertheless, in contrast to the other polymer matrices the reported optimum volume fraction of CNTs in PTFE was on the order of 15-20 vol.%.

Finally, to capitalize on this type of filler and take advantage of its remarkable properties many of the manufacturing problems, such as dispersion and alignment, as well as interface should be solved. More efforts should be directed to study and provide further insights into the mechanisms of sliding friction and wear with such materials.

2.2 Artificial Neural Network (ANN) Approach

2.2.1 Introduction to ANN

Artificial neural networks (ANNs) are biologically inspired computational models which operate in the same way as the brain's neural network (Fig. 2.5). They use interconnected nodes (called neurons or processing elements) to transfer information [184-188].

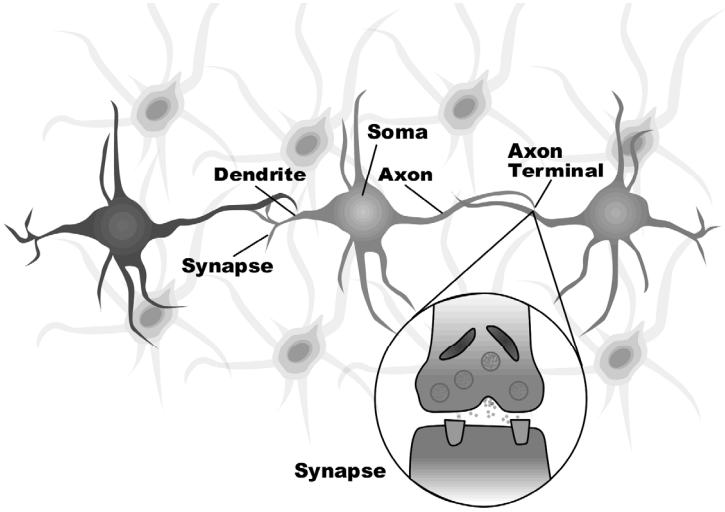

Figure 2.5: Schematic representation of biological neural network

ANNs collect their knowledge by detecting the patterns and relationships in data and learn through experience, not from programming [189, 190]. Thus, while they may interpolate between data with some confidence, they cannot accurately extrapolate, and any trials at such predictions should be viewed with great care [190]. Based on the fact that ANNs learn by example, it is not necessary for them to know the theory behind a phenomenon. The modeling process is opaque similar to a “black-box” operation, therefore it is difficult to ascertain any physical relationships within the dataset using an ANN [190-192].

The main advantage of the neural network approach over conventional regression analysis is that the network finds a solution without the need to specify the relationships or the form of relationships between variables. This feature is very helpful for modeling problems where the relationships between inputs and outputs are not clear enough or the solutions are not easily formulated in a short time [193, 194]. Additionally, ANNs are able to generalize and find patterns in large quantities of often noisy data [190]. Both biological and artificial networks exhibit the following major charac-

teristics: learning adaptation, generalization, massive parallelism, robustness, associative storage information and spatiotemporal information processing [195].

The structure of an ANN is divided into three segments: input layer, hidden layer, and output layer (Fig. 2.6a). The input layer neurons collect data from data file. The output layer neurons present the ANN's response to the input data. Hidden neurons communicate only with other neurons within the network. They belong to the large internal pattern that gives a solution to the problem. The numbers of neurons in the input and output layer are fixed to be equal to that of input and output variables. The hidden layer can contain more than one layer, and in each layer the number of neurons is flexible [184, 185, 189, 193, 196].

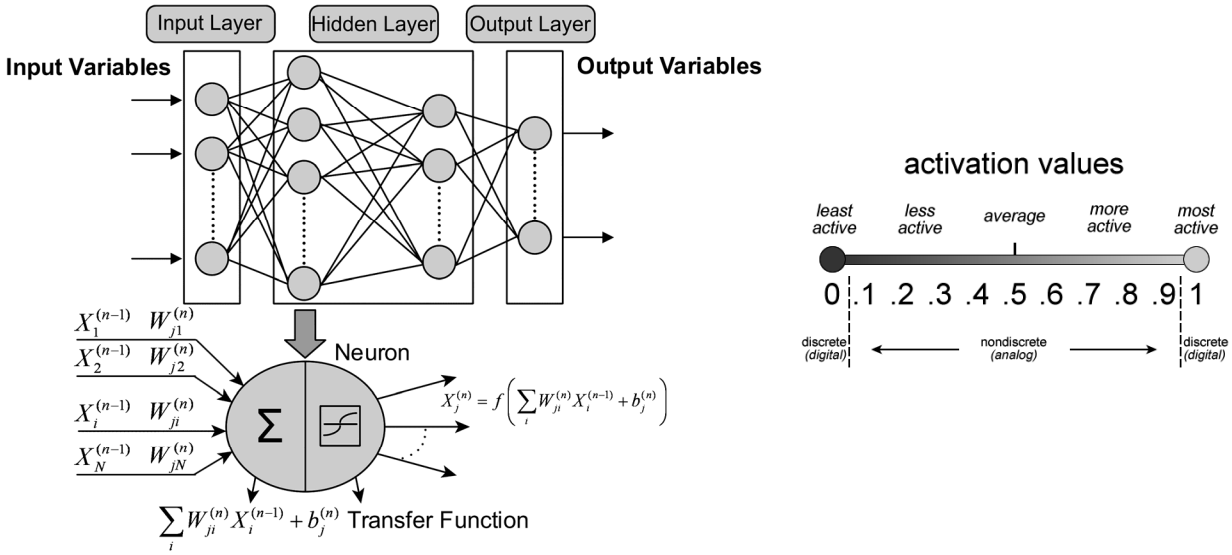

(a) (b)

Figure 2.6: Schematic representation of (a) ANN, (b) neuron activation values

The structure of an ANN can be expressed as:

$$N_{in} - [\, N_1 - N_2 - .. - N_h \,]_h - N_{out} \qquad (2.1)$$

in which N_{in} and N_{out} represent the number of input and output variables, respectively. N_1, N_2, and N_h are the numbers of the neurons in each hidden layer. The number of hidden layers is denoted by the subscript h.

Each processing element (neuron) has weighted inputs (synaptic weights or connection strengths), transfer function (activation or squashing function) and one output. To imitate a real neuron, each input or activation value (Fig. 2.6b) is weighted with a fraction between -1 and 1. The weight specifies how significant the incoming signal

for that input will be. All of the incoming signals weights are summed together and the total equals the net value of the neuron. Each artificial neuron is also set a number that corresponds to the threshold or point over which the artificial neuron will produce a signal (“fire”) and transfer it to another neuron. The output from the firing is then transferred to other neurons that are also weighted. In other words, the learned knowledge generated in the training process is memorized in terms of the state of these weights. This is the key to the ability of artificial neural networks to exhibit learning and memory. Additionally, the neural model includes an externally applied bias (offset) component, which task is to pull the inputs to the hidden and outputs into the correct range for the activation function. The connection strengths and thresholds are developed during training of the neural network [184, 185, 189, 193, 196-198].

Training (learning) is the act of continuously adjusting the connection weights, by strengthening or weakening them, until they reach distinctive values that allow the network to produce outputs close enough to the actual desired outputs. The two major categories of training with an ANN are the supervised and the unsupervised training. In the supervised training, the network output is compared to the desired target response. If the actual response does not correspond to the target response, the network generates an error signal which is then used to calculate the adjustment that should be made to the synaptic weights, so that the actual output equals the target one. In contrast, the unsupervised learning does not necessitate a target output. In the process of training the ANN receives input excitations or patterns and randomly organizes them into categories. When an incentive is later applied, the network gives an output response indicating the class to which this incentive belongs. Provided that such class cannot be found for the input incentive, a new class is created [186, 189, 198].

The action of the ANN is mostly governed by its architecture as well as values of the weights. There exists no simple method for determining the number of hidden neurons a network requires. In the process of training, inputs are adjusted (transformed) by the connection weights. Consequently, the number of connections has an important influence on the network performance. Whereas too few hidden neurons will obstruct the learning process, too many will lower the prediction capabilities through overtraining. By increasing the number of hidden neurons the ANN more closely fol-

lows the topology of the training dataset. Still, beyond a certain optimum number the network learns to deal only with the training data and its generalization capability severely drops [189, 196, 199]. Regarding the number of hidden layers, it has been shown in accordance with Kolmogorov's theorem that any function can be approximated by at most four layers. Looking at the published literature, though, discloses that most problems need (or at least are solved by) only one layer, and sometimes two layers, depending on the complexity of the problem [196].

The most commonly used ANN is a fully connected, supervised network with a backpropagation (BP) learning algorithm [186, 189, 196, 200, 201]. The error in prediction is fed backwards through the network to regulate the weights and minimize the error, accordingly avoiding the same error from reoccurring. This procedure is prolonged with multiple training sets until the error is minimized across many sets and yields mapping of inputs to outputs via a nonfigurative hidden layer [186, 189, 202, 203].

The algorithm of training a backpropagation network is summarized as follows [185, 186, 198, 202-205]:

1. **Initializion:** Initialize the weights and threshold values by setting them to small random values. Subsequently, these values will be adapted during each iteration of the training process until they converge to specific stable values. The derivative of the upper unit's activation function and the activation of the lower unit are decisive to the update of the weight between two units. Therefore, it is crucial to choose such values for the initial weights that would not make it possible to lead to zero activations or derivations of activations. If the initial values are too large, the initial input signals to each hidden or output unit will be likely to fall in the region where the derivative of the transfer function has a very small value, the so-called saturation region. If the initial weights are too small, the network input to a hidden or output unit will be close to zero, which will also cause extremely slow learning. Based on the aforesaid a common solution is to set the initial weights (and bias) to random values between -0.5 and 0.5 (or between -1 and 1). The values may be positive or negative because the final weights after training may be either sign too. Likewise, all the training pairs are marked as unused.

2. Feedforward:

I. An input signal x_i is received by each input unit ($X_i, i = 1,...,n$) and this signal is subsequently emitted to the hidden units in the layer above.

II. Each hidden unit (Z_j, $j = 1,..., p$) sums its weighted input signals,

$$z\_in_j = v_{0j} + \sum_{i=1}^{n} x_i v_{ij} \tag{2.2}$$

applies its activation function to compute its output signal

$$z_j = f\left(z\_in_j\right) \tag{2.3}$$

and sends this signal to all units in the layer above (output units).

III. Each output unit (Y_k, $k = 1,..., m$) sums its weighted input signals,

$$y\_in_k = w_{0k} + \sum_{j=1}^{p} z_j w_{jk} \tag{2.4}$$

and applies its activation function to compute its output signal

$$y_k = f\left(y\_in_k\right) \tag{2.5}$$

3. Backpropagation of Error:

I. Each output unit receives a target pattern corresponding to the input training pattern and computes its error information term,

$$\delta_k = (t_k - y_k) f'\left(y\_in_k\right) \tag{2.6}$$

Next, it calculates its weight correction term,

$$\Delta w_{jk} = \alpha \delta_k z_j \tag{2.7}$$

and bias correction term

$$\Delta w_{0k} = \alpha \delta_k, \tag{2.8}$$

and sends δ_k to the units in the layer below.

II. Each hidden unit sums its delta inputs from units in the layer above

$$\delta\_in_j = \sum_{k=1}^{m} \delta_k w_{jk} \tag{2.9}$$

and multiplies them by the derivative of its activation function to calculate its error information term

$$\delta_j = \delta\_in_j \; f'\left(z\_in_j\right) \tag{2.10}$$

as well as its weight correction term

$$\Delta v_{ij} = \alpha \delta_j x_i \tag{2.11}$$

and bias correction term

$$\Delta v_{0j} = \alpha \delta_j .$$

4. Update Weights and Biases:

I. Each output unit updates its bias and weights ($j = 0,..., p$):

$$w_{jk}^{(new)} = w_{jk}^{(old)} + \Delta w_{jk} \tag{2.12}$$

II. Each hidden unit updates its bias and weights ($i = 0,..., n$):

$$v_{ij}^{(new)} = v_{ij}^{(old)} + \Delta v_{ij} \tag{2.13}$$

5. Test Stopping Condition (Error < Threshold).

If the test stopping condition is not met, the feedforward and backpropagation steps should be repeated again. Usually, many epochs (a cycle through the entire set of training vectors) are required for training a BP neural network until the error is sufficiently low or the network settles.

The learning rate, α , is an important factor and determines the amount by which the weight is updated. A high value (≈ 1) will result in faster learning but raises the risk of the network overshooting the solution and then oscillating around it back and forth due to the large update step. A low value (< 0.1) avoids such problem but slows the process down [196, 206, 207].

Another key factor that can advance ANN training is the momentum, η . This term effectively adds inertia to the motion through weight space and contributes to faster convergence towards the minimum without causing divergent oscillations. In other words to stop the ANN from arriving at a solution that is a local but not true minimum, previous weight adjustments are permitted to continue smoothing the training. The weight correction term (eq. 2.7) is modified to include the momentum term as follows:

$$\Delta w_{jk}(t) = \eta \Delta w_{jk}(t-1) + \alpha \delta_k(t) z_j(t) \tag{2.14}$$

In this respect, the recorded value of the previous weight change will include the momentum term from the step before, i.e. it will merely be the value produced by eq. 2.14 at time (t-1). A high η value will lessen the risk of the network becoming caught in local minima but increase the risk of overshooting [196, 206, 207].

As mentioned before the basic task of an artificial neuron entails summing its weighted input signals and applying an output, or activation, function. For the inputs the activation function is the identity function. Typically, the same activation function is used for all the neurons in any particular layer of a neural network, although it is not compulsory. In most cases an activation function for a BP network should exhibit the following features: be continuous, differentiable, and monotonically non-decreasing. Sigmoid functions (S-shaped curves) are useful activation functions in this respect. The sigmoid activation function acts as a nonlinear gain for the output of a node. Its nonlinear characteristics help a neural network to handle the small as well as the large inputs. The sigmoid functions compress the range of the net input of the neuron such that the output activation value lies between 0 and 1. The logistic and the hyperbolic tangent functions (e.g. tan-sigmoidal transfer function defined by eq.2.15) are the most frequent ones [185, 198, 206, 208].

$$f(x) = \frac{1 - e^{-2x}}{1 + e^{-2x}} \tag{2.15}$$

In order to facilitate the comparisons between predicted values for different network parameters (learning rate, number of neurons in hidden layer) and desired values, there is a need for error evaluation. The following indices might be employed to estimate the performance of ANN:

- Mean relative error (MRE)

$$MRE = \frac{1}{n} \sum_{i=1}^{n} \frac{|d_i - o_i|}{d_i} \tag{2.16}$$

- Mean absolute error (MAE)

$$MAE = \frac{1}{n} \sum_{i=1}^{n} |d_i - o_i| \tag{2.17}$$

- Root mean squared error (RMSE)

$$RMSE = \left(\frac{1}{n} \sum_{i=1}^{n} \left(d_i - o_i \right)^2 \right)^{1/2} \tag{2.18}$$

- Coefficient of determination (COD)

$$COD = 1 - \frac{\sum_{i=1}^{n} \left(d_i - o_i \right)^2}{\sum_{i=1}^{n} \left(o_i - o \right)^2} \tag{2.19}$$

In which d_i is the desired value, o_i is the predicted output value, o is the average of o_i and n is the number of data (total number of entries) [196, 209, 210].

When the ANN produces the desired output, which means it is trained to a satisfactory level, the weighted links between the processing units are saved. These weights are then used as an analytical tool to predict results from a new set of input data (analogous to the training of biological neural networks). This is the so-called prediction phase when the ANN works only by forward propagation of data, i.e. without any backpropagation of error. The output of a forward propagation constitutes the predicted model for the validation data. In most cases the goal is to create an ANN solution capable of generalizing on examples, on which it was not trained, while maintaining an optimal level of accuracy for those on which it was.

It is also very important to appreciate the main drawbacks when working with ANN [211, 212] and to discuss briefly the possible pathways for their solution:

- Under-training: The ANN is insufficiently complex to model the data or an inappropriate set of training data is used. This is best solved by the utilization of an improved selection of training parameters for instance by simply scaling or converting some inputs to logarithmic scale or by using refined dimensional reduction techniques such as singular value decomposition.
- Non-convergence to global minimum i.e. getting trapped in local minima: Here it might help to either reduce the complexity of the network to a minimum or employ a second order solver such as the Levenberg-Marquart algorithm with multiple random starting values.

- Over-training and loss of generalization: Common methods that have proved effective for the prevention of over-training include reducing the complexity of the network as much as possible, adding a small amount of noise to the inputs or using an average of a number of trained networks. Alternatively, early stopping algorithm or Bayesian regularization might be employed. The first approach involves using one dataset for training and an independent dataset for validation. The network is trained until the error starts increasing in the independent dataset. Bayesian regularization involves minimization of a linear combination of squared errors and weights rather than simply minimizing the squared errors.
- Extrapolation beyond training data is unlikely to be reliable (except by good chance).
- Neural networks are purely phenomenological and do not inherently produce a mechanistic understanding of the process being modeled. However, the generalization of the behavior that is achieved with a well fitted neural network may contribute to the development of mechanistic understanding.

Finally, it is possible to apply commercial software and build an ANN quite easily. However, neural programs are not written in the same way as traditional computer programs. Nevertheless, a neural network, just like a computer program, must be seen as an object which is designed and built according to a plan. The plan sets out exactly what will be required at each stage along with a method for achieving each requirement. The neural network development cycle is summarized in Fig. 2.7.

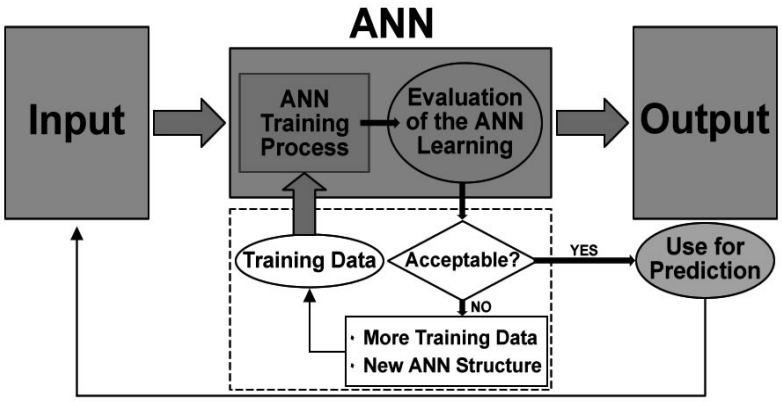

Figure 2.7: Schematic representation of ANN development cycle

In the usage of artificial neural networks an essential drawback might be the complexity of the network, which is directly related to problems such as poor generalization as well as over-fitting (i.e. the network only memorizes the data for training, but does not generalize correct knowledge). In other words, the initial network architecture supplies numerous interconnections between the neurons, some of which are not decisive for its performance. By eliminating these non-useful redundant connections the ANN structure might be simplified (Fig. 2.8) leading to improved generalization capability of the network and better prediction accordingly [213, 214].

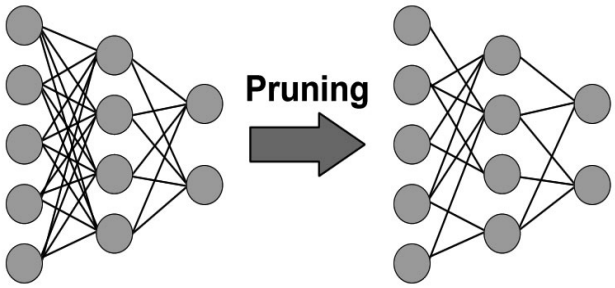

Figure 2.8: Schematic representation of ANN structure pruning

To know which weights should be eliminated is a difficult issue. There exist diverse approaches (or pruning algorithms) to optimize the network architecture, which are based on different criteria. Optimal Brain Surgeon (OBS) algorithm follows the criterion of minimal increase in error on the training data [214]. This method belongs to a class of sensitivity-base weight pruning methods that make use of second order derivatives to eliminate the least important weights in ANN. It does not only remove the weights but also optimally readjusts the remaining ones [215]. The single steps constituting the OBS optimization procedure can be summarized as follows:

1. Train a reasonably large network to minimum error.
2. Estimate the Hessian matrix of the second-order derivatives of the training error criterion with respect to the existing weights.
3. Evaluate the “saliency” of every weight, i.e. the increase in the training error resulting from the elimination of the weight.
4. Delete the weight with the smallest saliency and update the remaining weights.
5. Repeat steps 1-4 until the number of removals exceeds a threshold.

A detailed representation of the individual steps for pruning an ANN architecture via an OBS algorithm is given in [213-218].

2.2.2 Application of ANN to Polymer Composites

2.2.2.1 General Remarks

Correct prediction of material properties and behavior based on existing data has remained a continuous challenge for many researchers in the field of materials science. Very often, regression analysis has been applied where data are best fitted to a specified relationship. Still, this approach involves the following difficulties: (i) a relationship needs to be specified in advance, (ii) the specified relationship tends to be a linear or pseudo-linear equation, (iii) once derived the regression equation applies across the entire span of the input space, which might not always be reasonable [219, 220]. To avoid these difficulties, non-linear regression techniques such as the ANN method have received considerable attention and found many successful applications in modeling the relationship between characteristic properties of polymers and their composites and chosen influence factors, as reviewed by Zhang and Friedrich [15, 221] in addition to Kadi [222]. Important examples from the actual area of ANN prediction with these materials encompasses studies on mechanical behavior [223-227], creep behavior [216, 228, 229], damage assessment and growth [230-234], prediction of delamination [235, 236], crash behavior and energy absorption [237], dynamic mechanical properties [238-240], bond strength [241], effective thermal conductivity [242], materials manufacturing and processing parameters and control [243-249], other related examples [202, 250-255]. Likewise, the ANN method has successfully been applied by different groups to predict the fatigue life of polymer composites [194, 256-265]. When comparing the two examples of fatigue life prediction [257, 258], it can be seen that the use of fiber orientation as input data was able to achieve quite a high predictive quality with a training set of only 92 data points, taken from unidirectional (UD) composites [258], and the result was even better than the one achieved in [257] with more than 400 data points, taken from laminates. The last outcome underlines also the key aspect of fiber orientation in UD composites to their fatigue performance. Indisputably, the fatigue life of multi-axial laminates [257] is much more complex than that of unidirectional ones; consequently more extensive training of the neural network was required for capturing the relationships behind fa-

tigue behavior. The ANN approach has also been employed for friction and/or wear prediction. The scope and results of these investigations will be discussed briefly in the following subchapter.

2.2.2.2 ANN Applied for Friction and Wear Prediction

In a seminal paper of Jones, Jansen and Fusaro [266] from 1997 a preliminary investigation of neural networks techniques was done to predict the tribological properties of metals. The data from three different tribo test rigs were analyzed. The load, testing time, sliding distance and speed, viscosity of lubricants, temperature and frictional coefficient were the ANN input variables; the output parameter was the wear rate. Comparatively small datasets were used both for training and testing of the ANN. Yet, a satisfactory predictive quality could be achieved. Moreover, contribution strengths were applied to describe how strong the influence of the input variables to the output wear rate was by evaluating the weight factors between the input layer and hidden layers. Some other works in the field of ANNs for friction and/or wear prediction include [267-279].

With reference to polymer composites, Velten et al. [280] were the pioneers in exploring the application of ANNs to these materials and used an ANN to predict the wear volume of short-fiber/particle reinforced thermoplastics. A dataset of 72 independent wear measurements was utilized to train and test the neural network. The dataset was generated from fretting tests with various PA 46 material compositions. The input parameters of the ANN were both characteristic mechanical properties and measuring conditions. The automated Bayesian regularization of a backpropagation algorithm was selected as a learning rule. Nevertheless, at this early stage of research, the ANN model gave only reasonable accuracy and there was still room for improvement. In a later study of Zhang et al. [281] an enlarged dataset of 103 independent measurements was used for friction and wear studies. The utilized input data were: (1) material composition, (2) selected mechanical properties of the composites measured at different temperatures, (3) testing conditions. The output data were the wear characteristics. At first, the effect of the diverse groups of input parameters was analyzed. In all these cases, 88 data points were used for training and the remaining 15 for testing. In this initial part, the Bayesian algorithm was applied as the learning rule. It was demonstrated that the parameter “material composition”

strongly influences the performance of the ANN for achieving a reliable prediction of the corresponding materials properties. Subsequently, it was shown that the applied training algorithm and the ANN architecture exert strong impact on the predictive quality. Both Bayesian regularization and Powell-Beale conjugate gradient algorithm were distinguished as the most advantageous in terms of computational speed and prediction quality. Concerning the optimum network architecture the three-hidden layer network 9-[15-10-5]$_3$-1 exhibited the best results.

Zhang, Barkoula, Karger-Kocsis, and Friedrich [282] applied the ANN approach to study the erosive wear of three polymer-based materials, namely polyethylene (PE), polyurethane (PUR) and epoxy modified by hygrothermally decomposed PUR. It was shown that ranking of the importance of characteristic properties to the erosive wear rate via the coefficient of determination (equation 2.19) could offer some information about which property had a stronger relationship to the erosive wear of polymers. In the more recent study by Suresh, Harsha and Ghosh [283] an ANN was also used to model solid particle erosion of PPS and PPS reinforced by short glass fibers. A data-set containing only 48 independent measurements obtained from erosion wear tests was used to train and test the ANN. Impact angle, impact velocity and fiber content were chosen as input variables and the erosion rate was the output parameter. The optimized ANN had a structure of 3-[9-6-3]$_3$-1. The predicted profiles showed good agreement with the experimental data points. From the predicted profiles the dependence of the erosion wear rate of PPS and its composites on fiber content and testing conditions could be obtained over the entire knowledge domain. In a similar study Satapathy, Patnaik and Pradhan [284] modeled the erosive wear rate of fish scale filled epoxy matrix composites via ANNs using a much larger training dataset of 135 data points. Based on the least error criteria the selected network structure was 5-[12]$_1$-1. The predicted results by the ANN were of reasonable accuracy (the error between experimental and theoretical erosion wear rate lay in the range 0-14%).

Zhang et al. [285] investigated the effect of sliding velocity and applied load on the tribological behavior of SiC-filled PEEK coating using an ANN. The dataset was divided into three categories: 75 sets were used for training the network, 75 sets were used for testing the network and 20 sets were used for network validation after optimization. The input parameters were the applied load and sliding velocity. The output

parameters were the wear rate and frictional coefficient. The optimized ANN had an architecture of 2-[5-3]$_2$-2. Analogous to the other studies, the predicted tendencies by the ANN were close enough to the experimentally obtained results.

In a series of studies Jiang and coworkers [225, 286, 287] applied the ANN technique to predict the wear and mechanical properties of short fiber reinforced PA composites. The predicted property profiles as a function of short fiber content or testing conditions exemplified the remarkable capability of well-optimized neural networks for systematic parametric studies related to material optimization. Despite that the accuracy of prediction was satisfactory it was shown that the latter parameter might be further improved by expanding the training dataset. Likewise, the optimization of the ANN configuration illustrated that although this parameter exerts great influence on the performance of the ANN, there is still a lack of well-defined rules to attain the best ANN architecture. Finally, some recommendations were given by the authors as to determining optimum hidden layer structure, best neuron number as well as training algorithm.

Srinivasan et al. [288] used probabilistic neural networks for the development of a wear mechanism map for glass fiber reinforced epoxy materials. The wear mechanism map can be used subsequently for the selection of optimum working conditions. However, no detailed information was given as to the training of the ANN and its prediction accuracy. Liujie et al. [289] used back propagation ANN to study the effects of various pv-factors and sliding distances on the friction and wear behavior of carbon fiber reinforced PEEK composite (PEEK-CF30) at the contact temperature of 120°C. For generating the friction and wear dataset, a pin-on-disc test rig was used. The dataset was comparatively small and consisted of only 30 experimental data points, where 25 data points were selected for training and the rest for testing of the network. Regardless of the very limited dataset surprisingly low training errors were reached after only 10-12 cycles of training. From the predicted three dimensional plots of the frictional coefficient and wear loss against sliding distance and pv-factor it became obvious that for both tribo-parameters the sliding distance plays a more decisive role than the pv-factor in these materials. Yet, the results from the ANN prediction should be considered with great care as being system-related i.e. subsequent data streams presented to the trained network should be drawn from a statistically

similar distribution to the training PEEK-based data. Zhu et al. [290] applied an ANN to predict tribological properties of carbon fiber and micro TiO_2 reinforced PTFE composites. Initially the ANN structure and training algorithm were optimized to match the particular application. Once a sufficiently trained ANN was obtained, it was used to generate new results without performing time consuming tribo-experiments. The applied input parameters were material compositions, mechanical properties as well as testing conditions; the output was wear volume loss or frictional coefficient. Good predictive results could be gained. However, the predictive quality for the frictional coefficient was superior. The joint interplay of carbon fiber and micro-TiO_2 in PTFE proved beneficial for increasing the wear resistance of the composite, which was verified both experimentally and by the ANN prediction. These results correlate quite well with those of Jiang et al. [147]. In a more recent study Gyurova et al. [291] investigated the importance of various input characteristic properties for the frictional coefficient and wear rate of PPS composites. An analogous investigation for ranking the importance of characteristic properties to wear loss was formerly reported by Chang [27] for epoxy based composites.

2.3 Summary

In recent years the use of polymer composites as structural components, where friction and wear are critical issues, has undergone rapid growth. Polymers are favored in tribo-applications because of the prospect to tailor desired material features by proper incorporation of different phases as well as self-lubricity of the matrix itself. Modern tribo-fillers include: short fibers that improve mechanical and thermal performance as well as internal lubricants that lower friction and contribute to the formation of thin, uniform transfer film. Whereas, the former results in higher pv-limits, the latter is an essential prerequisite for diminishing wear. Currently, a huge international research effort is ongoing to quantify the properties and science of polymer nanocomposites. In the field of tribology, it has been shown that inorganic nano and submicro particles put forward a remarkable opportunity to develop multifunctional composites with customized physical and tribological properties. Moreover, the required filler loading fraction is much lower when compared to micro-scale particulate fillers. The combined action of short carbon fibers and nano/sub-micro particles led to a dramatic enhancement in both friction properties and wear resistance as well as an

increase in the load-carrying capacity of such materials. Possible mechanisms concerning this effect were discussed in terms of: (i) rolling action of the nano-filler alone or being embedded in matrix wear debris, (ii) improvement of the stability of the transfer film as well as (iii) increasing the stiffness of the matrix, consequently reducing both the stress concentration in the surface layer around the fibers as well as fibers deformation under tension. This is even now a fast developing area and it is the subject of further research for providing feasible explanation and appropriate models for predicting this behavior. Further beneficial effect on the performance of structural tribo-components can be expected with the addition of carbon nanotubes in polymer matrices. The solutions are not fully satisfactory as yet, and consequently, commercial application requires more research and development work.

In the process of wear of polymers and polymer composites, very complex and highly non-linear interactions are involved. Therefore, analytical models are difficult or impossible to obtain. Nevertheless, the improvement of performances and reliability of structural components as well as the appropriate selection of materials to diminish/control wear necessitates a full understanding of the effects of all system parameters. In this respect a novel, powerful modeling technique (ANNs) has emerged and was applied to study friction and wear of various materials including polymers and polymer composites. ANNs are designed to emulate a brain's ability to identify patterns and draw conclusions when presented with complex noisy and often irrelevant information. ANNs require no prior models, but they need large training datasets. After the network has satisfactorily been trained to solve a physical problem from a given set of examples, new data from the same knowledge domain can be predicted without performing too many, long lasting experiments. Likewise, these techniques are found superior over regression methods as the dimensionality and/or nonlinearity of the problem increases, which makes them ideal for modeling friction and wear phenomena. Up to now in the field of polymers and polymer-based composites most of the studies were concentrated on: (i) pattern completion for friction and wear properties provided that only a portion of an input pattern is available, (ii) parameter studies related to external testing conditions and (iii) indicator of the importance of various input characteristic properties for the frictional coefficient and wear rate. The results of these works indicated that ANNs might be used not only for designing new materials, but also for further understanding of the modeled nonlinear relations.

3 Objectives of the Study

To develop and test a new composite material for a specific application is a complicated process. It is necessary to select the right composition (matrix, fillers, reinforcing phase, lubricants, etc.), manufacturing process and to consider the operating parameters and environmental effects under which the material is going to function. Besides its complex nature, to study and understand the sliding wear process of polymer composites is, as a rule, time-consuming and involves high costs. A feasible solution can be the development of a predictive design tool that can operate with a comparatively small experimental database and be able to draw conclusions about non-linear relationships even from noisy and complex data. Moreover, this tool should show good conformation between predicted and measured results (i.e. give reasonable accuracy). ANN modeling exhibits unique qualities such as non-linearity, adaptive learning, generalization and model independence (“black box” modeling) and perfectly matches the imposed requirements.

The concept of a hybrid reinforcement by mixing two or more phases such as particles, layers or fibers, where at least one of the phases is in the nanometer (sub-micro meter) size has already been utilized in nature. Using natural reagents and polymers, for instance carbohydrates, lipids and proteins, nature makes strong, wear resistant composites such as bones and shells [134]. Following this approach in the field of tribology more and more research activities are focused nowadays on inorganic nano and sub-micro particles combined with a traditional reinforcement.

In this respect, the objectives of the present investigation were concentrated on the following aspects.

Methodology Study

Until now, the application of ANN to polymers and polymer composites, especially for dealing with tribological properties, is still at its basic research stage. Therefore, the exploration of the performance potential and the enhancement of the prognostic qualities are still matters of further research. To find the optimum neural network topology for modelling a particular problem is not an easy task and a matter of experimentation. In a methodology study using existing experimental friction and wear test

results it was endeavored to: (i) investigate the strategies for obtaining a suitable ANN architecture related to the friction and wear problem with polymers and polymer composites, (ii) find a proper architecture that avoids over-fitting or instability, (iii) analyze the various training/testing methodologies as well as evaluate predicted versus measured results for both training and testing phases.

Sliding Friction and Wear Measurement of PPS Matrix Composites

The knowledge gained within the methodology study was subsequently applied to a newly measured dataset of polyphenylene sulfide matrix composites filled with various traditional fillers (short carbon fibers, PTFE, graphite) and inorganic sub-micro particles. The selection of additives was based on obtaining an appropriate balance of mechanical, self-lubricating, wear resistance and operating temperatures properties using the existing know-how on thermosetting-based materials. Another key objective was to explore both experimentally and via the ANN approach the effects of these additives, acting alone or in combination, on the sliding friction and wear performance of thermoplastic matrix composites. The influence of the operating parameters contact pressure (p) and sliding speed (v) was also studied. At last, the ruling wear mechanisms in these hybrid materials were experimentally examined in detail.

Pruning via Optimal Brain Surgeon Algorithm (OBS)

In general, the intact network architecture provides more than adequate interconnections among the neurons. Therefore, the optimal brain surgeon algorithm (OBS) was applied to optimize the network performance by removing useless interconnections in its architecture and compare its performance to the fully-connected network.

Input Parameters Study

Within an importance analysis it was attempted to investigate the correlation between characteristic mechanical and tribological properties of polymer composites using the ANN. The latter might indicate to which properties material designers should pay more attention when tailoring a composite system for a particular tribological operation. Furthermore, the characteristic properties are normally easier to obtain than the complex tribological ones, and therefore the success of prediction could be of benefit to reduce the number of tribo-experiments.

Ball Bearing (“Rolling”) Effect on Sub-Micro Scale

It was previously established that the combination of short carbon fibers and particulate nano or sub-micro inorganic particles in a polymer matrix resulted in significant improvement in the tribo-performance of the composite material. Early theory suggested a positive “rolling effect” of the individual particles in the boundary layer, which helps keep the fibers in the matrix and decreases strongly the frictional coefficient. However, the rolling mechanism was so far only hypothetical and additional experimental research should be done to verify it. In this respect, it was the objective of this work to perform:

- Direct experimental observation not only of the individual contact surfaces but also of their sliding interface.
- In-depth analysis of the elemental composition of the resultant transfer particles.
- Investigation of the role of the mechanical characteristics such as Mohs’ hardness of the particulate filler on its “rolling effect”.

.

4 Experimental Procedures

4.1 Materials

The matrix material used in this study was PPS (Fortron grade 0214, Ticona GmbH). PPS is a semi-crystalline, high performance thermoplastic material with a melting temperature of 285-290°C, a glass transition temperature in the range of 85-95°C, very low water absorption, high hardness, rigidity as well as excellent creep resistance even at elevated temperatures [292-294]. Therefore, it is a good candidate as a polymer matrix for sliding friction and wear applications. Neat PPS, however, is a brittle material with a relatively low impact strength and wear resistance [50, 295]. For that reason, diverse traditional reinforcing agents and additives as well as sub-micro particles were chosen to enhance the matrix property profile: pitch-based short carbon fiber (Kureha M-2007S, Kureha Chemicals GmbH), graphite (Superior 9039, Superior Graphite Europe Ltd.), PTFE (Dyneon 9207, Dyneon), sub-micro TiO_2 (Kronos 2310, Kronos Titan GmbH), sub-micro ZnS (Sachtolit HD-S, Sachtleben Chemie GmbH). The properties of the fillers are summarized in Table 4.1 and Table 4.2. The structures of the fillers are given in Fig. 4.1 and Fig. 4.2.

Table 4.1: Selected properties of traditional reinforcing agents and additives used in this study [27, 296]

Product	**SCF Kureha M-2007S**	**Graphite Superior 9039**	**PTFE Dyneon 9207**
Manufacturer/ Distributor	Kureha Chemicals GmbH	Superior Graphite Europe Ltd.	Dyneon
Diameter [µm]	14.5	20	4
Fiber length [µm]	90	-	-
Mohs' hardness	6.0	-	-

Table 4.2: Selected properties of sub-micro fillers used in this study [27, 296-298]

Product	**TiO_2 Kronos 2310**	**ZnS Sachtolit HDS**
Manufacturer/Distributor	Kronos Titan GmbH	Sachtleben Chemie GmbH
APS [nm]	300	300
SSA [m^2/g]	18	18
Morphology	Spherical	Spherical
Surface modification	Al,Si,Zr,C (Purity ≥ 92.5%)	Not done (Purity 99%)
Mohs' hardness	6.0-6.5	3.0

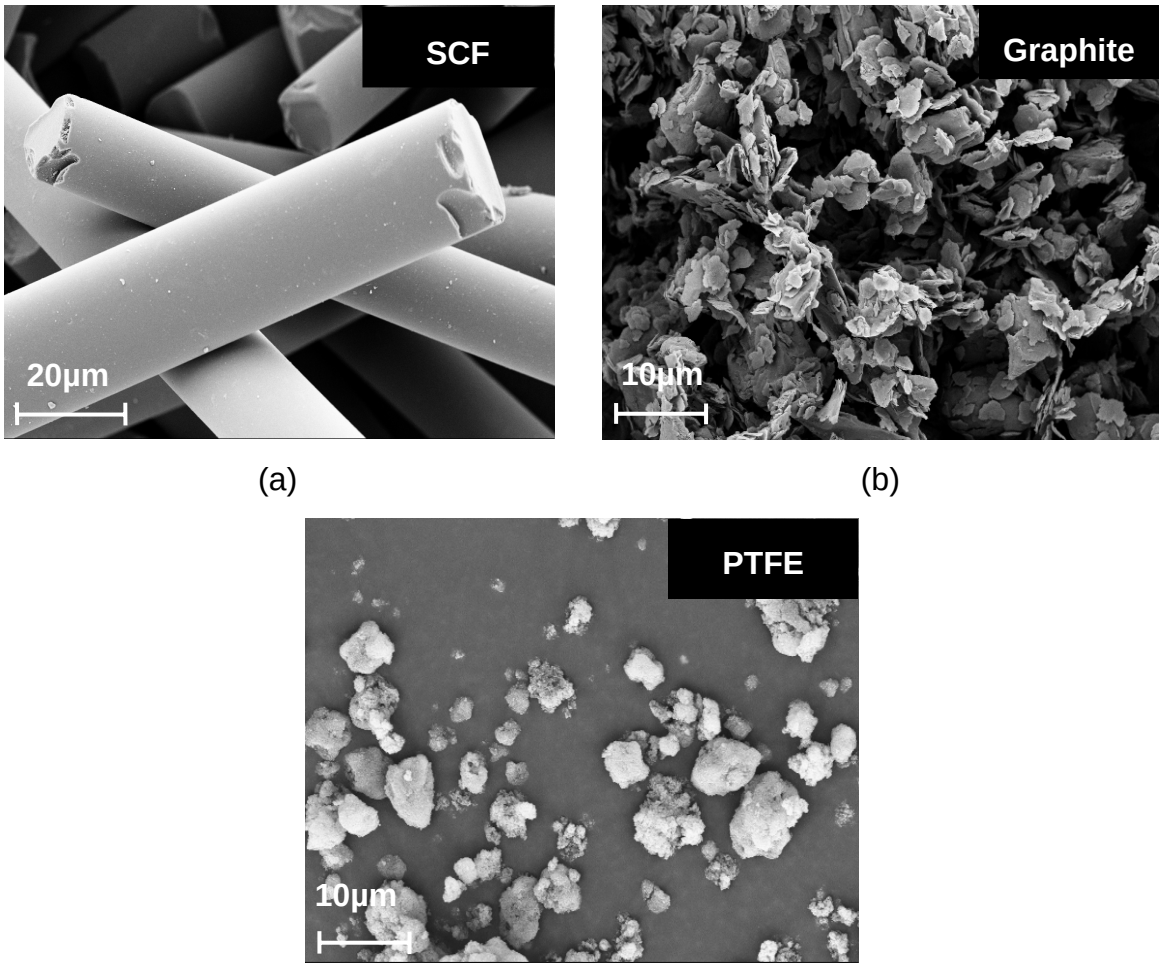

Figure 4.1: SEM micrographs of traditional reinforcing agents and additives used in this study

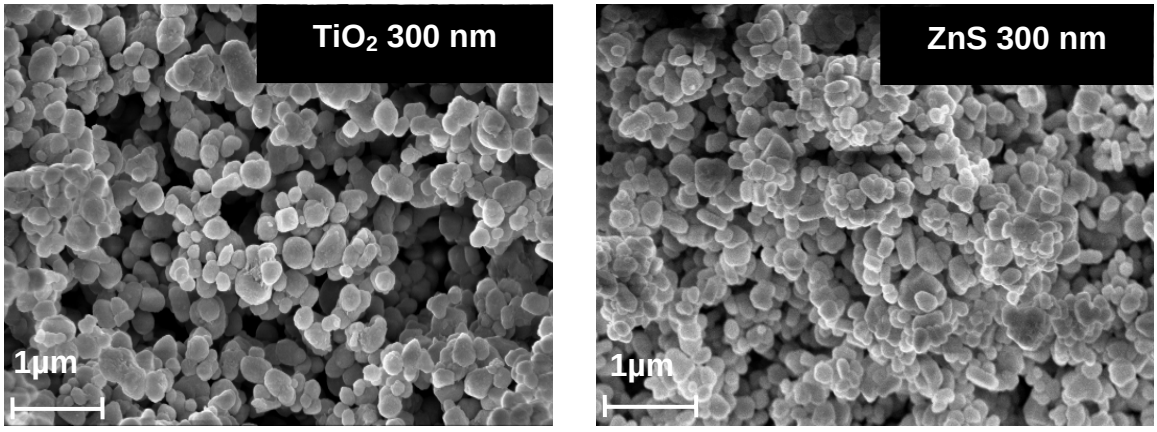

(a) (b)

Figure 4.2: SEM micrographs of sub-micro particles used in this study

4.2 Material Compounding

The investigated PPS compounds listed in Table 4.3 were fabricated by mixing the fillers with the matrix in a twin-screw extruder (ZE25Ax44D, Berstorff GmbH). Prior to extrusion, the matrix, reinforcing agents, additives and fillers were dried in a vacuum oven for a period of 72 hours at a temperature of 80°C. The screw speed and matrix feed rate during extrusion were set to 300 rpm and 8-9 kg/h, respectively. The extrusion temperature zones from hopper to die were selected as follows:

- Feed zone: 68°C-73°C ;
- Transition zone: 294°C-315°C;
- Metering zone: 310°C-315°C;
- Adapter (head temperature): 310°C-312°C;
- Die: 310°C-312°C;
- Melt temperature: 313-316°C.

The extruded strands were quenched in water and subsequently chopped into granules. Next, they were dried in a vacuum oven for at least 72 hours at a temperature of 80°C for moisture removal. Some of the compositions (marked with a star) were extruded at the company Ensinger GmbH.

Table 4.3: Material compositions of the manufactured PPS compounds

Code	PPS [vol.%]	SCF [vol.%]	TiO_2 [vol.%]	Gr [vol.%]	PTFE [vol.%]	ZnS [vol.%]
C1≡PPS1	100	0	0	0	0	0
C2≡PPS2	99	0	1	0	0	0
C3≡PPS4	97	0	3	0	0	0
C4≡PPS3	95	0	5	0	0	0
C5≡PPS5	93	0	7	0	0	0
C6≡PPS6	85	15	0	0	0	0
C7≡PPS7	84	15	1	0	0	0
C8≡PPS8	82	15	3	0	0	0
C9≡PPS9	80	15	5	0	0	0
C10≡PPS10	78	15	7	0	0	0
C11≡PPS13	75	20	5	0	0	0
C12*≡PPS16	85	10	5	0	0	0
C13*≡PPS18	75	10	5	10	0	0
C14*≡PPS19	70	10	5	10	5	0
C15*≡PPS20	65	10	5	10	10	0
C16*≡PPS21	70	10	5	5	10	0
C17*≡PPS22	75	10	5	5	5	0
C18*≡PPS23	90	10	0	0	0	0
C19*≡PPS24	70	10	0	10	10	0
C20*≡PPS25	75	10	5	0	10	0
C21≡PPS26	95	5	0	0	0	0
C22≡PPS27	93	5	2	0	0	0
C23≡PPS28	91	7	2	0	0	0
C24≡PPS29	89	6	5	0	0	0
C25≡PPS30	87	8	5	0	0	0
C26≡PPS31	81	5	4	0	0	0
C27≡PPS32	87	10	3	0	0	0
C28≡PPS33	77	15	8	0	0	0
C29≡PPS36	85	10	0	0	0	5

Finally, the materials were injection molded into rectangular plates (80 x 80 x 4 mm^3) using an injection molding machine (Allrounder, Arburg GmbH) at a barrel temperature of 310°C-335°C depending on the corresponding filler loading fraction. The mold temperature was set to 150°C.

4.3 Tribology Testing

The sliding friction and wear tests were performed on a Wazau pin-on-disc (P-o-D) test rig. During testing a rotating pin is pressed against a stationary disc (q.v. Fig. 1.1b in chapter 1). This test rig permits much better control of the experimental conditions and is becoming increasingly used in preference to other tribometers. Moreover, the experiments can be completed under comparatively steady conditions without systematic variations, e.g. in contact area, as they can occur in other tribometers [299].

For the purpose of testing, samples were cut into pins with a contact surface of 4 x 4 mm^2. In order to ensure identical flow conditions, only the middle section of the plates was chosen for machining the samples. All the samples were cut so that the loading applied was in the mold filling (melt flow) direction (Fig. 4.3).

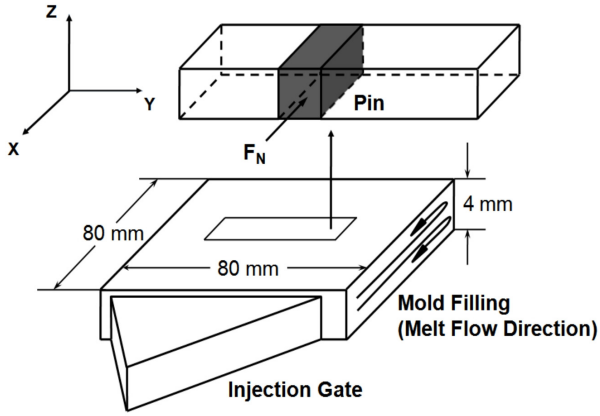

Figure 4.3: Schematic representation of sample selection for P-o-D testing

The sliding friction and wear tests were carried out under dry testing conditions and at room temperature. The testing parameters were varied as follows: applied pressure (p) in the range from 1 MPa to 4 MPa using an increment of 1 MPa; sliding speed (v) of 1 m/s and 3 m/s. At least three pins were tested per testing condition, and the average values were taken. The counterface was a 100 Cr6 (German standard DIN 616) steel disc (LS 2542, INA-Schaeffler KG), where the average surface roughness at the beginning of the test was about R_a = 0.19 µm and the hardness was around 63 HRC. Prior to executing the tests, the contact surface of the pin was polished by abrasion against silicon carbide paper (grit number P 400, Buehler) for a very short time to render the same level of surface finish for all the test specimens. Subsequently, the pin and steel counterface were cleaned with isopropanol and acetone, respectively, followed by drying. The testing time was fixed to 20 hours, allowing the system to reach steady-state tribological conditions. For some of the materials, e.g. pristine PPS, the test was stopped after 1 hour due to excessive wear. In the course of the experiments both the normal and friction forces were recorded simultaneously to determine the frictional coefficient (q.v. equation 1.1 in chapter 1). The latter is reported as a time-averaged value based on the data measured in steady state. The surface temperature was recorded by an embedded subsurface thermocouple fixed into the non-contacting surface, namely at the rear side of the stationary

counterface. Embedded thermocouples were found to provide a good indication of the transient changes in frictional heat generation which accompany coarse variations in the contact area [300]. The specific wear rate, w_s, was calculated from the mass loss of the specimen after the test over the total test duration (q.v. equation 1.2 in chapter 1). This includes some small inaccuracy, due to the averaging over the running-in and steady state phases, but makes the evaluation procedure easier [301].

4.4 Mechanical and Thermo-Mechanical Testing

4.4.1 Dynamic Microhardness Testing

Dynamic microhardness tests were done with a dynamic ultramicrohardness tester (DUH-202, Shimadzu Corporation). The test was performed by loading the sample up to a defined load level (1000 mN). Then the maximum load (1000 mN) was kept constant for 2 s. At the last stage unloading took place. Ten indentations were made on each sample, for which an average value was reported.

4.4.2 Tensile and Compression Testing

The tensile properties were determined using a universal testing machine (model 1485, Zwick GmbH) with a test speed of 1 mm/min. The tests were completed according to the standard DIN EN ISO 527-2 [302] using specimen type 1BA. The tensile modulus was evaluated as a secant modulus in the initial linear portion of the stress-strain curve above the load take-up region.

Compression tests were performed according to DIN ISO 604 [303] in a universal testing machine (model 1474, Zwick GmbH) with a sample having the dimensions 10 x 10 x 4 mm^3 and at a testing speed 1 mm/min. Two separate tests were carried out using different test specimens. In the initial tests for compressive strength determination the distance between the metal plates was measured using the integrated displacement measurement unit in the universal testing machine. In the subsequent tests for determining the compression modulus, a special inductive displacement transducer (W1T3, HBM GmbH) was employed. The accuracy with the inductive transducer was higher, but the working range was restricted to very small displacements. The compression modulus was then evaluated as a secant modulus in the initial linear portion of the stress-strain curve above the load take-up region.

4.4.3 Notch Charpy Impact Testing

Instrumented notch Charpy impact tests were carried out according to ISO-179-2 standard [304] on a pendulum impact testing machine (CEAST GmbH). Rectangular specimens, type 1, having the dimensions 80 x 10 x 4 mm^3 were used with a notch type A. The distance between the supports was set to 62 mm. The specimens were fractured at a speed of 2.9 m/s and impact energy of 4 J [305]. For measuring the area of the fracture surfaces from the notch Charpy impact tests optical micrographs were recorded with the help of a light stereomicroscope (SZH-ILLD, Olympus Optical Co. (Europa) GmbH). At least ten samples were tested from each material.

4.4.4 Dynamic Mechanical Thermal Analysis (DMTA)

Dynamic mechanical thermal analysis (DMTA) was conducted on dynamic material testing equipment (Eplexor, Gabo GmbH). The mechanical loss factor and storage modulus were continuously measured during a thermoscan within the temperature range of 20-250°C at a heating rate of 1°C/min. The specimen was of a rectangular shape and dimensions 50 x 10 x 4 mm^3. The tests were performed in a tensile mode with a static load 40 N and dynamic load 20 N at a constant frequency of 10 Hz.

4.5 Surface Analysis

4.5.1 Scanning Electron Microscopy

Surface micrography and analysis was conducted at the completion of the tribological testing on selected samples in order to generate information of the corresponding friction and wear processes. The interactive surfaces (worn pin, wear track) were observed by scanning electron microscope (Supra 40, Carl Zeiss MicroImaging GmbH). Prior to investigation a thin Au-Pd/carbon layer was sputtered over the worn pin surface (SCD 050, Balzers) for at least 70 s to allow electron conduction away from the impinging electron beam during inspection. In addition, X-ray photoelectron spectroscopy (XPS) was used to gain information on the elemental composition of the developed transfer films and wear debris. In certain cases energy dispersive X-ray (EDX) analysis was also performed.

4.5.2 Atomic Force Microscopy

Atomic force microscopy (AFM) was used to acquire quantitative determination and presentation of surface topography. Particularly, single fibers embedded in the surface of the worn composite pin were observed by the AFM apparatus (Digital Instruments), of which the lateral and vertical resolutions were 2 nm and 0.2 nm, respectively; the x/y-scanning was within the range: 0.3 to 150 µm. The AFM was operated in tapping mode.

4.6 Development of Graphical User Interface (GUI) for ANN Training and Prediction

User-friendly graphical interfaces were developed at the Institut für Verbundwerkstoffe GmbH (IVW) based on the Neural Network Toolbox in Matlab 7.0.4 (The Math Works Inc.) environment [306] for performing network optimization (Fig. 4.4, Fig. 4.5) and prediction (Fig. 4.6) with the ANN. The developed graphical interfaces enable the user to load the acquired training and/or prediction databases in Excel format which are then used for ANN training and/or prediction. They also permit the user to select the network architecture (input column, output column, and hidden layer), the training (learning) algorithm as well as some extra parameters such as learning rate, repeating times of the training/testing process, number of epochs and show period (the interval at which the training status is displayed).

The GUI for network optimization is developed in two different configurations. The initially developed configuration (Fig. 4.4) requires entering the hidden layer structure manually one by one. The improved second configuration (Fig. 4.5) is more convenient and allows faster evaluation of the best network architecture by automatic generation of the hidden layer structure. In this case instead of manually entering the hidden layer structures one by one, the GUI performs automatic evaluation of all network structures restricted by the number of hidden layers “Number Layers” and number of neurons in each hidden layer “Number Neurons” starting by default with 1 neuron and 1 hidden layer. The latter allows the computer program to be left running uninterrupted until the evaluation is finished. In this option the user can also define the initial conditions for the number of neurons in the pre-last hidden layer “I.C. for the Neurons”. Therefore, the problem of restarting from the very beginning when the PC is stopped or blocked is avoided.

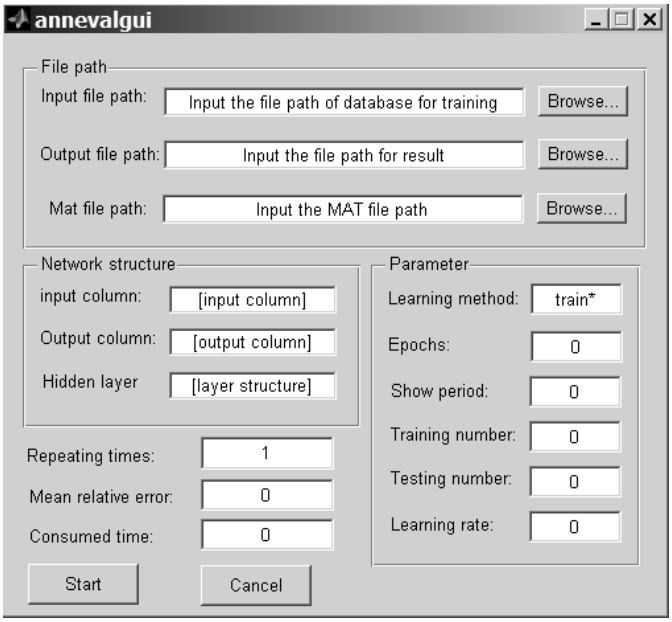

Figure 4.4: GUI for ANN optimization: annevalgui

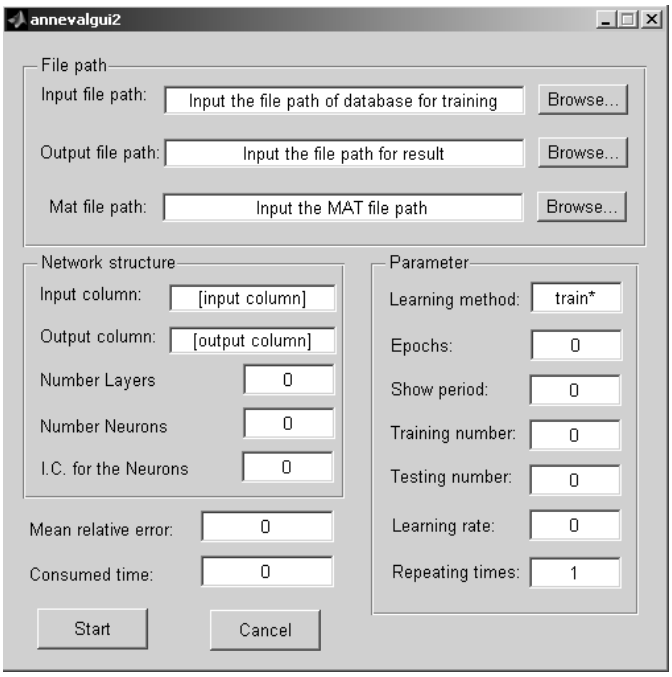

Figure 4.5 GUI for ANN optimization (improved configuration): annevalgui2

In the process of network optimization one part of the acquired data is used for training (≈ 75%) and the rest is used for testing of the ANN (≈ 25%). The network, however, is still trained on the entire dataset. The created GUIs (Fig. 4.4, Fig. 4.5) allow the user to set both the training number and the testing number of data. The computer program is written in a way to permit random distribution of the whole training

database each time when it is run in order to optimize the training process. Once the information is entered the user can click on the “Start” button (Fig. 4.4, Fig. 4.5) to activate the training process. While the training is running, the Matlab code automatically saves data to the output data file upon completion of each block of trials. Thereby it eliminates the necessity for the observers to be responsible for saving their own data to a file at the end of a data-collection session. After the training process is completed the observers are returned to the GUI where they can view the obtained training parameters i.e. the MRE and the consumed time (CPU time). The training process continues either to the end of the specified iterations or until reaching the target level of errors.

After optimizing the network parameters such as architecture and training algorithm the next step is to perform prediction to get new results in the same knowledge domain. The user can run the developed GUI (Fig. 4.6) and input the desired new combinations of input parameters as an Excel data file by using the browse button for the “Prediction database”.

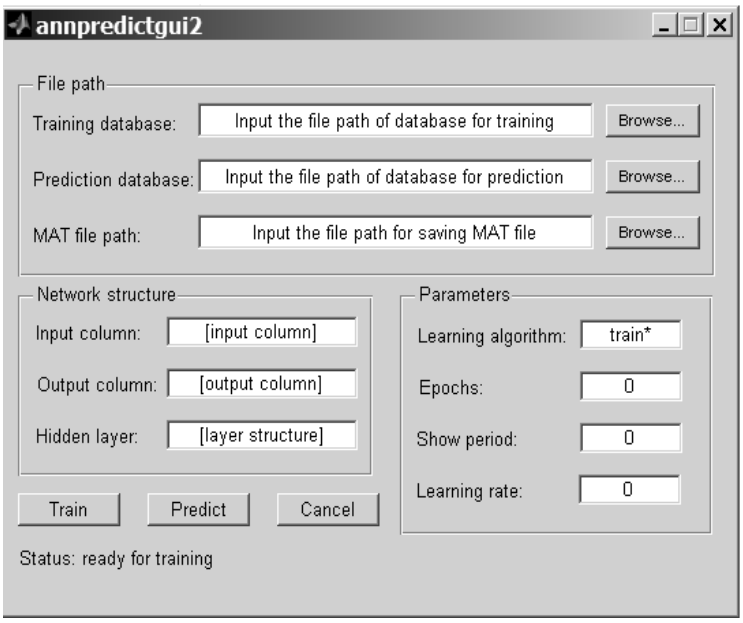

Figure 4.6: GUI for ANN prediction: annpredictgui2

Once all the information has been entered and the network has been trained the user activates the prediction by pressing the “Predict” button (Fig. 4.6). The output is returned to the GUI and saved in Excel format along with the MRE and the consumed time. The model will work with sufficient accuracy within the range of the dataset

used in the training. If the user defines input conditions outside this range the software will still generate an output but it may not be correct.

The computer program for finding the optimal case of trained neural network requires significant computational resources but once trained the model can quickly and easily predict new situations without a requirement for powerful resources. The user can also use the GUI interface to simulate results for new input parameters. No in-depth knowledge of Matlab or computer programming is necessary for successful navigation of the designed GUI.

4.7 Optimization of ANN via Optimal Brain Surgeon Algorithm (OBS)

For ANN optimization (calculation of saliencies), Java Neural Network Simulator (JavaNNS), Version 1.1 was used [307]. The software was developed at the Wilhelm-Schickard-Institute for Computer Science in Tübingen (Germany) based on the Stuttgart Neural Network Simulator (SNNS) 4.2 kernel with a new graphical user interface written in Java set on top of it. Through this software it was possible to prune the network by eliminating certain needless interconnections (Fig. 4.7a) which weights give a maximum decrease in the final prediction error (FPE) estimate (Fig. 4.7b) [308, 309]. The interface permits the selection of the following parameters: initializing, updating and learning functions along with the pruning method.

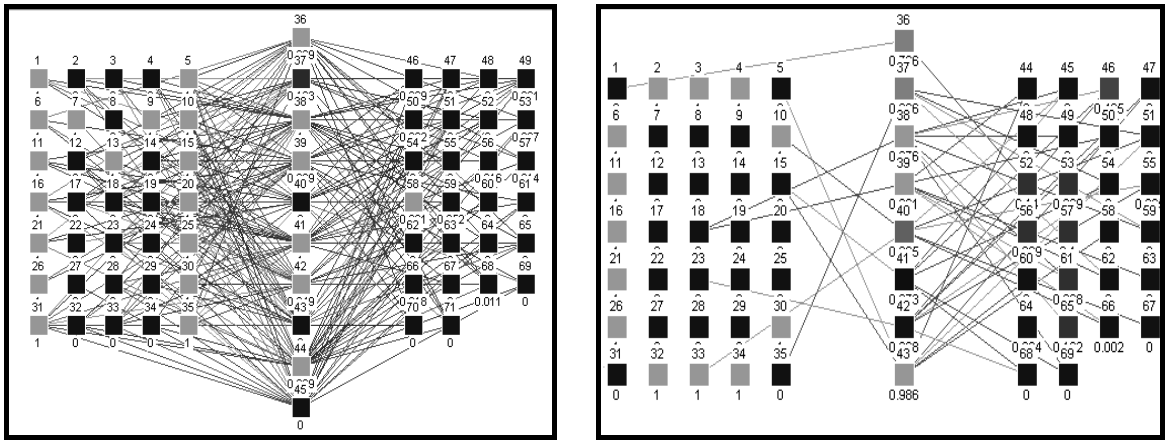

(a) (b)

Figure 4.7: Schematic representation of the ANN (a) prior to and (b) after pruning generated with JavaNNS (Version 1.1) [307]

5 Results and Discussion

5.1 Methodology Study

The major goal of this study was to investigate the applicability of an artificial neural network approach in predicting characteristic tribological properties of polymers and polymer composites. For comparison, a series of predictions were also performed on the much easier to obtain mechanical properties with these materials. The design and optimization of the networks and their topologies was carried out in the following three stages. During the first stage various training algorithms were tested. During the second stage the most appropriate number of hidden layers as well as the best number of neurons in each hidden layer was determined. In the third stage the influence of the size of the training dataset was investigated. Finally, the optimized ANNs were executed to predict new results in the same knowledge domain.

5.1.1 Datasets and Preprocessing

Two datasets extracted from available literature were used in the present work. One contained 101 independent fretting wear tests of PA 46 composites [36, 280]. The other was obtained from RTP Company [310]. It consisted of 93 groups of independent Izod impact, tension and bending tests of PA 66 composites. All measured parameters are listed in Table 5.1. The input variables include the material compositions (volume or weight fraction of the matrix, short fibers and fillers), the testing conditions (temperature, normal force, and sliding speed) for PA 46, and the manufacturing process (i.e. impact modification) of PA 66 composites. The output variables were the characteristic tribological properties of PA 46 composites (frictional coefficient and specific wear rate), and the mechanical properties of PA 66 composites (Izod impact energy, tensile and flexural strength, tensile and flexural modulus). It should be noted here that the following entries were used for indicating whether or not impact modification was applied: “1” ≡ yes; “0” ≡ no.

Table 5.1: Measured parameters and values used for input and output of ANN

	PA 46 composites	**PA 66 composites**
Input		
Material compositions	Matrix (69-100 vol.%)	Matrix (40-100 wt.%)
	Fiber (0-25 vol.%)	Fiber (0-60 wt.%)
	Filler (0-12 vol.%)	Filler (0-20 wt.%)
Testing conditions	Temperature (20-150°C)	/
	Normal force (10-30 N)	/
	Sliding speed (0.02-0.2 m/s)	/
Manufacturing process	/	Impact modification (0 or 1)
Output		
Mechanical properties	/	Izod impact energy with notched or unnotched specimens
	/	Tensile strength
	/	Tensile modulus
	/	Flexural strength
	/	Flexural modulus
Tribological characteristics	Frictional coefficient	/
	Specific wear rate	/

5.1.2 Optimization of ANN Architecture

There are many training algorithms (learning rules) using various strategies to optimize the performance of a neural network i.e. to yield a fast, robust and accurate neural network. However, different algorithms perform best on different problems [311]. In this respect, to choose the right one is the first challenge that should be solved before using the network for prediction. In the present work, five most commonly used training algorithms provided in the neural network toolbox of Matlab were studied and compared, namely: a) the Powell-Beale conjugate gradient algorithm, b) the gradient descent algorithm with momentum, c) the scaled conjugate gradient

algorithm, d) the BFGS quasi-Newton method, and e) the Levernberg-Marquardt algorithm, as listed in Table 5.2 (for detailed knowledge, q.v. [184, 312]).

Table 5.2: Learning algorithms used to train the ANN with brief descriptions [184, 286, 312]

Algorithm	**Acronym**	**Matlab code**	**Description**
Conjugate gradient with Powell/Beale restarts algorithm	CGB	traincgb	Generally has a faster rate of convergence
Gradient descent algorithm with momentum	GDM	traingdm	Faster than basic gradient descent algorithm
Scaled conjugate gradient algorithm	SCG	trainscg	The conjugate gradient algorithm requires no line search
BFGS quasi-Newton algorithm	BFG	trainbfg	Usually converges in fewer iterations but requires estimating Hessian matrix
Levenberg-Marquardt algorithm	LM	trainlm	One of the fastest training algorithms for networks of moderate size

The analysis of performance was done in the same environment and according to two parameters: prediction accuracy and computational cost. For each datasets mentioned in the previous subchapter, three networks with different hidden layer configurations were used in order to eliminate the disturbance of network structure (Table 5.3). The selection of the neurons in the hidden layer(s) was decided by using the rule of thumb. All the networks had 9 input variables (material compositions and testing conditions) and 1 output: specific wear rate for the dataset of PA 46; tensile strength for the dataset of PA 66. During the evaluation, the network was trained by 80 data, and tested by 10 data. All data were randomly selected from the datasets. For the sake of minimizing the accident error, this training and testing process was independently repeated 100 times. In order to facilitate the comparisons of performance for different network configurations, mean relative error (MRE) was introduced as a criteria (q.v. equation 2.16, subchapter 2.2.1). Obviously, the lower MRE becomes, the better the prediction quality of the network is.

Table 5.3: Network structures used for analysis of learning algorithm

Dataset of PA 46	**Dataset of PA 66**
9-$[3]_1$-1	9-$[2]_1$-1
9-$[3\text{-}1]_2$-1	9-$[3]_1$-1
9-$[9\text{-}4\text{-}2]_3$-1	9-$[3\text{-}1]_2$-1

In Fig. 5.1 and Fig. 5.2, the values of MRE and computation time are given for each learning algorithm and network structure, respectively.

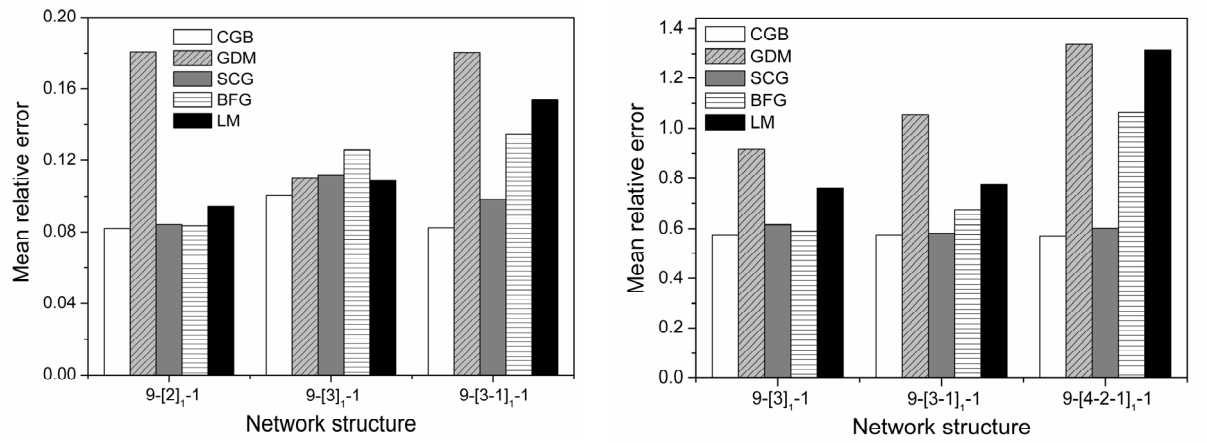

(a) (b)

Figure 5.1: A comparison of the prediction quality of various learning algorithms (a) prediction of tensile strength based on PA 66 dataset, (b) prediction of specific wear rate based on PA 46 dataset [225, 287]

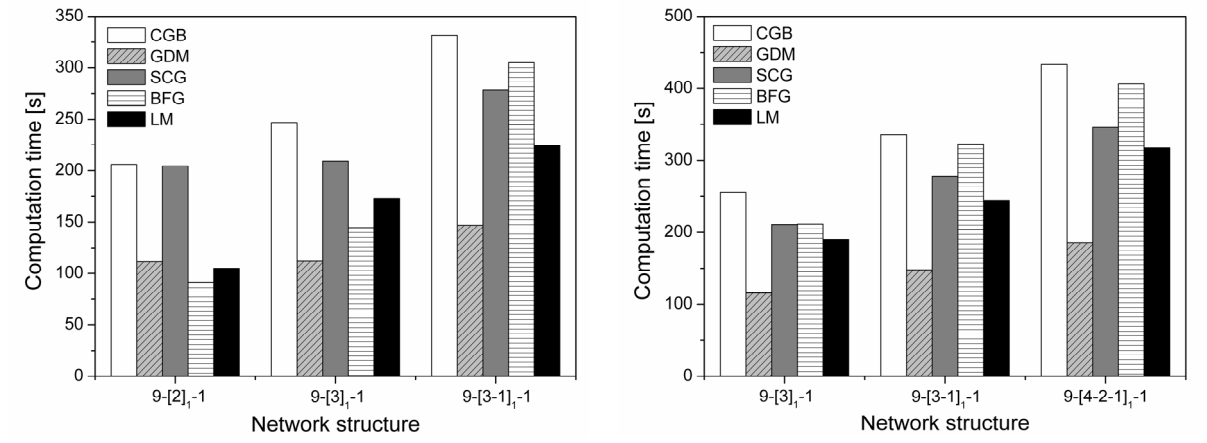

(a) (b)

Figure 5.2: A comparison of the computation time of various learning algorithms (a) prediction of tensile strength based on PA 66 dataset, (b) prediction of specific wear rate based on PA 46 dataset [225, 287]

It is difficult to generalize from these results which algorithm is evidently superior. For example, the GDM algorithm consumed the least time, but its prediction quality was less satisfactory. On the other hand, the SCG algorithm can give acceptable prediction accuracy, but only at a quite low speed. The CGB algorithm gave the highest prediction accuracy among the five algorithms, though it also consumed the most time. Yet, taking into account that the training and testing process was independently repeated 100 times, the difference of computation cost of these algorithms for a single training and prediction process was trivial (on the order of several seconds). Therefore, the CGB algorithm was considered to fit the present case better than the others and was selected to be used in the following work.

The next task was to determine the neural network topology, which includes the number of hidden layers and processing elements in each layer. The number of neurons in the input and output layers is governed by the dimensionality of the corresponding problem. However, there is no proven best answer or rule to define the optimum network topology for a particular application. This makes the task seem more like an “art” for the network designer [313]. Only some general strategies were picked up over time and followed by researchers (q.v. subchapter 2.2). In Fig. 5.3, a network possessing 9 input variables (material compositions and testing conditions) and 1 output variable (frictional coefficient or specific wear rate) was used to show the dependence of the prediction precision on the network complexity.

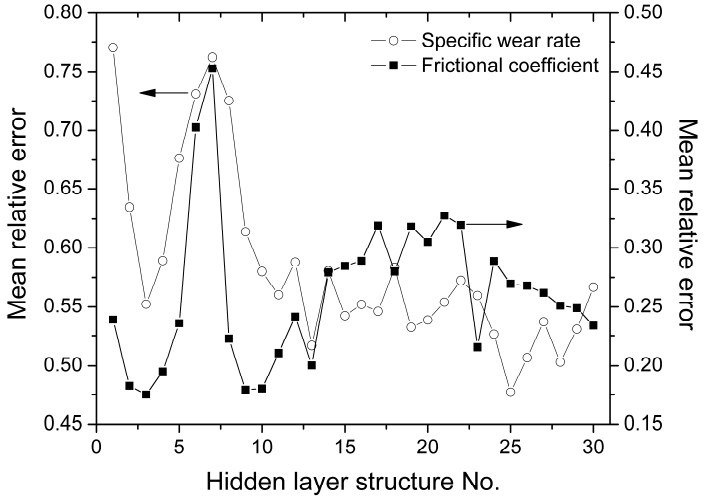

Figure 5.3: Dependence of mean relative error on the hidden-layer structure for the wear properties of PA 46 composites. The X-coordinate represents the network structure No., which can be found in Table 5.4 [225, 287]

Here, the X-coordinate refers to the network structures, which are listed in Table 5.4.

Table 5.4: Tested ANN architectures

No.	Hidden-layer structure PA 46 dataset	Hidden-layer structure PA 66 dataset	No.	Hidden-layer structure PA 46 dataset	Hidden-layer structure PA 66 dataset
1	9-$[1]_1$-1	9-$[1]_1$-6	16	9-$[8\text{-}2]_2$-1	9-$[8\text{-}6]_2$-6
2	9-$[2]_1$-1	9-$[2]_1$-6	17	9-$[10\text{-}4]_2$-1	9-$[10\text{-}1]_2$-6
3	9-$[3]_1$-1	9-$[3]_1$-6	18	9-$[12\text{-}1]_2$-1	9-$[10\text{-}6]_2$-6
4	9-$[4]_1$-1	9-$[4]_1$-6	19	9-$[12\text{-}4]_2$-1	9-$[12\text{-}1]_2$-6
5	9-$[6]_1$-1	9-$[5]_1$-6	20	9-$[13\text{-}4]_2$-1	9-$[12\text{-}6]_2$-6
6	9-$[12]_1$-1	9-$[6]_1$-6	21	9-$[14\text{-}4]_2$-1	9-$[15\text{-}1]_2$-6
7	9-$[18]_1$-1	9-$[9]_1$-6	22	9-$[15\text{-}2]_2$-1	9-$[15\text{-}6]_2$-6
8	9-$[1\text{-}1]_2$-1	9-$[12]_1$-6	23	9-$[4\text{-}2\text{-}1]_3$-1	9-$[16\text{-}8]_2$-6
9	9-$[2\text{-}1]_2$-1	9-$[18]_1$-6	24	9-$[9\text{-}4\text{-}2]_3$-1	9-$[4\text{-}3\text{-}2]_3$-6
10	9-$[3\text{-}1]_2$-1	9-$[1\text{-}1]_2$-6	25	9-$[12\text{-}6\text{-}3]_3$-1	9-$[6\text{-}4\text{-}2]_3$-6
11	9-$[3\text{-}3]_2$-1	9-$[2\text{-}1]_2$-6	26	9-$[12\text{-}9\text{-}6]_3$-1	9-$[9\text{-}6\text{-}3]_3$-6
12	9-$[4\text{-}3]_2$-1	9-$[3\text{-}2]_2$-6	27	9-$[15\text{-}9\text{-}6]_3$-1	9-$[12\text{-}9\text{-}11_3$-6
13	9-$[5\text{-}1]_2$-1	9-$[5\text{-}1]_2$-6	28	9-$[15\text{-}12\text{-}6]_3$-1	9-$[12\text{-}9\text{-}6]_3$-6
14	9-$[5\text{-}3]_2$-1	9-$[5\text{-}4]_2$-6	29	9-$[30\text{-}15\text{-}7]_3$-1	9-$[15\text{-}9\text{-}1]_3$-6
15	9-$[6\text{-}4]_2$-1	9-$[8\text{-}1]_2$-6	30	9-$[50\text{-}25\text{-}12]_3$-1	9-$[15\text{-}12\text{-}6]_3$-6

The evaluation was similar to that in the previous analysis for the learning algorithm. The network was trained by 80 data, and then tested by 10 data. This procedure was repeated 200 times. For the sake of saving computation time, the maximum number of iterations (epochs) was reduced by about 30%. This slightly lowered the prediction accuracy as compared to the above results. It was found, especially for the single hidden-layer network, that the mean relative error decreases with the increase of neurons in a certain range, and then increases again when more neurons are added (Fig. 5.3). The curves show that a network consisting of a single hidden layer with 3 neurons gave the best prediction quality for the frictional coefficient, whereas a structure of three hidden layers 9-$[12\text{-}6\text{-}3]_3$-1 yielded the lowest MRE for the specific wear

rate of PA 46 composites. Although it has been proven that a neural network necessitates at most two hidden layers to approximate any function to an arbitrary order of accuracy [216], this outcome indicates that for more complicated problems (i.e. wear evaluation), for which the output is a function of numerous parameters, the description of the relationship between output and inputs requires more elaborate architecture of the network.

Fig. 5.4 shows, for comparison, the results of PA 66 composites generated by a network with 9 inputs (compositions and manufacturing process) and 6 outputs (strength and modulus). The training and testing procedures were similar to the previous one, and the structures can also be found in Table 5.4.

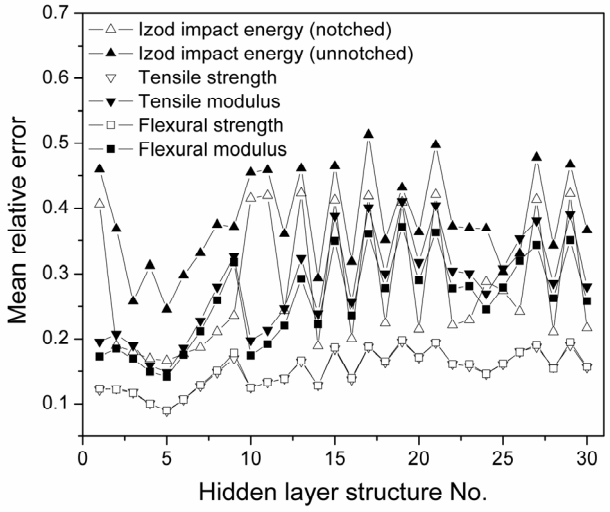

Figure 5.4: Dependence of the mean relative error on the hidden-layer structure for the mechanical properties of PA 66 composites. The X-coordinate represents the network structure No., which can be found in Table 5.4 [225, 287]

A structure of 9-$[5]_1$-6 was proved to achieve the lowest mean relative error for every output variable. The saturation state was also clearly evident for the single hidden-layer network. It should be noticed that the prediction quality of unnotched Izod impact energy was not as good as for the other mechanical properties. This can be attributed to the heterogeneity of the intact specimen, which resulted in a larger instability of the measured results.

Multi-dimensional modeling is among the key advantages of ANNs. As compared to other phenomenological modeling techniques, i.e. multiple regression analysis (MRA), the neural network possesses a strong capability to explore the interconnections be-

tween multiple input and output variables concurrently. Fig. 5.5 presents a comparison between the prediction quality of single output and multiple output networks for the frictional coefficient and specific wear rate of PA 46 composites.

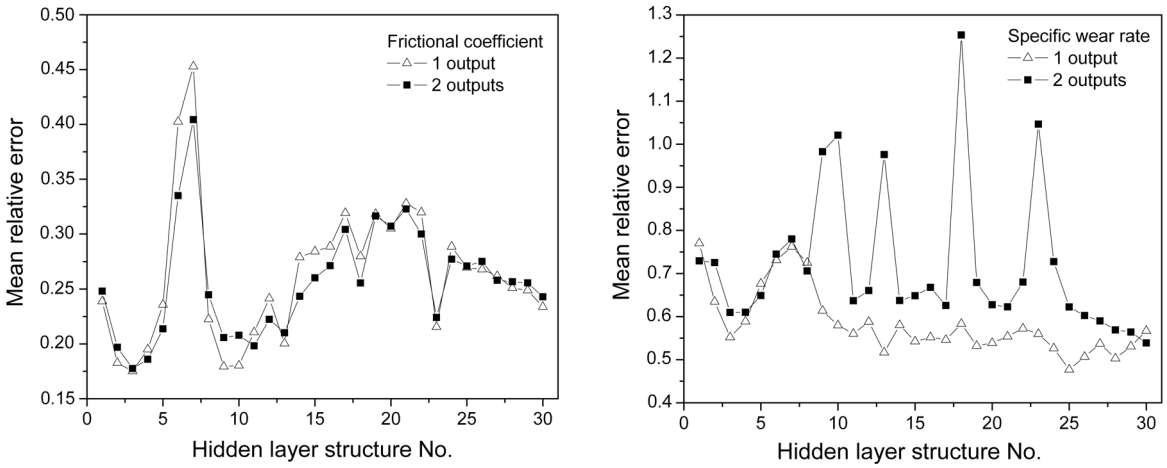

(a) (b)

Figure 5.5: Influence of the output number on the prediction quality for the wear properties of PA 46 composites (a) frictional coefficient, (b) specific wear rate. X-coordinate represents the network structure No., which can be found in Table 5.4 [225, 287]

While for the frictional coefficient the performance of both configurations was very similar (Fig. 5.5a), for the specific wear rate of PA 46 composites (Fig. 5.5b), the prediction results of the two-output network were subordinate to those of the single-output network. With reference to the mechanical properties (Fig. 5.6), although the required number of neurons for the maximum performance decreased with the reduced number of output variables, the distinction between the best results was barely noticeable. Taking into account the computation time, the multi-output network exhibited better efficiency. Furthermore, it can be found in Fig. 5.5b and Fig. 5.6b that the mean relative error is likely to increase sharply when the number of neurons in the last hidden layer is less than that in the output layer, i.e. $N_h < N_{out}$. Based on these results as well as the work of Zhang et al. [238] it can be concluded that the one-output neural network is recommended for achieving high level of prediction in practical engineering cases, especially when handling complex phenomena. In some cases, a multi-output neural network might be used to model some relatively simple problems due to its higher computation efficiency.

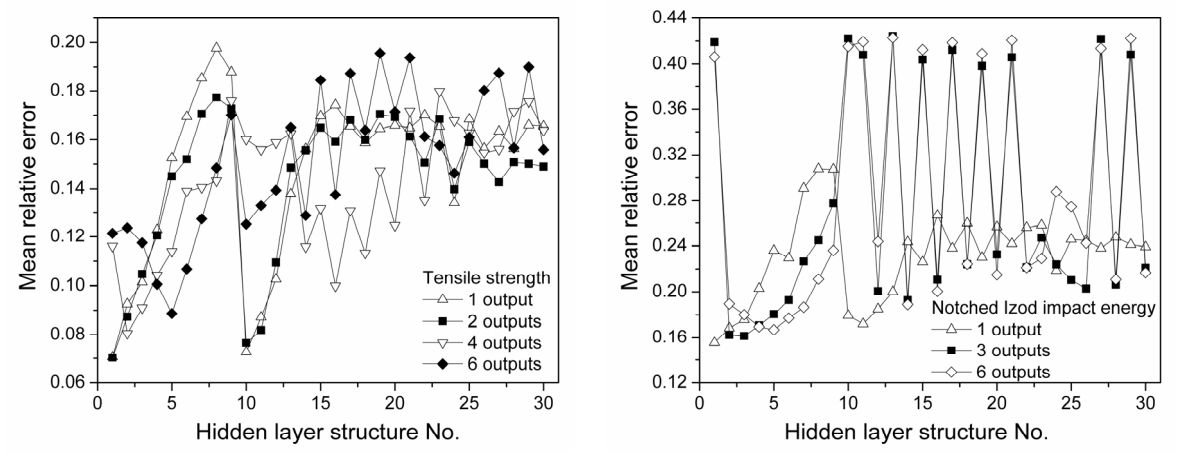

(a) (b)

Figure 5.6: Influence of the output number on the prediction quality for the mechanical properties of PA 66 composites (a) tensile strength, (b) notched Izod impact energy. X-coordinate represents the network structure No., which can be found in Table 5.4 [225, 287]

As a final point of the methodology study, the size of the training dataset was analyzed. The size of the training dataset is a very important aspect that also largely controls the predictive quality of the network. Fig. 5.7 provides a comparison of the different number of training data in terms of mean relative error for characteristic tribological properties determined on a PA 46 dataset as well as for mechanical properties on a PA 66 dataset. The utilized ANN architectures were 9-$[3]_1$-1 for frictional coefficient, 9-$[12\text{-}6\text{-}3]_3$-1 for specific wear rate and 9-$[5]_1$-6 for the mechanical properties. By applying curve fitting on the corresponding results, it is likely that MRE will be diminished to a stable level (0.1-0.2) when the number of training data reaches 180 for the tribological and 90 for the mechanical properties. This outcome might be related to the fact that wear is a complex phenomenon that is affected by many factors and is more likely to incur data scattering during testing. Similar results were established by Scott et al. [276] and Zhu et al. [290]. Accordingly, it can be concluded that the required amount of training data to export prediction results with high accuracy depends on the complexity of the property or behavior modeled.

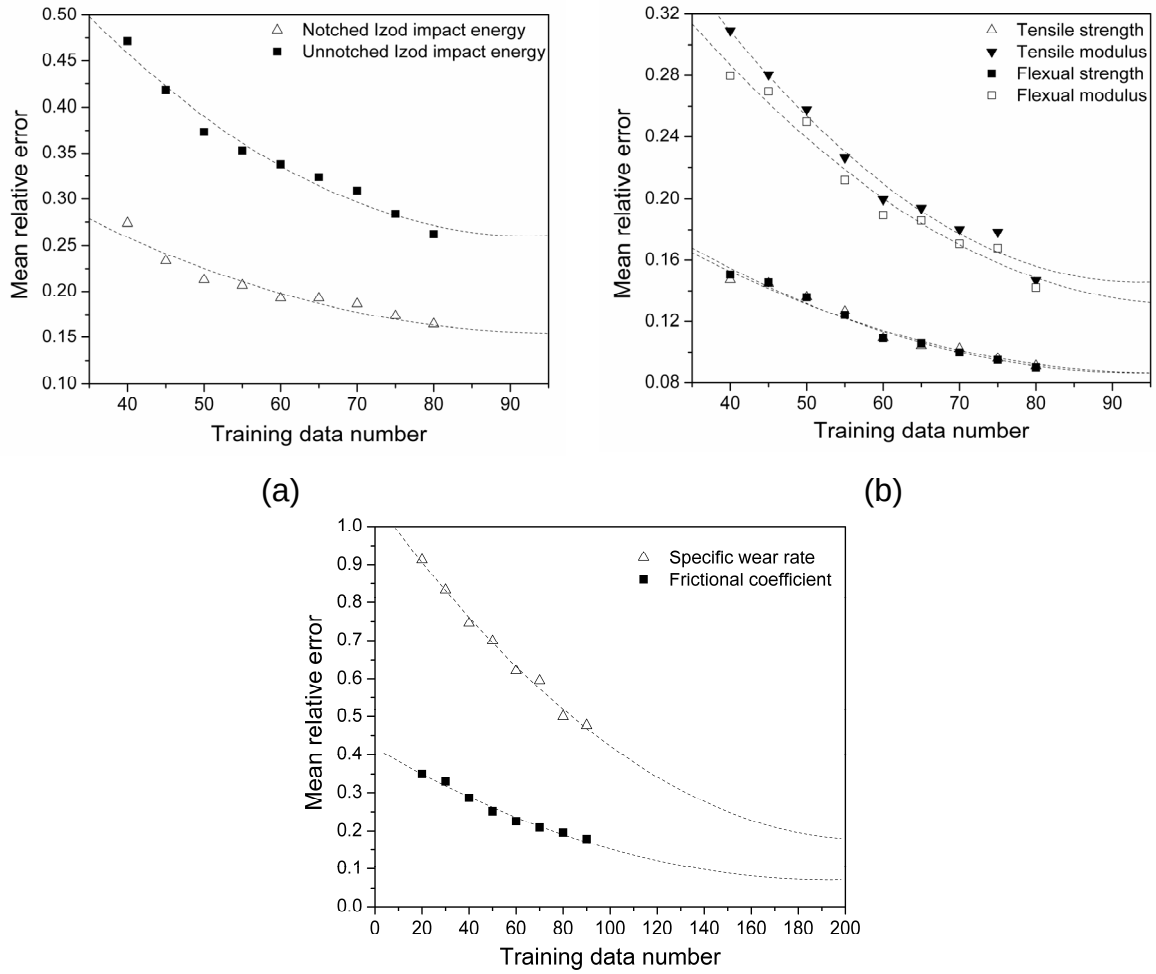

Figure 5.7: Dependence of the prediction quality (mean relative error) on the number of training data for (a) and (b) characteristic mechanical properties of PA 66 composites, (c) characteristic tribological properties of PA 46 composites [225, 287]

5.1.3 ANN Prediction

In the previous two subchapters, the optimal training algorithm and ANN topology were analyzed. For the sake of achieving the highest possible prediction quality, the optimized networks were trained by the whole experimental dataset. In this part the trained ANN models were tested for their interpolation capability using only input variables that had never been experienced by the networks. Still, most of them lie within the boundary of the existing training dataset because the extrapolation performance of an ANN for non-sampled points is unjustified and dangerous.

The predicted three-dimensional (3D) profiles of the frictional coefficient and specific wear rate for PA 46 composites as a function of glass fiber- and PTFE- volume content are displayed in Fig. 5.8. The predicted profiles exhibit good agreement with the measured data (dots with error bars). Furthermore, the prediction discloses the effect of the filler loading fraction on the friction and wear resistance. A continuous increase in the wear resistance is visualized with the increase of the volume content of both PTFE and short glass fibers. The lowest wear zone occurs at loading fractions of PTFE ≥ 5 vol.% and GF ≥ 10 vol.%. In this case, the wear is accompanied also by very low frictional coefficients (≈ 0.2).

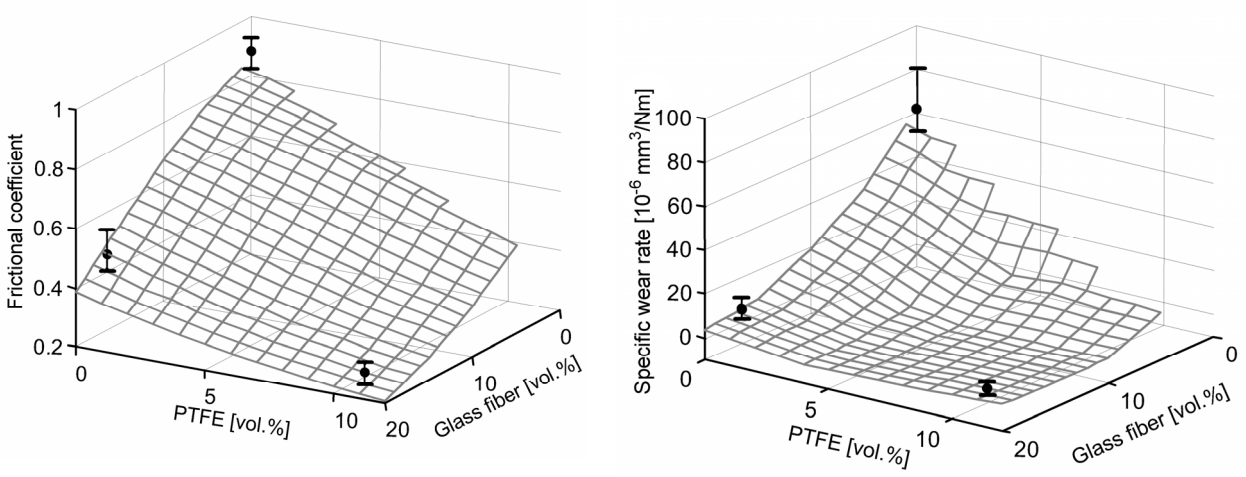

(a) (b)

Figure 5.8: Predicted tribological properties of PA 46 composites as functions of glass fiber- and PTFE- volume content at F_N = 10 N, v = 0.04 m/s, T = 20°C (a) frictional coefficient and (b) specific wear rate. The measured data points are plotted as black dots with error bars [225, 287]

The prediction of the friction and wear properties as a function of the corresponding testing conditions (normal force and sliding speed) was also performed by the trained networks (Fig. 5.9). The predicted profiles inferred that the sliding speed is more influential for the frictional coefficient, while the normal force seems more dominant for the specific wear rate. Yet, the speed dependence of the frictional coefficient within the experimental conditions appears to approach a steady state plateau at high loads (> 10 N); whereas wear starts to accelerate rapidly as the severity of the contact increases (especially with an increase in pressure or both pressure and speed).

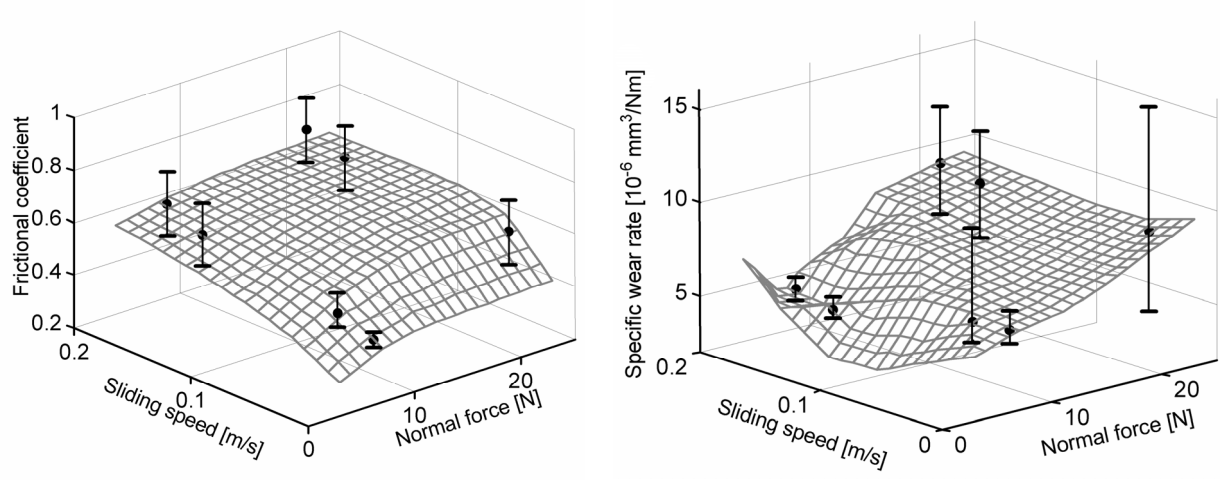

(a) (b)

Figure 5.9: Predicted tribological properties of PA 46 composites as functions of testing conditions at 20°C (a) frictional coefficient and (b) specific wear rate. The measured data points are plotted as black dots with error bars [225, 287]

Fig. 5.10 displays a series of mechanical properties of PA 66 composites simultaneously predicted by the trained ANN. The actual measured data points, marked as black dots, are plotted as check data. In these 3D profiles, a noticeable reinforcing effect can be visibly recognized with the increase in carbon fiber loading fraction. However, the incorporation of PTFE either alone or as a third phase leads to a slight deterioration in the composite strength, especially when its loading fraction reaches high values. In contrast to the other predicted mechanical properties, the prediction for the unnotched Izod impact strength displays a steep drop in its value for carbon fiber loadings between 0 and 10 wt.%. This is then followed by a continuous increase with higher weight fractions of carbon fibers (≥ 10 wt.%). The observed drop is a result of the network only being trained on the available data at 0 wt.% and 10 wt.%. No commercial data was available for the intermediate region, which is therefore not that well defined. Physically, this decrease in impact strength could be explained by the inability of the carbon fibers at low weight fractions to suppress fracture initiation, while at higher loading fractions the fibers effectively interact with the matrix to prevent crack initiation and propagation.

The prediction quality was better for the mechanical properties than for the tribological ones. From this, it can be inferred that the underlying dependence of the mechanical properties on material composition is more straightforward than that of the

wear parameters. Finally, the results of this section demonstrate that ANNs represent an effective way to test friction and wear correlational parameters and determine their severity.

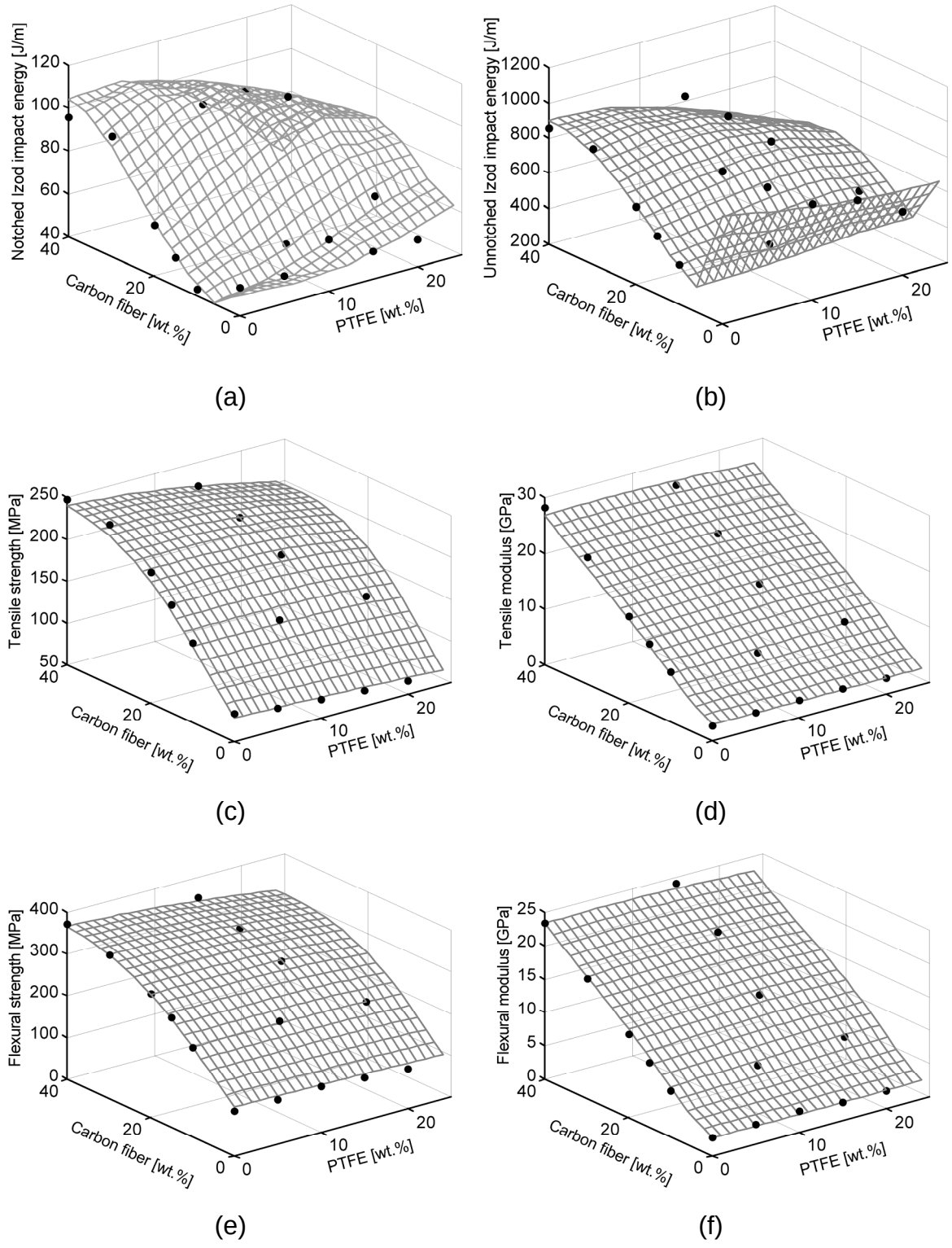

Figure 5.10: Predicted mechanical properties of PA 66 composites as functions of carbon fiber- and PTFE- volume content [225, 287]

5.2 Sliding Friction and Wear of PPS Matrix Composites: Experimental and ANN Approach

5.2.1 Datasets, Learning Algorithm and ANN Architecture

In order to build a well balanced model, it is important to collect a suitable dataset. Likewise, it is significant when training a neural network to collect data, which covers the entire operating range of the system at a sampling rate sufficient to capture its generalizable behavior [196]. Following these rules, a new measurement series was performed with PPS matrix composites. Five training datasets were collected or expanded throughout a period of three years (Fig. 5.11).

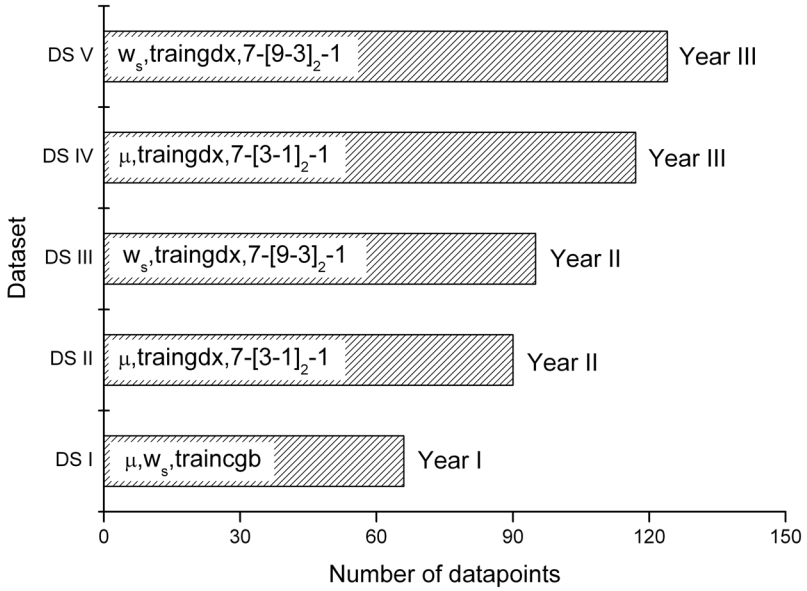

Figure 5.11: Datasets, learning algorithm and architecture of the ANN for sliding friction and wear prediction with PPS matrix composites

All datasets used for training and prediction (Fig. 5.11) are described in Table 5.5 and include the material compositions (volume fraction of matrix, reinforcing agents, lubricants and fillers), testing conditions (pressure and sliding speed) as well as some characteristic mechanical and thermo-mechanical properties of the PPS composites (e.g. tensile and compressive properties tested at room temperature along with DMTA properties determined in the range 23-230°C) as input parameters; the output parameters were the tribological properties (frictional coefficient and specific wear rate). In addition, the input variables in these datasets were classified as primary (material compositions and testing conditions) and secondary (mechanical and

thermo-mechanical properties). 80-90% of the data in each dataset was used for training, the remaining 10-20% of the dataset was utilized for testing the ANN. The experimentally measured values are presented in Table A1 in the appendix.

Table 5.5: Measured parameters and values used for input and output of the ANN

Input				
Material compositions	PPS matrix (65-100 vol.%)	Short carbon fiber (0-20 vol.%)	TiO_2 (0-7 vol.%)	PTFE (0, 5, 10 vol.%) Graphite (0, 5, 10 vol.%)
Testing conditions	Sliding speed (1, 3 m/s)	Applied pressure (1, 2, 3, 4 MPa)		
Mechanical and thermo-mechanical properties	Compressive and tensile properties (modulus, stress and strain)	Notch Charpy impact strength	Microhardness	Glass transition temperature, storage modulus, mechanical loss factor, etc.
Output				
Tribological characteristics	Frictional coefficient	Specific wear rate		

The data for the specific wear rate was initially normalized (logarithmically compressed) and scaled to the range [-1, 1] in order to improve the learning speed as these values fall in the region of the sigmoid transfer function. After training the normalized output values were converted to real values. The transfer functions used were the *tansig* function for the hidden layer and *purelin* function for the output layer. The training and testing processes were repeated 200 times. The maximum number of iterations (epochs) in the training process was set to 1000. The training process stopped when either the value of end iteration was reached or the MRE minimum was attained. The initial weights and biases of the network were generated automatically by the written program. Based on the methodology study (subchapter 5.1) the initially selected learning method with dataset I was CGB (traincgb). However, it has been established within later research activities using an expanded version of dataset I (in total 84 independent data measurement points with PPS matrix composites) that the variable learning rate algorithm GDX (traingdx) performs superiorly over CGB both in terms of replicating the training data (higher accuracy) and rapid convergence. Thus, the GDX algorithm has been used in the further training of the ANN. The initially selected learning rate was 0.02. The computer used for performing the training and prediction was a Pentium (R) 4 CPU at 2.00 GHz to 3.20 GHz.

The optimum network architectures for the frictional coefficient and specific wear rate are displayed in Fig. 5.11. These two network architectures were experimentally found in a train-test procedure with the expanded version of dataset I (in total 84 independent data measurement points with PPS matrix composites). In this train-test procedure the performance of the neural network was continuously monitored by varying systematically both the number of hidden layers (between 1 and 2) and the number of neurons in the hidden layer (between 1 and 20). The train-test procedure was repeated each time the network architecture was modified. Both networks (Fig. 5.11) produced optimum results for the available inputs (i.e. low MRE and acceptable computation time) compared to the other tested combinations.

5.2.2 Effect of Short Carbon Fibers and Sub-micro TiO_2 Particles

Fig. 5.12 compares the frictional coefficient and specific wear rate of the neat polymer matrix with that of the PPS based composites.

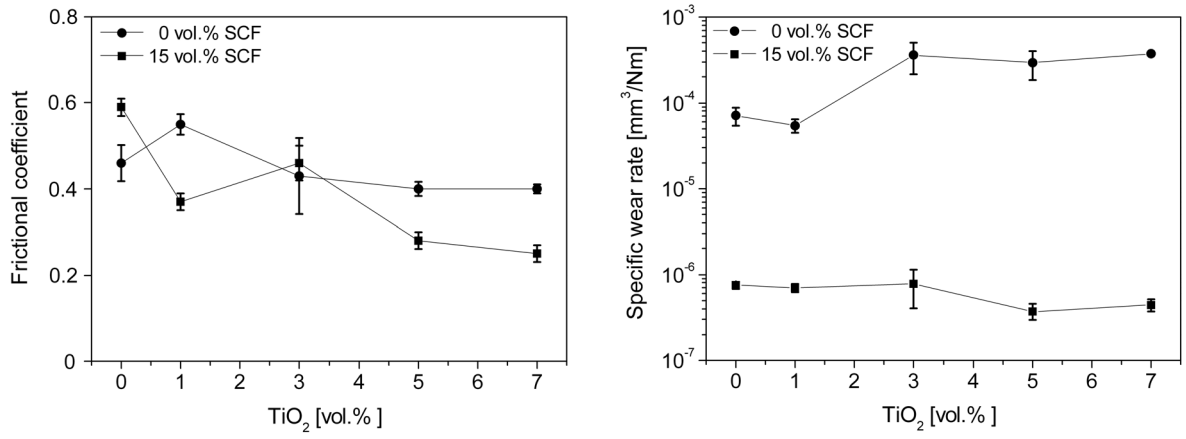

Figure 5.12: Characteristic tribological properties of PPS and PPS-based composites as a function of SCF- and sub-micro TiO_2-volume content (a) frictional coefficient (average value in steady state) and (b) specific wear rate. The testing conditions were: p = 1 MPa, v = 1m/s

The results show that short carbon fibers when acting alone did not cause a decrease, but increased the frictional coefficient of the PPS matrix (Fig. 5.12a). However, the addition of sub-micro (300 nm) TiO_2 particles as third phase did not only neutralize this effect, but even diminished the frictional coefficient by more than a factor of 2 as compared to SCF-reinforced PPS. Regarding the specific wear rate, the sole incorporation of sub-micro (300 nm) particles exerted a detrimental impact on

the wear resistance of the PPS matrix. As a consequence, an upward trend in the specific wear rate originated, especially when the content of sub-micro TiO_2 increased. A significant improvement in the wear resistance (approximately two orders of magnitude) was obtained by adding short carbon fibers, either as a single or as a second reinforcing phase. It has already been reported in previous investigations (summarized in subchapter 2.1.1.1) that short carbon fibers are one of the key fillers for improving the wear resistance of polymers. Likewise, the hybrid synergistic reinforcement of short carbon fibers and sub-micro particles began to reduce the wear rate even more (by a factor of two) when compared to the single reinforcement with short carbon fibers. A similar synergistic effect was established with the addition of TiO_2 nanoparticles (5-10 nm) to hybrid glass/PTFE fabric composites [145].

The success of a neural network depends mainly on its architecture and the size of the collected training data. Throughout this section the impact of these two factors will be illustrated for the specific wear rate of PPS composites. It has been shown above that the network architecture is usually determined in a train-test procedure. The greater the complexity of the considered problem, the larger the number of weights required to model it [196]. As a consequence, too many adjustable parameters might lead to data overfitting - the network no longer generalizing the data but fitting also its noisy peculiarities [314]. In this respect, research activities are directed to the application of the so-called “weight elimination” or “pruning” techniques, which aim to generate a network with as small number of weights as possible. The pruning process involves the following steps: first take an existing network, which adequately fits the data and subsequently remove connections, even whole nodes with their pendant connections, without sacrificing the fitting capabilities of the network. In this respect, it was attempted to determine if network pruning presents advantages over the fully-connected network for predicting the specific wear rate of PPS composites. The OBS algorithm was used to perform the pruning and the GDX learning method to train the network. The OBS algorithm follows the criterion of minimal increase in error on the training data. The increase in the training error (saliency) is evaluated using the Hessian matrix of the second-order derivatives when weights are being eliminated. The weights with the smallest saliency are deleted. After that, the remaining weights are updated (q.v. subchapter 2.2.1). The procedure was applied to a set of 95 independent data measurement points (DSIII, Fig. 5.11). In order to demonstrate

the effectiveness of the proposed OBS algorithm, the whole network (7-[9-3]$_2$-1, Fig. 5.11) was first trained using the GDX algorithm; subsequently the conditioned and insensitive nodes were identified and pruned by the OBS algorithm. Finally, retraining was done with the GDX algorithm keeping the pruned weights equal to zero. Java Neural Network Simulator (JavaNNS), Version 1.1 was used to prune the network (q.v. subchapter 4.7). Training was performed through the Control Panel. In the “Initializing” tab (Fig. 5.13a), an initialization function (“Random Weights” for this particular case) and its parameters (min.: -1.0; max.: 1.0) were adjusted. The “Init” button (also available in the tab “Learning”) completed the initialization.

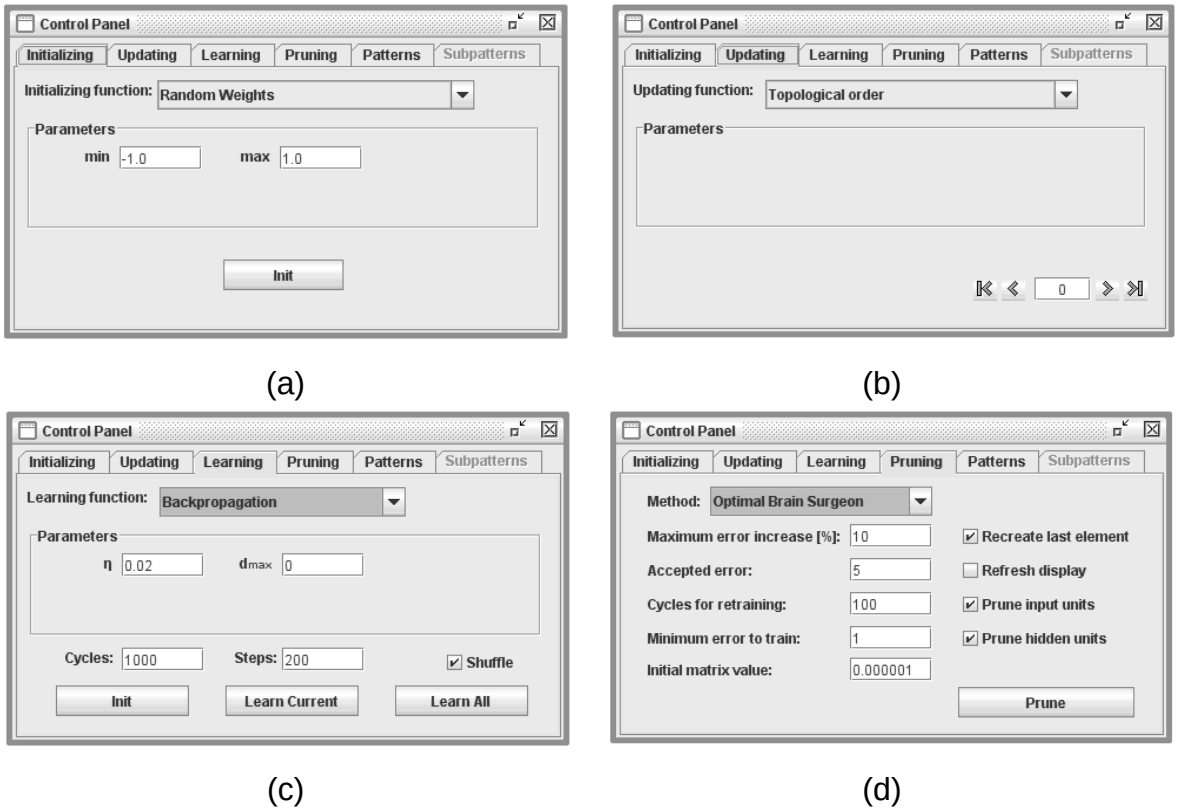

Figure 5.13: Control panel (a) initializing, (b) updating, (c) learning and (d) pruning

The same “Control Panel” tag (Fig. 5.13b) was implemented for selecting the updating function and its parameters for the training stage. “Topological order” was chosen as the updating function. This mode is the most favorable mode for feedforward ANNs. One step is sufficient to propagate information from input to output. With other update modes or with recursive networks, several steps might be needed [308]. In Fig. 5.13c, the button "Learn All" performs training with all patterns from the pattern set. Although activations can be propagated through the network without patterns

defined, learning can be performed only with patterns present. A set of patterns belonging to the same task is called a pattern set. As previously explained, there are in the usual case two pattern sets when dealing with a neural network. One for training the network (training pattern set), and one for testing purposes to check the learning ability of the network (test pattern set).

The parameters selected herein were the learning factor, the number of cycles (epochs) and steps (repeating times). To allow for random selection of the patterns it was necessary to activate “Shuffle”. The chosen options and controls for pruning networks can be found under the Pruning tab (Fig. 5.13d) in the Control Panel.

The architecture of the ANN prior to pruning and after pruning is shown in Fig. 5.14 (a)-(b), respectively. As expected the number of hidden nodes after pruning was strongly reduced from 9 to 2 in the first and from 3 to 2 in the second hidden layer.

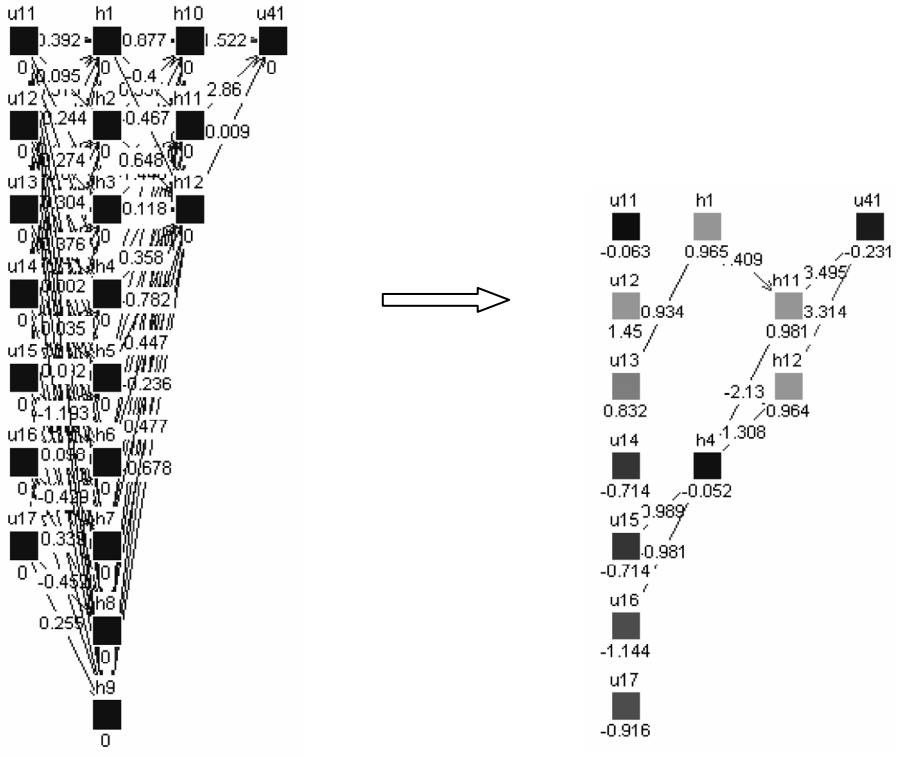

(a) (b)

Figure 5.14: ANN architecture (a) initial and (b) pruned

Next, the computational times of the ANN before and after pruning were also compared. Both networks performed equally well and their results were not significantly different (Table 5.6).

Nevertheless, the refinement of the neural network structure via OBS required exhaustive computations for inputting the data into a format that JavaNNS Software (subchapter 4.7) can recognize i.e. for creating the corresponding network files (containing information on network topology and learning rules) and pattern files (containing information on the training and test data). Therefore, future work is needed to optimize this step.

Table 5.6: Comparison of the consumed time with and without pruning step

Operation	**Consumed CPU time [s]**	
	Network trained	Prediction completed
Train and predict	10.26	1.60
Train, prune and predict	11.13	1.32

The prediction performance of the network before and after pruning is displayed in Fig. 5.15. In both cases the prediction fitted the experimentally generated results reasonably well. Yet, pruning resulted in a somewhat better input-output mapping over the fully connected network. This might be attributed to the elimination of the effect of irrelevant or redundant inputs. Further investigations are required to clarify these results.

It can be observed that there is a sudden drop in the data for the specific wear rate at 10 vol.% (Fig. 5.15). This is due to the fact that at this stage of the study the network was used to predict results only for the discrete fiber volume fractions of 0 vol.%, 10 vol.% and 15 vol.% SCF. No prediction was made for the intermediate concentrations of SCF and the “meshgrid” command in Matlab [306] was used for constructing the 3D surface plots. However, as it will be seen subsequently, at the latest research stage the prediction data for these volume fractions have been generated.

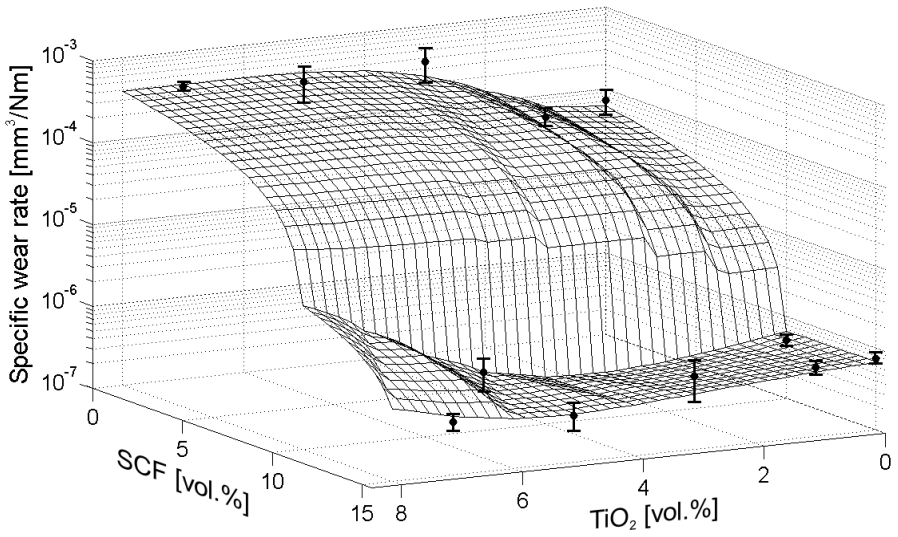

(a)

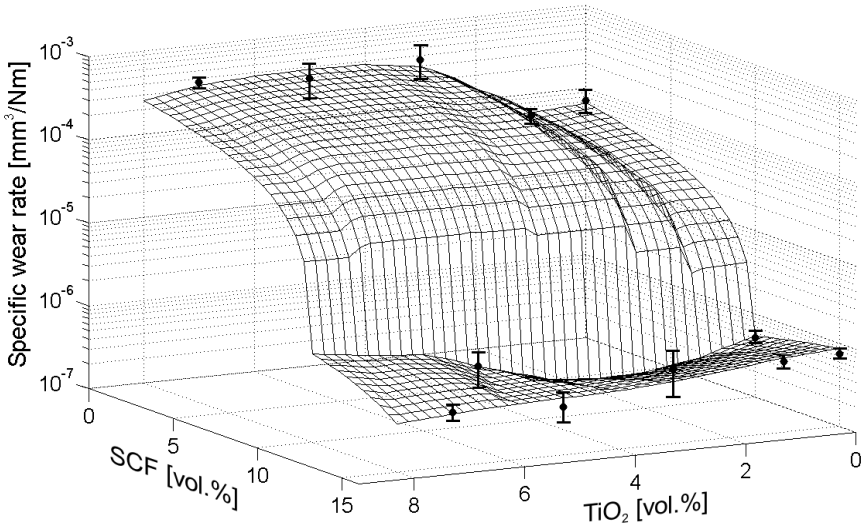

(b)

Figure 5.15: ANN predicted 3D profiles of the specific wear rate as a function of SCF- and sub-micro TiO_2-volume content (a) without pruning, (b) with pruning. The testing conditions were: p = 1 MPa, v = 1m/s

In subchapter 5.1.2. (Fig. 5.7) given above, significant emphasis has been placed on the importance of the number of training points for the quality of a neural network prediction. A comparison of the MRE generated after training of the ANN with the different training datasets (Table 5.7) shows that the predicting performance improves significantly with the enlarged datasets.

Table 5.7: MRE evaluation of output data with the different training datasets

Dataset	Number of data points	Property	MRE
DS I	66	Frictional coefficient	> 0.11
DS I	66	Specific wear rate	> 1.0
DS II	90	Frictional coefficient	0.11
DS III	95	Specific wear rate	0.72
DS IV	117	Frictional coefficient	≤ 0.10
DS V	124	Specific wear rate	≤ 0.55

Fig. 5.16a shows the predicted results as 3D plots of the specific wear rate based on the largest dataset collected in this work (124 independent data points, DS V, Fig. 5.11). In contrast to the former predictions (Fig. 5.15), in this case the prediction was done for the continuous range of carbon fiber loading fraction, namely 0-15 vol.% using an increment value of 1 vol.% prior to applying the “meshgrid” command. Using a smaller increment of fiber volume fraction avoids the sudden drop in the predicted specific wear rate data since the wear rate decreases rapidly as SCF volume fraction increases. As for the concentration range of TiO_2 particles in both cases it was kept the same, namely 0-8 vol.% with 1 vol.% increment value.

It is clearly seen that the predicted results (Fig. 5.16a) are either very close or identical to the corresponding experimentally measured values (plotted as dots with error bars). At this stage it can be concluded that the training of the network is satisfactory, i.e. the network has learnt the complex relationship between the selected input and the corresponding output for the examples presented in the training dataset.

The developed and trained ANN model until now successfully mapped the relationship between various input parameters and the output specific wear rate values. Still, for its practical use it must be checked if it is also able to generalize this relationship. A simple method for ensuring an acceptable level of generalization is to test the network on independent validation dataset (q.v. Table A2 in the appendix) that has not been used in training and testing processes before. The validation of the network model for the specific wear rate is presented in Fig. 5.16b. All validation test points were predicted exactly (or within the error bands limits). These results indicate that the developed ANN model for predicting the specific wear rate is both reasonably correct and able to generalize well.

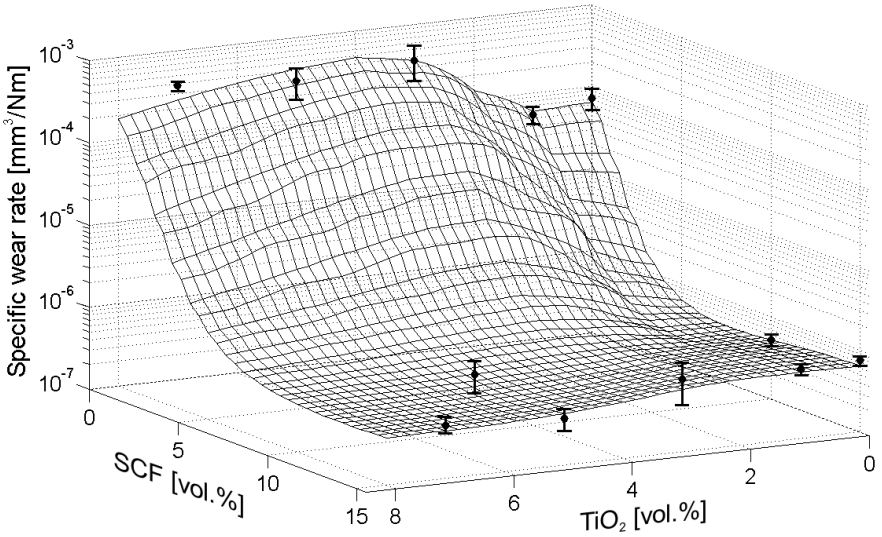

(a)

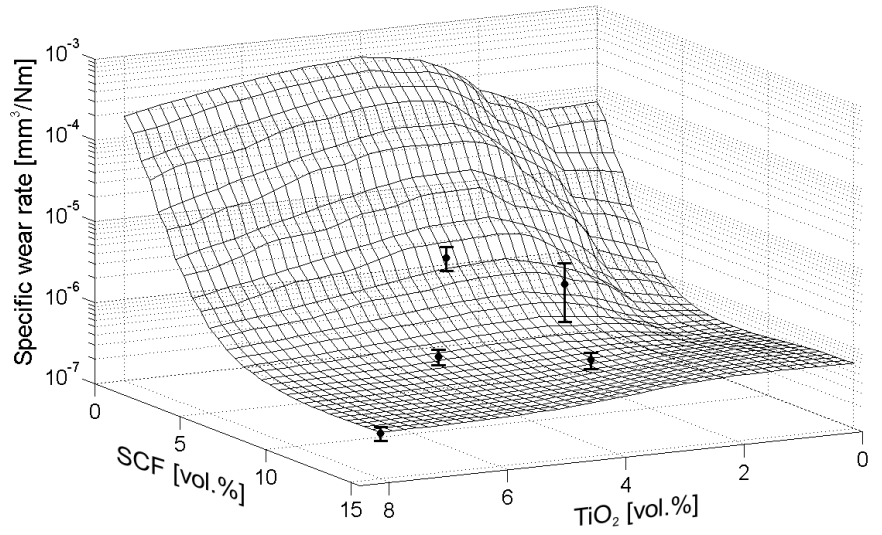

(b)

Figure 5.16: Experimental (black points with error bars) vs. predicted (3D mesh) values of the specific wear rate as a function of SCF- and sub-micro TiO_2-volume content (a) training dataset, (b) validation dataset. The testing conditions were: p = 1 MPa, v = 1m/s

Fig. 5.17a presents the predicted results as 3D plots for the frictional coefficient based on a training dataset of 117 independent data points (DS IV, Fig. 5.11). Similar to the specific wear rate, the predicted results are either close or identical to the corresponding experimentally measured values. Likewise, excellent agreement is observed between the experimentally measured and predicted frictional coefficient val-

ues for the validation test points within the range of the examined experimental conditions (Fig. 5.17b).

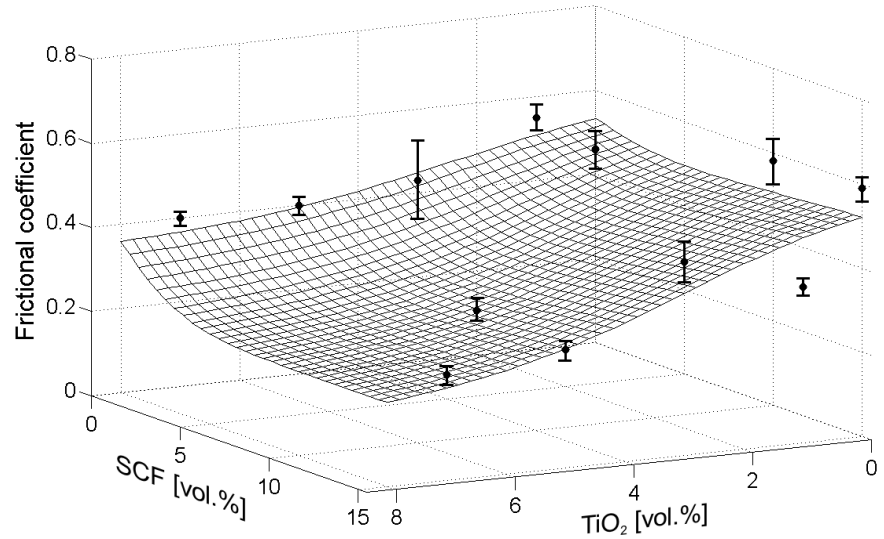

(a)

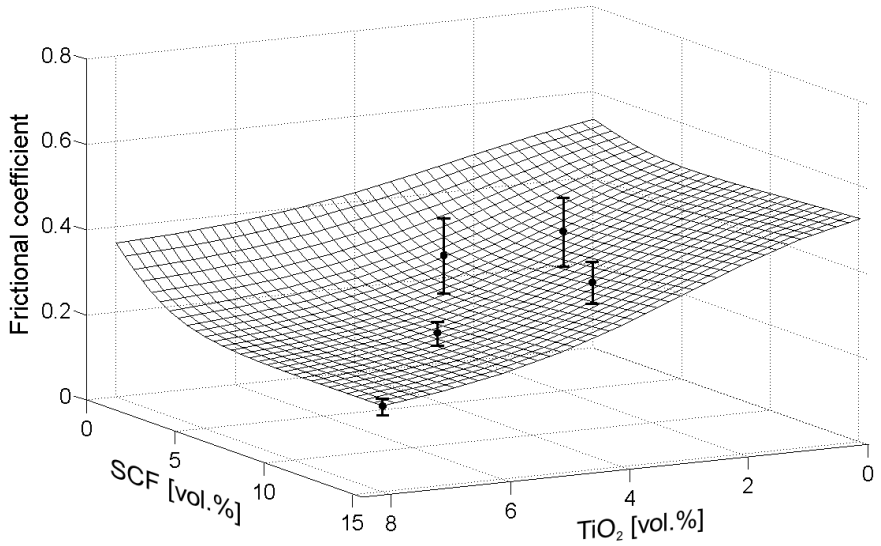

(b)

Figure 5.17: Experimental (black points with error bars) vs. predicted (3D mesh) values of the frictional coefficient (average value in steady state) as a function of SCF- and sub-micro TiO_2-volume content (a) training dataset, (b) validation dataset. The testing conditions were: p = 1 MPa, v = 1m/s

At this stage, it is possible to use the excellent generalization capability of the optimized ANN to analyze the impact of the two fillers, namely SCF and sub-micro TiO_2, on the sliding friction and wear properties of PPS composites over a much broader range without performing exhaustive experimental work. It is obvious from Fig. 5.17 that the combination of the two fillers results in a lower frictional coefficient. Although the mechanisms of reduction in frictional coefficient contributed by each of the two fillers are different, which will be discussed subsequently in subchapter 5.4, it is clear that they can work together simultaneously and make the respective effects superposed. As shown above, short carbon fibers play a key role in improving the wear resistance of PPS, as a single or second reinforcing phase. It is predicted that the specific wear rate decreases with increasing volume fraction of SCF, however less steeply at larger volume fractions (≥ 7 vol.%). With the incorporation of both short carbon fibers and TiO_2 sub-micro particles in PPS matrix, a hybrid reinforcement effect can be found. For higher SCF concentrations (≥ 8 vol.%), the specific wear rate exhibited a drop-off tendency with the increase of TiO_2 content in the range 1-8 vol.%. This type of relationship is in agreement with the experimental results of Friedrich et al. [25] for epoxy composites. Such favorable synergistic effect between carbon fibers and sub-micro TiO_2 has also been envisaged by ANNs in PTFE matrix composites [290]. According to both the experimental results and the ANN prediction, the composition of PPS with 15 vol.% SCF and 8 vol.% TiO_2 (300 nm) gives the best wear resistance (i.e. the lowest specific wear rate).

5.2.3 Effect of Internal Lubricants

The significance of transfer film formation for the tribological performance of a given polymer system is well established in the community and has been illustrated in chapter 2. In this respect solid lubricants are regarded as essential component for achieving the formation of thin, uniform transfer film. Within this work the effects of solid lubricants (PTFE powders and Gr flakes) on the sliding friction and wear performance of a hybrid composite system (PPS reinforced with 10 vol.% SCF and 5 vol.% sub-micro TiO_2) was studied. Fig. 5.18 illustrates the dependence of the frictional coefficient and specific wear rate on the filler content of internal lubricants at standard testing conditions.

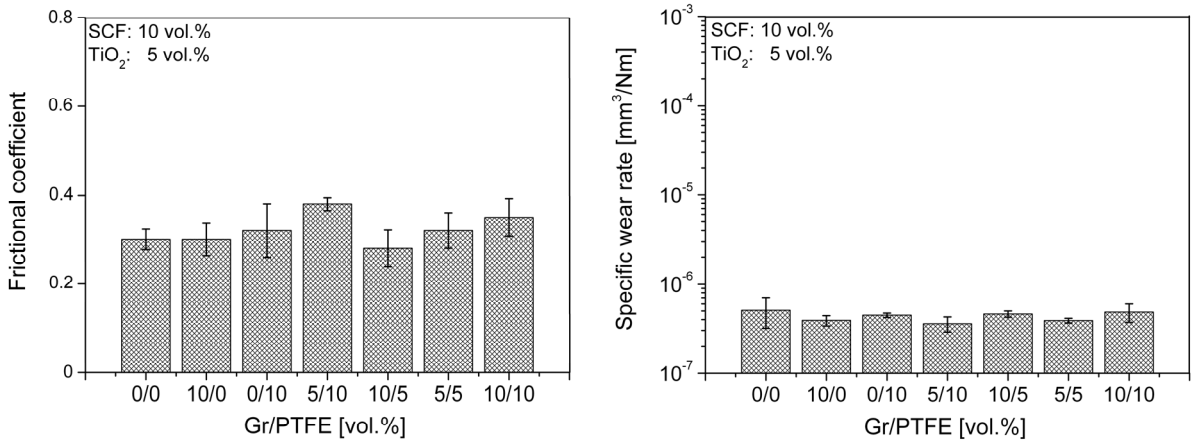

(a) (b)

Figure 5.18: Effect of internal lubricants (Gr and PTFE) on characteristic tribological properties of a hybrid reinforced PPS/SCF/TiO_2 system (a) frictional coefficient (average value in steady state) and (b) specific wear rate. The testing conditions were: p = 1 MPa, v = 1m/s

While for the specific wear rate only marginal or no improvement over the reference material (without internal lubricants) could be recognized, for the frictional coefficient a slight increase resulted with the compositions containing high volume fraction of PTFE (10 vol.%). With the analysis of the ruling wear mechanisms in the following subchapter 5.4.2 an explanation will be given for this effect.

The developed ANN models were also applied for studying the effect of loading fraction of Gr and PTFE in a hybrid reinforced PPS system containing 10 vol.% SCF and 5 vol.% TiO_2. It is readily apparent that the predicted results (Fig. 5.19) exhibit good correlation with the measured values. Under these mild conditions the average frictional coefficient in steady state (Fig. 5.19a) is more or less insensitive to the addition of both lubricants. Nevertheless, as it will be seen subsequently, the addition of internal lubricants induces notable smoothing of frictional oscillations. The specific wear rate shows a decreasing trend when the loading fraction of both fillers is increased up to a center level and then reduces only slightly. Optimum results can be attained with a Gr loading fraction of 3 vol.% and PTFE loading fraction of 6-7 vol.%. Likewise, it can be seen that a high loading fraction of Gr or PTFE (10 vol.%) when acting as single lubricating phase is also beneficial in diminishing wear. The results for the specific wear rate conform well to former experimental results with a PEEK thermoplastic matrix [33].

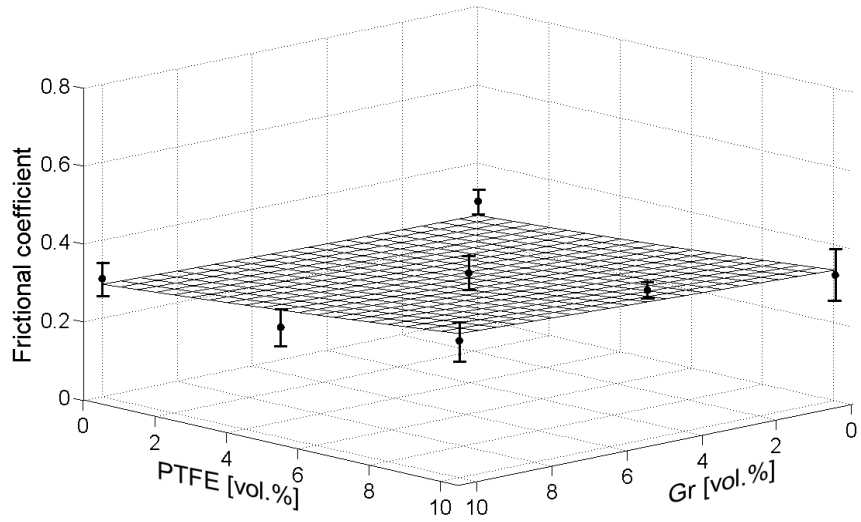

(a)

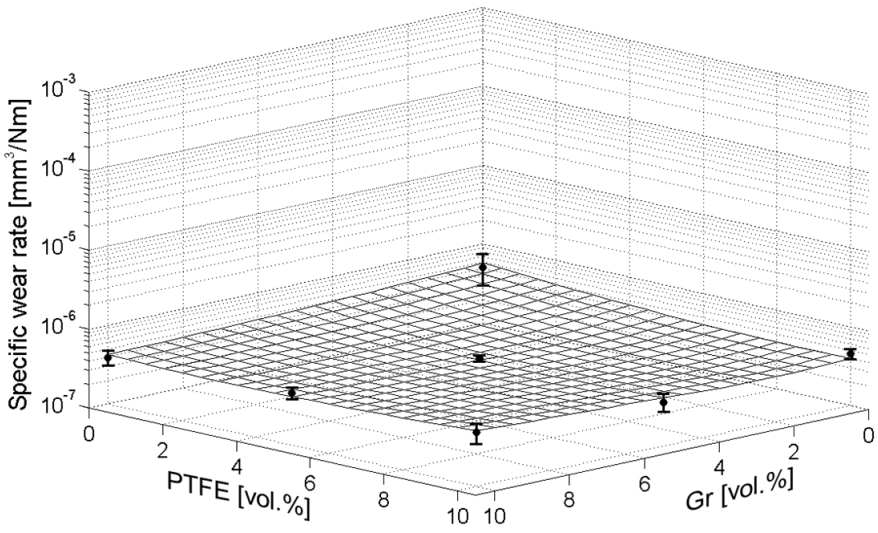

(b)

Figure 5.19: ANN predicted 3D plots of (a) frictional coefficient (average value in steady state) and (b) specific wear rate of a hybrid reinforced PPS/SCF/TiO_2 system as function of Gr- and PTFE-volume content. The measured data are plotted as black points with error bars. The testing conditions were: p = 1 MPa, v = 1m/s

5.2.4 Effect of Operating Parameters

Typical time variations in the frictional coefficient obtained at standard testing conditions are presented in Fig 5.20.

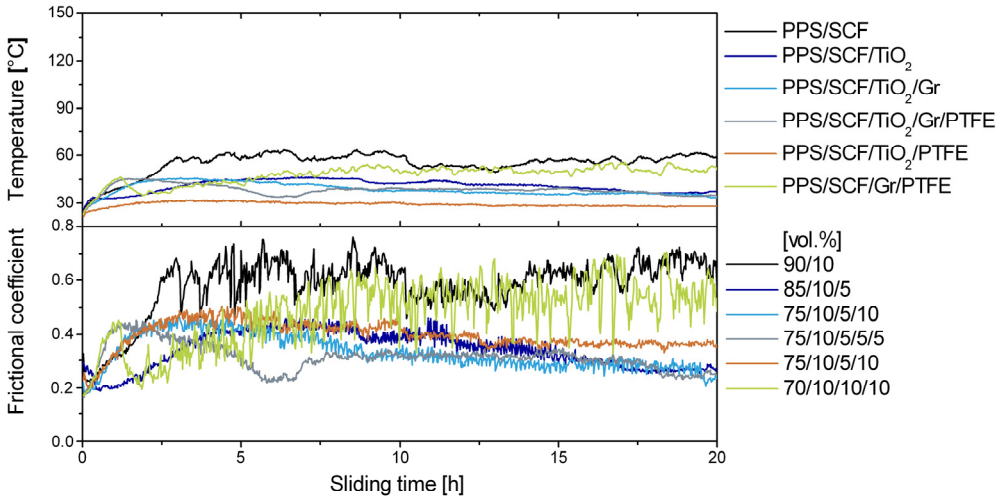

Figure 5.20: Variation of frictional coefficient with sliding time for PPS composites at p = 1 MPa, v = 1m/s

In the initial, running-in period, both sub-micro TiO_2 acting alone or in combination with internal lubricants proved very effective in keeping the frictional coefficient relatively low in short carbon fiber reinforced PPS. Though, the effectiveness of sub-micro reinforcement is revealed to a greater extent in the subsequent steady state. In this longer range, the compositions with TiO_2 (300 nm) demonstrate strongly diminished frictional coefficient when compared to the compounds without TiO_2. Moreover, it can be seen that the materials incorporating TiO_2 in combination with internal lubricants (Gr and/or PTFE) and short carbon fibers generate optimum effects in both, the running-in and subsequent steady state phases. The latter is a consequence of the positive contribution of each reinforcing phase resulting in synergistic interactions, which govern the tribological performance of such a multiphase system. These results are in good agreement with those generated by Zhang and coworkers [25-27].

The measured temperature profiles in the process of sliding follow similar trends. This is expected because nearly all of the energy dissipated in frictional contacts is transformed into heat, i.e. the rate of energy dissipation is directly proportional to the frictional coefficient [300]. No significant influence of the incorporation of internal lu-

bricants to PPS/SCF composite could be seen. This might be related to the slow release and furnishing of the internal lubricants from the polymer matrix to the sliding interface under these operating conditions.

A plot of the frictional coefficient versus time for the same material combinations at higher pressure and speed is shown in Fig. 5.21.

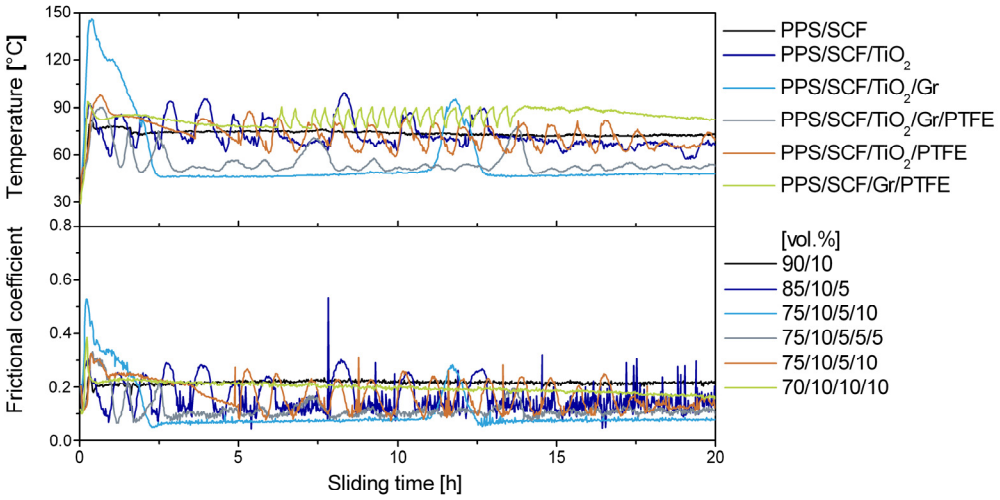

Figure 5.21: Variation of frictional coefficient with sliding time for PPS composites at p = 3 MPa, v = 3 m/s

According to these results, significant reduction of the running-in stage is evident with all composites under higher pv-conditions accompanied with a strong rise in contact temperature. The highest temperature was measured with the composite containing Gr in the running-in period. The hybrid system PPS/SCF/TiO_2 gave erratic behavior typically exhibiting stick-slip. Stick-slip is a phenomenon where the instant sliding speed of a material does not remain close to the average sliding speed, but fluctuates between nearly still periods and moments of very high speed. Stick-slip is found to be a function of the friction and wear mechanisms as well as sliding velocity. A fundamental barrier to smooth sliding occurs when the sliding surfaces are likely to adhere to each other or if the rate of change of the coefficient of kinetic friction as a function of velocity at the particular sliding velocity employed is negative [128, 315].

In comparison with the low pv-factor (Fig. 5.20), where no significant influence could be observed with internal lubricants, the addition of either graphite or graphite in combination with PTFE effectively eliminated the stick-slip sliding motion of the

PPS/SCF/TiO_2 system in the high pv-range. The best results were achieved by the composite with graphite or blending graphite and PTFE. These materials displayed the lowest and almost constant frictional coefficient in steady state. This outcome is in good agreement with trends recognized on similar systems in other polymer matrices [27]. The material containing SCF and a combination of the two internal lubricants displayed no jerky stick-slip motion, but a higher and constant frictional coefficient in steady state than the compositions with additional inclusion of sub-micro TiO_2 particles. This might be related to the fact that with this material no contribution from rolling friction occurs as with the other materials, which effect will be discussed in subchapter 5.5. Equally, the material reinforced by SCF as a single reinforcing phase did not show stick-slip, but the highest measured value of frictional coefficient in steady state. The addition of PTFE as a single lubricating phase to the system PPS/SCF/TiO_2 could eliminate the stick slip sliding motion completely only in the last 3-4 hours. Yet, at severe sliding conditions (12 MPa·m/s) the presence of PTFE in the composite PPS/SCF/TiO_2 caused a complete transition to smooth sliding after merely 5 hours running-in. This might be related to a quicker discharge of the lubricant in the wear process between the two sliding surfaces.

The pv-limit is regarded in general as the performance criterion for tribo-materials and is used to categorize the severity of application [3, 12]. Fig. 5.22 illustrates the interrelationship between the time related depth wear rate and load carrying capacity for diverse material combinations, where the slope of the curve corresponds to the specific wear rate (q.v. equation 1.4, chapter 1). It can be seen that the curve is essentially linear for all compounds in the low, moderate and high pv-range (up to 9 MPa·m/s). This means that within this range the specific wear rate of these materials is independent of both p and v and is equal to the basic wear factor k_0*. Still, in the very high pv-range (12 MPa·m/s) a strong increase in the depth wear rate with almost all compositions resulted. Some even underwent excessive wear accompanied with the formation of lips and trailing strands of material on the downstream side of the worn specimens. This might be associated with a temperature induced drop of the material's properties with rising interfacial temperature [49]. Nevertheless, it becomes clear that the pv-product of the hybrid system PPS/SCF/TiO_2 might be enhanced through the additional incorporation of the two solid lubricants.

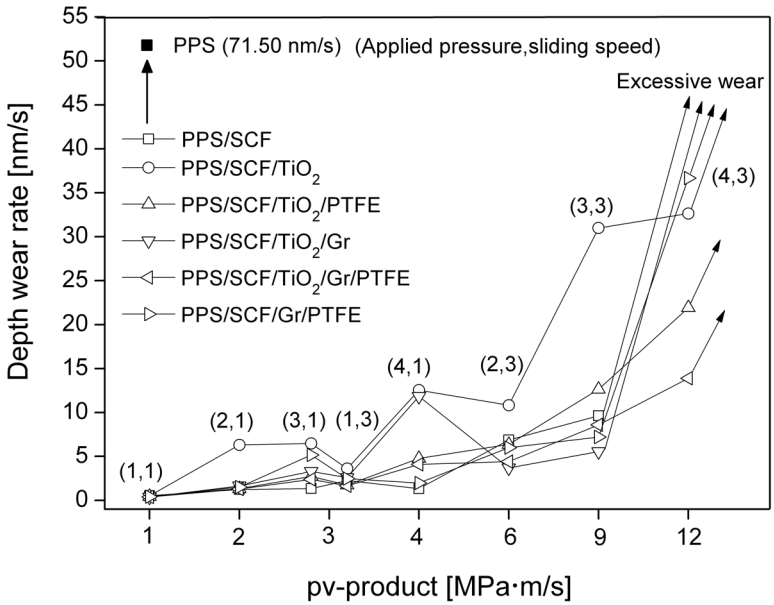

Figure 5.22: Depth wear rate of PPS composites as a function of pv-product

The best results were obtained by blending comparatively low amounts of graphite and PTFE (≈ 5 vol.% from each additive). At higher concentrations (> 10 vol.%), the lubricants combined with TiO_2 were inferior to the wear resistance. It was also interesting to observe that the wear rate of the material containing graphite as a single lubricant (PPS/SCF/TiO_2/Gr composition) showed much higher sensitivity to the applied pressure than to the sliding speed. At low sliding speed (1 m/s) the depth wear rate of this material drastically increased when the applied pressure was raised to 4 MPa and was even much higher than the value measured at 3 MPa and 3 m/s. Further increase in the sliding speed to 3 m/s at 4 MPa led to extreme wear and severe surface damage. The reason for this behavior is believed to lie in the low load carrying capacity of graphite films [316]. Likewise, higher loads might raise the contact temperature and strain energy more than the sliding speed, resulting in a higher level of disruption and shear deformation [317]. Such load dependence of graphite on the tribological behavior of a composite has already been established by Zhan and Zhang [318]. At low loads graphite particles imparted the composites with good tribological characteristics, whereas at high loads high loading fraction of graphite deteriorated the mechanical properties and resulted in delamination wear.

Fig. 5.23 displays the simultaneous functional dependence of the frictional coefficient and specific wear rate with respect to the sliding speed and applied pressure for the composition PPS with 10 vol.% SCF and 5 vol.% TiO_2.

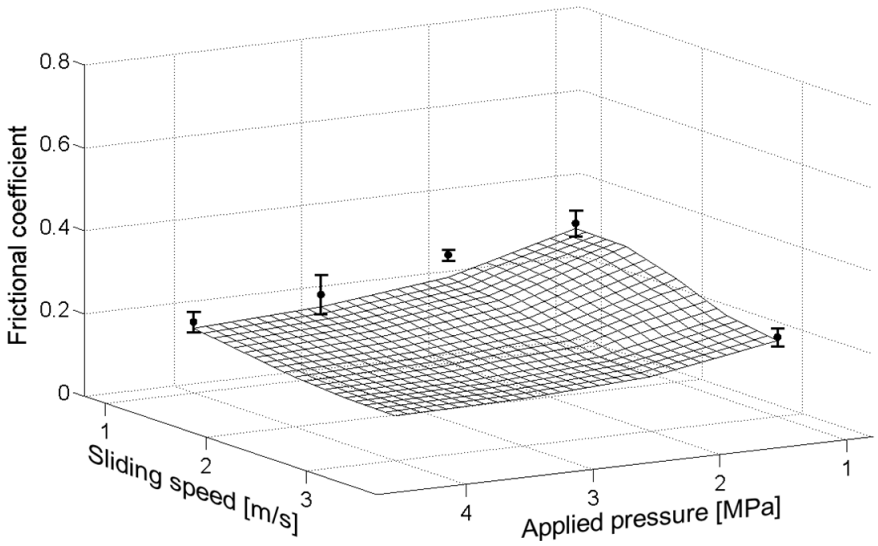

(a)

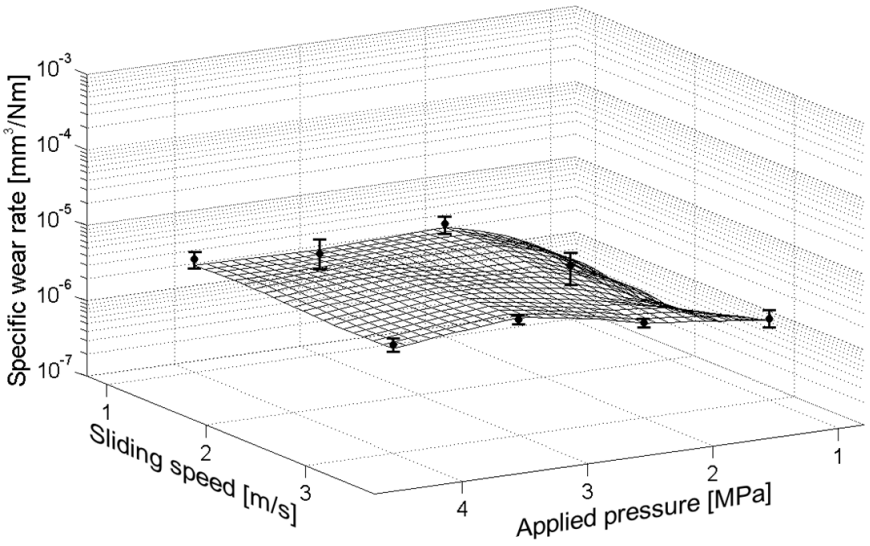

(b)

Figure 5.23: ANN predicted 3D profiles of (a) frictional coefficient (average value in steady state), (b) specific wear rate as a function of sliding speed and applied pressure for the hybrid system PPS/SCF/TiO_2 [85/10/5 vol.%]. The measured data are plotted as black points with error bars

Initial inspection of Fig. 5.23a reveals that the frictional coefficient exhibits a trend to monotonic decrease when either sliding speed or applied pressure is increased. It can be estimated that a very low value of friction will be achieved under the pv-conditions of 12 MPa·m/s (p = 4 MPa, v = 3 m/s). However, under these conditions despite the fact that the frictional coefficient of this material was greatly reduced it responded with stick-slip sliding. Consequently, no accurate values of friction could

be obtained. While, the specific wear rate rises visibly with the applied pressure in a stepwise fashion, it seems that it is less sensitive to the increase in the sliding speed. The latter might be associated with the dependence of the wear resistance on the mechanical properties of a composite at high loading conditions [81].

The frictional coefficient of the compound PPS/SCF/TiO_2/Gr/PTFE seems to be more sensitive to pressure variations at lower speeds (Fig. 5.24a).

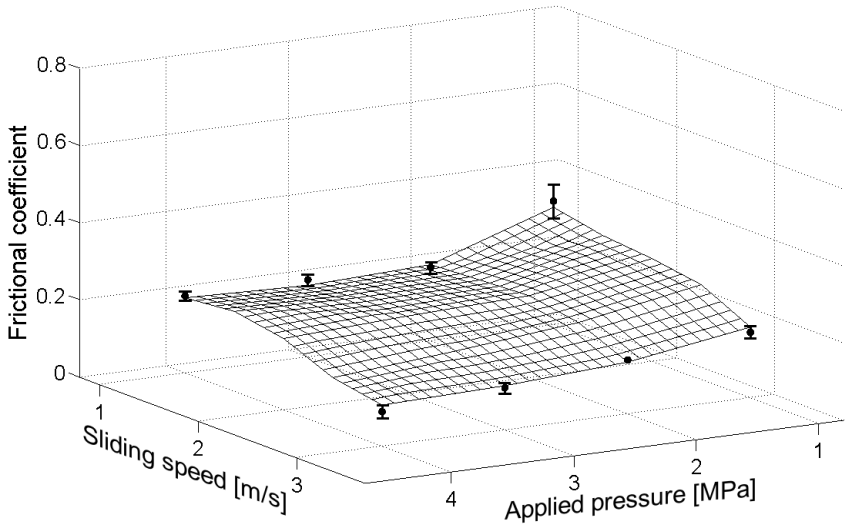

(a)

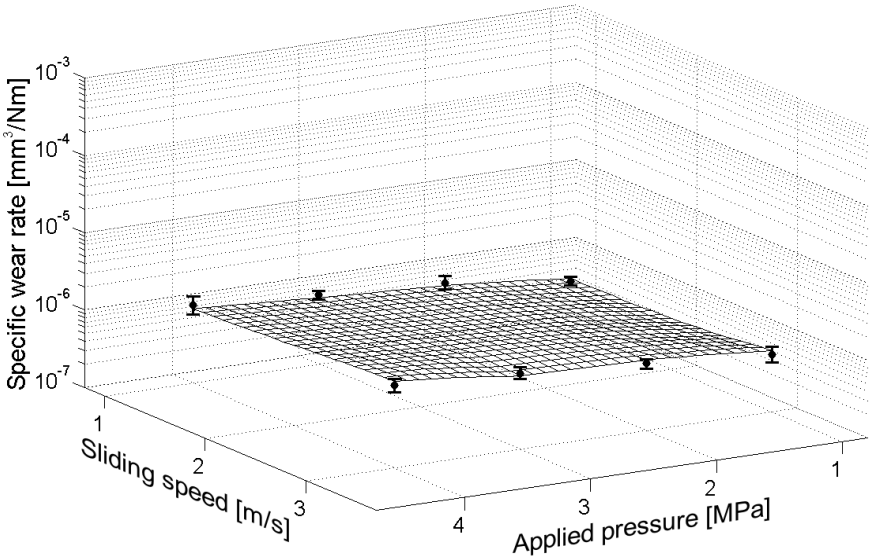

(b)

Figure 5.24: ANN predicted 3D profiles of (a) frictional coefficient (average value in steady state), (b) specific wear rate as a function of sliding speed and applied pressure for the hybrid system PPS/SCF/TiO_2/Gr/PTFE [85/10/5/5/5 vol.%]. The measured data are plotted as black points with error bars

Yet, its minimum might be obtained at both elevated pressure and speed. This is due to the fact that in the high pv-range the transfer film can form faster owing to the increase in adhesive force between the film and the counterpart with the increased load as well as the reduced surface contact time and increased real area of contact [82]. The tendency for the specific wear rate (Fig. 5.24b) is similar to that of the composition without solid lubricants (Fig. 5.23b). Nevertheless, the compound filled with solid lubricants principally exhibits lower wear rates over the complete pv-range as well as less sensitivity to increases in pressure or speed.

Finally, as Fig. 5.23 and Fig. 5.24 illustrate, the predictions of the ANN are very close or even identical to the experiment based results plotted as dots with error bars. Hence, the trained ANNs were able to learn the modeled relationship. Equally, these graphs demonstrate that a well-trained ANN and additionally one that is able to generalize might be successfully used in analyzing the effects of operating parameters on the sliding friction and wear behavior of a given compound over a broad range of testing conditions without performing the complete time-consuming testing program. This type of analysis would be extremely beneficial to the design engineer to avoid testing conditions which would be expected to lead to results different from the respective material specifications.

5.3 Input Parameters Study

It can be speculated that the sliding friction and wear behavior of a material must be controlled by a number of variables such as material composition, mechanical and thermo-mechanical properties and the testing conditions. Nevertheless, the degree of influence of those variables might not be the same. By now, it has been demonstrated that material compositions and testing conditions are essential to obtain realistic predictions of friction and wear [15, 147, 225, 281, 282, 286, 287]. At the same time, properly selected input parameters might assist to reach satisfactory prediction accuracy even with a relatively small training dataset [15, 259, 290]. For instance, the comparison of the two examples of fatigue life prediction [15, 257, 259], showed that the use of fiber orientation as input data yielded quite a high prediction quality with a training set of barely 92 data points, taken from unidirectional composites [259], and the result was even better than the one achieved in [257] with more than 400 data points, taken from laminates. In a preliminary work of Zhang et al. [282] it was estab-

lished that some secondary parameters exert great influence on the prediction quality. In this respect, it was the goal of this work to investigate the relative importance of the so-called secondary parameters (subchapter 5.2.1), on sliding friction and wear. By choosing the secondary parameters (q.v. Table A3-A5 in the appendix) as additional input together with the seven primary parameters (referred to as “Base”) allowed the ranking of their relative importance to the prediction quality in terms of the mean relative error (MRE). Moreover, the secondary parameters are in the usual case simple parameters that can be precisely and easily controlled and measured unlike the complex tribological ones. Consequently, the success of prediction could be of benefit to reduce the required number of tribo-experiments. Dataset II and dataset III (Fig. 5.11) were used in training the ANNs for the frictional coefficient and specific wear rate, respectively.

The predictive quality results for the frictional coefficient are shown in Fig. 5.25. From this figure it can be seen that the microhardness and storage modulus are the most influential in improving the quality of prediction when compared to the reference case (“Base”). Yet, the strength of this improvement was not as pronounced as for the specific wear rate. The remaining parameters were inferred to have no strong correlation to the sliding friction behavior of PPS composites.

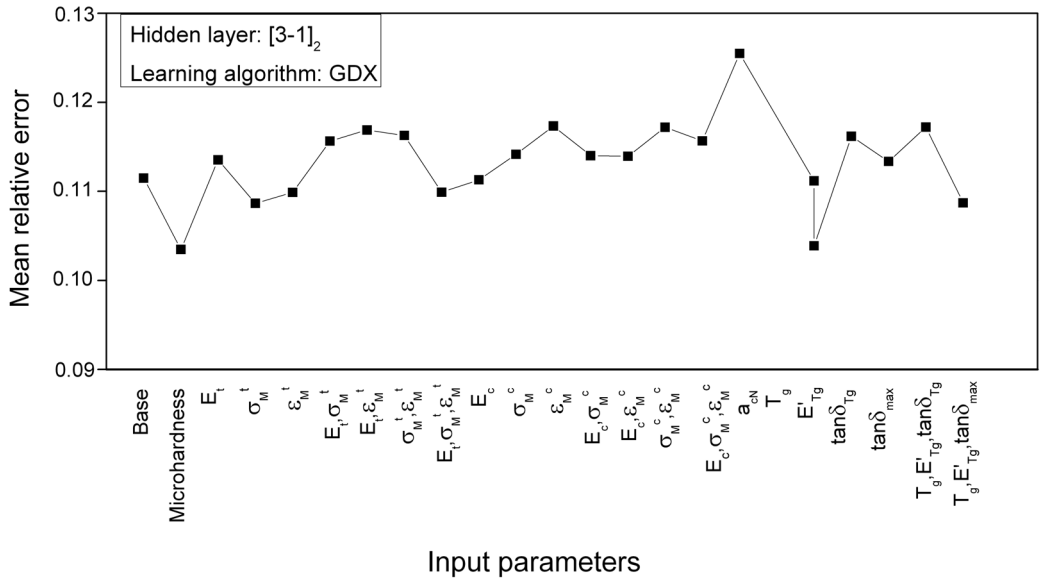

Figure 5.25: Ranking of the importance of various input variables to frictional coefficient of PPS composites by ANN (DS II)

It has already been established by Zhang et al. [282] in an importance analysis study that the yield stress exhibits significant ranking to erosive wear of thermoplastic polymer (PE) compared to other properties such as Young's modulus, crystallinity, yield strain or fracture energy. This trend was also experimentally confirmed in a former publication of Friedrich [319]. For sliding wear, it was found in the present investigation (Fig. 5.26) that a combination of tensile modulus and strain represents the strongest correlation with wear performance (MRE $\leq$ 0.68). This outcome conforms fairly well to the experimentally established trends by Gyurova et al. [320] for the same PPS-materials as well as by Tsukizoe and Ohmae for fiber reinforced plastics [321].

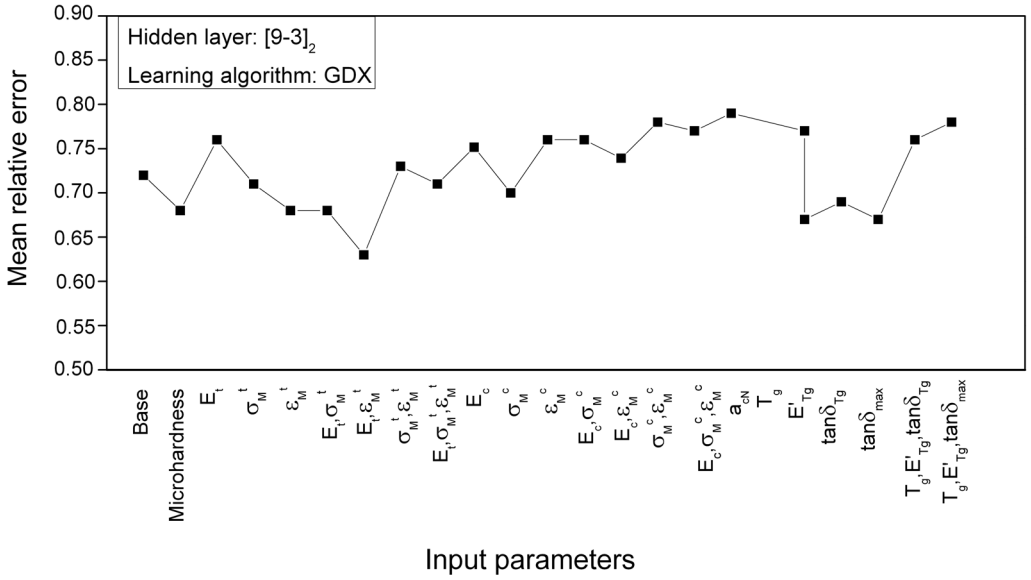

Figure 5.26: Ranking of the importance of various input variables to specific wear rate of PPS composites by ANN (DS III)

The amount of wear of a material due to contact pressure and relative motion of a solid counterpart is based largely on diverse adhesive and abrasive wear mechanisms [5, 12]. From microscopic observations of polymer matrix surfaces worn by steel counterparts it has been established that the major contributions to wear are caused by a series of plastic deformation and rupture in a thin surface layer, plowing a larger material volume and subsequent cutting of plastically deformed areas [12]. The mathematical description of such behavior should follow the correlation that the wear volume is inversely proportional to the hardness of the wearing material (resistance of the material against indentation of counterpart asperities) [5, 12]. In addition,

the wear volume depends through the wear coefficient and the geometry of the surface morphology on two kinds of material physical properties: the surface energy, which is associated with adhesion and friction forces (given by the frictional coefficient) and those properties of the material that are responsible for the mechanisms by which material is detached from the surface. These are basically mechanical properties such as ultimate tensile strength and elongation to fracture [12]. Moreover, higher stiffness lessens the real contact area yielding lower adhesion, hence lower wear [31]. It was observed that an almost linear relationship exists between the wear volume and the reciprocal of the ultimate elongation at break [11]. All this explains the predicted strong correlation of the tensile properties to wear performance.

Damping properties (storage modulus, mechanical loss factor) as well as microhardness maintain the second place (Fig. 5.26). The latter suggests that damping behavior might be a key factor in controlling the sliding wear process. Such a relationship has previously been observed for the erosive wear of PUR [282] and is in good agreement with the formula describing the deformation component of friction [31]. Nevertheless, the inclusion of glass transition temperature data in combination with storage modulus and mechanical loss factor as input reduces this strong correlation to sliding wear performance of the last two parameters and even renders worse results. The reason for this might be attributed to the very similar values of glass transition temperatures of the investigated materials (q.v. Table A5 in the appendix). As to the microhardness results, most tribological cases involve conditions where a hard body indents, impinges or slides against another softer surface. Therefore, the hardness, work hardening ability and strain to fracture of each material involved in the mechanical interaction are crucial parameters, which control the extent and depth to which strain builds up below each surface prior to microfracture and wear loss. Furthermore, the magnitude of the stresses as well as the rate at which strain energy is conveyed and dissipated between two bodies during their interaction, also determines the respective levels of subsurface strain buildup and fracture [322]. The compressive properties along with notch Charpy impact strength are found to exert minor influence in determining the specific wear rate, except for the compressive strength. The weak correlation between the wear resistance of these materials and their notch Charpy impact strength was also experimentally ascertained in [320]. The importance of compressive strength for the wear behavior of the investigated compositions could

be attributed to the fact that during sliding the material is normally subjected to compressive loading.

Finally, it can be seen in Fig. 5.25 that the reference value of MRE for sliding friction is much lower than for the specific wear rate (Fig. 5.26). This outcome is in agreement with the results discussed in subchapter 5.1.2 (q.v. Fig. 5.7). Likewise, whereas for the specific wear rate the values scatter in a very wide range, for the frictional coefficient the values scatter was smaller (q.v. Table A1 in the appendix). Therefore, it is more difficult with the specific wear rate to adjust the weights to perfectly match all the values in the output layer.

5.4 Surface Analysis

5.4.1 Effect of Short Carbon Fibers and Sub-micro TiO_2

Fig. 5.27 illustrates the morphology of the worn surfaces as well as the typical wear mechanisms involved in the wear process of both unfilled and reinforced PPS against a standard steel disc (R_a = 0.2 μm). Arrow lines at the left top corner mark the relative sliding directions of the sample surfaces (currently under microscopic observation). Wear grooves (furrows) are clearly visible on the worn surface of the neat PPS (Fig. 5.27a). These features are caused by the plowing and cutting action of the hard asperities of the steel counterface (as compared to the softer polymer matrix). Likewise, small surface cracks are formed perpendicular to the sliding direction (Fig. 5.27b). These cracks are a result of a high frictional coefficient and a locally high strain rate [12]. Back transferred wear particles are also visible. Sub-micro TiO_2 (300 nm) introduced as reinforcement increases the rigidity of the matrix material. However, because of its high hardness (6-6.5 Mohs' hardness) grooving by these particles occurs and contributes additionally to the abrasive component of wear (Fig. 5.27c and Fig. 5.27d). The process of abrasive wear is further intensified especially at high filler content, possibly due to the formation of agglomerates and loss of the matrix integrity. The wear mechanisms change considerably with the short carbon fibers as reinforcing component (Fig. 5.27e). The fact that short carbon fibers usually improve the wear resistance of a polymer matrix under sliding wear conditions has already been broadly discussed in subchapter 2.1.1.1 and was attributed to several factors such as

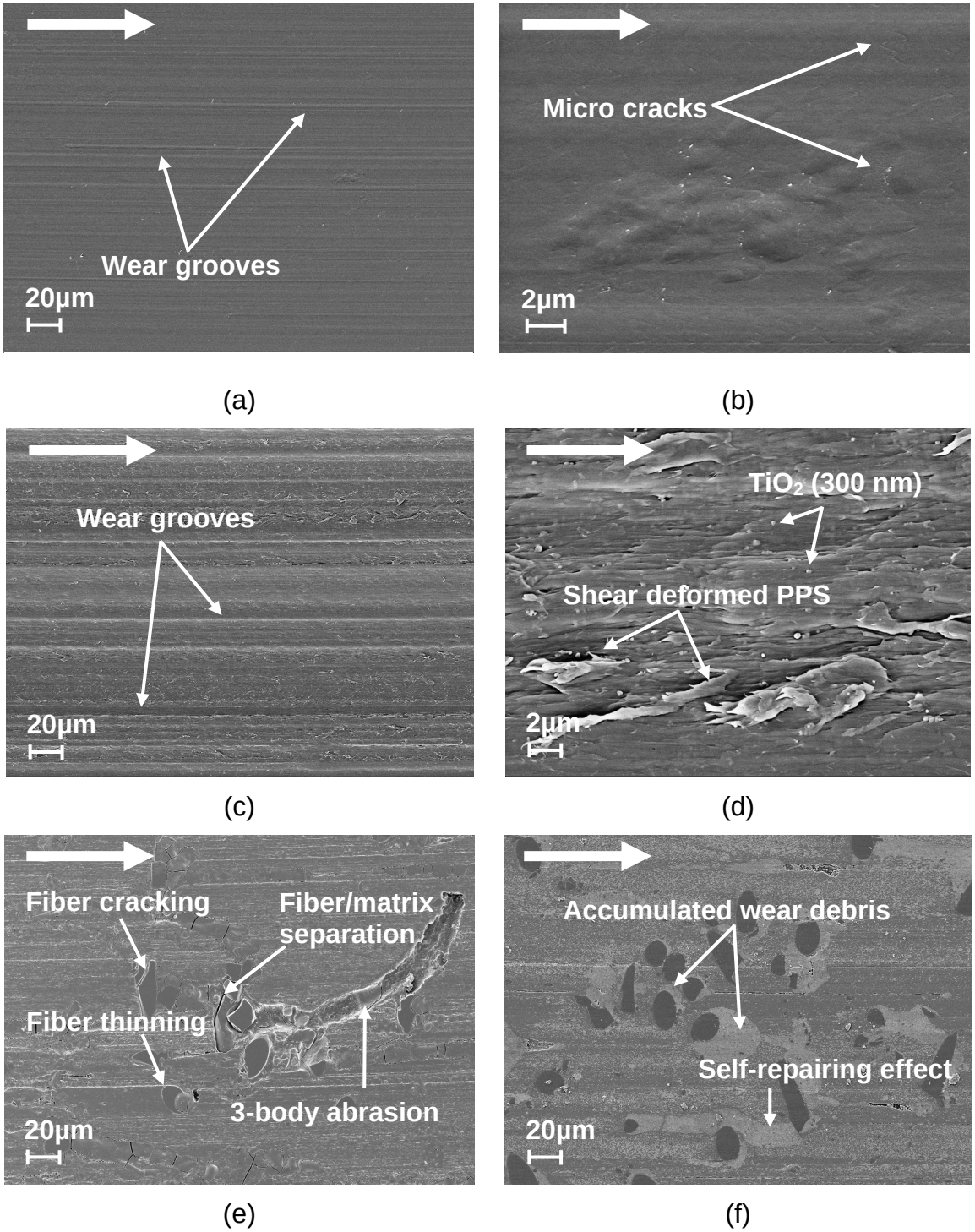

Figure 5.27: SEM micrograph of worn pin surface of (a), (b) unfilled PPS, (c), (d) PPS/TiO_2 [95/5 vol.%], (e) PPS/SCF [90/10 vol.%], (f) PPS/SCF/TiO_2 [85/10/5 vol.%]. The arrows in the left upper corner indicate the relative sliding directions of the pins. The testing conditions were: p = 1 MPa, v = 1m/s

load supporting effect, reduced micro-cutting or micro-plowing from the hard steel asperities, good thermal conductivity as well as reduction of interfacial shear force due to partial graphite structure of the fibers. In particular, wear of the matrix material

on and around the fibers, fiber thinning, multiple fiber cracking, fiber pulverization and fiber/matrix separation along the interfaces (fiber removal) occur as classical wear scenario [12, 27, 38, 41, 50]. Some of these mechanisms can also be recognized in Fig. 5.27e. It can be seen that the broken and detached fiber pieces are subsequently swept away easily and might result in third body abrasion of the polymer surface. The combination of both short carbon fibers and sub-micro TiO_2 led to a strong decrease in the specific wear rate. This outcome can be related to a synergistic interaction between the two components. On the one side, the carbon fibers boost the mechanical performance of the compound. On the other side, the particulate sub-micro filler helps keep the fibers in the matrix material by segregating around the fibers in the process of sliding (Fig. 5.27f). Furthermore, the matrix embedded sub-micro particles might successfully fill and repair the induced abrasive microscopic furrows from the detached fiber pieces yielding a much smoother surface with few tiny scratches in comparison to the PPS filled with short carbon fibers without TiO_2. A similar self-repairing effect has been established with short carbon fibers and nano-SiO_2 epoxy hybrid composites [141]. An additional positive effect of the sub-micro TiO_2 particles is considered to be occurring. The sub-micro TiO_2 particles, when being used in combination with the much larger short carbon fibers, are not easily plowed out of the matrix by the counterpart asperities. Instead, they are gradually released and presumably start to act as a rolling body between the two mating surfaces. Still, this ball bearing (“rolling”) mechanism has been so far only hypothetical. It will be addressed experimentally in detail in subchapter 5.5.

5.4.2 Effect of Internal Lubricants

The dominant wear mechanisms with the hybrid system PPS/SCF/TiO_2 containing internal lubricants (Fig. 5.28) did not show significant difference under standard testing conditions (p = 1 MPa, v = 1 m/s) when compared with the reference material without internal lubricants (Fig. 5.27f). Still, for the compositions with higher volume fraction of PTFE, larger contributions from abrasive wear can be identified. The microhardness measured with these materials (q.v. Table A3 in the appendix) was also lower. As outlined in the literature the grooving term of the frictional coefficient increases strongly with decreasing hardness of the wearing material [3]. These factors explain the observed increase in the frictional coefficient, as shown in Figure 5.18.

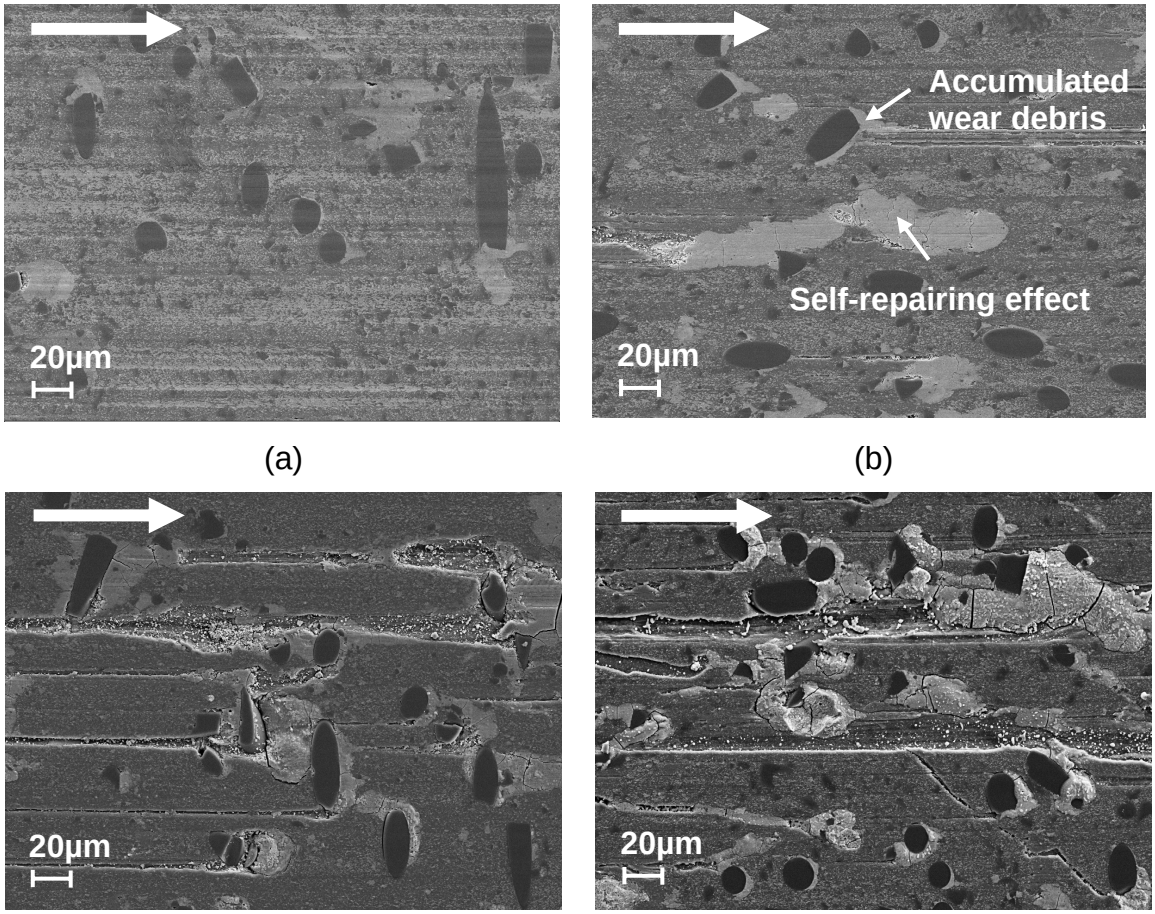

Figure 5.28: SEM micrograph of worn pin surface of (a) PPS/SCF/TiO_2/Gr [75/10/5/10 vol.%], (b) PPS/SCF/TiO_2/Gr/PTFE [75/10/5/5/5 vol.%], (c) PPS/SCF/TiO_2/PTFE [75/10/5/10 vol.%], (d) PPS/SCF/TiO_2/Gr/PTFE [70/10/5/5/10 vol.%]. The arrows in the left upper corner indicate the relative sliding directions of the pins. The testing conditions were: p = 1 MPa, v = 1m/s

As for the transfer film morphologies developed in the process of sliding on the steel counterfaces (Fig. 5.29), it can be seen that for all the materials a comparatively thin, uniform and well-bonded transfer films resulted. The wear rates recorded with these materials were also very similar (Fig. 5.22), as if they are a single material. However, it will be seen in the following subchapter that at a higher pv-factor the wear mechanisms and/or their magnitude change with these materials and are mostly determined by the mechanical properties as well as the thermal conductivity and heat conduction capacity of the entire hybrid system. In this respect the incorporation of appropriate amounts of carbon fibers (load bearing phase) and solid lubricants plays a decisive role.

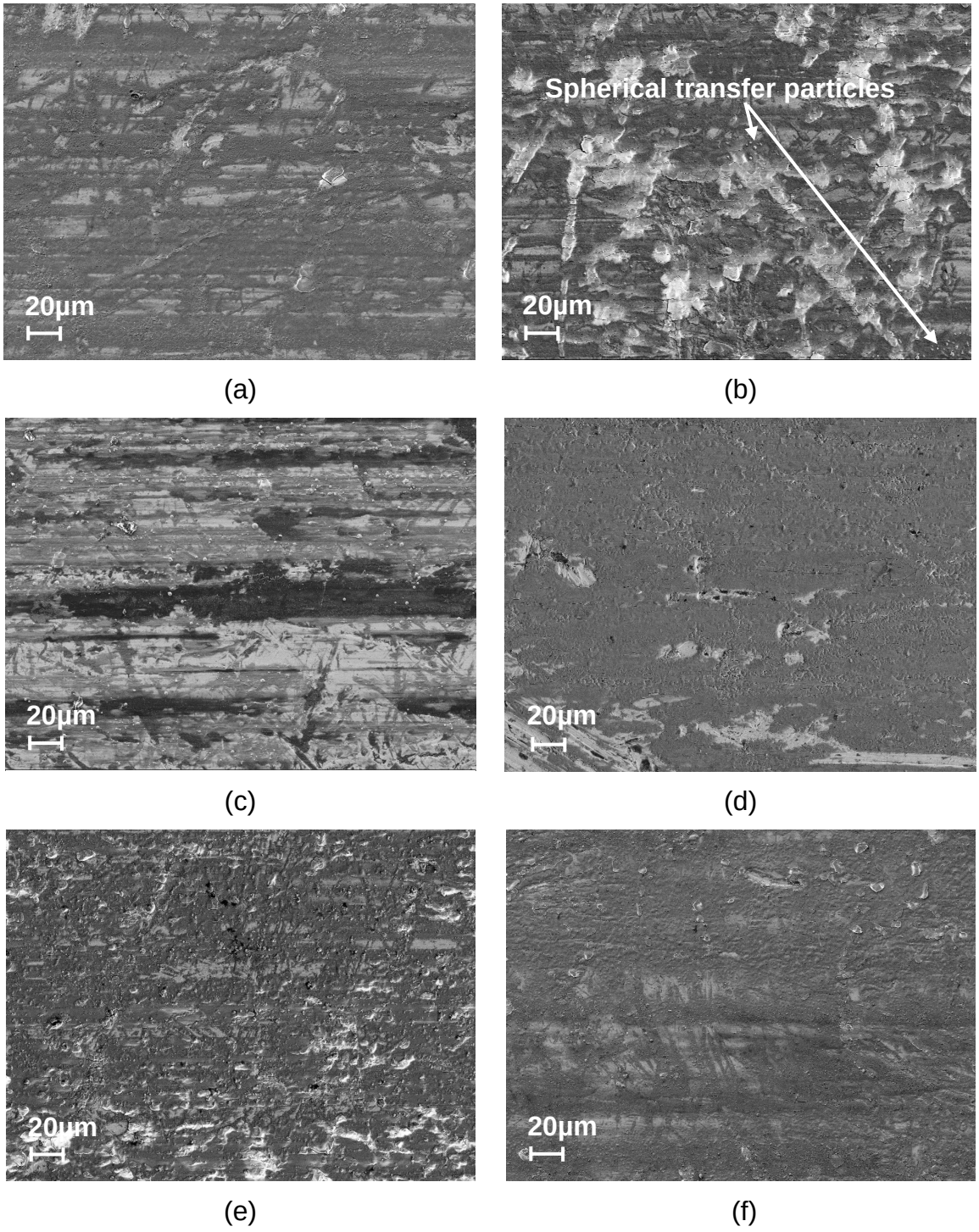

Figure 5.29: SEM micrograph of transfer film developed on the counterface of (a) PPS/SCF [90/10 vol.%], (b) PPS/SCF/TiO_2 [85/10/5 vol.%], (c) PPS/SCF/TiO_2/Gr [75/10/5/10 vol.%], (d) PPS/SCF/TiO_2/PTFE [75/10/5/10 vol.%], (e) PPS/SCF/TiO_2/Gr/PTFE [75/10/5/5/5 vol.%], (f) PPS/SCF/Gr/PTFE [70/10/10/10 vol.%]. The testing conditions were: p = 1 MPa, v = 1 m/s

5.4.3 Effect of Operating Parameters

Increasing the pv-product resulted in smoother surfaces (Fig. 5.30) with almost all compositions as compared to the standard testing conditions (Fig. 5.27 and Fig. 5.28). The worn surfaces of the composite containing Gr (10 vol.%) as a sole internal lubricant (Fig. 5.30c) or Gr (5 vol.%) in combination with PTFE (5 vol.%) (Fig. 5.30e) appear to be the smoothest without evidences of severe fiber removal, or fiber pulverization. Such surfaces provide a more uniform interface stress distribution and yield lower wear [64]. Actually, the measured wear rate with these materials under these testing conditions (Fig. 5.22) was among the lowest. The average frictional coefficient in steady state was also very low (0.09-0.11). This result can be related to the superimposed action of several factors: (i) the beneficial effect of internal lubricants, (ii) the development of thin, coherent transfer film (Fig. 5.31c and Fig. 5.31e) that can substantially lower friction, as well as (iii) the positive ball-bearing action of the accumulated sub-micro TiO_2 transfer structures. The latter alleviates friction and helps keeping the fibers in the matrix material leading to a fine working tribological system. The details of this effect will be discussed in the next subchapter 5.5. Still, it should be born in mind that the composition containing high loading fraction of graphite (10 vol.%) could not withstand higher loads corresponding to contact pressure of 4 MPa, and underwent excessive wear accompanied with the formation of lips and trailing strands of material on the downstream side of the worn specimen.

Flake-like shear tongues are formed on the worn surface of the composition for which stick-slip friction was observed (Fig. 5.30b), indicating an adhesive wear mode. It was discovered in a fractographic analysis that the fracture surface of the flake-like shear tongues shows the fracture mode of compression and shear [5]. The latter is in good agreement with the rather low compressive properties measured for this material (q.v. Table A4 in the appendix). As already mentioned, a fundamental barrier to smooth sliding appears when the sliding surfaces tend to adhere to each other. In the usual case, adhesive wear is a wear mode generated under plastic contact. Provided that the contact interface between two surfaces under plastic contact has sufficient adhesive bonding strength to oppose relative sliding, large plastic deformation generated by disruption is introduced in the contact region under compression and shearing. As a result of such large deformation in the contact region, a crack is set off

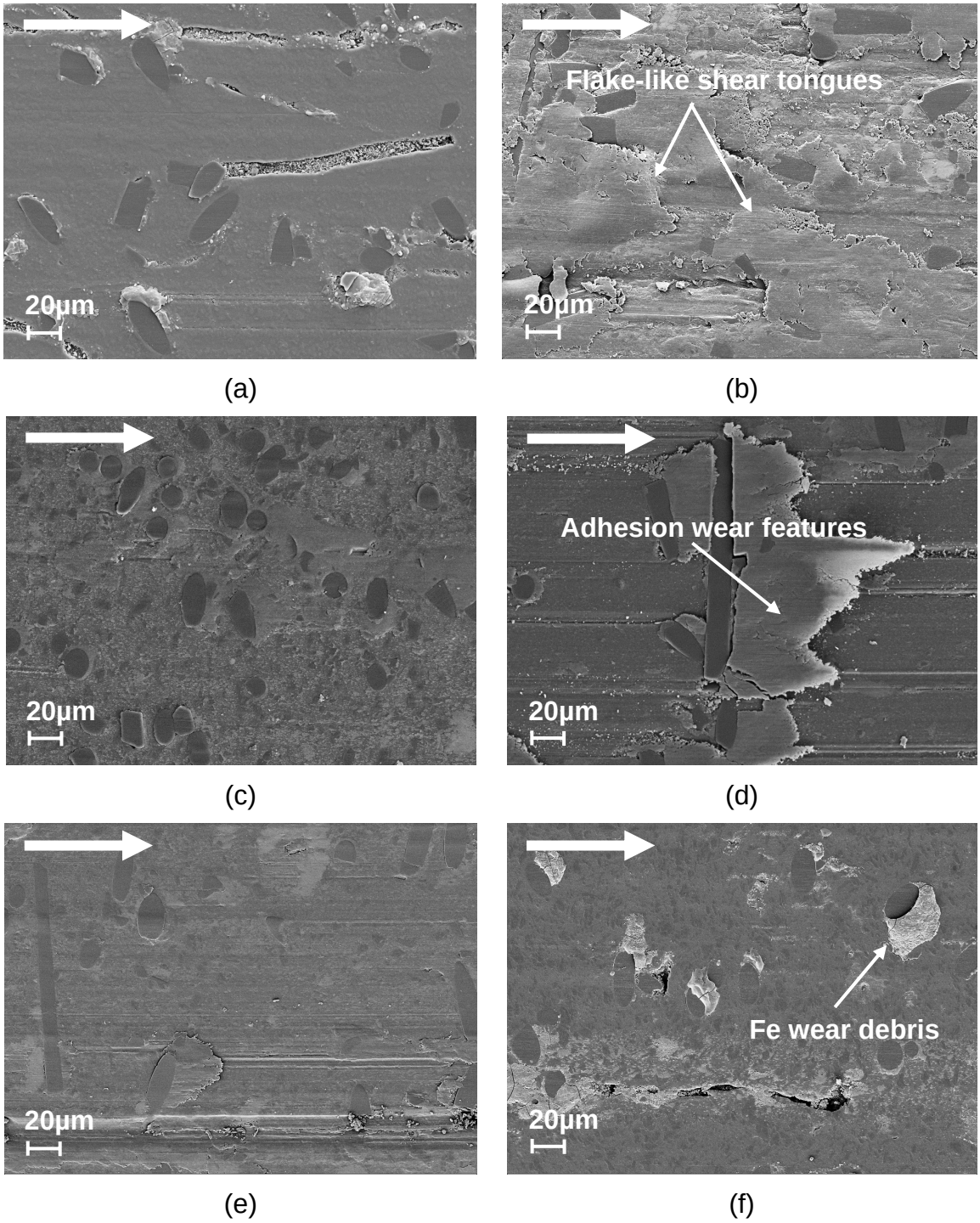

Figure 5.30: SEM micrograph of worn pin surface of (a) PPS/SCF [90/10 vol.%], (b) PPS/SCF/TiO_2 [85/10/5 vol.%], (c) PPS/SCF/TiO_2/Gr [75/10/5/10 vol.%], (d) PPS/SCF/TiO_2/PTFE [75/10/5/10 vol.%], (e) PPS/SCF/TiO_2/Gr/PTFE [75/10/5/5/5 vol.%], (f) PPS/SCF/Gr/PTFE [70/10/10/10 vol.%]. The arrows in the left upper corner indicate the relative sliding directions of the pins. The testing conditions were: p = 3 MPa, v = 3 m/s

and is propagated in the combined fracture mode of tensile and shearing. When the crack arrives at the contact interface, a wear particle is created and adhesive transfer

is completed [5]. Likewise, in the slipping regime a very low frictional coefficient was measured (≈ 0.05), which might arise from temperature-induced softening [3] and local melting phenomena (“hot spots” effects [4]). These mechanisms govern the material removal behavior at high values of the pv-factor and account for the abrupt sharp increase in the wear rates measured.

For the multiphase system PPS/SCF/TiO_2/PTFE (Fig. 5.30d) adhesive wear features are also visible, which explains the observed fluctuations in frictional coefficient over time (Fig. 5.21). For the case of the system filled only with traditional reinforcement and internal lubricants (Fig. 5.30f), SEM-EDX analysis revealed that tribochemical reactions occurred in the process of sliding involving the transfer of counterface metal Fe at the worn pin’s surface (q.v. Fig. A.1 in the appendix). The major Fe-distribution was detected around the tips of the fibers. Previous investigations of Kong et al. [323] disclosed that such oxide films yield both low frictional coefficient and mild wear. Such Fe-transfer was also established via XPS analysis in the composition containing short carbon fibers as single reinforcing phase (q.v. Fig. A2 in the appendix) and is in agreement with other investigations [52].

The SEM micrographs of the corresponding transfer films formed onto the rubbing steel surfaces in the process of sliding revealed the development of a thin and fairly tenacious transfer film with the hybrid compositions PPS/SCF/TiO_2 containing Gr as a single lubricant or in combination with PTFE (Fig. 5.31c and Fig. 5.31e). Such transfer films favor the reduction in frictional coefficient and wear rate. One supplementary issue that should be considered here are the so-called tribochemical reactions occurring in the process of sliding with filled PPS. These reactions might lead to improved bonding of the transfer film to the counterface, and therefore enhanced wear resistance [61, 66, 77, 98]. Bahadur and Sunkara [66] showed that when TiO_2 was used as filler in a PPS matrix, a thin and relatively continuous transfer film resulted on the counterface steel discs. XPS analysis of the transfer film disclosed the reduction of TiO_2 filler into elemental Ti. The Ti-element possesses greater attraction towards the steel surface and introduces additional chemical bonding of the transfer film to the counterface [66]. The transfer film of the composition displaying stick-slip motion appeared with thick irregular discrete regions (Fig. 5.31b). It is believed that these features are the result of material removal in adhesive mode. Such thick and

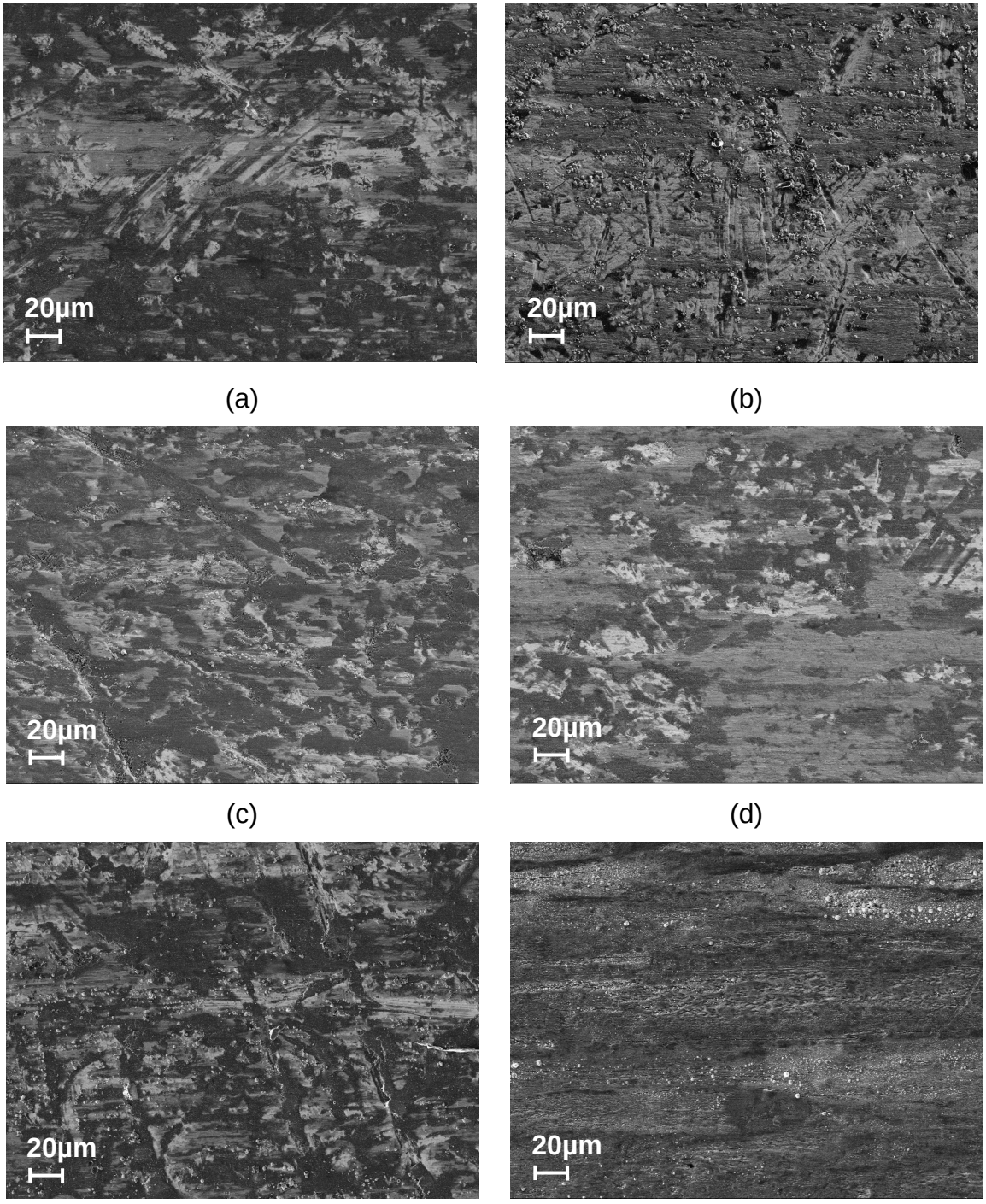

Figure 5.31: SEM micrograph of transfer film developed on the counterface of (a) PPS/SCF [90/10 vol.%], (b) PPS/SCF/TiO_2 [85/10/5 vol.%], (c) PPS/SCF/TiO_2/Gr [75/10/5/10 vol.%], (d) PPS/SCF/TiO_2/PTFE [75/10/5/10 vol.%], (e) PPS/SCF/TiO_2/Gr/PTFE [75/10/5/5/5 vol.%], (f) PPS/SCF/Gr/PTFE [70/10/10/10 vol.%]. The testing conditions were: p = 3 MPa, v = 3 m/s

discrete transfer film lumps may not be stable. Therefore, their removal, or incomplete removal, and reoccurrence might be responsible for the great fluctuations in

friction. Another possible cause for the jerky stick-slip motion might be a strong adhesion between the agglomerated TiO_2 wear particles and the asperities of the steel counterface, which effect has already been observed with inorganic fullerene nanoparticles under severe contact conditions [151]. The addition of PTFE to the multiphase material PPS/SCF/TiO_2 contributed positively to the formation of smoother and thinner tribolayer (Fig. 5.31d) and was able to suppress the stick-slip due to the well-know lubricating effect of PTFE [69]. It can be seen that for this composition, fine spherical TiO_2 transfer particles can be found in the tribolayer, which size agrees well with the gap between the two contact surfaces. The composite PPS/SCF also formed a thin and consistent transfer film (Fig. 5.31a), which explains the much lower and stable steady state frictional coefficient with this material when compared to the standard testing conditions (p = 1 MPa, v = 1 m/s). Nevertheless, the steady state frictional coefficient of this material was the highest among the investigated compositions. This can be clarified by the nature of the transfer film containing more abrasive wear debris (e.g. broken and/or pulverized fiber pieces). Moreover, the transfer film of this material displayed tiny cracks in its topography and no spherical wear debris. It has been shown in this work that the system containing only traditional fillers (SCF, Gr, and PTFE) without sub-micro TiO_2 particles exhibited good wear resistance and moderately low friction under the presently discussed conditions (p = 3 MPa, v = 3 m/s). This might be associated with the lubricating action of Gr and PTFE along with tribochemical effects of the polymer matrix and metal counterface leading to the formation of compounds such as FeS, $FeSO_4$, and/or $Fe_2(SO_4)_3$, FeO and Fe_3O_4. These compounds positively contribute to the transfer film bonding and/or lessening friction [77, 98, 99, 323]. Still, the temperature measured continuously in the process of sliding with this composite was the highest among all materials (≈ 90°C). This temperature is very close to the glass transition temperature of this material (98.35°C determined via DMTA according to the 2% offset-method [293]). Therefore, softening of the material (transition in rubbery state) might have taken place with loss of modulus, and consequently plastic deformation. The latter might explain the compacted but undulating transfer film appearance (Fig. 5.31f). Finally, it can be concluded that the wear reducing function of graphite is obviously limited in these systems up to a certain volume fraction and loading range above which undesirable effects occur in both cases.

5.5 Ball Bearing ("Rolling") Effect on a Sub-Micro Scale

Recent tribological studies [25-28, 41, 135-138, 146-148] have demonstrated that the combination of short carbon fibers and sub-micro TiO_2 particles (300 nm) in various thermoplastic and thermosetting matrices can have a substantial beneficial impact on their friction and wear properties. Chang, Friedrich, Zhang and coworkers [25-28, 41, 135-138] proposed a positive rolling effect of the particulate filler between the materials' pairs. The benefit of the rolling effect was mainly attributed to the following three aspects: (i) the substantial reduction of the frictional coefficient, (ii) the restriction of grooving/cutting wear as well as (iii) protection of short carbon fibers from serious fiber removal effects. Yet, the range of applicability of this model is limited to a particle size that agrees well with the gap between the sliding surfaces [27].

In order to better understand the behavior of the particulate filler in the boundary layer of the first bodies, after testing both mating surfaces (polymer pin and steel counterface) were joined together via a specially designed fixing steel element using commercial adhesive. The system was then removed from the test rig and embedded in epoxy resin (q.v. Fig. A3 in the appendix). Subsequently, cross-sectional cuts were made both parallel and transverse to the sliding direction via abrasive water jet cutting. Due to the suboptimal quality of the investigated surfaces after water jet cutting, the samples were polished and then observed under SEM. This investigation experimentally complements the results generated by Zhang and co-workers as well as previously reported assumptions [147].

It can be seen from Fig. 5.32 that in the boundary layer spherical or quasi-spherical debris are present, very similar to the ones identified on the counterface (q.v. Fig. A4 in the appendix). XPS analysis (q.v. Fig. A5 and Fig. A6 in the appendix) revealed that the following elements were the principal components of these structures: titanium (Ti), oxygen (O), sulfur (S), carbon (C). Based on this observation it can be concluded that these debris stand for TiO_2 particles wrapped in matrix material. This element analysis also agrees well with the one done on the counterface (q.v. Fig. A7 in the appendix) as well as the EDX analysis of the worn pin surface (q.v. Fig. A8 in the appendix). Additionally, iron (Fe) from the steel counterface was detected. It has already become clear that some oxidation occurs during sliding which leads to the formation of iron oxides that are afterward visibly blended into the debris (q.v. sub-

chapter 5.4.3). The micrographs for the transverse cross-sections as well as those taken of the original system prior to being embedded in epoxy resin can be seen in Fig. A9 and Fig. A10 in the appendix, respectively.

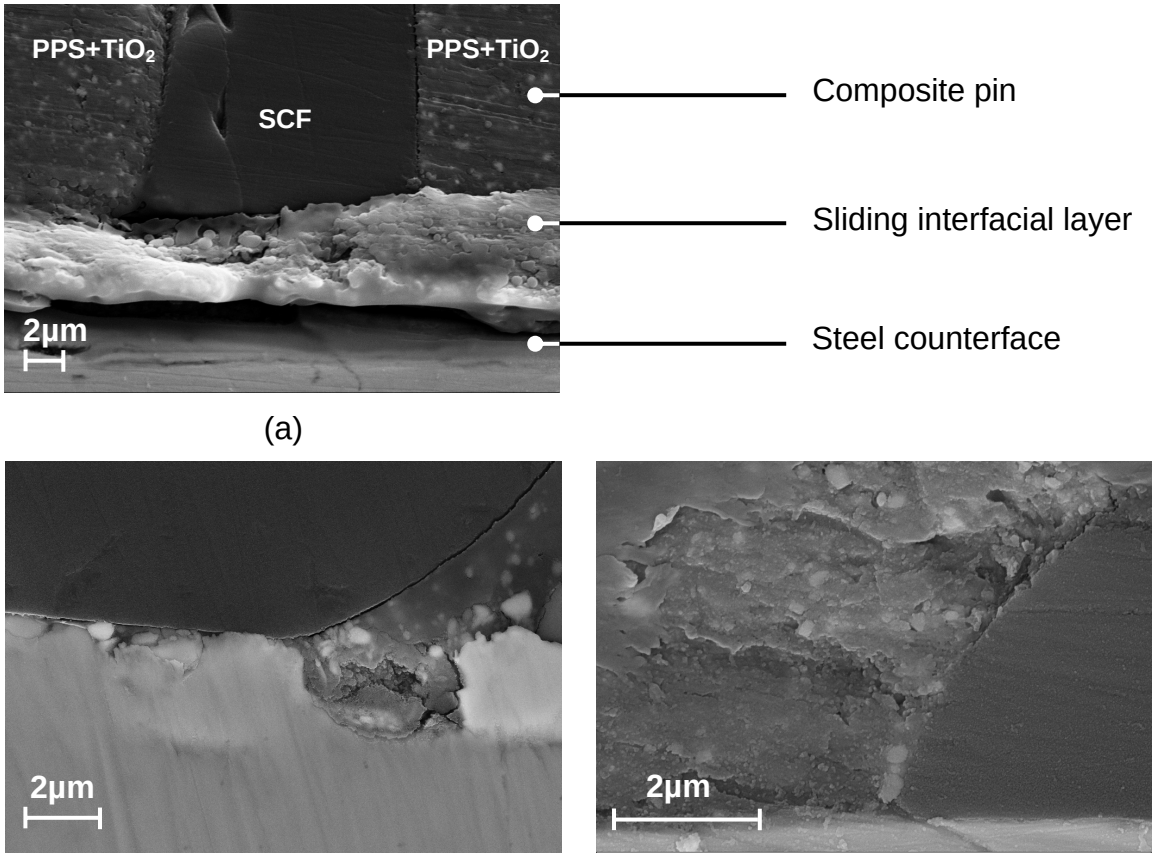

Figure 5.32: SEM micrographs of longitudinal cross-section showing the sliding interfacial layer between PPS/SCF/TiO_2 [85/10/5 vol.%] composite and 100 Cr6 steel disc. The testing conditions were: p = 1 MPa, v = 1 m/s

Recent molecular dynamics simulations by Rigney et al. [324] for a composite filled with hard (WC) nanoparticles revealed that the hard particles do not deform under shear and compression conditions, but migrate and agglomerate during sliding. The latter is associated with the following two factors: (i) thermodynamic driving force related to the strong bonding between the atoms of the hard particles, (ii) kinetic factor (i.e. vorticity) that enables the hard particles to migrate fast enough to act in response to the thermodynamic driving force. Moreover, the mechanical mixing that occurs during sliding is associated with nanoscale rotational flow in material where the strain rates are the highest leading to long-range mass transport normal to the principal shear direction [325].

These results are in slight contradiction with the original hypothesis proposed by Chang and coworkers [27, 41], who presumed that the rolling mechanism is induced by the individual metal oxide particles only. However, it should be born in mind that at this early stage of research, no direct observation of the sliding interfacial region (boundary layer) between the contact surfaces was done or could have been done by the authors. Only the separated sliding partners were investigated via SEM. Similarly, no in-depth analysis of the elemental composition of the resultant wear debris was performed.

Subsequent examination of the worn pin contact area using atomic force microscopy revealed that the fiber remained parallel to the worn surface during sliding and is more or less intact. Although its surface is fairly smooth, tiny nanoscale grooves (circa 70-90 nm in width) are discernible. The particulate filler can be seen gathered around the fiber, especially at its leading edge. For comparison, AFM observations (q.v. Fig. A11 in the appendix) disclosed that for the composite without sub-micro particles the fiber surface was strongly damaged, especially at the leading edge and tilted towards the worn surface.

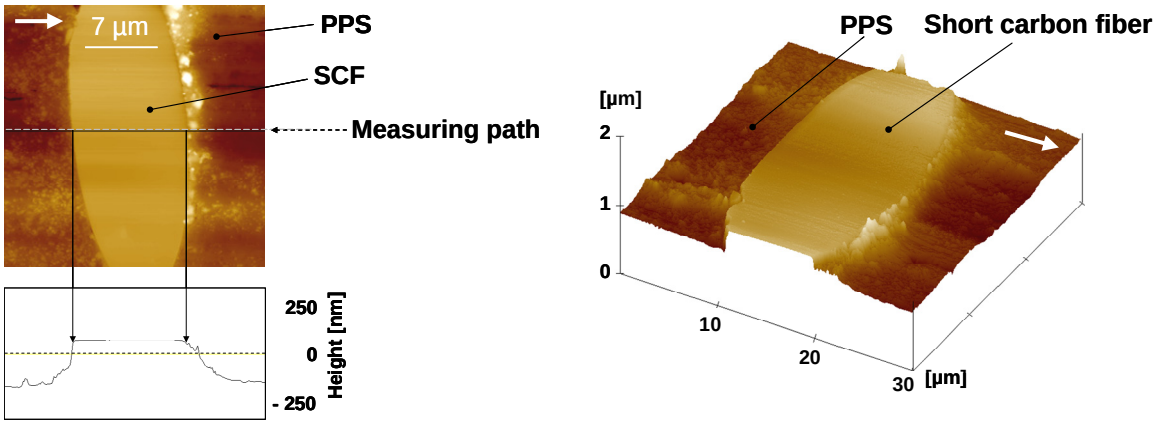

(a) (b)

Figure 5.33: AFM images and the respective measurement profiles of a fiber in the worn pin surface of PPS/SCF/TiO_2 [85/10/5 vol.%] composite. The white arrows indicate the relative sliding directions of the sample surfaces (currently under microscopic observation). The testing conditions were: p = 1 MPa, v = 1 m/s

Based on the above results and observations, the following modified wear scenario can be constructed for the sliding wear behavior of the multiphase polymer composite system against 100 Cr6 steel counterface (Fig. 5.34). When sliding commences, wear processes lead to a removal of the soft polymer matrix and exposure of the

near surface components. This allows slow release and gradual supply of the sub-micro particles from the polymer matrix to the contact surface. Once in the interface region, the sub-micro particles start filling the crevices of the counterface (can enter the roughness valleys) as well as they are free to roll and/or slide under the resulting shear forces similar to fullerene-like WS_2 nano-particles [150]. During their rolling and/or sliding action the particles tend to agglomerate (Fig. 5.34a) and are mixed with soft matrix material in addition to Fe from the counterface. The structure evolves as the material mixes, perhaps in such a way as to minimize the work during sliding [324]. These accumulated debris (“rollers”) serve as spacers [150, 157], decrease the real contact area and prevent the contact between the hard steel asperities and the soft polymer pin, thus causing a transition from solid body friction to a kind of three body mild abrasion. The latter would not be surprising taking into consideration the accumulating evidence for the significance of mixing processes in tribological interfaces [326].

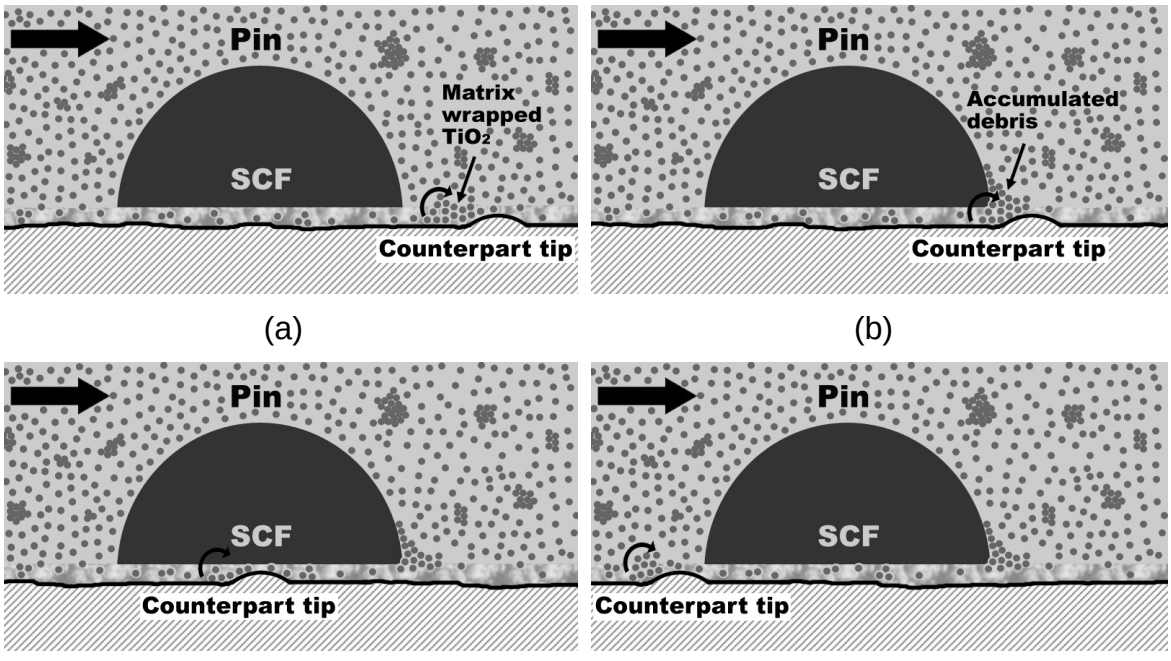

Figure 5.34: Schematic illustration of the ball bearing effect on a sub-micro scale. The thick black arrows in the upper left corner indicate the relative sliding direction of the pins. The small black arrows at the leading edge of the counterpart tip indicate the rolling direction of the transfer particles

The hardness of the particulate filler (TiO_2) is almost the same as that of the carbon fibers, but clearly higher than that of the soft polymer matrix. Therefore, when the rolling debris encounter a fiber they are hindered by the exposed fiber and partially

remain blocked at its front (leading) edge (Fig. 5.34b). Next, the quasi-spherical complexes start rolling over the fiber surface thus preventing severe fiber damage and adverse scratching from the much harder steel asperities (Fig. 5.34c). Finally, when reaching the trailing edge of the fiber, the quasi-spherical debris transfer again on the softer matrix material and in part remain embedded there. The residue continues moving and expanding again. In this way these transfer particles act as tiny ball bearings [327] in the sliding contact, ease the relative movement between the two antagonist surfaces, alleviate friction, protect the fibers from sever damaging and prevent rapid wear.

It was also interesting to observe a continuous reduction in the frictional coefficient over time (Fig. 5.20), which indicates the ongoing process of TiO_2 phase accumulation in the friction contact and justifies their efficiency in the steady state. It should be mentioned that the clearance (average surface roughness) between the two sliding surfaces is close to the mean diameter of the pristine particles. On the other hand, under severe contact conditions stick slip behavior was observed with this hybrid composite. As already mentioned, one of the causes of this effect could be a strong adhesion between the accumulated sub-micro particles and the asperities of the counterface thus limiting their rolling friction [151]. It has already been demonstrated that the introduction of solid lubricant reservoirs (e.g. Gr and PTFE) is an acceptable solution in this case. Solid lubricants act similarly to the lubricants used in real ball bearings [328], provide low shear resistance and avert stick-slipping.

There exist also other theories in the community as to the protective effect of nano-, sub-micro- and micro-particles on short carbon fibers in a hybrid reinforced polymer composite. Zhang and Schlarb [140] presumed that the increased stiffness of the PEEK matrix through the incorporation of the SiO_2 nanoparticles (13 nm, 7.5 Mohs' scale hardness [296]) might decrease the stress concentration on SCF in the surface layer as well as their deformation by tensile stresses. Similar results were reported by Zhu et al. [290] for PTFE/SCF/TiO_2 composites. In this latter case due to their higher hardness than that of PTFE, the beneficial effect of TiO_2 microparticles (1 μm) was related to the enhanced toughness and stiffness of the matrix rather than to their ball bearing action. For the investigated PPS materials in the present work, only a negligible improvement in the mechanical properties (tensile properties, compressive

properties) could be recorded through the incorporation of TiO_2 particles. Consequently, one can view the beneficial role of hard spherical particulate filler in the SCF/polymer composite as either superposition of all the above-mentioned effects or their sole action.

The introduction of softer sub-micro particles (ZnS, 3 Mohs' scale hardness [296]) yielded a much different behavior during sliding and could not give the desired ball bearing effect (Fig. 5.35).

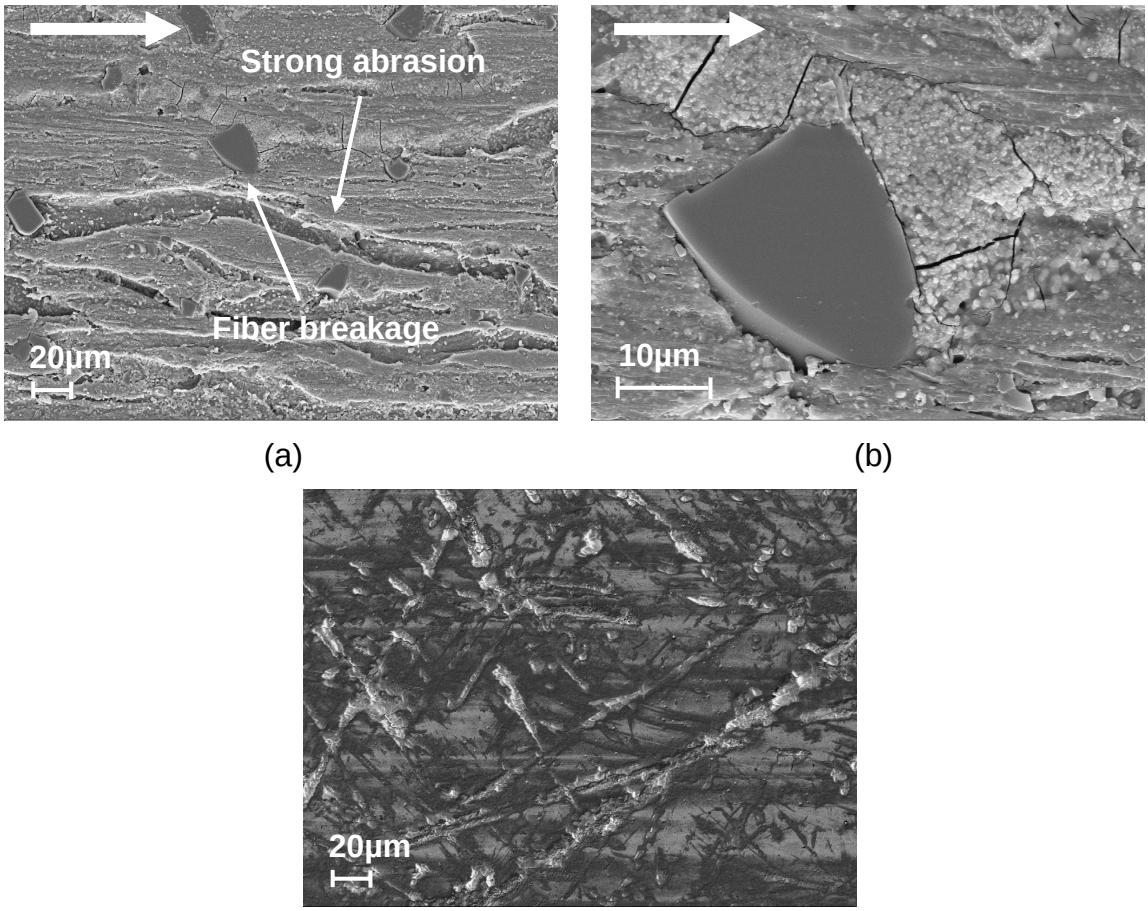

(a) (b)

(c)

Figure 5.35: SEM micrographs of (a), (b) worn pin surface, (c) transfer film developed on the counterface of PPS/SCF/ZnS [85/10/5 vol.%] composite. The testing conditions were: p = 1 MPa, v = 1 m/s

Due to their soft nature these particles can easily be deformed and damaged under shear by the hard asperities leading to formation of lubricious surface tribo-layers [324]. It can be seen from the SEM micrographs (Fig. 5.35a and Fig. 5.35b) that, although the particles were collected around the fiber tips, strong fiber breakage and interfacial removal resulted. The worn surface was rough with typical microscopic

furrows produced by a plowing process. These features of the worn surface were very similar to those with PPS/SCF composite (Fig. 5.27e). Consequently, the soft ZnS particles were not that effective in this case for providing proper protection of the fibers from the hard asperities. As to the counterface, although the SEM analysis (Fig. 5.35c) showed a good development of a continuous interfacial layer, due to the intensive fiber breakage events within this material the tribo-layer contained more abrasive transfer components (e.g. broken fiber pieces). Finally, it should be taken into consideration that with ZnS the Gibbs free energy change (ΔG) is positive, so that no chemical reaction is likely to occur between this filler and the steel counterface [103].

6 Summary and Outlook

One of the main objectives pursued in this study was to assess the potential of using artificial neural networks to predict characteristic tribological properties of polymer-based composites. Through the application of the ANN technique to pre-existing datasets collected from the published literature and commercial databanks, it was demonstrated how an ANN model can be developed in order to predict accurately enough not only frictional coefficient and specific wear rate, but also simple mechanical properties of short fiber reinforced polyamide composites. During the development of the network architecture, which has a remarkable influence on the performance of the network, the following practical rules were derived:

- In most cases, a simple structure of one hidden layer including several neurons has an adequate capability to model straightforward relationships. However, complicated phenomena e.g. wear behavior, require more complex network topology.
- The determination of the best neuron number is case dependent. The prediction quality increases in a certain range when the number of neurons increases, yet it deteriorates when the neuron number exceeds a given saturation value.
- Generally speaking, one-output network can avoid the disturbance of the relationships between inputs and different outputs, and provide a higher prediction quality. Nevertheless, a multi-output network might be used for some simple problems, such as prediction of certain mechanical properties. The reason is that the computation time needed by a multi-output network in these cases is markedly less without significant differences in the accuracy of prediction to the one-output network.

The ANN models developed here were capable of identifying the relationship between the chosen input and output variables for the SFR-PA composites with reasonable accuracy. It should be noted that once the network was trained, the time required to output results for a given set of input was nearly instantaneous on a personal computer. This indicates that this technique may have considerable potential for solving time-consuming complex problems such as friction and wear. The main

benefit is that the modeling is based purely on the data and not on preconceptions, and that the ANN can interpolate effects by learning trends and patterns, even when complete datasets are not yet available.

Subsequently, the sliding friction and wear behavior of PPS based composites filled with various traditional fillers and inorganic sub-micro particles was both experimentally studied and modeled by implementing the ANN approach. In developing the ANN models the variable learning rate GDX algorithm was selected for training. Input variables of material composition and testing conditions were used. Two networks with the structures of 7-[3-1]$_2$-1 and 7-[9-3]$_2$-1 were chosen in a trial and error procedure for modeling the frictional coefficient and wear rate, respectively. The following important results were obtained:

- A favorable synergistic interaction was found between the short carbon fiber (SCF) reinforcement and sub-micro TiO_2 (300 nm) particles. The sub-micro TiO_2 particles had a similar Mohs' hardness as the short carbon fibers (Mohs' scale 6-6.5). From the SEM and AFM characterization performed after testing, several phenomena were proposed to explain this anti-wear ability and friction reducing properties. The general idea is that while the SCFs boost the mechanical performance of the compound, the particulate sub-micro filler helps keeping the fibers in the matrix material by segregating around the fibers in the process of sliding. Additionally, the sub-micro TiO_2 particles, when being used in combination with the much larger short carbon fibers, are not easily plowed out of the matrix by the counterpart asperities. Instead, they are gradually released, tend to mix with soft matrix material and Fe from the steel counterface giving rise to quasi-spherical transfer particles that serve as spacers and apparently roll between the two mating surfaces. Finally, a self-repairing effect was established with this hybrid system where the matrix wrapped TiO_2 particles might successfully fill and repair the induced abrasive furrows from the detached fiber pieces.
- The positive synergistic effect between short carbon fibers and sub-micro TiO_2 particles was also envisaged by the ANN. There was either a very close or perfect agreement between the input-output mapping computed by the network for both training test data as well as validation test data that has never been used in creating or training the network. According to both the experimental results and the

ANN predictions, the composition of PPS with 15 vol.% SCF and 8 vol.% TiO_2 gives the best wear resistance (i.e. the lowest specific wear rate). These results exemplify the ability of well-trained ANNs to perform useful non-linear interpolations based on simple data for complex and poorly defined problems such as sliding wear behavior of polymer composites.

- Sliding results for a short carbon fiber composite with soft sub-micro (300 nm) particles (ZnS) resulted in quite a different behavior compared with the case of composites with hard sub-micro particles (TiO_2). The soft sub-micro particles (Mohs' scale 3) deformed under shear and compression conditions and were unable to provide proper protection of the fibers from the hard asperities. Likewise, these particles could not serve as tiny rollers in a sliding contact and facilitate relative movement between the two contacting surfaces, thereby leading to lower friction.

- In comparison with the low pv-factors, where no significant influence could be observed with internal lubricants, the addition of either graphite or graphite in combination with PTFE effectively eliminated the stick-slip sliding motion of the hybrid system PPS/SCF/TiO_2 in the high pv-range. The solid lubricants acted in this case as lubricant reservoirs, similarly to the lubricants used in real ball bearings, and generated the lowest and almost constant frictional coefficient in steady state. Therefore, such multiphase systems PPS/SCF/TiO_2/Gr/PTFE might be used in sliding bearings with the additional benefit of rolling friction typical with ball bearings.

- The materials containing either SCF alone or in combination with the two internal lubricants displayed no jerky stick-slip motion in the upper pv-range, but they exhibited a higher and constant frictional coefficient in steady state than the compositions with sub-micro TiO_2 particles. This might be related to the fact that with these materials no contribution from rolling friction occurred, as it was the case with the other sub-micro TiO_2-filled composites.

- Solid lubricants also enhanced the load bearing capacity of the hybrid system PPS/SCF/TiO_2. The best results were obtained by blending comparatively low amounts of graphite and PTFE (≈ 5 vol.% from each additive). At higher concentrations (> 10 vol.%), the lubricants combined with TiO_2 were inferior to the wear

resistance. Moreover, the wear reducing function of graphite is limited in these systems not only up to a certain volume fraction but also load level above which undesirable effects (delamination wear) occurred.

- The predicted surface plots by the trained ANN and the actual data exhibited very good conformity. These results illustrated the power of the neural network approach to predict the evolution of characteristic tribological parameters as a function of material type, applied pressure and sliding speed without having to perform the total number of experimental combinations.

Optimal brain surgeon (OBS) algorithm, an effective technique for network optimization, was used to improve the performance and efficiency of the artificial neural network by removing irrelevant network nodes and then comparing its performance to the fully-connected network. Although the forecasting quality of the pruned network was to some extent superior over the fully connected network, it should be taken into consideration that at this stage pruning the network demands intensive efforts for inputting the data into a form which is usable by the software.

The present study focused also on defining the role of various input variables on sliding friction and wear of polymers. The variables that affect wear can exert synergistic effects on one another. An ANN can identify and use these effects in its predictions. The importance analysis revealed that in addition to material composition and pv-data the most relevant variables for frictional coefficient were microhardness, tensile properties, compressive modulus and especially storage modulus. For the specific wear rate the neural network inferred that along with material composition and testing conditions the second most influential parameters were the tensile modulus and strain, microhardness as well as damping properties. The compressive properties as well as the notch Charpy impact strength seemed to have a small impact on sliding wear of PPS composites, except for the compressive strength. This was broadly in line with the published literature.

Finally, the results of this work have proven so far the general applicability of the ANN approach in simulating the complex, multi-dimensional, non-linear relationship between sliding friction and wear behavior of polymer composites filled with diverse fillers (e.g. short fibers, sub-micro particles, internal lubricants) and selected input

parameters (e.g. material composition, testing conditions). Yet, it leaves potential for further improvements and future research activities on:

- Reduce the error level for the specific wear rate as well as increase the robustness of the developed ANN so that it can make predictions with a smaller amount of training data.
- Development of a method to effectively handle and integrate the pruning step into the GUI for training and prediction.
- Using the developed ANN tool for designing new wear resistant polymer matrix composites for sliding friction and wear applications.
- Applying the practical knowledge gained herein by the ANN for the elucidation of other complex phenomena such as abrasive or corrosive wear of polymer-based composites.

As to the ball bearing effect on a sub-micro scale, future investigations are required in order to unravel the exact tribological mechanism of this complex interface prior to the application of these materials into engineering practice, with particular emphasis on:

- Longer tests, which are needed to observe if the generation of the quasi-spherical wear debris during sliding ceases at a certain point or if they become less significant after extended sliding.
- Additional tests, which are required to determine the range of operating conditions where the sub-micro particles are most effective in reducing sliding friction and wear. Likewise, the operating parameters that influence the performance of the sub-micro particles should be closely examined.
- Further tests on the effectiveness of the sub-micro particles in the high pv-range due to possible destruction of the quasi-spherical structures under high loads (> 4 MPa) and sliding velocities (> 3 m/s), thus causing an inability to provide rolling friction any longer.
- Analysis of the influence of the particulate filler’s surface modification and type for their rolling friction.

7 References

[1] Axen, N.; Hogmark, S.; Jacobson, S.: Friction and Wear Measurement Techniques. In: Bhushan, B. (Ed.): Modern Tribology Handbook. Vol I. Boca Raton: CRC Press, 2001, 493-510

[2] Stachowiak, G.W.; Batchelor, A.W.; Stachowiak, G.B.: Introduction. In: Stachowiak, G.W.; Batchelor, A.W.; Stachowiak, G.B. (Eds.): Experimental Methods in Tribology. Amsterdam: Elsevier, 2004, 1-12

[3] Zum Gahr, K.H.: Microstructure and Wear of Materials. New York: Elsevier, 1987

[4] Ludema, K.: Friction. In: Bhushan, B. (Ed.): Modern Tribology Handbook. Vol I. Boca Raton: CRC Press, 2001, 205-233

[5] Kato, K.; Adachi, K.: Wear Mechanisms. In: Bhushan, B. (Ed.): Modern Tribology Handbook. Vol I. Boca Raton: CRC Press, 2001, 273-300

[6] Bhushan, B.; Gupta, B.K.: Friction, Wear and Lubrication. In: Bhushan, B.; Gupta, B.K. (Eds.): Handbook of Tribology: Materials, Coatings, and Surface Treatments. New York: McGraw-Hill, 1991, 2.1-2.36

[7] Friedrich, K.: Traditional and New Approaches to the Development of Wear-Resistant Polymer Composites. Journal of Synthetic Lubrication, Vol. 18, No. 4 (2002), 275-290

[8] Norm ASTM G77 - 05e1 Standard Test Method for Ranking Resistance of Materials to Sliding Wear Using Block-on-Ring Wear Test

[9] Norm ASTM G99 - 05 Standard Test Method for Wear Testing with a Pin-on-Disk Apparatus

[10] Friedrich, K.: On the Sliding Wear Performance of Polymer Composite Systems. Research Report CCM-90-19. Newark: Center for Composite Materials, University of Delaware, 1990

[11] Tewari, U.S.; Bijwe, J.: Recent Developments in Tribology of Fiber Reinforced Composites with Thermoplastic and Thermosetting Matrices. In: Friedrich, K. (Ed.): Advances in Composite Tribology. Amsterdam: Elsevier, 1993, 159-207

[12] Friedrich, K.: Wear of Reinforced Polymers by Different Abrasive Counterparts. In: Friedrich, K. (Ed.): Friction and Wear of Polymer Composites. Amsterdam: Elsevier, 1986, 233-287

[13] Anderson, J.C.: The Wear and Friction of Commercial Polymers and Composites. In: Friedrich, K. (Ed.): Friction and Wear of Polymer Composites. Amsterdam: Elsevier, 1986, 329-362

[14] Hutchings, I.M.: The Challenge of Wear. In: Stachowiak, G. W. (Ed.): Wear-Materials, Mechanisms and Practice. Chichester: John Wiley & Sons, 2005, 1-7

[15] Zhang, Z.; Friedrich, K.: Artificial Neural Networks Applied to Polymer Composites: a Review. Composites Science and Technology, Vol. 63, No. 14 (2003), 2029-2044

[16] Barber, A.J.; Renner, T.E.; You, S.; Sandlass, G.S.; Maki, A.: Predicting Tire Handling Performance Using Neural Network Models. Society of Automotive Engineers 2004-01-1574 (2004), 1-9

[17] Wolverton, M.P.; Talley, K.; Theberge, J.E.: Friction and Wear of Thermoplastic Composites. In: Henry, S.D. (Ed.): ASM Handbook. Vol.18. Friction, Lubrication, and Wear Technology. ASM International, 1992, 820-826

[18] Briscoe, B.J.; Sinha, S.K.: Tribology of Polymeric Solids and Their Composites. In: Stachowiak, G.W. (Ed.): Wear-Materials, Mechanisms and Practice. Chichester: John Wiley & Sons, 2005, 223-267

[19] Bhushan, B.; Gupta, B.K.: Solid Lubricants and Self-Lubricating Solids. In: Bhushan, B.; Gupta, B.K. (Eds.): Handbook of Tribology: Materials, Coatings, and Surface Treatments. New York: McGraw-Hill, 1991, 5.1-5.75

[20] Friedrich, K.; Lu, Z.; Haeger, A.M.: Recent Advances in Polymer Composites' Tribology. Wear, Vol. 190 (1995), 39-144

[21] Kukureka, S.N.; Hooke, C.J.; Rao, M.; Liao, P.; Chen, Y.K: The Effect of Fibre Reinforcement on the Friction and Wear of Polyamide 66 under Dry Rolling-Sliding Contact. Tribology International, Vol. 32 (1999), 107-116

[22] Erdemir, A.: Solid Lubricants and Self-Lubricating Films. In: Bhushan, B. (Ed.): Modern Tribology Handbook. Vol II. Boca Raton: CRC Press, 2001, 787-825

[23] Wetzel, B.; Haupert, H.; Friedrich, K.; Zhang, M.Q.; Rong, M.Z.: Impact and Wear of Polymer Nanocomposites at Lower Filler Content. Polymer Engineering and Science, Vol. 42 (2002), 1919-1927

[24] Wetzel, B.; Haupert, F.; Zhang, M.Q.: Epoxy Nanocomposites with High Mechanical and Tribological Performance. Composites Science and Technology, Vol. 63 (2003), 2055-2067

[25] Zhang, Z.; Friedrich, K.: Tribological Characteristics of Micro- and Nanoparticle Filled Polymer Composites. In: Friedrich, K.; Fakirov, S.; Zhang, Z. (Eds.): Polymer Composites: From Nano-to Macro-Scale. New York: Springer, 2005, 169-185

[26] Friedrich, K.; Zhang, Z.; Schlarb, A.K.: Effects of Various Fillers on the Sliding Wear of Polymer Composites. Composites Science and Technology, Vol. 65 (2005), 2329-2343

[27] Chang, L.: Friction and Wear of Nanoparticle Filled Polymer Composites. Kaiserslautern: Institut für Verbundwerkstoffe, 2005. ISBN 3-934930-56-5

[28] Chang, L.; Zhang, Z.; Ye, L.; Friedrich, K.: Synergistic Effects of Nanoparticles and Traditional Tribo-fillers on Sliding Wear of Polymeric Hybrid Composites. In: Friedrich, K.; Schlarb, A.K. (Eds.): Tribology of Polymeric Nanocomposites, Friction and Wear of Bulk Materials and Coatings. Amsterdam: Elsevier, 2008, 35-61

[29] Zhang, G.; Schlarb, A.K.; Tria, S.; Elkedim, O.: Tensile and Tribological Behaviors of PEEK/Nano-SiO_2 Composites Compounded Using a Ball Milling Technique. Composites Science and Technology, Vol. 68 (2008), 3073-3080

[30] Wagner, H.D.: Reinforcement. In Mark, H.F. (Ed.): Encyclopedia of Polymer Science and Technology. 3., Ed. Vol. 4. New York: John Wiley & Sons, 2005, 94-115

[31] Song, J.; Ehrenstein, G.W.: Friction and Wear of Self-reinforced Thermoplastics. In: Friedrich, K. (Ed.): Advances in Composite Tribology. Amsterdam: Elsevier, 1993, 19-63

[32] Friedrich, K.: Reibung und Verschleiß von Polymer-Verbundwerkstoffen. Zeitschrift für Werkstofftechnik, Vol. 17 (1986), 434-443

[33] Haeger, A.M.; Davies, M.: Short-fibre Reinforced, High Temperature Resistant Polymers for a Wide Field of Tribological Applications. In: Friedrich, K. (Ed.): Advances in Composite Tribology. Amsterdam: Elsevier, 1993, 107-157

[34] Dayananda Jawali, N.; Siddeswarappa, B.; Siddaramaiah: Physicomechanical Properties, Machinability, and Morphological Behavior of Short Glass Fiber-Reinforced Nylon 6 Composites. Journal of Reinforced Plastics and Composites, Vol. 25, No. 13 (2006), 1409-1418

[35] Reinicke, R.: Eigenschaftsprofil neuer Verbundwerkstoffe für Tribologische Anwendungen im Automobilbereich. Kaiserslautern: Institut für Verbundwerkstoffe, 2000. ISBN-3-934930-17-4

[36] Reinicke, R.; Haupert, F.; Friedrich, K.: On the Tribological Behaviour of Selected Injection Moulded Thermoplastic Composites. Composites Part A, Vol. 29 (1998), 763-771

[37] Lancaster, J.: The effect of Carbon Fiber Reinforcement on the Friction and Wear of Polymers. Journal of Applied Physics, Vol. 1 (1968), 549-559

[38] Jain, V.K.: Investigation of the Wear Mechanism of Carbon-Fiber-Reinforced Acetal. Wear, Vol. 92 (1983), 279-292

[39] Newell, J.: Carbon Fibers. In: Mark, H.F. (Ed.): Encyclopedia of Polymer Science and Technology. 3., Ed. Vol. 9. New York: John Wiley & Sons, 2005, 91-112

[40] Floeck, J.; Friedrich, K.; Yuan, Q.: On the Friction and Wear Behaviour of PAN- and Pitch-Carbon Fiber Reinforced PEEK Composites. Wear, Vol. 225-229 (1999), 204-311

[41] Zhang, Z.; Chang, L.: Tribological Properties of Epoxy Nanocomposites: Part II. A Combinative Effect of Short Carbon Fibre with Nano-TiO_2. Wear, Vol. 260 (2006), 869-878

[42] Crosa, G.; Baumvol, I.J.R: Tribology of Polymer Composites Used as Frictional Materials. In: Friedrich, K. (Ed.): Advances in Composite Tribology. Amsterdam: Elsevier, 1993, 583-626

[43] Schulte, K.; Friedrich, K.; Jacobs, O.: Fretting and Fretting Fatigue of Advanced Composite Laminates. In: Friedrich, K. (Ed.): Advances in Composite Tribology. Amsterdam: Elsevier, 1993, 669-722

[44] Wu, Y.T.: How Short Aramid Fiber Improves Wear Resistance, Du Pont Co., Textile Fibers Dept., 2003 – Corporate Literature

[45] http://www.addcomp.com/articles/general/features/strengtheningJanFeb07.html (30.08.2007)

[46] Bourbigot, S.; Flambard, X: Heat Resistance and Flammability of High Performance Fibres: a Review. Fire and Materials, Vol. 26 (2002), 155-168

[47] Lin, J.S.: Effect of Surface Modification by Bromination and Metalation on Kevlar Fiber Epoxy Adhesion. European Polymer Journal, Vol. 38, No. 1 (2002), 79-86

[48] Tarantili, P.A.; Andreopoulos, A.G.: Mechanical Properties of Epoxies Reinforced with Chloride-Treated Aramid Fibers. Journal of Applied Polymer Science, Vol. 65 (1998), 267-276

[49] Larsen, T.Ø.; Andersen, T.L.; Thorning, B.; Vigild, M.E.: The Effect of Particle Addition and Fibrous Reinforcement on Epoxy-Matrix Composites for Severe Sliding Conditions. Wear, Vol. 264 (2008), 857-868

[50] Lhymn, C.; Bozolla, J: Friction and Wear of Fiber Reinforced PPS Composites. Advances in Polymer Technology, Vol. 7, No. 4 (1987), 451-461

[51] Chen, J.; Jia, J.; Zhou, H.; Chen, J.; Yang, S.; Fan, L.: Tribological Behavior of Short-Fiber-Reinforced Polyimide Composites under Dry-Sliding and Water-Lubricated Conditions. Journal of Applied Polymer Science, Vol. 107 (2008), 788-796

[52] Paulo Davim, J.; Cardoso, R.: Effect of the Reinforcement (Carbon or Glass Fibers) on Friction and Wear Behavior of the PEEK against Steel Surface at Long Dry Sliding. Wear, Vol. 266 (2009), 795-799

[53] Zhang, S.W.: State-of-the-Art of Polymer Tribology. Tribology International, Vol. 31 (1998), 49-60

[54] Voss, H.; Friedrich, K.: Wear Performance of a Bulk Liquid Crystal Polymer and Its Short Fibre Composites. Tribology International, Vol. 19, No. 3 (1986), 145-156

[55] Xian, G.; Zhang, Z.: Sliding Wear of Polyetherimide Matrix Composites I. Influence of Short Carbon Fibre Reinforcement. Wear, Vol. 258 (2005), 776-782

[56] Lu, Z.P.; Friedrich, K.: On Sliding Friction and Wear of PEEK and Its Composites. Wear, Vol. 181-183 (1995), 624-631

[57] Suresha, B.: Friction and Dry Slide Wear of Short Glass Fiber Reinforced Thermoplastic Polyurethane Composites. Journal of Reinforced Plastics and Composites, http://jrp.sagepub.com/cgi/rapidpdf/0731684408097763v1.pdf (10.12.2009)

[58] Zhang, H.; Zhang, Z.: Comparison of Short Carbon Fibre Surface Treatments on Epoxy Composites: II. Enhancement of the Wear Resistance. Composites Science and Technology, Vol. 64 (2004), 2031-2038

[59] Voss, H.; Friedrich, K.: On the Wear Behaviour of Short-Fibre-Reinforced PEEK Composites. Wear, Vol. 116 (1987), 1-18

[60] Yu, L.; Bahadur, S.: An Investigation of the Transfer Film Characteristics and the Tribological Behaviors of Polyphenylene Sulfide Composites in Sliding against Tool Steel. Wear, Vol. 214 (1998), 245-251

[61] Zhao, Q.; Bahadur, S.: A Study of the Modification of the Friction and Wear Behavior of Polyphenylene Sulfide by Particulate Ag_2S and PbTe Fillers. Wear, Vol. 217 (1998), 62-72

[62] Schwartz, C.J.; Bahadur, S.: Studies on the Tribological Behavior and Transfer Film-Counterface Bond Strength for Polyphenylene Sulfide Filled with Nanoscale Alumina Particles. Wear, Vol. 237 (2000), 261-273

[63] Bahadur, S.: The Development of Transfer Layers and Their Role in Polymer Tribology. Wear, Vol. 245 (2000), 92-99

[64] Schwartz, C.J.; Bahadur, S.: The Role of Filler Deformability, Filler-Polymer Bonding, and Counterface Material on the Tribological Behaviour of Polyphenylene Sulphide (PPS). Wear, Vol. 251 (2001), 1532-1540

[65] Cho, M.H., Bahadur. S.: Study of the Tribological Synergistic Effects in Nano CuO-filled and Fiber Reinforced Polyphenylene Sulfide Composites. Wear, Vol. 258 (2005), 835-845

[66] Bahadur, S.; Sunkara, C.: Effect of Transfer Film Structure, Composition and Bonding on the Tribological Behaviour of Polyphenylene Sulphide Filled with Nano Particles of TiO_2, ZnO, CuO and SiC. Wear, Vol. 258 (2005), 1411-1421

[67] Lansdown, A.R.: Molybdenum Disulfide Lubrication. Amsterdam: Elsevier, 1999, 207-244

[68] Tanaka, K.: Effect of Various Fillers on the Friction and Wear of PTFE-Based Composites. In: Friedrich K. (Ed.): Friction and Wear of Polymer Composites. Amsterdam: Elsevier, 1986, 137-174

[69] Biswas, S.K.: Friction and Wear of PTFE-a Review. Wear, Vol. 158 (1992), 193-211

[70] Samyn, P.; Quintelier, J.; Ost, W.; De Baets, P.; Schoukens, G.: Sliding Behaviour of Pure Polyester and Polyester-PTFE Filled Bulk Composites in Overload Conditions. Polymer Testing, Vol. 24 (2005), 588–603

[71] Liu, X.; Li, T.; Tian, N.; Liu, W.: Note, Tribological Properties of PTFE-Filled PMIA. Journal of Applied Polymer Science, Vol. 74 (1999), 747-751

[72] Cho, M.H.; Bahadur, S.; Pogosian, A.K.: Friction and Wear Studies Using Taguchi Method on Polyphenylene Sulfide with a Complex Mixture of MoS_2, Al_2O_3, and Other Compounds. Wear, Vol. 258 (2005), 1825-1835

[73] Oster, F.: Hochtemperaturbeständige Polymer-Beschichtungen für tribologische Anwendungen. Kaiserslautern: Institut für Verbundwerkstoffe, 2005. ISBN 3-934930-49-2

[74] Dresselhaus, M.S.; Dresselhaus, G.; Eklund, P.C.: Science of Fullerenes and Carbon Nanotubes. San Diego: Academic Press Inc., 1996, 15-59

[75] Zhang, X.; Liao, G.; Jin, Q.; Feng, X.; Jian, X.: On Dry Sliding Friction and Wear Behavior of PPESK Filled with PTFE and Graphite. Tribology International, Vol. 41 (2008), 195-201

[76] Winer, W.O.: Molybdenum Disulfide as a Lubricant: a Review of the Fundamental Knowledge. Wear, Vol. 10 (1967), 422-452

[77] Yu, L.; Yang, G.S.; Liu, W.; Xue, W.: An Investigation of the Friction and Wear Behaviors of Polyphenylene Sulfide Filled with Solid Lubricants. Polymer Engineering and Science, Vol. 40 (2000), 1825-1832

[78] Wang, J.; Gu, M.; Songhao, B.; Ge, S.: Investigation of the Influence of MoS_2 Filler on the Tribological Properties of Carbon Fiber Reinforced Nylon 1010 Composites. Wear, Vol. 225 (2003), 774-779

[79] Bolvari, A.; Glenn, S.; Janssen, R.; Elliset, C.: Wear and Friction of Aramid Fiber and PTFE Filled Composites. Wear, Vol. 203-204 (1997), 7-9

[80] Zhang, Z., Breidt, C., Chang, L., Friedrich, K.: Correlation between Tribological and Mechanical Properties of Short-fiber/Particle Reinforced PEEK. 6th International Tribology Conference (AUSTRIB 2002), Perth (Australia), December 2-5, 2002, 589-594

[81] Xian, G.; Zhang, Z.: Effects of the Combination of Solid Lubricants and Short Carbon Fibres on the Sliding Performance of Poly(Etherimide) Matrix Composites. Journal of Applied Polymer Science, Vol. 94 (2004), 1428-1434

[82] Zhang, X.R.; Pei, X.Q.; Wang, Q.H.: Effect of Solid Lubricant on the Tribological Properties of Polyimide Composites Reinforced with Carbon Fibers. Journal of Reinforced Plastics and Composites, Vol. 27 (2008), 2005-2012

[83] Bijwe, J.; Rajesh, J.J.; Jeyakumar, A.; Ghosh, A.; Tewari, U.S.: Influence of Solid Lubricants and Fiber Reinforcement on Wear Behaviour of Polyethersulphone. Tribology International, Vol. 33 (2000), 697-706

[84] Bijwe, J.; Indumathi, J.; Rajesh, J.J.; Fahim, M.: Friction and Wear Behaviour of Polyetherimide Composites in Various Wear Modes. Wear, Vol. 249 (2001), 715-726

[85] Chand, N.; Fahim, M.: Wear and Friction of FRP Composites. In: Chand, N.; Fahim, M. (Eds.): An Introduction to Tribology of FRP Materials. New Delhi: Allied Publishers Ltd., 2000, 132-255

[86] Khoddamzadeh, A.; Liu, R.; Wu, X.: Novel Polytetrafluoroethylene (PTFE) Composites with Newly Developed Tribaloy Alloy Additive for Sliding Bearings. Wear, Vol. 266, No. 7-8 (2009), 646-657

[87] Lu, Z.: Geschmierte Hochtemperatur-Verbundwerkstoffe für Anwendungen als Gleitelemente. Egelsbach: Hänsel-Hohenhausen, 1994. ISBN 3-89349-527-4

[88] Theiler, G.; Hübner, W.; Gradt, T.; Klein, P.: Friction and Wear of Carbon Fibre Filled Polymer Composites at Room and Low Temperatures. Materialwissenschaft und Werkstofftechnik, Vol. 35 (2004), 683-689

[89] Klein, P.: Tribologisches Eigenschaftsprofil kurzfaserverstärkter Polytetrafluorethylen/Polyetheretherketon-Verbundwerkstoffe. Kaiserslautern: Institut für Verbundwerkstoffe, 2005. ISBN 3-934930-50-6

[90] Thostenson, E.T., Chunyu, L., Chou, T.W.: Nanocomposites in Context. Composites Science and Technology, Vol. 65, 2005, 491-516

[91] Durand, J.M.; Vardavoulias, M.; Jeandin, M.: Role of Reinforcing Ceramic Particles in the Wear Behaviour of Polymer-based Model Composites. Wear, Vol. 181-183 (1995), 833-839

[92] Bahadur, S.; Gong, D.: The Role of Copper Compounds as Fillers in the Transfer and Wear Behavior of Polyetheretherketone. Wear, Vol. 154 (1992), 151-165

[93] Bahadur, S.; Gong, D.; Anderegg, J.W.: The Role of Copper Compounds as Fillers in the Transfer Film Formation and Wear of Nylon. Wear, Vol. 154 (1992), 207-223

[94] Bahadur, S.; Gong, D.: The Transfer and Wear of Nylon and CuS-Nylon Composites: Filler Proportion and Counterface Characteristics. Wear, Vol. 162-164 (1993), 397-406

[95] Bahadur, S.; Gong, D.; Anderegg, J.W.: Tribochemical Studies by XPS Analysis of Transfer Films of Nylon 11 and Its Composites Containing Copper Compounds. Wear, Vol. 165 (1993), 205-212

[96] Bahadur, S.; Kapoor, A.: The Effect of ZnF_2, ZnS and PbS Fillers on the Tribological Behavior of Nylon 11. Wear, Vol. 155 (1992), 49-61

[97] Bahadur, S.; Gong, D.; Anderegg, J.W.: Investigation of the Influence of CaS, CaO, and CF_2 Fillers on the Transfer and Wear of Nylon by Microscopy and XPS Analysis. Wear, Vol. 197 (1996), 271-279

[98] Zhao, Q.; Bahadur, S.: The Mechanism of Filler Action and the Criterion of Filler Selection for Reducing Wear. Wear, Vol. 225-229 (1999), 660-668

[99] Jintang, G.: Tribochemical Effects in Formation of Polymer Transfer Film. Wear, Vol. 245 (2000), 100-106

[100] Xing, X.S.; Li, R.K.Y.: Wear Behaviour of Epoxy Matrix Composites Filled with Uniform Sized Sub-Micron Spherical Silica Particles. Wear, Vol. 256 (2004), 21-26

[101] Wetzel, B.; Rosso, P.; Haupert, F.; Friedrich, K.: Epoxy Nanocomposites - Fracture and Toughening Mechanisms. Engineering Fracture Mechanics, Vol. 73 (2006), 2375-2398

[102] Dasari, A.; Yu, Z.Z.; Mai, Y.W.: Fundamental Aspects and Recent Progress on Wear/Scratch Damage in Polymer Nanocomposites, Materials Science and Engineering R, Vol. 63 (2009), 31-80

[103] Bahadur, S.; Schwartz, C.J.: The Influence of Nanoparticle Fillers in Polymer Matrices on the Formation and Stability of Transfer Film during Wear. In: Friedrich, K.; Schlarb, A.K. (Eds.): Tribology of Polymeric Nanocomposites, Friction and Wear of Bulk Materials and Coatings. Amsterdam: Elsevier, 2008, 17-34

[104] Zhang, M.Q.; Rong, M.Z.; Yu, S.L.; Wetzel, B.; Friedrich, K.: Improvement of Tribological Performance of Epoxy by the Addition of Irradiation Grafted Nano-Inorganic Particles. Macromolecular Materials and Engineering, Vol. 287 (2002), 111-115

[105] Putnam, S.A.; Cahill, D.G.; Ash, B.J.; Schadler, L.S.: High-precision Thermal Conductivity Measurements as a Probe of Polymer/Nanoparticle Interfaces. Journal of Applied Physics, Vol. 94, No. 10 (2003), 6785-6788

[106] Xue, Q.; Wang, Q.: Wear Mechanisms of Polyetheretherketone Composites Filled with Various Kinds of SiC. Wear, Vol. 213 (1997), 54-58

[107] Rong, M.Z.; Zhang, M.Q.; Liu, H.; Zeng, H.M.; Wetzel, B.; Friedrich, K.: Microstructure and Tribological Behavior of Polymeric Nanocomposites. Industrial Lubrication and Tribology, Vol. 53 (2001), 72-77

[108] Shao, X.; Liu, W.; Xue, Q.: The Tribological Behavior of Micrometer and Nanometer TiO_2 Particle-Filled Poly(phthalazine ether sulfone ketone) Composites. Journal of Applied Polymer Science, Vol. 92 (2004), 906-914

[109] Shi, G.; Zhang, Q.; Rong, M.Z.; Wetzel, B.; Friedrich, K.: Friction and Wear of Low Nanometer Si_3N_4 Filled Epoxy Composites. Wear, Vol. 254 (2003), 784-796

[110] Wang, Q.; Xu, J.; Shen, W.; Liu, W.: An Investigation of the Friction and Wear Properties of Nanometer Si_3N_4 Filled PEEK. Wear, Vol. 196 (1996), 82-86

[111] Zhang, M.Q.; Rong, M.Z.; Yu, S.L.; Wetzel, B.; Friedrich, K.: Effect of Particle Surface Treatment on the Tribological Performance of Epoxy Based Nanocomposites. Wear, Vol. 253 (2000), 1088-1095

[112] Hou, X.; Shan, C.X.; Choy, K.L.: Microstructures and Tribological Properties of PEEK-based Nanocomposites Coatings Incorporating Inorganic Fullerene-like Nanoparticles. Surface and Coatings Technology, Vol. 202 (2008), 2287-2291

[113] Wang, Q.; Xue, Q.; Liu, H.; Shen, W.; Xu, J.: The Effect of Particle Size of Nanometer ZrO_2 on the Tribological Behaviour of PEEK. Wear, Vol. 198 (1996), 216-219

[114] Wang, Q.; Xue, Q.; Shen, W.: The Friction and Wear Properties of Nanometer SiO_2-Filled Polyetheretherketone. Tribology International, Vol. 30 (1997), 193-197

[115] Wang, Q.; Xu, J.; Shen, W.; Xue, Q.: The Effect of Nanometer SiC Filler on the Tribological Behaviour of PEEK. Wear, Vol. 209 (1997), 316-321

[116] Wang, Q.; Xue, Q.; Shen, W.; Zhang, J.: The Friction and Wear Properties of Nanometer ZrO_2-Filled Polyetheretherketone. Journal of Applied Polymer Science, Vol. 69 (1998), 135-141

[117] Sreekala, M.S.; Eger, C.: Property Improvements of an Epoxy Resin by Nanosilica Particle Reinforcement. In: Friedrich, K.; Fakirov, S.; Zhang, Z. (Eds.): Polymer Composites - from Nano- to Macroscale. New York: Springer, 2005, 91-105

[118] Garcia, M.; de Rooij, M.; Winnubst, L.; van Zyl, W.E.; Verweij, H.: Friction and Wear Studies on Nylon-6/SiO_2 Nanocomposites. Journal of Applied Polymer Science, Vol. 92 (2004), 1855-1862

[119] Li, F.; Hu, K.; Li, J.; Zhao, B.: The Friction and Wear Characteristics of Nanometer ZnO Filled Polytetrafluoroethylene. Wear, Vol. 249 (2002), 877-882

[120] Sawyer, W.G.; Freudenberg, K.D.; Bhimaraj, P.; Schadler, L.S: A Study on the Friction and Wear Behavior of PTFE Filled with Alumina Nanoparticles. Wear, Vol. 254 (2003), 573-580

[121] Lai, S.Q.; Li, T.S.; Liu, X.J.; Lv, R.G.: A Study on the Friction and Wear Behavior of PTFE Filled with Acid Treated Nano-attapulgite. Macromolecular Material Engineering, Vol. 289 (2004), 916-922

[122] Gyurova, L.A.; Schlarb, A.K.: State-of-the-art: On the Action of Various Reinforcing Fillers and Additives for Improving the Sliding Friction and Wear Performance of Polymer Composites. Part 1: Short Fibers, Internal Lubricants, Particulate Fillers. Journal of Plastic Technology, Vol. 4, No. 6 (2008), 1-31

[123] Burris, D.L.; Sawyer, W.G.: Improved Wear Resistance in Alumina-PTFE Nanocomposites with Irregular Shaped Nanoparticles. Wear, Vol. 260 (2006), 915-918

[124] Lai, S.Q.; Li, T.S.; Hu, Z.M.: The Friction and Wear Properties of Polytetrafluoro-ethylene Filled with Ultrafine Diamond. Wear, Vol. 260 (2006), 462-468

[125] Burris, D.l.; Boesl, B.; Bourne, G.R.; Sawyer, W.G.: Polymeric Nanocomposites for Tribological Applications. Macromolecular Materials and Engineering, Vol. 292 (2007), 387-402.

[126] Ji, Q.L.; Zhang, M.Q.; Rong, M.Z.; Wetzel, B.; Friedrich, K.: Friction and Wear of Epoxy Containing Surface Modified SiC Nanoparticles. Tribology Letters, Vol. 20 (2005), 115-123

[127] Zhang, M.Q.; Rong, M.Z.; Luo, Y.: Sliding Wear Performance of Epoxy-based Nanocomposites, In: Friedrich, K.; Schlarb, A.K. (Eds.): Tribology of Polymeric Nanocomposites, Friction and Wear of Bulk Materials and Coatings. Amsterdam: Elsevier, 2008, 108-129

[128] Stachowiak, G.W.; Batchelor, A.W.: Fundamentals of Contact between Solids. In: Stachowiak, G.W.; Batchelor, A.W. (Eds.): Engineering Tribology. Amsterdam: Elsevier, 1993, 527-556

[129] Palabiyik, M.; Bahadur, S.: Tribological Studies of Polyamide 6 and High-density Polyethylene Blends Filled with PTFE and Copper Oxide and Reinforced with Short Glass Fibers. Wear, Vol. 253 (2002), 369-376

[130] Bahadur, S.; Gong, D.; Anderegg, J.W.: Studies of Worn Surfaces and the Transfer Film Formed in Sliding by CuS-Filled and Carbon Fiber-Reinforced Nylon Against a Steel Surface. Wear, Vol. 181-183 (1995), 227-235

[131] Bahadur S.; Polineni, V.K.: Tribological Studies of Glass Fabric-Reinforced Polyamide Composites Filled with CuO and PTFE. Wear, Vol. 200 (1996), 95-104

[132] Xian, G.; Zhang, Z.; Friedrich, K.: Tribological Properties of Micro- and Nanoparticles-Filled Poly(etherimide) Composites. Journal of Applied Polymer Science, Vol. 101 (2006), 1678-1686

[133] Vande Voort, J.; Bahadur, S.: The Growth and Bonding of Transfer Film and the Role of CuS and PTFE in the Tribological Behavior of PEEK. Wear, Vol. 181-183 (1995), 212-221

[134] Hussain, F.; Hojjati, M.; Okamoto, M.; Gorga, R.E.: Review Article: Polymer-Matrix Nanocomposites, Processing, Manufacturing and Application, an Overview. Journal of Composite Materials, Vol. 40, No. 7 (2006), 1511-1575

[135] Zhang, Z.; Breidt, C.; Chang, L.; Haupert, F.; Friedrich, K.: Enhancement of the Wear Resistance of Epoxy: Short Carbon Fibre, Graphite, PTFE and Nano-TiO_2. Composites Part A, Vol. 35 (2004), 1385-1392

[136] Chang, L.; Zhang, Z.; Breidt, C.; Friedrich, K.: Tribological Properties of Epoxy Nanocomposites: I. Enhancement of the Wear Resistance by Nano-TiO_2 Particles. Wear, Vol. 258 (2005), 141-148

[137] Chang, L.; Zhang, Z.; Zhang, H.; Friedrich, K.: Effect of Nanoparticles on the Tribological Behaviour of Short Carbon Fibre Reinforced Poly(etherimide) Composites. Tribology International, Vol. 38 (2005), 966-973

[138] Chang, L.; Zhang, Z.; Zhang, H.; Schlarb, A.K.: On the Sliding Wear of Nanoparticles Filled Polyamide 66 Composites. Composites Science and Technology, Vol. 66 (2006), 3188-3198

[139] Larsen, T.Ø.; Andersen, T.L.; Thorning, B.; Horsewell, A.; Vigild, M.E.: Changes in the Tribological Behavior of an Epoxy Resin by Incorporating CuO Nanoparticles and PTFE Microparticles. Wear, Vol. 265 (2008), 203-213

[140] Zhang, G.; Schlarb, A.K.: The Roles of Nano-SiO_2 Particles on the Tribololgical Behavior of Short Carbon Fiber Reinforced PEEK. Composites Science and Technology, Vol. 69 (2009), 1029-1035

[141] Guo, Q.B.; Rong, M.Z.; Jia, G.L.; Zhang, M.Q.: Sliding Wear Performance of Nano-SiO_2/Short Carbon Fiber/Epoxy Hybrid Composites. Wear, Vol. 266 (2009), 658-665

[142] McCook, L.; Boesl, B.; Burris, D.L.; Sawyer, W.G.: Epoxy, ZnO, and PTFE Nanocomposite: Friction and Wear Optimization. Tribology Letters, Vol. 22 (2006), 253-257

[143] Su, F.; Zhang, Z.; Liu, W.: Friction and Wear Behavior of Hybrid Glass/PTFE Fabric Composite Reinforced with Surface Modified Nanometer ZnO. Wear, Vol. 265 (2008), 311-318

[144] Xian, G.; Walter, R.; Haupert, F.: A Synergistic Effect of Nano-TiO_2 and Graphite on the Tribological Performance of Epoxy Matrix Composites. Journal of Applied Polymer Science, Vol. 102 (2006), 2391-2400

[145] Su, F.; Zhang, Z.; Liu, W.: Tribological Behavior of Hybrid Glass/PTFE Fabric Composites with Phenolic Resin Binder and Nano-TiO_2 Filler. Wear, Vol. 264 (2008), 562-570

[146] Gyurova, L.A.; Jiang, Z.; Friedrich, K.; Zhang, Z.; Schlarb, A.K: On the Tribological Behavior of Selected PPS Nanocomposites Designed for Tribological Exploitation. In: Reibung, Schmierung und Verschleiß, Vol. 1. 47. Tribologie-Fachtagung, Göttingen (Germany), September 25-27, 2006. Aachen: Gesellschaft für Tribologie e.V., 2006, 30/1-30/10

[147] Jiang, Z.; Gyurova, L.A.; Schlarb, A.K.; Friedrich, K.; Zhang, Z.: Study on Friction and Wear Behavior of Polyphenylene Sulfide Composites Reinforced by Short Carbon Fibers and Sub-Micro TiO_2 Particles. Composites Science and Technology Vol. 68 (2008), 734-742

[148] Gyurova, L.A.; Jiang, Z.; Schlarb, A.K.; Friedrich, K.; Zhang, Z.: Study on the Wear and Friction of Short Carbon Fiber and/or Nano-TiO_2 Reinforced Polyphenylene Sulfide Composites Using Artificial Neural Networks. In: Fisher, A.; Bobzin, K. (Eds.): Friction, Wear and Wear Protection, International Symposium on Friction, Wear and Wear Protection 2008, Aachen (Germany), April 9-11, 2008. Weinheim: VCH, 2009, 417-422

[149] Rapoport, L.; Lvovsky, M.; Lapsker, I.; Leshchinsky, V.; Volovik, Y.; Feldman, Y.; Zak, A.; Tenne, R.: Slow Release of Fullerene-like WS_2 Nanoparticles as a Superior Solid Lubrication Mechanism in Composite Matrices. Advanced Engineering Materials, Vol. 3 (2001), 71-75

[150] Rapoport, L.; Lvovsky, M.; Lapsker, I.; Leshchinsky, V.; Volovik, Y.; Feldman, Y.; Margolin, A.; Rosentsveig, R.; Tenne, R.: Slow Release of Fullerene-like WS_2 Nanoparticles from Fe-Ni Graphite Matrix: A Self-lubricating Nanocomposite. Nanoletters, Vol. 1 (2001), 137-140

[151] Rapoport, L.; Nepomnyashchy, O.; Lapsker, I.; Verdyan, A.; Soifer, Y.; Popovitz-Biro R.; Tenne; R.: Friction and Wear of Fullerene-like WS_2 under

Severe Contact Conditions: Friction of Ceramic Materials. Tribology Letters, Vol. 19, No. 2 (2005), 143-149

[152] Joly-Pottuza, L.; Dassenoya, F.; Belina, M.; Vachera, B.; Martina; J.M.; Fleischer, N.: Ultralow-friction and Wear Properties of IF-WS_2 under Boundary Lubrication. Tribology Letters, Vol. 18, No. 4 (2005), 477-485

[153] Rapoport, L.; Fleischer, N.; Tenne, R.: Applications of WS_2 (MoS_2) Inorganic Nanotubes and Fullerene-like Nanoparticles for Solid Lubrication and for Structural Nanocomposites. Journal of Materials Chemistry, Vol. 15 (2005), 1782-1788

[154] Yang, H.; Liu, S.; Li, J.; Li, M.; Peng, G.; Zou, G.: Synthesis of Inorganic Fullerene-like WS_2 Nanoparticles and their Lubricating Performance. Nanotechnology, Vol. 17 (2006), 1512-1519

[155] Cizaire, L.; Vacher, B.; Le Mogne, T., Martin, J.M.; Rapoport, L.; Margolin, A.; Tenne, R.: Mechanisms of Ultra-low Friction by Hollow Inorganic Fullerene-like MoS_2 Nanoparticles. Surface and Coatings Technology, Vol. 160 (2002), 282-287

[156] Huanga, H.D.; Tua, J.P.; Zoua, T.Z.; Zhanga, L.L.; Heb, D.N.: Friction and Wear Properties of IF–MoS_2 as Additive in Paraffin Oil. Tribology Letters, Vol. 20, No. 3-4 (2005), 247-250

[157] Zou, T.; Tu, J.; Huang, H.; Lai, D.; Zhang, L.; He, D.: Preparation and Tribological Properties of Inorganic Fullerene-like MoS_2. Advanced Engineering Materials, Vol. 8, No. 4 (2006), 289-293

[158] Margolin, A.; Popovitz-Biro, R.; Albu-Yaron, A.; Rapoport, L.; Tenne, R.: Inorganic Fullerene-like Nanoparticles of TiS_2. Chemical Physics Letters, Vol. 411 (2005), 162-166

[159] Wang, Q.; Xue, Q.; Liu, W.; Chen, J.M.: The Friction and Wear Characteristics of Nanometer SiC and Polytetrafluoroethylene Filled Polyetheretherketone. Wear, Vol. 243 (2000), 140-146

[160] Khare, R.; Bose, S.: Carbon Nanotube Based Composites- a Review. Journal of Minerals & Materials Characterization & Engineering, Vol. 4 (2005), 31-46

[161] Ahir, S.V.; Terentjev, E.M.: Polymer Containing Carbon Nanotubes: Active Composite Materials. In: Nalwa, H.S. (Ed.): Polymeric Nanostructures and Their Applications. Vol. 1. Los Angeles: American Scientific Publishers (2006), 1-48

[162] Wang, L.Y.; Tu, J.P.; Chen, W.X.; Wang, Y.C.; Liu, X.K.; Olk, C.; Cheng, D.H.; Zhang, X.B.: Friction and Wear Behaviour of Electroless Ni-Based CNT Composite Coatings. Wear, Vol. 254 (2003), 1289-1293

[163] Suhr, J.; Koratkar, N.; Keblinski, P.; Ajayan, P.: Viscoelasticity in Carbon Nanotube Composites. Nature Materials, Vol. 4 (2005), 134-137

[164] Bright, I.; Koutsos, V.; Li, Q.; Cheung, R.: Carbon Nanotubes for Integration into Nanocomposite Materials. Microelectronic Engineering, Vol. 83 (2006), 1542-1546

[165] Joly-Pottuz, L.; Dassenoy, F.; Vacher, B.; Martin, J.M.; Mieno, T.: Ultralow Friction and Wear Behaviour of Ni/Y-based Single Wall Carbon Nanotubes (SWNTs). Tribology International, Vol. 37 (2004), 1013-1018

[166] Chen, X.H.; Chen, C.S.; Xiao, H.N.; Liu, H.B.; Zhou, L.P.; Li, S.L.; Zhang, G.: Dry Friction and Wear Characteristics of Nickel/Carbon Nanotube Electroless Composite Deposits. Tribology International, Vol. 39 (2006), 22-28

[167] Chen, C.; Chen, X.; Yang, Z.; Li, W.; Xu, L.; Yi, B.: Effect of Multi-walled Carbon Nanotubes as Reinforced Fibres on Tribological Behaviour of Ni-P Electroless Coatings. Diamond and Related Materials, Vol. 15 (2006), 151-156

[168] Dong, S.R.; Tu, J.P.; Zhang, X.B.: An Investigation of the Sliding Wear Behaviour of Cu-Matrix Composite Reinforced by Carbon Nanotubes. Materials Science and Engineering A, Vol. 313 (2001), 83-87

[169] An, J.W.; You, D.H.; Lim, D.S.: Tribological Properties of Hot-pressed Alumina-CNT Composites. Wear, Vol. 255 (2003), 677-681

[170] Lim, D.S.; You, D.H.; Choi, H.J.; Lim, S.H.; Jang, H.: Effect of CNT Distribution on Tribological Behaviour of Alumina-CNT Composites. Wear, Vol. 259 (2005), 539-544

[171] Lim, D.S.; An, J.W.; Lee, H.J.: Effect of Carbon Nanotube Addition on the Tribological Behaviour of Carbon/Carbon Composites. Wear, Vol. 252 (2002), 512-517

[172] Gong, Q.M.; Li, Z.; Zhang, Z.; Wu, B.; Zhou, X.; Huang, Q.Z.; Liang, J.: Tribological Properties of Carbon Nanotube-doped Carbon/Carbon Composites. Tribology International, Vol. 39 (2006), 937-944

[173] Tanaka, A.; Umeda, K.; Yudasaka, M.; Suzuki, M.; Ohana, T.; Yumura, M.; Iijima, S.: Friction and Wear of Carbon Nanohorn-containing Polyimide Composites. Tribology Letters, Vol. 19 (2005), 135-142

[174] Cai, H.; Yan, F.; Xue, Q.: Investigation of Tribological Properties of Polyimide/Carbon Nanotube Nanocomposites. Materials Science and Engineering A, Vol. 364 (2004), 94-100

[175] Yang, Z.; Dong, B.; Huang, Y.; Liu, L.; Yan, F.Y.; Li, H.L.: A Study on Car-bon Nanotubes Reinforced Poly(methyl methacrylate) Nanocomposites. Materials Letters, Vol. 59 (2005), 2128-2132

[176] Yang, Z.; Dong, B.; Huang, Y.; Liu, L.; Yan, F.Y.; Li, H.L.: Enhanced Wear resistance and Microhardness of Polystyrene Nanocomposites by Carbon Nanotubes. Materials Chemistry and Physics, Vol. 94 (2005), 109-113

[177] Dong, B.; Wang, C.; He, B.L.; Li, H.L.: Preparation and Tribological Properties of Poly(methyl mathacrylate)/Styrene/MWCNTs Copolymer Nanocomposites. Journal of Applied Polymer Science, Vol. 108 (2008), 1675-1679

[178] Xue, Y.; Wu, W.; Jacobs, O.; Schädel, B.: Tribological Behaviour of UHMWPE/HDPE Blends Reinforced with Multi-wall Carbon Nanotubes. Polymer Testing, Vol. 25 (2006), 221-229

[179] Dong, B.; Yang, Z.; Huang, Y.; Li, H.L.: Study on Tribological Properties of Multi-walled Carbon Nanotubes/Epoxy Resin Nanocomposites. Tribology Letters, Vol. 20 (2005), 251-254

[180] Zhang, L.C.; Zarudi, I.; Xiao, K.Q.: Novel Behaviour of Friction and Wear of Epoxy Composites Reinforced by Carbon Nanotubes. Wear, Vol. 261 (2006), 806-811

[181] Sulong, A.B.; Park, J.; Lee, N.; Goak, J.: Wear Behavior of Functionalized Multi-walled Carbon Nanotube Reinforced Epoxy Matrix Composites. Journal of Composite Materials, http://jcm.sagepub.com/cgi/rapidpdf/0021998306061305v1.pdf (10.12.2009)

[182] Jacobs, O.; Schädel, B.: Wear Behavior of Carbon Nanotube-Reinforced Polyethylene and Epoxy Composites. In: Friedrich, K.; Schlarb, A.K. (Eds.): Tribol-ogy of Polymeric Nanocomposites, Friction and Wear of Bulk Materials and Coatings. Amsterdam: Elsevier, 2008, 209-244

[183] Chen, W.X.; Li, F.; Han, G.; Xia, J.B.; Wang, L.Y.; Tu, J.P.; Xu, Z.D.: Tribological Behavior of Carbon-Nanotube-Filled PTFE Composites. Tribology Letters, Vol. 15 (2003), 275-278

[184] Haykin, S.: Neural Networks: a Comprehensive Foundation. 2., Ed. New Jersey: Prentice Hall, 1999

[185] Fausett, L.: Fundamentals of Neural Networks, Architectures, Algorithms and Applications. New Jersey: Prentice Hall, 1994

[186] Arslan, A.; Ince, R.: The Neural Network Approximation to the Size Effect in Fracture of Cementitious Materials. Engineering Fracture Mechanics, Vol. 54 (1996), 249-261

[187] Warde, J.; Knowles, D.M.: Application of Neural Networks to Mechanical Property Determination of Ni-base Superalloys. ISIJ International, Vol. 39 (1999), 1006-1014

[188] Hayajneh, M.T.; Hassan, A.M.; Mayyas, A.T.: Artificial Neural Network Modeling of the Drilling Process of Self-lubricated Aluminum/Alumina/Graphite Hybrid Composites Synthesized by Powder Metallurgy Technique. Journal of Alloys and Compounds, Vol. 478 (2009), 559-565

[189] Agatonovic-Kustrin, S.; Beresford, R.: Review: Basic Concepts of Artificial Neural Network (ANN) Modeling and Its Application in Pharmaceutical Research. Journal of Pharmaceutical and Biomedical Analysis, Vol. 22 (2000), 717-727

[190] Schooling, J.M.; Brown, M.; Reed, P.A.S.: An Example of the Use of Neural Computing Techniques in Materials Science: the Modeling of Fatigue Thresh-

olds in Ni-base Superalloys. Materials Science and Engineering A, Vol. 260, No. 1-2 (1999), 222-239

[191] Gareth Pierce, S.; Worden, K.; Bezazi, A.: Uncertainty Analysis of a Neural Network Used for Fatigue Lifetime Prediction. Mechanical Systems and Signal Processing, Vol. 22 (2008), 1395-1411

[192] Malinov, S.; Sha, W.: Software Products for Modeling and Simulation in Materials Science. Computational Materials Science, Vol. 28 (2003), 179-198

[193] Tchaban, T.; Griffin, J.P.; Taylor, M.J.: A Comparison between Single and Combined Backpropagation Neural Networks in Prediction of Turnover. Engineering Applications of Artificial Intelligence, Vol. 11 (1998), 41-47

[194] Jia, J.; Davalos, J.F.: An Artificial Neural Network for the Fatigue Study of Bonded FRP-Wood Interfaces. Composite Structures, Vol. 74 (2006), 106-114

[195] Lolas, S.; Olatunbosun, O.A.: Prediction of Vehicle Reliability Performance Using Artificial Neural Networks. Expert Systems with Applications, Vol. 34 (2008), 2360-2369

[196] Swingler, K.: Applying Neural Networks, a Practical Guide. 3., Ed. San Francisco: Morgan Kaufman Publishers Inc., 2001

[197] Genel, K.: Application of Artificial Neural Network for Predicting Strain-life Fatigue Properties of Steel on the Basis of Tensile Tests. International Journal of Fatigue, Vol. 26 (2004), 1027-1035

[198] Zeng, P.: Neural Computing in Mechanics. Applied Mechanics Reviews, Vol. 51, No. 2 (1998), 173-197

[199] Dumortier, C.; Lehert, P.: Statistical Modeling of Mechanical Tensile Properties of Steels by Using Neural Networks and Multivariate Data Analysis. ISIJ International, Vol. 39 (1999), 980-985

[200] Lin, S.C.; Lin, R.J.: Tool Wear Monitoring in Face Milling Using Force Signals. Wear, Vol. 198 (1996), 136-142

[201] Venkatesh, V.; Rack, H.J.: A Neural Network Approach to Elevated Temperature Creep-Fatigue Life Prediction. International Journal of Fatigue, Vol. 21 (1999), 225-234

[202] Sumpter, B.G.; Noid, D.W.: On the Use of Computational Neural Networks for the Prediction of Polymer Properties. Journal of Thermal Analysis, Vol. 46 (1996), 833-851

[203] Forouzan, S.; Akbarzadeh, A.: Prediction of Effect of Thermo-Mechanical Parameters on Mechanical Properties and Anisotropy of Aluminium Alloy AA3004 Using Artificial Neural Network. Materials and Design, Vol. 28, No. 5 (2007), 1678-1684

[204] Han, Y.L.: Artificial Neural Network Technology as a Method to Evaluate the Fatigue Life of Weldments with Welding Defects. International Journal of Pressure Vessels and Piping, Vol. 63 (1995), 205-209

[205] Kang, J.Y.; Song, J.H.: Neural Network Applications in Determining the Fatigue Crack Opening Load. International Journal of Fatigue, Vol. 20 (1998), 57-69

[206] Bishop, C.M.: Neural Networks for Pattern Recognition. New York: Oxford University Press, 1995

[207] Todd Pleune, T.; Chopra, O.K.: Using Artificial Neural Networks to Predict the Fatigue Life of Carbon and Low-alloy Steel. Nuclear Engineering and Design, Vol. 197 (2000), 1-12

[208] De Veaux, R.D.; Schumi, J.; Schweinsberg, J.; Ungar, L.H.: Prediction Intervals for Neural Networks via Nonlinear Regression. Technometrics, Vol. 40, (1998), 273-282

[209] Genel, K.; Kurnaz, S.C.; Durman, M.: Modeling of Tribological Properties of Alumina Fiber Reinforced Zinc-aluminum Composites Using Artificial Neural Network. Materials Science and Engineering A, Vol. 363 (2003), 203-210

[210] Li, Y.: Predicting Materials Properties and Behavior Using Classification and Regression Trees. Materials Science and Engineering A, Vol. 433 (2006), 261-268

[211] Cottis, R.A.; Qing, L.; Owen, G.; Gartland, S.J.; Helliwell, I.A.; Turega, M.: Neural Network Methods for Corrosion Data Reduction. Materials and Design, Vol. 20 (1999), 169-178

[212] Danaher, S.; Datta, S.; Waddle, I.; Hackney, P.: Erosion Modeling Using Bayesian Regulated Artificial Neural Networks. Wear, Vol. 256 (2004), 879-888

[213] Hassibi, B.; Stork, D.G.; Wolff, G.J.: Optimal Brain Surgeon and General Network Pruning. In: Proceedings of IEEE International Conference on Neural Networks (ICNN), Vol. 1, San Francisco (USA), March 28-April 1, 1993, 293-299

[214] Hassibi, B.; Stork, D.G.: Second Order Derivatives for Network Pruning: Optimal Brain Surgeon. In: Lippman, D.S.; Moody, J.E.; Touretzky, D.S. (Eds.): Advances in Neural Information Processing Systems. Vol. 5. San Mateo: Morgan Kaufmann Publishers Inc., 1993, 164-171

[215] Mak, B.; Chan, K.W.: Pruning Hidden Markov Models with Optimal Brain Surgeon. IEEE Transactions on Speech and Audio Processing, Vol. 13, No. 5 (2005), 993-1003

[216] Al-Haik, M.S.; Hussaini, M.Y.; Garmestani, H.: Prediction of Nonlinear Viscoelastic Behavior of Polymeric Composites Using an Artificial Neural Network. International Journal of Plasticity, Vol. 22 (2006), 1367-1392

[217] Poppi, R.J.; Massart, D.L.: The Optimal Brain Surgeon for Pruning Neural Network Architecture Applied to Multivariate Calibration. Analytica Chimica Acta, Vol. 375 (1998), 187-195

[218] Attik, M.; Bougrain, L.; Alexandre, F.: Neural Network Topology Optimization. In: Duch, W.; Kacprzyk, J.; Oja, E.; Zadrozny, S. (Eds.): Artificial Neural Networks: Formal Models and Their Applications. Proceedings of the 15th International Conference (ICANN 2005), Part II, Warsaw (Poland), September 11-15, 2005. Berlin-Heidelberg: Springer Verlag, 2005, 53-58

[219] Bhadeshia, H.K.D.H.: Neural Networks in Materials Science. ISIJ International, Vol. 39, No. 10 (1999), 966-979

[220] Pao, H.T.: A Comparison of Neural Network and Multiple Regression Analysis in Modeling Capital Structure. Expert Systems with Applications, Vol. 35, No. 3 (2008), 720-727

[221] Zhang, Z.; Friedrich, K.: Artificial Neural Network in Polymer Composites. Proceedings of the 3rd Asian-Australasian Conference on Composite Materials (ACCM-3), Auckland (New Zealand), July 15-17, 2002, 105-118

[222] El Kadi, H.: Modeling the Mechanical Behavior of Fiber-Reinforced Polymeric Composite Materials Using Artificial Neural Networks-a Review. Composite Structures, Vol. 73 (2006), 1-23

[223] Lee, C.S.; Hwang, W.; Park, H.C.; Han, K.S.: Failure of Carbon/Epoxy Composite Tubes under Combined Axial and Torsional Loading 1. Experimental Results and Prediction of Biaxial Strength by the Use of Neural Networks. Composites Science and Technology, Vol. 59, No. 12 (1999), 1779-1788

[224] Seyhan, A.T; Tayfur, G.; Karakurt, M.; Tanoglu, M: Artificial Neural Network (ANN) Prediction of Compressive Strength of VARTM Processed Polymer Composites. Computational Materials Science, Vol. 34, No. 1 (2005), 99-105

[225] Jiang, Z.; Gyurova, L.; Zhang, Z.; Friedrich, K.; Schlarb, A.K.: Neural Network Based Prediction on Mechanical and Wear Properties of Short Fibers Reinforced Polyamide Composites. Materials and Design, Vol. 29 (2008), 628-637

[226] Liang, G.; Chandrashekhara, K.: Neural Network Based Constitutive Model for Elastomeric Foams. Engineering Structures, Vol. 30 (2008), 2002-2011

[227] Stylianopoulos, T.; Bashur, C.A.; Goldstein, A.S.; Guelcher, S.A.; Barocas, V.H.: Computational Predictions of the Tensile Properties of Electrospun Fibre Meshes: Effect of Fibre Diameter and Fibre Orientation. Journal of the Mechanical Behavior of Biomedical Materials, Vol. I (2008), 326-335

[228] Al-Haik, M.S.; Garmestani, H; Navon, I.M.: Truncated-Newton Training Algorithm for Neurocomputational Viscoplastic Model. Computer Methods in Applied Mechanics and Engineering, Vol. 192 (2003), 2249-2267

[229] Al-Haik, M.S.; Garmestani, H.; Savran, A.: Explicit and Implicit Viscoplastic Models for Polymeric Composite. International Journal of Plasticity, Vol. 20, No. 10 (2004), 1875-1907

[230] Ramu, S.A.; Johnson, V.T.: Damage Assessment of Composite Structures-a Fuzzy Logic Integrated Neural Network Approach. Computers and Structures, Vol. 57, No. 3 (1995), 491-502

[231] Okafor, A.C.; Otieno, A.W.; Dutta, A.; Rao, V.S.: Detection and Characterization of High-velocity Impact Damage in Advanced Composite Plates Using Multi-sensing Techniques. Composite Structures, Vol. 54, No. 2-3 (2001), 289-297

[232] Su, Z.; Ye, L.: Artificial Neural Algorithm-based Damage Assessment for Laminated Composite Structures Using Distributed Actuators/Sensors. In: Proceedings of the 5th International Symposium on Advanced Composites, Corfu (Greece), May 5-7, 2003

[233] Garg, A.K; Mahapatra, D.R; Suresh, S; Gopalakrishnan, S; Omkar, S.N.: Estimation of Composite Damage Model Parameters Using Spectral Finite Element and Neural Network. Composites Science and Technology, Vol. 64, No. 16 (2004), 2477-2493

[234] Ye, L.; Lu, Y.; Su, Z.; Meng, G.: Functionalized Composite Structures for New Generation Airframes: a Review. Composites Science and Technology, Vol. 65, No. 9 (2005), 1436-1446

[235] Valoor, M.T.; Chandrashekhara, K.: A Thick Composite-beam Model for Delamination Prediction by the Use of Neural Networks Approach. Composites Science and Technology, Vol. 60, No. 9 (2000), 1773-1779

[236] Karnik, S.R.; Gaitonde, V.N.; Campos Rubio, J.; Esteves Correia, A.; Abrao, A.M.; Paulo Davim, J.: Delamination Analysis in High Speed Drilling of Carbon Fiber Reinforced Plastics (CFRP) Using Artificial Neural Network Model. Materials and Design, Vol. 29 (2008), 1768-1776

[237] Mahdi, E.S.; Kady, H.El.: Crushing Behavior of Laterally Compressed Composite Elliptical Tubes: Experiments and Prediction Using Artificial Neural Networks. Composite Structures, Vol. 83 (2008), 399-412

[238] Zhang, Z.; Klein, P.; Friedrich, K.: Dynamic Mechanical Properties of PTFE Based Short Carbon Fiber Reinforced Composites: Experiment and Artificial Neural Network Prediction. Composites Science and Technology, Vol. 62, No. 7-8 (2002), 1001-1009

[239] Bertinetto, C.; Duce, C.; Micheli, A.; Solaro, R.; Starita, A.; Tine, M.R.: Prediction of the Glass Transition Temperature of (Meth)acrylic Polymers Containing Phenyl Groups by Recursive Neural Network. Polymer, Vol. 48 (2007), 7121-7129

[240] Khan, A.; Shamsi, M.H.; Choi, T.S.: Correlating Dynamic Mechanical Properties with Temperature and Clay Composition of Polymer-clay Nanocomposites. Computational Materials Science, Vol. 45, No. 2 (2009), 257-265

[241] Park, D.K.; Jang, H.; Ahn, N.: Development of Bond Strength Model for FRP Plates Using Back-propagation Algorithm. Journal of Applied Polymer Science, Vol. 100 (2006), 5119- 5127

[242] Turias, I.J.; Gutierres, J.M.; Galindo, P.L.: Modelling the Effective Thermal Conductivity of an Unidirectional Composite by the Use of Artificial Neural Networks. Composites Science and Technology, Vol. 65 (2005), 609-619

[243] Rai, N.; Pitchumani, R.: Optimal Cure Cycles for the Fabrication of Thermosetting Matrix Composites. Polymer Composites, Vol. 18, No. 4 (1997), 566-581

[244] Su, H.B.; Fan, L.T.; Schlup, J.R.: Monitoring the Process of Curing of Epoxy/Graphite Fiber Composites with a Recurrent Neural Network as a Soft Sensor. Engineering Applications of Artificial Intelligence, Vol. 11, No. 2, (1998), 293-306

[245] Nascimento, C.A.O.; Giudici, R.: Neural Network Based Approach for Optimisation Applied to an Industrial Nylon-6,6 Polymerisation Process. Computers & Chemical Engineering, Vol. 22, Supplement 1 (1998), 595-600

[246] Heider, D.; Gillespie Jr., J.W.; Piovoso, M.J.: Intelligent Control of the Thermoplastic Composite Tow Placement Process. Journal of Thermoplastic Composite Materials, Vol. 11 (1998), 573-595

[247] Allan, G.; Yang, R.; Fotheringham, A.; Mather, R.: Neural Modelling of Polypropylene Fiber Processing: Predicting the Structure and Properties and Identifying the Control Parameters for Specified Fibers. Journal of Materials Science, Vol. 36 (2001), 3113-3118

[248] Heider, D.; Piovoso, M.J.; Gillespie Jr., J.W.: Application of a Neural Network to Improve an Automated Thermoplastic Tow-placement Process. Journal of Process Control, Vol. 12 (2002), 101-111

[249] Gonzaga, J.C.B.; Meleiro, L.A.C.; Kiang, C.; Maciel Filho, R.: ANN-based Soft-sensor for Real-time Process Monitoring and Control of an Industrial Polymerization Process. Computers & Chemical Engineering, Vol. 33 (2009), 43-49

[250] Jayatheertha, C.; Webber, J.P.H.; Morton, S.K.: Application of Artificial Neural Networks for the Optimum Design of a Laminated Plate. Computers & Structures, Vol. 59, No. 5 (1996), 831-845

[251] Chandrashekhara, K.; Okafor, A.C.; Jiang, Y.P.: Estimation of Contact Force on Composite Plates Using Impact-induced Strain and Neural Networks. Composites Part B: Engineering, Vol. 29, No. 4 (1998), 363-370

[252] Ulmer II, C.W.; Smith, D.A.; Sumpter, B.G.; Noid, D.I.: Computational Neural Networks and the Rational Design of Polymeric Materials: the Next Generation Polycarbonates. Computational and Theoretical Polymer Science, Vol. 8, No. 3-4 (1998), 311-321

[253] Gotlib, V.A.; Sato, T.; Beltzer, A.I.: Neural Computations of Effective Response of Random Composites. International Journal of Solids and Structures, Vol. 37, No. 33 (2000), 4527-4538

[254] Karnik, S.R.; Gaitonde, V.N.; Mata, F.; Paulo Davim, J.: Investigative Study on Machinability Aspects of Unreinforced and Reinforced PEEK Composite Machining Using ANN Model. Journal of Reinforced Plastics and Composites, Vol. 27 (2008), 751-768

[255] Sarkar, K.; Ghalia, M.B.; Wu, Z.; Bose, S.C.: A Neural Network Model for the Numerical Prediction of the Diameter of Electro-spun Polyethylene Oxide Nanofibers. Journal of Materials Processing Technology, Vol. 209, No. 7 (2009), 3156-3165

[256] Aymerich, F.; Serra, M.: Prediction of Fatigue Strength of Composite Laminates by Means of Neural Networks. Key Engineering Materials, Vol. 144 (1998), 231-240

[257] Lee, J.A.; Almond, D.P.; Harris, B.: The Use of Neural Networks for the Prediction of Fatigue Lives of Composite Materials. Composites Part A: Applied Science and Manufacturing, Vol. 30, No. 10 (1999), 1159-1169

[258] Al-Assaf, Y.; El Kadi, H.: Fatigue Life Prediction of Unidirectional Glass Fibre/Epoxy Composite Laminate Using Neural Networks. Composite Structures, Vol. 53, No. 1 (2001), 65-71

[259] El Kadi, H.; Al-Assaf, Y.: Prediction of the Fatigue Life of Unidirectional Glass Fiber/Epoxy Composite Laminate Using Different Neural Network Paradigms. Composite Structures, Vol. 55 (2002), 239-246

[260] El Kadi, H.; Al-Assaf, Y.: Energy-based Fatigue Life Prediction of Fiber-Glass/Epoxy Composites Using Modular Neural Networks. Composites Structures, Vol. 57 (2002), 85-89

[261] Choi, S.W.; Song, E.J.; Hahn, H.T.: Prediction of Fatigue Damage Growth in Notched Composite Laminates Using an Artificial Neural Network. Composites Science and Technology, Vol. 63 (2003), 661-675

[262] El Mahi, A.; Khawar Farooq, M.; Sahraoui S.; Bezazi, A.: Modelling the Flexural Behaviour of Sandwich Composite Materials under Cyclic Fatigue. Materials and Design, Vol. 25 (2004), 199-208

[263] Al-Assaf, Y., El Kadi, H.: Fatigue Life Prediction of Composite Materials Using Polynomial Classifiers and Recurrent Neural Networks. Composite Structures, Vol. 77 (2007), 561-569

[264] Bezazi, A.; Gareth Pierce, S., Worden, K., Harkati, E.H.: Fatigue Life Prediction of Sandwich Composite Materials under Flexural Tests Using a Bayesian Trained Artificial Neural Network. International Journal of Fatigue, Vol. 29 (2007), 738-747

[265] Freire Jr., R.C.S.; Doria Netto, A.D.; Aquino, E.M.F.: Comparative Study between ANN Models and Conventional Equations in the Analysis of Fatigue Failure of GFRP. International Journal of Fatigue, Vol. 31, No. 5 (2009), 831-839

[266] Jones, S.P.; Jansen, R.; Fusaro, R.: Preliminary Investigation of Neural Network Techniques to Predict Tribological Properties. Tribology Transactions, Vol. 40 (1997), 312-320

[267] Lin, S.C.; Lin, R.J.: Tool Wear Monitoring in Face Milling Using Force Signals. Wear, Vol. 198 (1996), 136-142

[268] Das, S.; Roy, R.; Chattopadhyay, A.B.: Evaluation of Wear of Turning Carbide Inserts Using Neural Networks. International Journal of Machine Tools and Manufacturing, Vol. 36 (1996), 789-797

[269] Umeda, A.; Sugimura, J.; Yamamoto, Y.: Characterization of Wear Particles and Their Relations with Sliding Conditions. Wear, Vol. 216 (1998), 220-228

[270] Myshkin, N.K.; Kwon, O.K.; Grigoriev, A.Ya.; Ahn, H.S.; Kong, H.: Classification of Wear Debris Using Neural Network. Wear, Vol. 203-204 (1997), 658-662

[271] Subrahmanyam, M.; Sujatha, C.: Using Neural Networks for the Diagnosis of Localized Defects in Ball Bearings. Tribology International, Vol. 30 (1997), 739-752

[272] Sahraoui, T.; Guessasma, S.; Fenineche, N.E.; Montavon, G.; Coddet, C.: Friction and Wear Behaviour Prediction of HVOF Coatings and Electroplated Hard Chromium Using Neural Network Computing. Materials Letters, Vol. 58 (2004), 654-660

[273] Cetinel, H.; Öztürk, H.; Celik, E.; Karlik, B.: Artificial Neural Network-based Prediction Technique for Wear Loss Quantities in Mo Coatings. Wear, Vol. 261 (2006), 1064-1068

[274] Aleksendric, D.; Duboka, Č.: Prediction of Automotive Friction Material Characteristics Using Artificial Neural Networks-cold Performance. Wear, Vol. 261 (2006), 269-282

[275] Ramesh, R.; Gnanamoorthy, R.: Artificial Neural Network Prediction of Fretting Wear Behavior of Structural Steel, En 24 against Bearing Steel, En 31. Journal of Materials Engineering and Performance, Vol. 16 (2007), 703-709

[276] Scott, D.J.; Coveney, P.V.; Kilner, J.A.; Rossiny, J.C.H.; Alford, N.Mc.N.: Prediction of the Functional Properties of Ceramic Materials from Composition Using Artificial Neural Networks. Journal of European Ceramic Society, Vol. 27 (2007), 4425-4435

[277] Srinivasa Pai, P.; Mathew, M.T.; Stack, M.M.; Rocha, L.A.: Some Thoughts on Neural Network Modeling of Microabrasion-corosion Processes. Tribology International, Vol. 41 (2008), 672-681

[278] John Presin Kumar, A.; Kingsly Jeba Singh, D.: Artificial Neural Network-based Wear Loss Prediction for A390 Aluminum Alloy. Journal of Theoretical and Applied Information Technology, Vol. 4 (2008), 961-964

[279] Hayajneh, M.; Hassan, A.M.; Alrashdan, A.; Mayyas, A.T.: Prediction of Tribological Behavior of Aluminum-Copper Based Composite Using Artificial Neural Network. Journal of Alloy and Compounds, Vol. 470 (2009), 584-588

[280] Velten, K.; Reinicke, R.; Friedrich, K.: Wear Volume Prediction with Artificial Neural Networks. Tribology International, Vol. 33 (2000), 731-736

[281] Zhang, Z.; Friedrich, K.; Velten, K.: Prediction of Tribological Properties of Short Fibre Composites Using Artificial Neural Networks. Wear, Vol. 252 (2002), 668-675

[282] Zhang, Z.; Barkoula, N.M.; Karger-Kocsis, J.; Friedrich, K.: Artificial Neural Network Predictions on Erosive Wear of Polymers. Wear, Vol. 255 (2003), 708-713

[283] Suresh, A.; Harsha, A.P.; Ghosh, M.K.: Solid Particle Erosion Studies on Polyphenylene Sulfide Composites and Prediction on Erosion Data Using Artificial Neural Networks. Wear, Vol. 266 (2009), 184-193

[284] Satapathy, A.; Patnaik, A.; Pradhan, M.K.: A Study on Processing, Characterization and Erosion Behavior of Fish (Labeo-rohita) Scale Filled Epoxy Matrix Composites. Materials and Design, Vol. 30 (2009), 2359-2371

[285] Zhang, G.; Guessasma, S.; Liao, H.; Coddet, C.; Bordes, J. M.: Investigation of Friction and Wear Behaviour of SiC-Filled PEEK Coating Using Artificial Neural Network. Surface and Coatings Technology, Vol. 200, No. 8 (2006), 2610-2617

[286] Jiang, Z.; Zhang, Z.; Friedrich, K.: Prediction on Wear Properties of Polymer Composites with Artificial Neural Network. Composites Science and Technology, Vol. 67 (2007), 168-176

[287] Jiang, Z.; Gyurova, L.; Zhang, Z.; Friedrich, K.; Schlarb, A.K.: Artificial Neural Network Based Prediction of Wear and Mechanical Properties of Polyamide Composites Reinforced by Short Fibers. In: Reibung, Schmierung und Verschleiß, Vol. 1. 47. Tribologie-Fachtagung, Göttingen (Germany), September 25-27, 2006. Aachen: Gesellschaft für Tribologie e.V., 2006, 4/1-4/14

[288] Srinivasan, V.; Maheshkumar, K.V.; Karthikeyan, R; Palanikumar, K.: Application of Probabilistic Neural Network for the Development of Wear Mechanism Map for Glass Fiber Reinforced Plastics. Journal of Reinforced Plastics and Composites, Vol. 26 (2007), 1893-1906

[289] Liujie, X.; Cardoso, R.; Davim, J.P.: Modelling the Tribological Behaviours of Composite PEEK-CF30 Using BP Neural Networks. Materials Science-Poland, Vol. 26 (2008), 495-504

[290] Zhu, J.; Shi, Y.; Feng, X.; Wang, H.; Lu, X.: Prediction on Tribological Properties of Carbon Fiber and TiO_2 Synergistic Reinforced Polytertrafluoroethylene Composites with Artificial Neural Networks. Materials and Design, Vol. 30 (2009), 1042-1049

[291] Gyurova, L.A.; Miniño-Justel, P.; Schlarb, A.K.: Modeling the Sliding Wear and Friction Properties of Polyphenylene Sulfide Composites Using Artificial Neural Networks. Wear, Vol. 268, No. 5-6 (2010), 708-714

[292] Domininghaus, H.: Die Kunststoffe und ihre Eigenschaften. Berlin: Springer-Verlag, 1998, 887-906

[293] Ehrenstein, G.W.; Riedel, G.; Trawiel, P.: Praxis der thermischen Analyse von Kunststoffe. München: Hanser Verlag, 1998

[294] Quintelier, J.; Samyn, P.; De Baets, P.; Tuzolana, T.: Wear Behaviour of Carbon Fiber Reinforced Poly(Phenylene Sulfide). Polymer Composites, Vol. 27, No. 1 (2006), 92-98

[295] Lu, D.; Mai, Y.W.; Li, R.K.Y.; Ye, L.: Impact Strength and Crystallization Behavior of Nano-SiO_x/Poly(Phenylene Sulfide) (PPS) Composites with Heat-treated PPS. Macromolecular Materials and Engineering, Vol. 288, No. 9 (2003), 693-698

[296] Katz, H.S.; Milewski, J.V.: Handbook of Fillers for Plastics. New York: Van Nostrand Reinhold, 1987

[297] Kronos International Inc.: TiO_2 Product Data Sheet, Kronos 2310, http://www.kronos.de/, (20.10.2008)

[298] Sachtleben Chemie GmbH: Produktinformation, Sachtolit HDS, http://www.sachtleben.de (30.10.2008)

[299] Stachowiak, G.W.; Batchelor, A.W.; Stachowiak, G.B.: Tribometers. In: Stachowiak, G.W.; Batchelor, A.W.; Stachowiak, G.B. (Eds.): Experimental Methods in Tribology. Amsterdam: Elsevier, 2004, 25-78

[300] Kennedy, F.E.: Frictional Heating and Contact Temperatures. In: Bhushan, B. (Ed.): Modern Tribology Handbook. Vol I. Boca Raton: CRC Press, 2001, 235-272

[301] Harrass, M.; Friedrich, K.; Almajid, A.A.: Tribological Behavior of Selected Engineering Polymers under Rolling Contact. Tribology International, Vol. 43, No. 3 (2010), 635-646

[302] Norm DIN EN ISO 527-2 Kunststoffe - Bestimmung der Zugeigenschaften - Teil 2: Prüfbedingungen für Form- und Extrusionsmassen (ISO 527-2 : 1993 einschließlich Corr. 1-1994); Deutsche Fassung EN ISO 527-2 : 1996

[303] Norm DIN EN ISO 604, Ausgabe 2003-12 Kunststoffe - Bestimmung von Druckeigenschaften (ISO 604 : 2002); Deutsche Fassung EN ISO 604 : 2003

[304] Norm ISO-179-2 Kunststoffe - Bestimmung der Charpy-Schlageigenschaften - Teil 2: Instrumentierte Schlagzähigkeitsprüfung (ISO 179-2 : 1997); Deutsche Fassung EN ISO 179 - 2 : 1999

[305] Norm ISO-179-1 Kunststoffe - Bestimmung der Charpy-Schlagzähigkeit (ISO 179 : 1993); Deutsche Fassung EN ISO 179 : 1996

[306] Matlab 7.0.4: Mathworks: http://www.mathworks.com

[307] JavaNNS: http://www.ra.cs.uni-tuebingen.de/downloads/JavaNNS/

[308] SNNS Stuttgart Neural Network Simulator: User Manual, Version 4.2, http://www.ra.cs.uni-tuebingen.de/downloads/SNNS/SNNSv4.2.Manual.pdf (18.11.2009)

[309] Fischer, I.; Henecke, F.; Bannes, C.; Zell, A.: JavaNNS Java Neural Network Simulator, User Manual, Version 1.1, http://www.ra.cs.uni-tuebingen.de/software/JavaNNS/manual/JavaNNS-manual.html (18.11.2009)

[310] RTP Company, http://www.rtpcompany.com/, (02.03.2005)

[311] Koker, R.; Altinkok, N.; Demir, A.: Neural Network Based Prediction of Mechanical Properties of Particulate Reinforced Metal Matrix Composites Using Various Training Algorithms. Materials and Design, Vol. 28, No. 2 (2007), 616-627

[312] Demuth, H.; Beale, M.: Neural Network Toolbox for Use with Matlab. User's guide, Version 3.0. The MathWorks, Inc., 1998

[313] Anderson, D.; McNeill, G.: Artificial Neural Networks Technology. New York: Kaman Sciences Corporation, 1992

[314] Morgan, P.; Curry, B.; Malcom, B.: Pruning Neural Networks by Minimization of the Estimated Variance. European Journal of Economic and Social System, Vol. 14, No. 1 (2000), 1-16

[315] Bhushan, B.: Principles and Applications of Tribology. New York: John Wiley & Sons, 1999

[316] Stachowiak, G.W.; Batchelor, A.W.: Solid Lubrication and Surface Treatments. In: Stachowiak, G.W.; Batchelor, A.W. (Eds.): Engineering Tribology. Amsterdam: Elsevier, 1993, 485-526.

[317] Jarratt, M.; Stallard, J.; Renevier, N.M.; Teer, D.G.: An Improved Diamond-like Carbon Coating with Exceptional Wear Properties. Diamond and Related Materials, Vol. 12 (2003), 1003-1007

[318] Zhan, Y.; Zhang, G.: Friction and Wear Behavior of Copper Matrix Composites Reinforced with SiC and Graphite Particles. Tribology Letters, Vol. 17, No. 1 (2004), 91-98

[319] Friedrich, K.: Erosive Wear of Polymer Surfaces by Steel Ball Blasting. Journal of Materials Science, Vol. 21 (1986), 3317-3323

[320] Gyurova, L.A.; Jiang, Z.; Friedrich, K.; Zhang, Z.; Schlarb, A.K.: Tribological and Mechanical Properties of Selected PPS Nanocomposites Designed for Tribological Service. In: Proceedings of 2nd Vienna International Conference Micro-and Nano-Technology (VienNano'07), Vienna (Austria), March 14-16, 2007. Vienna: Österreichische Tribologische Gesellschaft, 2007, 349-356

[321] Tsukizoe. T.; Ohmae, N.: Friction and Wear Performance of Unidirectionally Oriented Glass, Carbon, Aramid and Stainless Steel Fiber-Reinforced Plastics. In Friedrich, K. (Ed.): Friction and Wear of Polymer Composites. Amsterdam: Elsevier, 1986, 205-231

[322] Wilson, S.; Ball, A.: Performance of Metal Matrix Composites under Various Tribological Conditions. In Friedrich, K. (Ed.): Advances in Composite Tribology. Amsterdam: Elsevier, 1993, 311-366

[323] Kong, H.; Yoon, E.S.; Kwon, O.K.: Self-formation of Protective Oxide Films at Dry Sliding Mild Steel Surfaces under a Medium Vacuum. Wear, Vol. 181 (1995), 325-333

[324] Wu, J.H.; Karthikeyan, S.; Falk, M.L.; Rigney, D.A.: Tribological Characteristics of Diamond-like Carbon (DLC) Based Nanocomposite Coatings. Wear, Vol. 259 (2005), 744-751

[325] Fu, X.Y.; Rigney, D.A.; Falk, M.L.: Sliding and Deformation of Metallic Glass: Experiments and MD Simulations. Journal of Non-Crystalline Solids, Vol. 317 (2003), 206-214

[326] Wu, J.H.; Sanghavi, M.; Sanders, J.H.; Voevodin, A.A.; Zabinski, J.S.; Rigney, D.A.: Sliding Behavior of Multifunctional Composite Coatings Based on Diamond-like Carbon. Wear, Vol. 255 (2003), 859-868

[327] Greenberg, R.; Halperin, G.; Etsion, I.; Tenne, R.: The Effect of WS_2 Nanoparticles on Friction Reduction in Various Lubrication Regimes. Tribology Letters, Vol. 17, No. 2 (2004), 179-186

[328] http://www.ntnamerica.com/pdf/Ball_Bearings.pdf (01.11.2009)

8 Appendix

A1 Sliding Friction and Wear Properties of PPS Composites in MFD

Table A.1: Sliding friction and wear properties of PPS composites

Code	Sliding friction and wear properties in MFD: training data for ANN					
	Pressure [MPa]	Sliding speed [m/s]	Frictional coefficient	St.Dev	Specific wear rate [mm^3/Nm]	St.Dev
C1≡PPS1	1	1	0.46	0.04	7.15E-05	1.71E-05
C2≡PPS2	1	1	0.55	0.02	5.42E-05	9.72E-06
C3≡PPS4	1	1	0.43	0.09	3.60E-04	1.44E-04
C4≡PPS3	1	1	0.40	0.02	2.95E-04	1.09E-04
C5≡PPS5	1	1	0.40	0.01	3.76E-04	1.98E-05
C6≡PPS6	1	1	0.59	0.02	7.49E-07	6.76E-08
C6≡PPS6	1	3	0.50	0.02	1.14E-06	9.97E-08
C6≡PPS6	2	1	0.27	0.07	1.02E-06	1.22E-07
C6≡PPS6	2	3	0.32	0.04	1.03E-06	8.91E-07
C6≡PPS6	3	1	0.22	0.05	7.76E-07	8.38E-08
C6≡PPS6	3	3	0.20	0.01	1.37E-06	1.02E-07
C6≡PPS6	4	1	0.20	0.02	6.18E-07	8.12E-08
C7≡PPS7	1	1	0.37	0.02	7.00E-07	8.06E-08
C7≡PPS7	1	3	0.15	0.01	5.90E-07	5.13E-08
C7≡PPS7	2	1	0.24	0.02	5.86E-07	3.86E-08
C7≡PPS7	2	3	0.12	0.02	4.88E-07	9.51E-09
C7≡PPS7	3	1	0.15	0.03	8.19E-07	1.84E-07
C7≡PPS7	3	3	0.14	0.03	6.94E-07	2.49E-08
C7≡PPS7	4	1	0.13	0.01	2.19E-06	2.09E-07
C8≡PPS8	1	1	0.46	0.04	7.74E-07	3.72E-07
C8≡PPS8	1	3	0.17	0.01	6.95E-07	1.29E-07
C8≡PPS8	2	1	0.17	0.01	7.16E-07	5.04E-08
C8≡PPS8	2	3	0.12	0.02	7.61E-07	6.89E-08
C8≡PPS8	3	1	0.15	0.00	1.27E-06	6.26E-08
C8≡PPS8	3	3	Stick-slip	-	9.23E-07	9.70E-08
C8≡PPS8	4	1	0.14	0.02	1.25E-06	1.44E-07
C8≡PPS8	4	3	Stick-slip	-	1.36E-06	2.58E-07
C9≡PPS9	1	1	0.28	0.02	3.74E-07	7.99E-08
C9≡PPS9	1	3	0.17	0.01	5.86E-07	7.93E-08
C9≡PPS9	2	1	0.16	0.00	6.46E-07	7.39E-08
C9≡PPS9	2	3	0.10	0.00	6.53E-07	9.54E-08
C9≡PPS9	3	1	0.15	0.01	1.35E-06	7.79E-08
C9≡PPS9	3	3	Stick-slip	-	8.29E-07	9.71E-08
C9≡PPS9	4	1	0.14	0.01	1.24E-06	9.72E-08
C10≡PPS10	1	1	0.25	0.02	4.44E-07	7.28E-08
C10≡PPS10	1	3	0.17	0.01	5.55E-07	6.16E-08
C10≡PPS10	2	1	0.14	0.01	7.31E-07	1.38E-07
C10≡PPS10	2	3	0.11	0.00	1.09E-07	7.08E-09
C10≡PPS10	3	1	0.14	0.00	8.68E-07	1.22E-07
C10≡PPS10	3	3	Stick-slip	-	1.00E-06	1.73E-07
C10≡PPS10	4	1	0.15	0.01	1.71E-06	8.09E-08
C11≡PPS13	1	1	0.33	0.03	4.33E-07	7.78E-08
C11≡PPS13	1	3	0.17	0.01	6.18E-07	3.49E-08

Table A.1: Sliding friction and wear properties of PPS composites - continued

Code	Sliding friction and wear properties in MFD: training data for ANN					
	Pressure [MPa]	Sliding speed [m/s]	Frictional coefficient	St.Dev	Specific wear rate [mm^3/Nm]	St.Dev
C11≡PPS13	2	1	0.21	0.02	1.13E-06	1.66E-07
C11≡PPS13	2	3	0.10	0.01	6.60E-07	1.06E-07
C11≡PPS13	3	1	0.22	0.01	1.06E-06	1.42E-07
C11≡PPS13	3	3	0.10	0.03	1.92E-06	3.93E-07
C11≡PPS13	4	1	0.15	0.02	1.02E-06	5.72E-08
C11≡PPS13	4	3	0.12	0.03	3.72E-06	5.40E-07
C12*≡PPS16	1	1	0.30	0.02	5.10E-07	1.92E-07
C12*≡PPS16	1	3	0.19	0.02	1.20E-06	2.41E-07
C12*≡PPS16	2	1	0.26	0.01	3.16E-06	4.66E-07
C12*≡PPS16	2	3	Stick-slip	-	1.81E-06	7.18E-08
C12*≡PPS16	3	1	0.20	0.04	2.16E-06	7.04E-07
C12*≡PPS16	3	3	Stick-slip	-	3.44E-06	1.19E-07
C12*≡PPS16	4	1	0.17	0.02	3.13E-06	5.00E-07
C12*≡PPS16	4	3	Stick-slip	-	2.72E-06	2.64E-07
C13*≡PPS18	1	1	0.30	0.04	3.91E-07	5.24E-08
C13*≡PPS18	1	3	0.18	0.01	8.62E-07	6.23E-08
C13*≡PPS18	2	1	0.17	0.01	8.24E-07	1.46E-07
C13*≡PPS18	2	3	0.10	0.01	6.16E-07	3.01E-08
C13*≡PPS18	3	1	0.16	0.03	1.10E-06	2.32E-07
C13*≡PPS18	3	3	0.08	0.01	6.16E-07	9.83E-08
C13*≡PPS18	4	1	0.17	0.00	2.96E-06	6.93E-07
C14*≡PPS19	1	1	0.28	0.04	4.62E-07	3.76E-08
C14*≡PPS19	1	3	0.19	0.02	6.35E-07	5.57E-08
C14*≡PPS19	2	1	0.21	0.01	5.58E-07	5.17E-08
C14*≡PPS19	2	3	0.12	0.01	7.60E-07	5.22E-08
C14*≡PPS19	3	1	0.20	0.01	7.33E-07	6.64E-08
C14*≡PPS19	3	3	0.09	0.01	7.37E-07	6.35E-08
C14*≡PPS19	4	1	0.20	0.01	8.06E-07	8.84E-08
C14*≡PPS19	4	3	0.11	0.03	1.30E-06	4.06E-07
C15*≡PPS20	1	1	0.35	0.04	4.86E-07	1.15E-07
C15*≡PPS20	1	3	0.21	0.01	6.83E-07	1.37E-07
C15*≡PPS20	2	1	0.22	0.01	6.19E-07	5.44E-08
C15*≡PPS20	2	3	0.13	0.01	7.92E-07	6.01E-08
C15*≡PPS20	3	1	0.23	0.01	6.53E-07	3.47E-08
C15*≡PPS20	3	3	0.07	0.01	2.31E-06	6.44E-07
C15*≡PPS20	4	1	0.25	0.00	5.95E-07	6.18E-08
C15*≡PPS20	4	3	0.11	0.04	1.16E-06	2.59E-07
C16*≡PPS21	1	1	0.38	0.02	3.58E-07	6.95E-08
C16*≡PPS21	1	3	0.18	0.02	5.36E-07	5.36E-08
C16*≡PPS21	2	1	0.21	0.01	5.62E-07	6.39E-08
C16*≡PPS21	2	3	0.15	0.01	6.88E-07	8.74E-08
C16*≡PPS21	3	1	0.21	0.01	6.24E-07	7.10E-08
C16*≡PPS21	3	3	0.10	0.01	8.29E-07	8.09E-08
C16*≡PPS21	4	1	0.22	0.00	9.33E-07	8.77E-08
C16*≡PPS21	4	3	0.09	0.01	1.11E-06	2.08E-07
C17*≡PPS22	1	1	0.32	0.04	3.89E-07	2.34E-08
C17*≡PPS22	1	3	0.17	0.01	5.51E-07	9.73E-08
C17*≡PPS22	2	1	0.19	0.01	6.39E-07	7.09E-08
C17*≡PPS22	2	3	0.14	0.00	7.34E-07	1.70E-08

Table A.1: Sliding friction and wear properties of PPS composites - continued

Code	Sliding friction and wear properties in MFD: training data for ANN					
	Pressure [MPa]	Sliding speed [m/s]	Frictional coefficient	St.Dev	Specific wear rate [mm^3/Nm]	St.Dev
C17*≡PPS22	3	1	0.20	0.01	7.97E-07	5.74E-08
C17*≡PPS22	3	3	0.11	0.00	9.55E-07	8.39E-08
C17*≡PPS22	4	1	0.20	0.01	1.02E-06	1.89E-07
C17*≡PPS22	4	3	0.09	0.01	1.16E-06	1.64E-07
C18*≡PPS23	1	1	0.58	0.05	5.24E-07	5.73E-08
C18*≡PPS23	1	3	0.36	0.03	7.50E-07	6.87E-08
C18*≡PPS23	2	1	0.34	0.07	6.16E-07	1.04E-07
C18*≡PPS23	2	3	0.25	0.00	1.14E-06	3.97E-08
C18*≡PPS23	3	1	0.30	0.04	4.47E-07	3.95E-08
C18*≡PPS23	3	3	0.21	0.01	1.07E-06	5.90E-08
C18*≡PPS23	4	1	0.26	0.01	3.30E-07	8.21E-09
C19*≡PPS24	1	1	0.50	0.09	4.08E-07	1.27E-07
C19*≡PPS24	1	3	0.40	0.04	8.26E-07	6.98E-08
C19*≡PPS24	2	1	0.48	0.01	7.48E-07	4.11E-08
C19*≡PPS24	2	3	0.28	0.01	1.00E-06	4.01E-08
C19*≡PPS24	3	1	0.24	0.01	1.72E-06	5.25E-07
C19*≡PPS24	3	3	0.18	0.01	8.01E-07	3.04E-08
C19*≡PPS24	4	1	0.36	0.03	4.92E-07	6.86E-08
C19*≡PPS24	4	3	0.12	0.00	3.05E-06	3.15E-07
C20*≡PPS25	1	1	0.32	0.06	4.48E-07	2.60E-08
C20*≡PPS25	1	3	0.19	0.01	5.80E-07	9.46E-08
C20*≡PPS25	2	1	0.21	0.01	6.67E-07	1.56E-07
C20*≡PPS25	2	3	0.15	0.01	1.06E-06	1.03E-07
C20*≡PPS25	3	1	0.22	0.01	9.10E-07	1.98E-07
C20*≡PPS25	3	3	0.14	0.02	1.40E-06	1.70E-07
C20*≡PPS25	4	1	0.21	0.02	1.19E-06	3.70E-07
C20*≡PPS25	4	3	0.20	0.02	1.83E-06	7.40E-08
C21≡PPS26	1	1	0.53	0.07	7.53E-07	2.30E-07
C21≡PPS26	3	1	0.21	0.01	6.02E-07	1.08E-07
C23≡PPS28	1	1	0.33	0.03	8.30E-07	1.68E-08
C23≡PPS28	3	1	0.19	0.01	9.50E-06	7.78E-07
C24≡PPS29	1	1	0.23	0.02	6.18E-07	6.04E-08

Table A.2: Sliding friction and wear properties of PPS composites - validation data

Code	Sliding friction and wear properties in MFD: validation data for ANN					
	Pressure [MPa]	Sliding speed [m/s]	Frictional coefficient	St.Dev	Specific wear rate [mm^3/Nm]	St.Dev
C22≡PPS27	1	1	0.37	0.08	1.33E-06	8.71E-07
C25≡PPS30	1	1	0.22	0.02	5.03E-07	7.36E-08
C26≡PPS31	1	1	0.35	0.08	4.06E-06	1.12E-06
C27≡PPS32	1	1	0.34	0.04	4.70E-07	8.28E-08
C28≡PPS33	1	1	0.20	0.02	3.69E-07	5.43E-08

A2 Mechanical Properties of PPS Composites in MFD

Table A.3: Microhardness and notch Charpy impact strength of PPS composites

Code	Density [g/cm^3]	Microhardness in MFD		Instrumented notch Charpy impact strength in MFD	
		Microhardness [MPa]	St.Dev	a_{cN} [kJ/m^2]	St.Dev
C1≡PPS1	1.354	206.99	3.63	3.38	1.20
C2≡PPS2	1.373	212.88	0.98	3.36	0.85
C3≡PPS4	1.418	225.63	4.22	2.53	0.90
C4≡PPS3	1.464	218.76	3.73	2.60	0.79
C5≡PPS5	1.492	216.80	5.69	2.66	0.89
C6≡PPS6	1.386	239.36	10.10	3.47	0.29
C7≡PPS7	1.414	251.14	13.64	3.11	0.51
C8≡PPS8	1.459	255.06	7.16	3.05	0.76
C9≡PPS9	1.503	271.74	9.42	2.64	0.65
C10≡PPS10	1.560	266.83	12.56	2.65	0.32
C11≡PPS13	1.518	256.04	15.89	2.61	0.62
C12*≡PPS16	1.488	234.46	15.60	3.11	0.35
C13*≡PPS18	1.542	258.00	18.93	Not measured	Not measured
C14*≡PPS19	1.648	250.16	9.42	1.85	0.51
C15*≡PPS20	1.668	243.29	10.79	1.28	0.14
C16*≡PPS21	1.623	218.76	10.40	1.63	0.54
C17*≡PPS22	1.585	242.31	23.05	1.58	0.65
C18*≡PPS23	1.374	233.48	19.62	3.30	0.71
C19*≡PPS24	1.520	214.84	12.36	1.85	0.56
C20*≡PPS25	1.603	222.69	13.44	2.66	0.67
C21≡PPS26	1.363	204.29	4.99	3.13	1.50
C22≡PPS27	1.400	207.12	3.17	2.42	0.93
C23≡PPS28	1.404	211.66	2.66	2.97	1.50
C24≡PPS29	1.490	219.39	3.11	2.66	0.67
C25≡PPS30	1.495	219.07	2.51	2.29	1.13
C26≡PPS31	1.471	211.86	3.78	2.56	0.85
C27≡PPS32	1.429	219.62	1.94	2.49	0.99
C28≡PPS33	1.591	261.70	9.62	2.50	0.58
C29≡PPS36	1.505	225.72	7.36	3.59	0.88

Table A.4: Tensile and compression properties of PPS composites

Code	Tensile properties in MFD					
	E_t [MPa]	St.Dev	σ_M [MPa]	St.Dev	ε_M [%]	St.Dev
C1≡PPS1	3741.57	103.12	86.80	0.63	2.37	0.13
C2≡PPS2	3631.04	133.99	74.80	8.04	1.98	0.28
C3≡PPS4	3852.16	129.73	64.34	4.14	1.59	0.12
C4≡PPS3	3744.17	130.83	72.89	6.17	1.87	0.19
C5≡PPS5	3795.29	277.46	68.04	4.64	1.72	0.18
C6≡PPS6	4777.00	340.68	65.97	3.43	1.61	0.12
C7≡PPS7	5401.91	379.61	65.12	3.53	1.48	0.08
C8≡PPS8	5237.81	383.17	60.46	7.57	1.17	0.18
C9≡PPS9	5506.27	196.80	68.55	1.13	1.33	0.12
C10≡PPS10	5748.87	480.52	49.22	7.82	0.85	0.16
C11≡PPS13	5866.46	223.68	67.83	2.19	1.30	0.08
C12*≡PPS16	5158.88	318.10	70.66	2.67	1.57	0.08

Table A.4: Tensile and compression properties of PPS composites - continued

Code	Tensile properties in MFD					
	E_t [MPa]	St.Dev	σ_M [MPa]	St.Dev	ε_M [%]	St.Dev
C13*≡PPS18	4786.90	467.23	28.80	2.84	0.61	0.10
C14*≡PPS19	4759.78	700.25	29.16	3.19	0.60	0.10
C15*≡PPS20	5311.68	220.62	36.23	3.10	0.70	0.05
C16*≡PPS21	4493.61	228.08	32.89	0.85	0.74	0.03
C17*≡PPS22	4904.72	407.67	33.95	2.89	0.70	0.05
C18*≡PPS23	4764.10	346.65	67.22	1.43	1.66	0.12
C19*≡PPS24	5294.82	326.60	36.37	6.02	0.72	0.12
C20*≡PPS25	4320.29	119.87	52.57	1.62	1.46	0.09
C21≡PPS26	3935.82	341.37	72.53	2.62	1.90	0.10
C22≡PPS27	4244.47	297.48	74.03	2.56	2.05	0.08
C23≡PPS28	4415.18	162.50	65.39	4.34	1.60	0.10
C24≡PPS29	4633.56	182.34	69.87	0.93	1.79	0.10
C25≡PPS30	5359.67	394.42	66.30	1.46	1.55	0.09
C26≡PPS31	4613.38	383.20	73.98	1.90	1.93	0.10
C27≡PPS32	5145.12	385.12	64.04	1.25	1.68	0.14
C28≡PPS33	5975.74	288.58	52.41	1.37	0.87	0.02
C29≡PPS36	5564.53	242.38	79.67	0.73	1.53	0.07
Code	**Compression properties in MFD**					
	E_c [MPa]	St.Dev	σ_M^c [MPa]	St.Dev	ε_M^c [%]	St.Dev
C1≡PPS1	3134.42	280.74	115.34	4.57	8.94	1.91
C2≡PPS2	2665.94	463.12	115.12	6.83	8.98	2.57
C3≡PPS4	2977.09	302.59	111.41	4.54	8.36	1.90
C4≡PPS3	2974.11	429.88	117.88	3.05	8.99	1.63
C5≡PPS5	3251.14	435.38	110.57	2.61	7.51	1.23
C6≡PPS6	3396.74	644.29	117.72	1.72	7.72	0.91
C7≡PPS7	3838.93	427.98	121.36	2.74	7.11	1.20
C8≡PPS8	3596.95	445.80	119.58	0.85	6.17	0.49
C9≡PPS9	3938.62	578.48	121.78	4.62	8.00	2.06
C10≡PPS10	3595.24	407.71	120.43	2.73	6.87	0.72
C11≡PPS13	4575.45	393.44	129.25	2.69	14.46	3.37
C12*≡PPS16	3723.01	237.35	122.11	4.31	9.34	1.65
C13*≡PPS18	4161.91	330.01	118.79	1.89	8.43	1.48
C14*≡PPS19	3759.10	190.44	113.86	2.16	11.05	1.36
C15*≡PPS20	3462.65	261.66	104.19	2.20	9.23	1.36
C16*≡PPS21	3600.99	155.73	110.27	2.47	18.54	2.04
C17*≡PPS22	3318.72	520.96	113.77	2.67	15.38	3.30
C18*≡PPS23	3734.52	314.39	125.96	5.48	18.51	5.74
C19*≡PPS24	3652.79	115.54	106.64	1.51	17.06	2.30
C20*≡PPS25	3265.38	254.76	96.29	1.38	7.05	0.64
C21≡PPS26	2787.37	314.25	112.96	2.64	10.28	0.95
C22≡PPS27	2718.87	196.64	118.02	3.16	13.35	1.59
C23≡PPS28	2653.86	367.27	115.76	4.47	10.27	1.99
C24≡PPS29	2862.24	181.25	119.85	4.56	11.11	1.92
C25≡PPS30	3090.76	296.47	113.88	1.43	7.05	0.64
C26≡PPS31	2831.59	288.59	116.62	2.58	11.70	1.30
C27≡PPS32	2874.88	235.41	115.31	3.14	9.93	1.82
C28≡PPS33	3144.78	533.05	121.09	2.31	7.64	1.17
C29≡PPS36	2068.71	389.90	127.69	3.96	18.64	5.46

A3 Thermo-Mechanical Properties of PPS Composites in MFD

Table A.5: Thermo-mechanical properties of PPS composites

Code	DMTA properties in MFD							
	T_g^{onset} [°C]	$T_g^{E''}$ [°C]	E'at $T_g^{E''}$ [MPa]	St.Dev	tanδ at $T_g^{E''}$	St.Dev	$tan\delta_{max}$	St.Dev
C1≡PPS1	94.20	112.20	1673.00	84.85	0.14	0.00	0.17	0.00
C2≡PPS2	97.30	111.20	1695.50	27.58	0.14	0.01	0.17	0.00
C3≡PPS4	98.25	110.35	1805.50	3.54	0.14	0.00	0.17	0.00
C4≡PPS3	98.20	110.20	1826.50	37.48	0.14	0.00	0.17	0.00
C5≡PPS5	94.25	110.05	1756.00	145.66	0.15	0.00	0.19	0.00
C6≡PPS6	96.30	112.15	2585.00	130.11	0.11	0.00	0.13	0.00
C7≡PPS7	96.37	111.03	2716.67	249.08	0.11	0.00	0.13	0.00
C8≡PPS8	94.35	110.25	2786.00	156.98	0.11	0.00	0.13	0.00
C9≡PPS9	94.35	110.25	2973.00	179.61	0.11	0.00	0.13	0.00
C10≡PPS10	96.20	110.25	2685.50	313.25	0.12	0.00	0.14	0.01
C11≡PPS13	96.90	110.33	2897.67	120.29	0.12	0.00	0.14	0.00
C12*≡PPS16	99.40	111.25	2377.50	191.63	0.13	0.00	0.15	0.00
C13*≡PPS18	96.25	110.25	3345.00	48.08	0.11	0.00	0.14	0.00
C14*≡PPS19	96.30	112.35	3303.50	48.79	0.11	0.00	0.12	0.00
C15*≡PPS20	97.35	112.30	3532.50	12.02	0.11	0.00	0.12	0.00
C16*≡PPS21	96.15	112.40	2857.50	204.35	0.11	0.00	0.12	0.00
C17*≡PPS22	96.30	110.30	2881.50	224.15	0.12	0.00	0.14	0.00
C18*≡PPS23	98.35	112.30	2224.00	111.72	0.14	0.00	0.16	0.00
C19*≡PPS24	98.35	112.20	2774.00	258.80	0.11	0.00	0.13	0.00
C20*≡PPS25	96.30	110.25	2296.50	16.26	0.12	0.00	0.15	0.00
C21≡PPS26	98.40	110.15	1866.95	62.93	0.14	0.00	0.16	0.00
C22≡PPS27	98.20	110.30	1874.20	60.04	0.14	0.00	0.17	0.00
C23≡PPS28	96.40	110.20	1992.73	85.62	0.14	0.00	0.16	0.00
C24≡PPS29	96.30	108.15	2319.31	34.97	0.13	0.00	0.16	0.00
C25≡PPS30	96.30	109.15	2264.94	72.91	0.13	0.00	0.15	0.00
C26≡PPS31	96.20	108.35	2093.72	47.22	0.13	0.00	0.16	0.00
C27≡PPS32	96.20	110.30	2115.27	41.66	0.13	0.00	0.15	0.00
C28≡PPS33	96.15	110.25	2957.52	110.03	0.13	0.01	0.15	0.00
C29≡PPS36	94.10	110.35	2886.51	366.98	0.15	0.01	0.17	0.01

A4 SEM-EDX Analysis and XPS Spectra of Selected PPS Composites

In the following section the information gained on the elemental composition of the wear debris, transfer particles and films developed during sliding of selected PPS/SCF composites with and without TiO_2 sub-micro particles and/or internal lubricants against 100 Cr6 steel discs will be given. Likewise, observations of the boundary layer between the tribo-surfaces (polymer-based pin and 100 Cr6 steel disc) will be provided. Additionally, a schematic representation of the method of joining the tribo-surfaces will be shown after P-o-D testing and prior to performing cross-sectional water jet cutting.

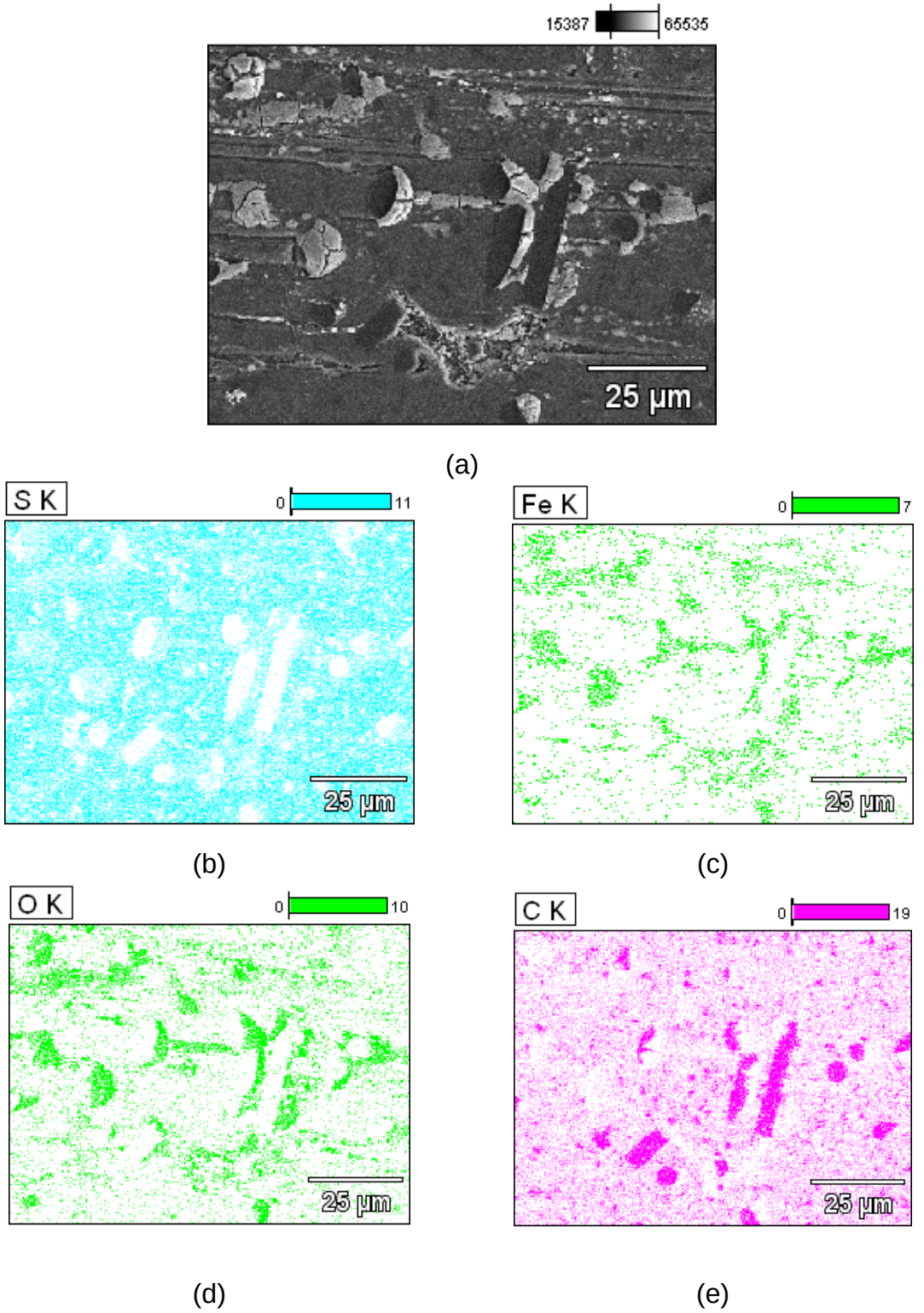

Figure A.1: SEM-EDX analysis of PPS/SCF/Gr/PTFE [70/10/10/10 vol.%] worn pin surface (a) chemical contrast, (b) S distribution, (c) Fe distribution, (d) O distribution, (e) C distribution. Testing conditions: p = 1 MPa, v = 3 m/s

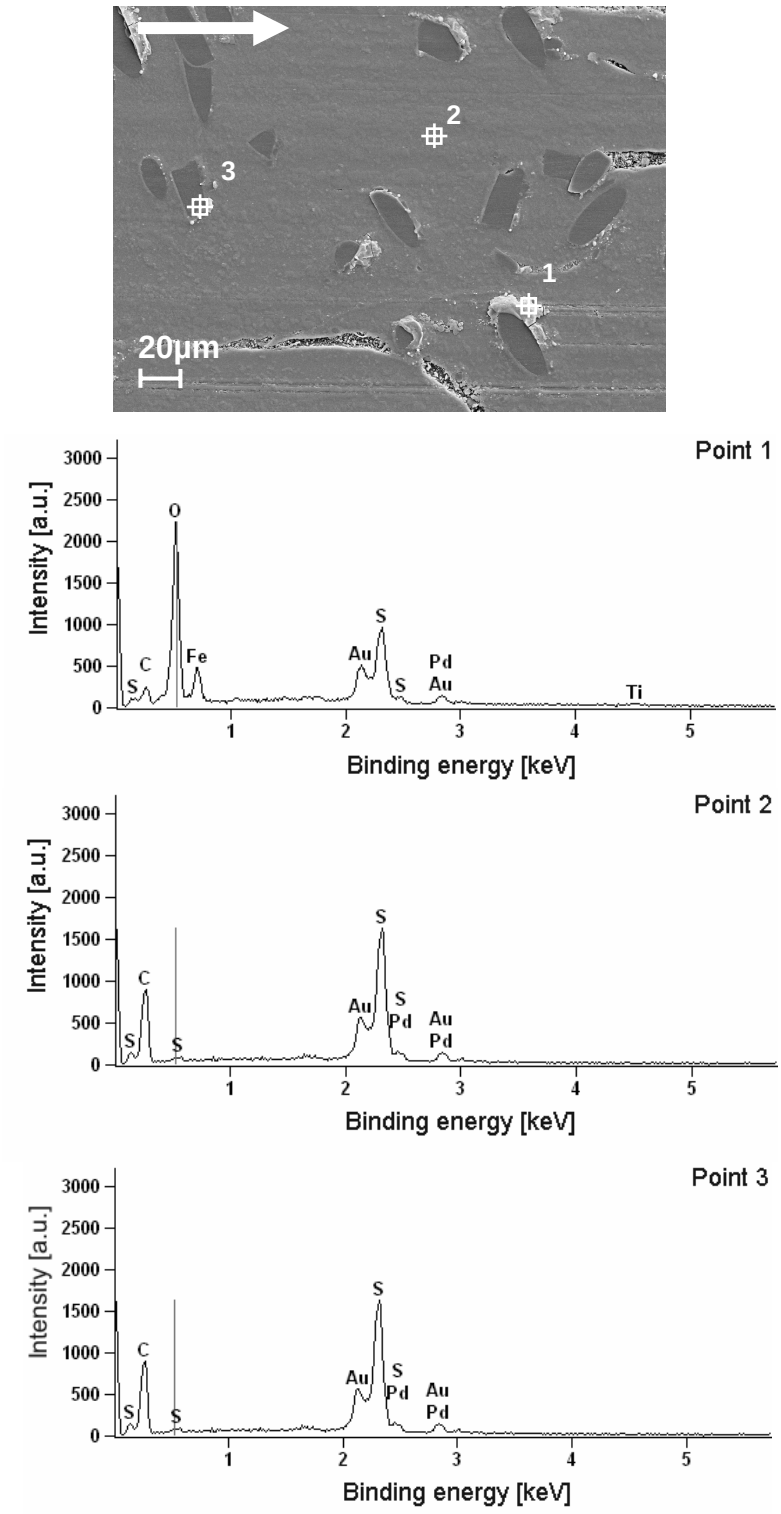

Figure A.2: SEM micrograph and XPS patterns for PPS/SCF [90/10 vol.%] worn pin surface. The arrow in the upper left corner indicates the relative sliding direction of the pin. Testing conditions: p = 3 MPa, v = 3 m/s

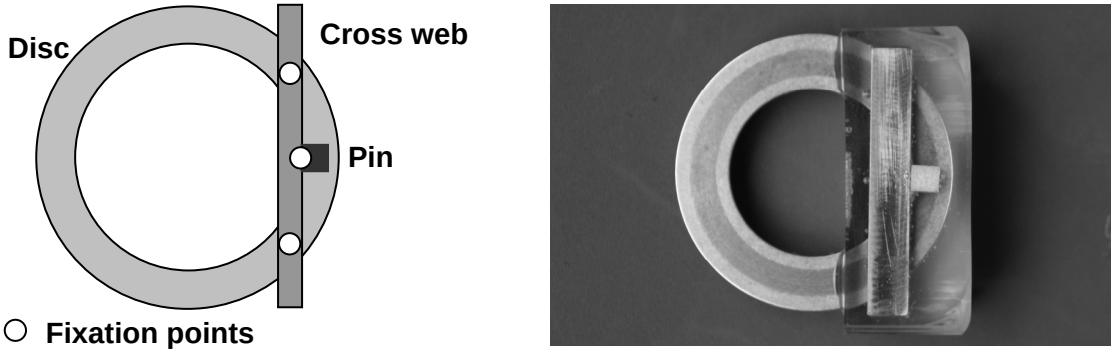

(a) (b)

Figure A.3: (a) Schematic representation of joining both mating surfaces (polymer pin and 100 Cr6 steel disc) immediately after pin-on-disc testing, (b) picture of the joined mating surfaces imbedded in epoxy resin prior to water jet cutting

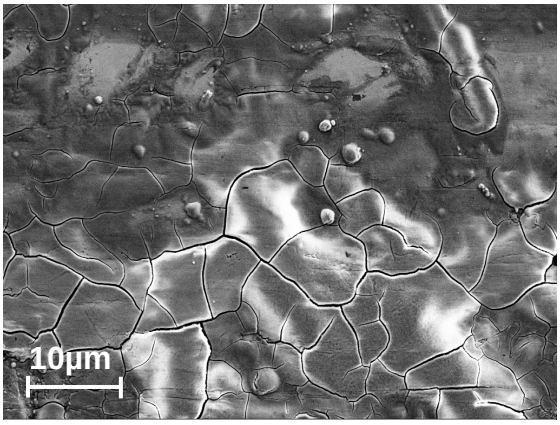

Figure A.4: SEM micrograph of the transfer film generated on the steel counterface after sliding against PPS/SCF/TiO_2 [85/10/5 vol.%]. Testing conditions: p = 1 MPa, v = 1 m/s

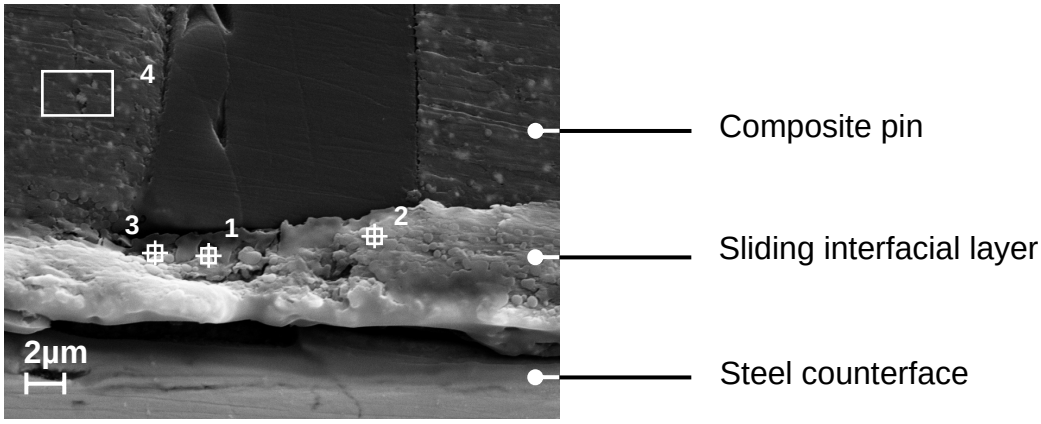

Figure A.5: SEM micrograph of longitudinal cross-section showing the sliding interfacial layer between PPS/SCF/TiO_2 [85/10/5 vol.%] composite and 100 Cr6 steel counterface with the corresponding XPS patterns. Testing conditions: p = 1 MPa, v = 1 m/s

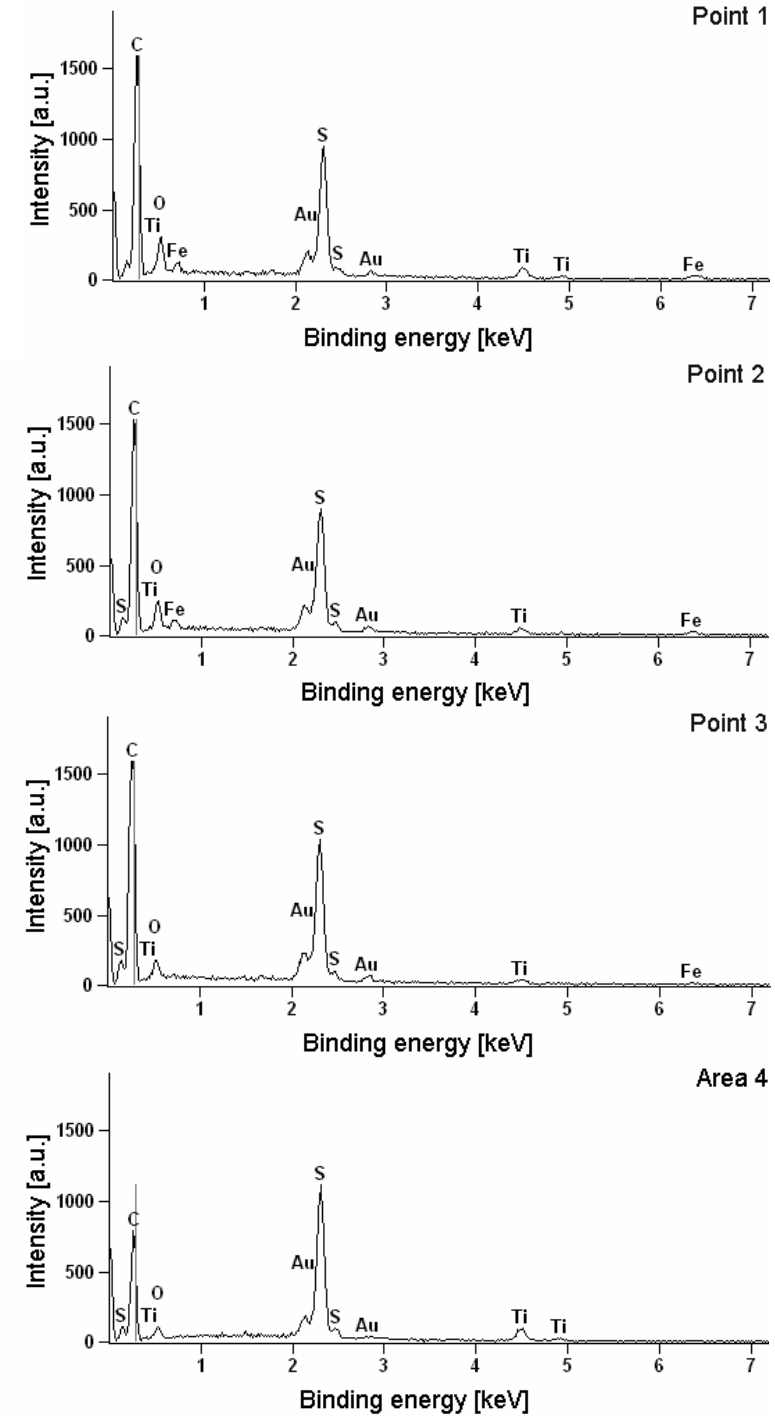

Figure A.5: SEM micrograph of longitudinal cross-section showing the sliding interfacial layer between PPS/SCF/TiO_2 [85/10/5 vol.%] composite and 100 Cr6 steel counterface with the corresponding XPS patterns. Testing conditions: p = 1 MPa, v = 1 m/s - continued

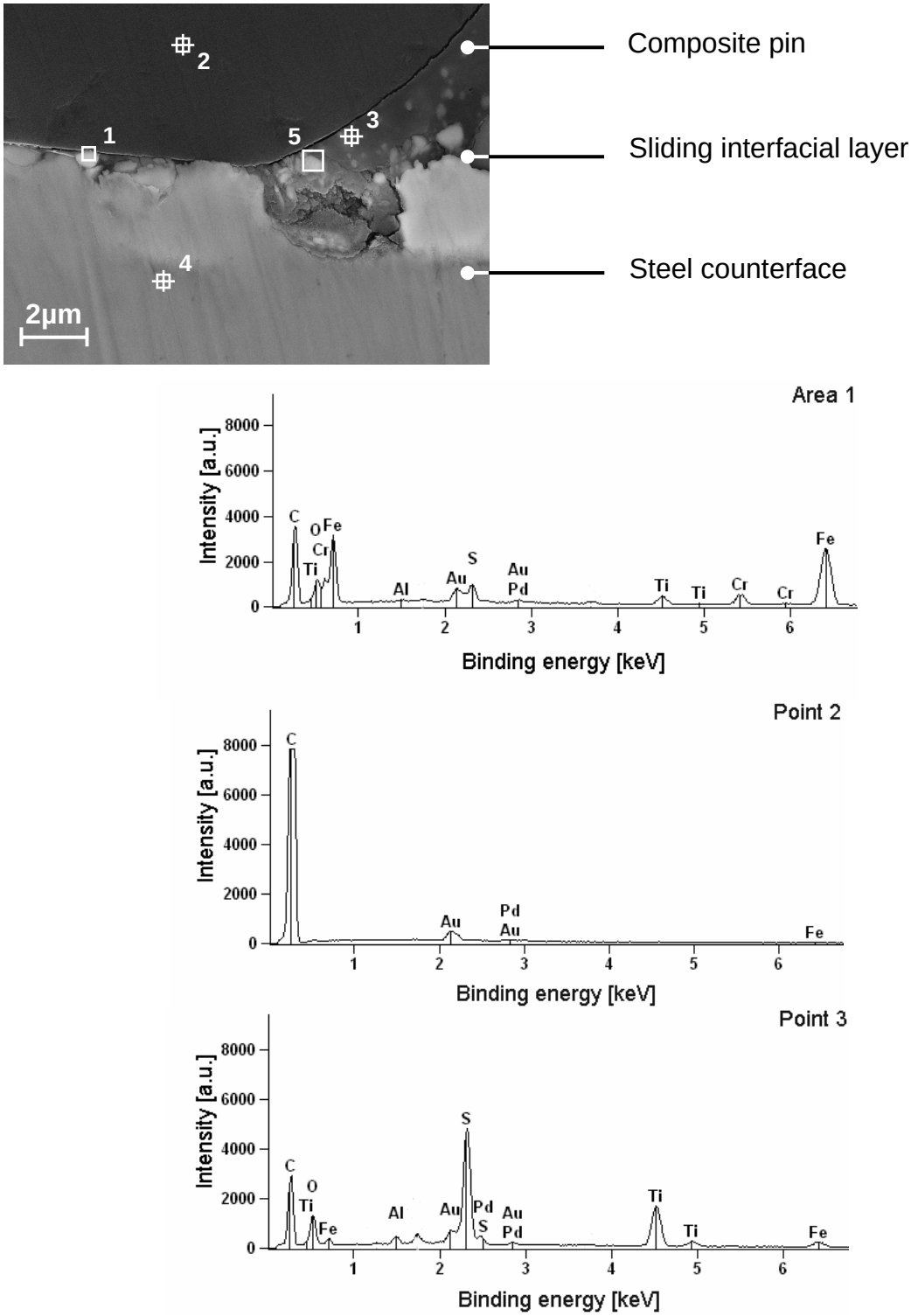

Figure A.6: SEM micrograph of longitudinal cross-section showing the sliding interfacial layer between PPS/SCF/TiO_2 [85/10/5 vol.%] composite and 100 Cr6 steel counterface with the corresponding XPS patterns. Testing conditions: p = 1 MPa, v = 1 m/s

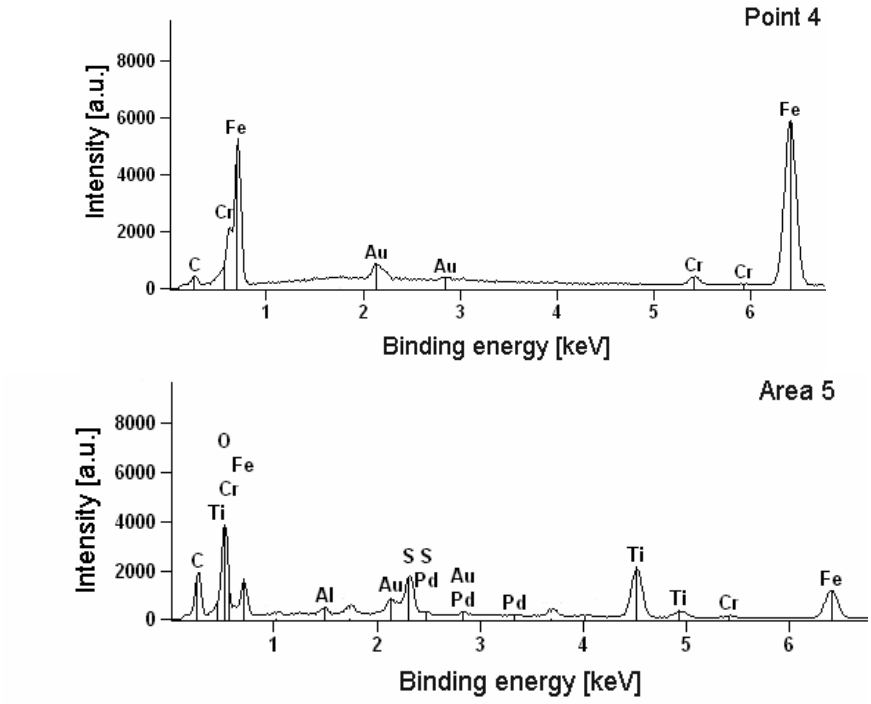

Figure A.6: SEM micrograph of longitudinal cross-section showing the sliding interfacial layer between PPS/SCF/TiO_2 [85/10/5 vol.%] composite and 100 Cr6 steel counterface with the corresponding XPS patterns. Testing conditions: p = 1 MPa, v = 1 m/s - continued

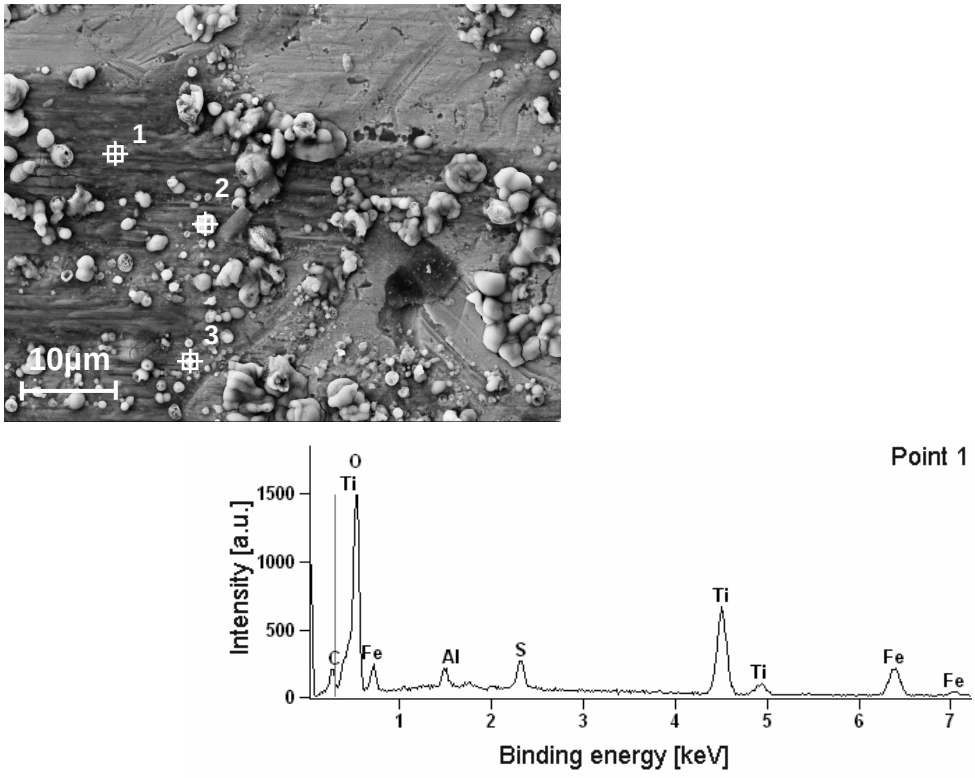

Figure A.7: SEM micrograph and XPS patterns for 100 Cr6 steel counterface after sliding against PPS/SCF/TiO_2 [85/10/5 vol.%] composite. Testing conditions: p = 3 MPa, v = 3 m/s

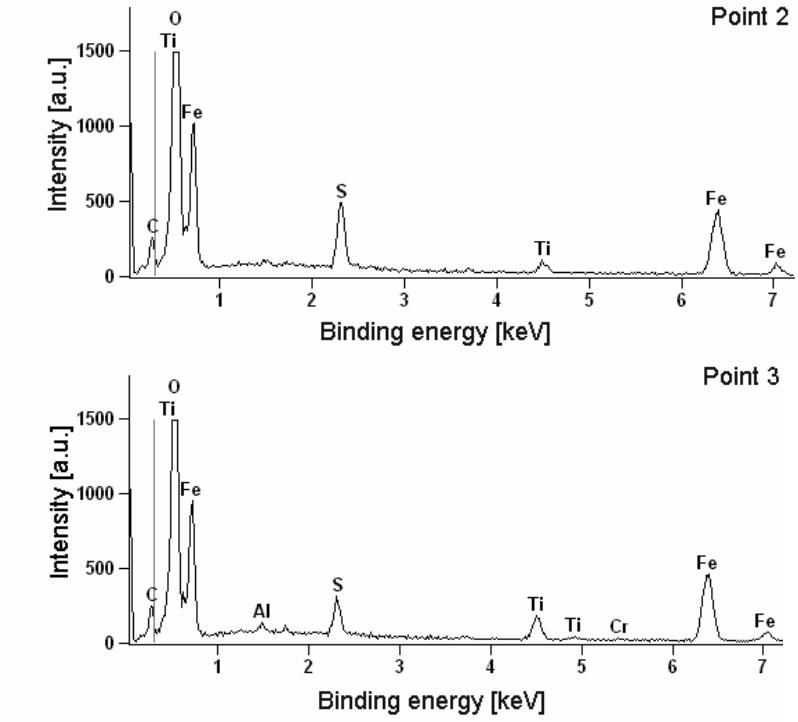

Figure A.7: SEM micrograph and XPS patterns for 100 Cr6 steel counterface after sliding against PPS/SCF/TiO_2 [85/10/5 vol.%] composite. Testing conditions: p = 3 MPa, v = 3 m - continued

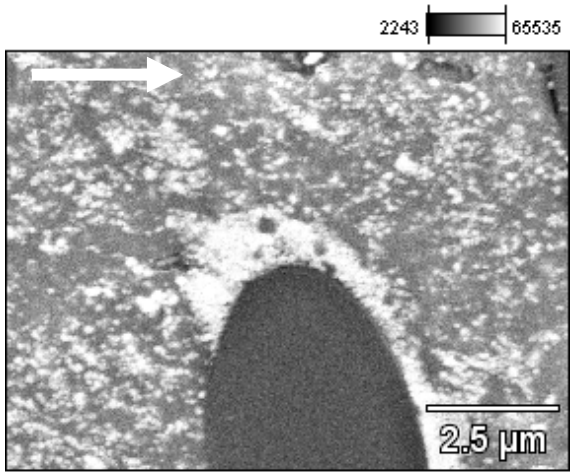

(a)

Figure A.8: SEM-EDX analysis of PPS/SCF/TiO_2 [80/15/5 vol.%] worn pin surface tested against 100 Cr6 steel counterface (a) chemical contrast, (b) S distribution, (c) Ti distribution, (d) O distribution, (e) C distribution. The arrow in the upper left corner indicates the relative sliding direction of the pin. Testing conditions: p = 1 MPa, v = 1 m/s

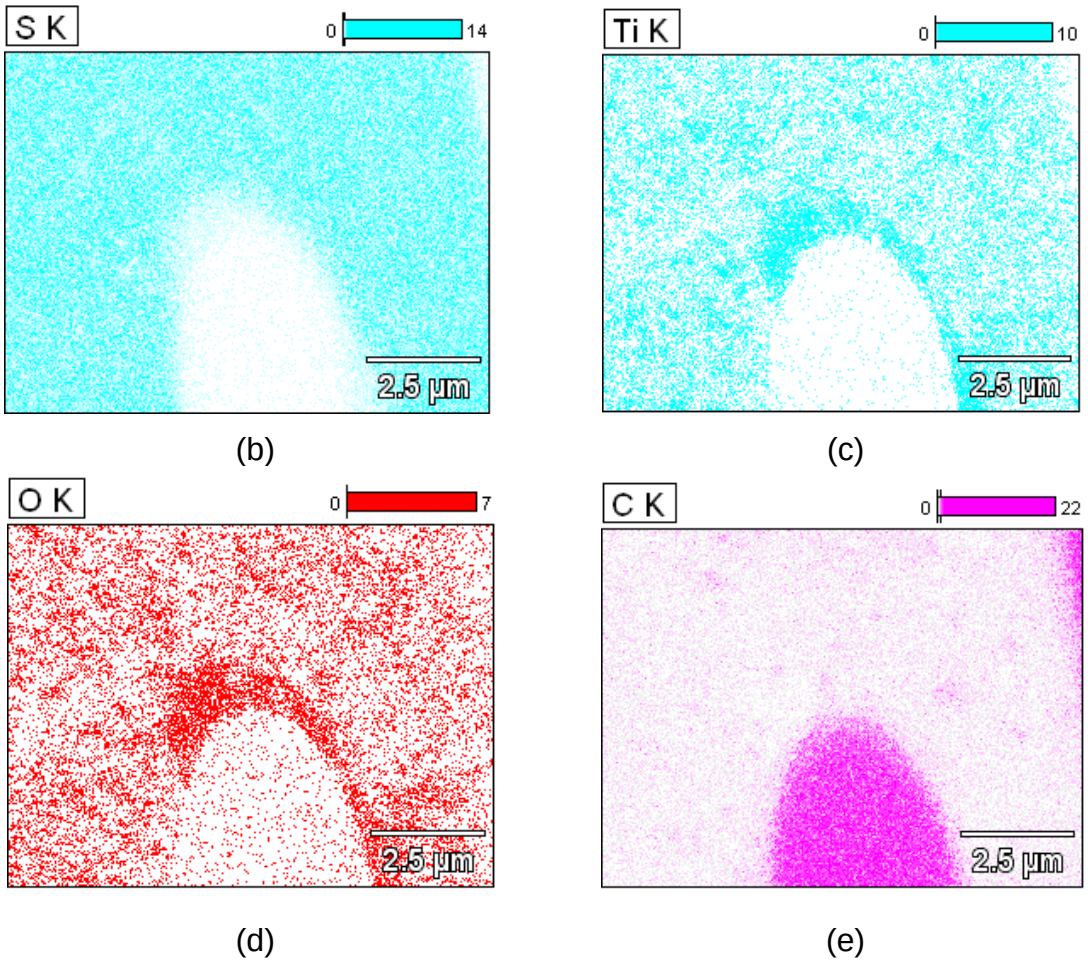

Figure A.8: SEM-EDX analysis of PPS/SCF/TiO_2 [80/15/5 vol.%] worn pin surface tested against 100 Cr6 steel counterface (a) chemical contrast, (b) S distribution, (c) Ti distribution, (d) O distribution, (e) C distribution. The arrow in the upper left corner indicates the relative sliding direction of the pin. Testing conditions: p = 1 MPa, v = 1 m/s - continued

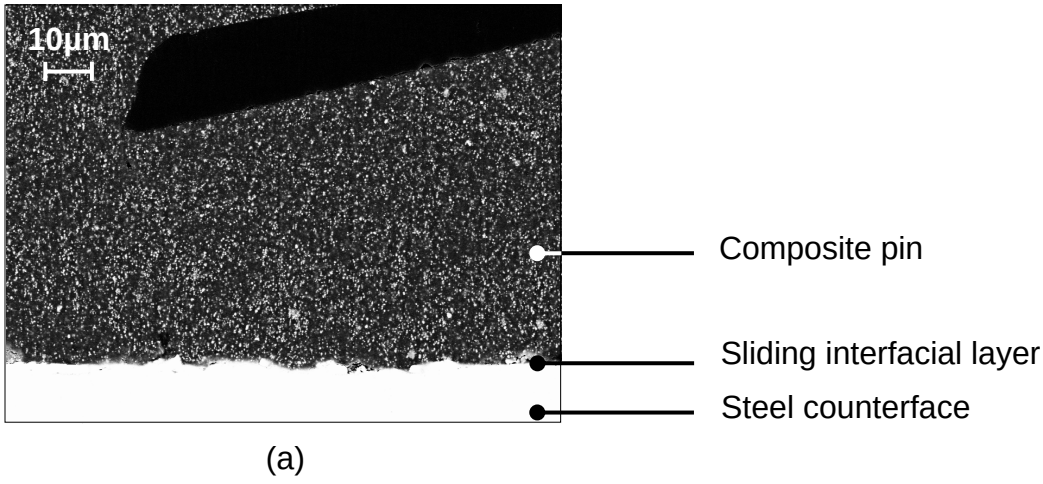

Figure A.9: SEM micrographs of transverse cross-section showing the sliding interfacial layer between PPS/SCF/TiO_2 [85/10/5 vol.%] composite and 100 Cr6 steel counterface. Testing conditions: p = 1 MPa, v = 1 m/s

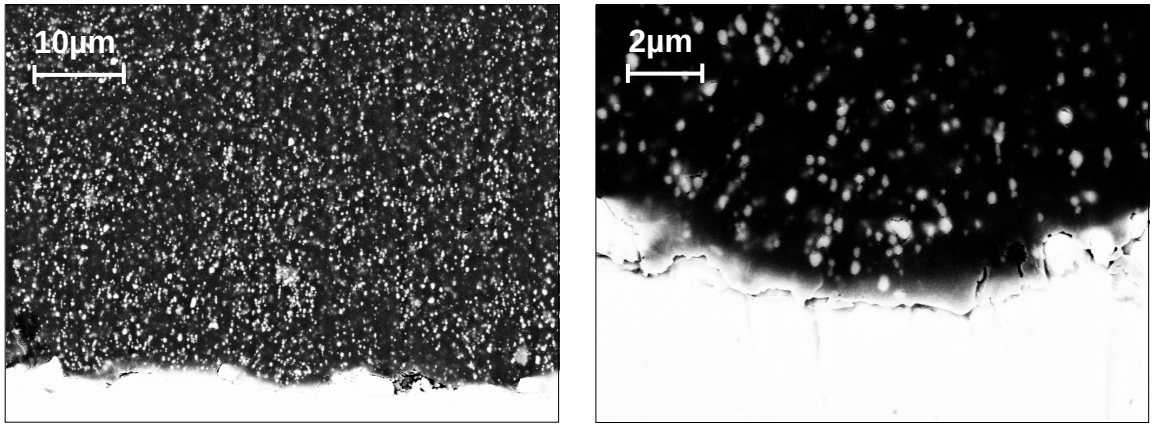

(b) (c)

Figure A.9: SEM micrographs of transverse cross-section showing the sliding interfacial layer between PPS/SCF/TiO_2 [85/10/5 vol.%] composite and 100 Cr6 steel counterface. Testing conditions: p = 1 MPa, v = 1 m/s - continued

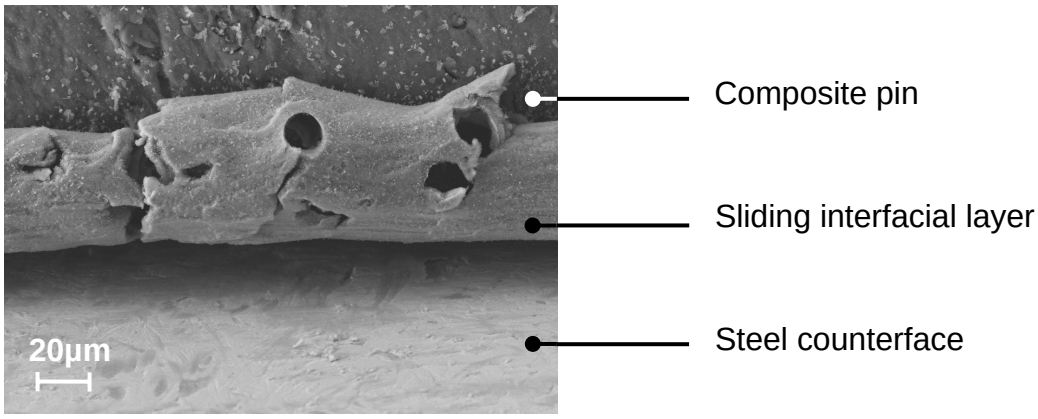

(a)

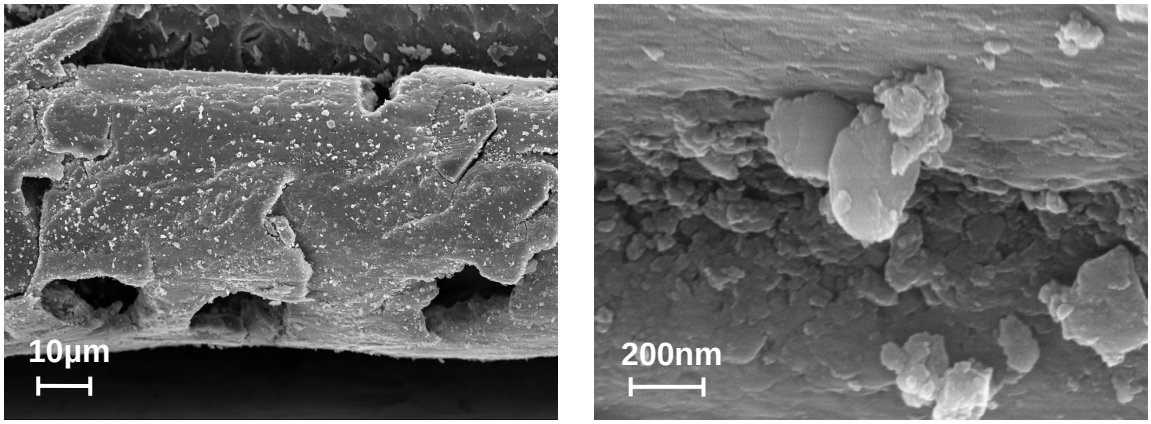

(b) (c)

Figure A.10: SEM micrographs of the joined mating surfaces (PPS/SCF/TiO_2 [85/10/5 vol.%] composite and 100 Cr6 steel counterface) immediately after P-o-D testing. Testing conditions: p = 1 MPa, v = 1 m/s

A5 AFM Observation of a Fiber in the Worn Pin Surface of PPS/SCF

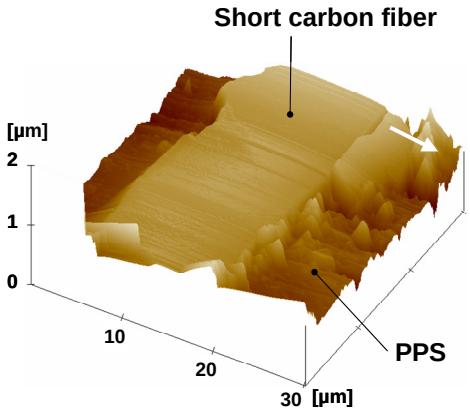

Figure A.11: AFM image of a fiber in the worn pin surface of PPS/SCF [90/10 vol.%] composite. The white arrow indicates the relative sliding direction of the sample surface (currently under microscopic observation). Testing conditions: p = 1 MPa, v = 1 m/s

List of Own Publications

1. Gyurova, L.A.; Miniño-Justel, P.; Schlarb, A.K.: Modeling the Sliding Wear and Friction Properties of Polyphenylene Sulfide Composites Using Artificial Neural Networks. Wear, Vol. 268, No. 5-6 (2010), 708-714

2. Gyurova, L.A.; Schlarb, A.K.: The Influence of Different Additives on Friction and Sliding Wear of Polyphenylene Sulfide Composites. In: Proceedings of the World Tribology Congress 2009 (WTC2009), Kyoto (Japan), September 6-11, 2009, 169

3. Gyurova, L.A.; Jiang, Z.; Schlarb, A.K.; Friedrich, K.; Zhang, Z.: Study on the Wear and Friction of Short Carbon Fiber and/or Nano-TiO_2 Reinforced Polyphenylene Sulfide Composites Using Artificial Neural Networks. In: Fisher, A.; Bobzin, K. (Eds.): Friction, Wear and Wear Protection, International Symposium on Friction, Wear and Wear Protection 2008, Aachen (Germany), April 9-11, 2008. Weinheim: VCH, 2009, 417-422

4. Gyurova, L.A.; Schlarb, A.K.: State-of-the-art: On the Action of Various Reinforcing Fillers and Additives for Improving the Sliding Friction and Wear Performance of Polymer Composites. Part 1: Short Fibers, Internal Lubricants, Particulate Fillers. Journal of Plastic Technology, Vol. 4, No. 6 (2008), 1-31

5. Jiang, Z.; Gyurova, L.A.; Schlarb, A.K.; Friedrich, K.; Zhang, Z.: Study on Friction and Wear Behavior of Polyphenylene Sulfide Composites Reinforced by Short Carbon Fibers and Sub-Micro TiO_2 Particles. Composites Science and Technology, Vol. 68 (2008), 734-742

6. Jiang, Z.; Gyurova, L.; Zhang, Z.; Friedrich, K.; Schlarb, A.K.: Neural Network Based Prediction on Mechanical and Wear Properties of Short Fibers Reinforced Polyamide Composites. Materials and Design, Vol. 29 (2008), 628-637

7. Gyurova, L.A.; Jiang, Z.; Friedrich, K.; Zhang, Z.; Schlarb, A.K.: Tribological and Mechanical Properties of Selected PPS Nanocomposites Designed for Tribological Service. In: Proceedings of 2nd Vienna International Conference Micro-and Nano-Technology (VienNano'07), Vienna (Austria), March 14-16, 2007. Vienna: Österreichische Tribologische Gesellschaft, 2007, 349-356

8. Jiang, Z.; Gyurova, L.; Zhang, Z.; Friedrich, K.; Schlarb, A.K.: Artificial Neural Network Based Prediction of Wear and Mechanical Properties of Polyamide Composites Reinforced by Short Fibers. In: Reibung, Schmierung und Verschleiß, Vol. 1. 47. Tribologie-Fachtagung, Göttingen (Germany), September 25-27, 2006. Aachen: Gesellschaft für Tribologie e.V., 2006, 4/1-4/14

9. Gyurova, L.A.; Jiang, Z.; Friedrich, K.; Zhang, Z.; Schlarb, A.K: On the Tribological Behavior of Selected PPS Nanocomposites Designed for Tribological Exploitation. In: Reibung, Schmierung und Verschleiß, Vol. 1. 47. Tribologie-Fachtagung, Göttingen (Germany), September 25-27, 2006. Aachen: Gesellschaft für Tribologie e.V., 2006, 30/1-30/10

List of Supervised Student Research Projects

1. Pérez Calvo, J.A.: On the Ball Bearing Effect of Nano (Sub-Micro) Particles in Short Carbon Fiber Reinforced Polymer Composites, IVW Bericht 09-018. Kaiserslautern: Institut für Verbundwerkstoffe GmbH, 2009

2. Bereciartua-Dudagoitia, A.: On the Tribological and Functional Behavior of Novel Epoxy/Carbon Nanotube Composites, IVW Bericht 08-032. Kaiserslautern: Institut für Verbundwerkstoffe GmbH, 2008

3. Minino-Justel, P.: Study on the Wear and Friction of Polymer Based Composites Using Artificial Neural Network, IVW Bericht 08-013. Kaiserslautern: Institut für Verbundwerkstoffe GmbH, 2008